Role of a Novel Iron Transport System in *Brucella* Pathogenicity and Intracellular Survival

A thesis submitted for the degree of Doctor of Philosophy
by

Christopher Moon

Division of Microbiology

School of Biological Sciences

THE UNIVERSITY OF READING

Reading

UK

and

Chemical, Biological and Radiological Division

DEFENCE SCIENCE AND TECHNOLOGY LABORATORY

Porton Down

UK

THE UNIVERSITY OF READING - DECLARATION

Declaration:

I confirm that this is my own work and the use of all material from other sources has been properly and fully acknowledged.

Signed: _____ Christopher Moon

Date: _____

Abstract:

The *mbfA* (**m**embrane **b**ound **f**erritin **A)** gene is carried by all *Brucella* species and is widely conserved in α-Proteobacteria. *mbfA* encodes a novel iron-export protein comprising an N-terminal peroxide reductase (erythrin) domain and a C-terminal, membrane-embedded, iron-export domain (**v**acuolar **i**ron **t**ransport, VIT). In this thesis, for the first time, the role of *mbfA* in *Brucella suis* 1330 and *Brucella melitensis* 16M was investigated, and the contributions of the two domains towards a novel mechanism of oxidative-stress resistance was considered. In addition, any part played by MbfA in enhancing *Brucella* survival within the macrophage 'Brucella-containing vacuole' (BCV) was investigated.

The isolated erythrin domain was shown to bind two iron atoms (as expected) or zinc which stabilized the protein, but no substantive peroxidase activity was exhibited, presumably due to lack of a reduction partner. *mbfA* complemented an *E. coli* mutant that was devoid of catalases/alkyl-hydroperoxidases, enhanced growth of a *fur* mutant with deregulated iron uptake, and impaired growth of a mutant lacking iron-uptake capacity. These findings support a role for MbfA in peroxide resistance and iron export. MbfA was shown to export ^{55}Fe when expressed in *E. coli*, and this activity was found to be O_2 and H_2O_2 dependent. Similar results were obtained using a *Burkholderia multivorans mbfA* mutant. In addition, MbfA mediated the decomposition of exogenous H_2O_2, which was mainly achieved by degradation of exogenous peroxide by exported iron. MbfA provided peroxide resistance in wildtype *E. coli* but only when endogenous catalases/peroxidases were inhibited by NO. Thus, MbfA is not markedly NO inhibited. MbfA iron export was found to be partly dependent on the presence of iron stores, in the form of bacterioferritin.

A naturally-occurring single-nucleotide substitution in the proximal coding region of the *mbfA* gene renders this gene cryptic in *B. melitensis* (although *mbfA* appears functional in all other *Brucella* spp.). Thus, a *B. melitensis mbfA* mutant exhibited no observable phenotype whereas a *B. suis mbfA* mutant displayed enhanced sensitivity to both Fe^{2+}- and H_2O_2-mediated oxidative stress. It is hypothesized that MbfA exports ferric iron into the luminal space of the endosomal *Brucella*-containing vacuole (eBCV) to counteract both the respiratory burst generated by NADPH oxidase as well as the export of iron into the macrophage cytoplasm by NRAMP1. Exported iron causes

disproportionation of peroxide externally, thus reducing the potential for harmful oxygen- and nitrogen-radical formation within the bacterial cell. Macrophage survival assays show that the absence of functional *mbfA* decreases intracellular survival during the early colonization phase in the eBCV, suggesting a reduced capacity to resist the redox stress of the endosomal and transient lysosomal compartments in the macrophage, which precede transition to the replicative BCV. Additionally, *in vivo*, *mbfA* contributes significantly to the maintenance of chronic infection within the murine liver and spleen. Further, MbfA provided a greater advantage in NRAMP1^{+} macrophages, than in NRAMP1^{-} macrophages. This finding supports a role for MbfA in countering the iron export role of NRAMP1 within the phagolysosome, such that the purpose of this NRAMP1 actiy would be to preserve peroxide against iron-catalysed degradation. In summary, the results are therefore consistent with a role for *mbfA* in intracellular survival and redox stress resistance in *Brucella*.

Table of Contents

Table of Figures

Chapter 1: Introduction

Chapter 2: Methods

Chapter 3: Bioinformatics

Chapter 4: Genetic Reagents

Chapter 5: Erythrin Domain Biochemistry

Chapter 6: Characterisation of MbfA function in *E. coli*

Chapter 7: Characterisation of MbfA in *Brucella*

Chapter 8: Discussion

Chapter 9: Appendix

Acknowledgements

Firstly, I would like to thank my supervisor, Professor Simon Andrews for his invaluable support and encouragement during the duration of my research project that I conducted at the University of Reading. In addition, I would also like to express my gratitude to the guidance and support that I received from my supervisor, Dr Helen Atkins and mentor Dr Philip Ireland at the Defence, Science and Technology Laboratory, Porton Down. Many thanks also to my additional supervisors Dr Malcolm East (University of Southampton) and Dr Kimon Andreas (University of Reading), as well as the collaboration with Dr Ehmke Pohl (University of Durham).

I would like to thank the past and present laboratory colleagues from the University of Reading, Ameer, Nancy, Afrah, Salem, Kang, Aida, Rana, Ian, Marwa, Dhama, Arvind and Fawzi, as well as the undergraduate and masters students that have collaborated on projects related to MbfA, Lucinda, Mark, Jonathan, Hannah and Alex and the technical staff and technicians for their help and guidance. I would like to thank my laboratory colleagues from DSTL, Helen, Mark, Andy and Karleigh for their experience and expertise with particular regards to the *in vivo* studies conducted.

Lastly, I would like to thank my partner Laura as well as my family; my parents and brother for their continued support throughout my research and writing of my thesis.

Publications and Presentations

1. **"The erythrin-VIT1 hybrid protein (MbfA) of *Brucella melitensis* acts as an iron exporter and protects against H_2O_2-mediated oxidative stress."**
   Moon C, Ireland P, Atkins H and Andrews SC.
   Midlands Molecular Microbiology Meeting
   University of Birmingham Sept. 2014

2. **"MbfA, a novel iron export system involved in *Brucella* pathogenicity and intracellular survival"**
   Moon C, Ireland P, Atkins H and Andrews SC.
   67th International Brucellosis Research Conference
   Marriott Hotel Chicago, USA Dec. 2015

3. **"MbfA, a novel iron export system involved in *Brucella* pathogenicity and intracellular survival"**
   Moon C, Ireland P, Karatzas A, East M, Atkins H and Andrews SC.
   Microbiology Society Annual Conference
   Arena and Convention Centre Liverpool Mar. 2016

4. **"MbfA, a novel iron export system involved in *Brucella* pathogenicity and intracellular survival"**
   Moon C, Ireland P, Karatzas A, East M, Atkins H and Andrews SC.
   10th International Biometals Symposium
   Art'otel Dresden, Germany July 2016

5. **"MbfA, a novel iron export system involved in *Brucella* pathogenicity and intracellular survival"**
   Moon C, Ireland P, Karatzas A, East M, Atkins H and Andrews SC.
   68th International Brucellosis Research Conference
   National Agricultural Science Centre (NASC), New Delhi, India Nov. 2016

Abbreviations

2,3-DHBA	2,3 dihydroxybenzoic acid	kDa	Kilo-daltons
APS	Ammonium persulphate	MbfA	Membrane bound ferritin A
BCV	*Brucella* containing vacuole	MES	2-(N-morpholino)ethanesulfonic acid
BSA	Bovine serum albumin	MOI	Multiplicity of Infection
CCC1	Calcium cross-complementer 1	MPO	Myeloperoxidase
CCCP	Carbonyl cyanide m-chlorophenyl hydrazone	MWCO	Molecular weight cut off
CV	Column volume	NADPH	Nicotinamide adenine dinucleotide phosphate
DAB	3,3'-diaminobenzidine	NRAMP1	Natural resistance-associated macrophage protein 1
DEAE	Diethylaminoethyl	O_2^-	Superoxide
DMEM	Dulbeccos modified Eagle media	OH•	Hydroxyl radical
DTPA	Diethylenetriaminepentaacetic acid	PCR	Polymerase chain reaction
eBCV	Endosomal BCV	PVDF	Polyvinylidene fluoride
EDTA	Ethylenediaminetetraacetic acid	rBCV	Replicative BCV
ESI-MS	Electrospray ionisation - mass spectroscopy	RNS	Reactive nitrogen species
FCS	Foetal calf serum	ROS	Reactive oxygen species
Fe^{2+}	Ferrous iron	SDS-PAGE	Sodium dodecyl sulphate - polyacrylamide gel electrophoresis
Fe^{3+}	Ferric iron	TAPS	N-Tris(hydroxymethyl)methyl-3-aminopropanesulfonic acid
H_2O_2	Hydrogen peroxide	TBE	Tris Borate EDTA Buffer
HEPES	2-[4-(2-hydroxyethyl)piperazin-1-yl]ethanesulfonic acid	TEMED	Tetramethylethylenediamine
ICP-OES	Inductively coupled plasma - optical emission spectroscopy	TRIS	Tris(hydroxymethyl)aminomethane
IPTG	Isopropyl β-D-1-thiogalactopyranoside	VIT	Vacuolar iron transporter
Irr	Iron response regulator		

Chapter 1: Introduction

1.1: Biological Importance of Iron

Iron is an essential nutrient required for growth, replication and survival; its acquisition in sufficient quantities is paramount for the propagation of nearly all organisms, including both pathogenic and non-pathogenic bacteria. This importance of iron in cellular biology is due to its role as a co-factor for proteins involved in numerous essential cellular processes. For instance, enzymes such as aconitase, part of the tricarboxylic acid cycle, and cytochromes, essential components of respiratory electron transport chains, require iron for their activity. Iron, as a co-factor, is incorporated into proteins in various forms, mostly as: the 'free' metal in mono- or di-nuclear form; as part of an iron-sulphur cluster; or combined with a protoporphyrin ring in the form of haem. The usefulness of iron as a co-factor component is largely dependent on its ability to readily switch between, and maintain, alternative redox states (ferrous - Fe^{2+}/ferric - Fe^{3+}) and adopts a wide range of redox potentials, allowing iron to mediate a variety of cellular redox reactions. However, this property can also be deleterious as it enables free iron within the cell to engage in illicit redox processes with molecular oxygen (and derived species) to generate toxic, reactive oxygen species (ROS: superoxide, O_2^-; hydrogen peroxide, H_2O_2 and the hydroxyl radical, ·HO) through Fenton and Haber-Weiss chemistry (Koppenol 2001), indicated below:

$$\text{Haber-Weiss: } Fe^{3+} + O_2^- \rightarrow Fe^{2+} + O_2$$

$$\text{Fenton: } Fe^{2+} + H_2O_2 + H^+ \rightarrow Fe^{3+} + HO\cdot + H_2O$$

$$\text{Net Radical Production: } O_2^- + H_2O_2 \rightarrow HO\cdot + OH^- + O_2$$

Such ROS can cause uncontrolled damage to various cell components, in particular lipid membranes, proteins and nucleic acids, leading to loss of cell viability. Thus, the deployment of iron within the cell must be carefully balanced to avoid iron toxicity whilst ensuring iron sufficiency.

In addition to its potential toxicity, iron presents problems of poor availability despite its abundance as the 4th most common element in the Earth's crust. This is caused by the very low solubility (1.4×10^{-9} M at pH 7; (Ratledge and Dover 2000)) of the environmentally predominant oxidised, ferric iron. Reduced, ferrous iron is soluble (0.1 M at pH 7.0), but is readily oxidised by molecular oxygen and so does not persist under

atmospheric conditions at neutral pH or higher. An effective and efficient mechanism for the acquisition of iron is an essential feature of a successful pathogen. Upon entry of a pathogen into the host, the bacterial cell experiences an environment in which iron is limited, this process is termed nutritional immunity.

1.2: Iron Acquisition by Pathogenic Bacteria

Under aerobic conditions, which prevail within the tissues of the mammalian host, iron primarily exists in the oxidized ferric form at a concentration below that required to support and maintain microbial growth. The host maintains free iron levels in the serum at even lower levels (10^{-24} M) as part of its innate resistance to microbial infection. This selective pressure has led pathogenic bacteria to develop mechanisms to counteract the iron withdrawal strategy of the host. These mechanisms can assimilate both the ferrous and ferric forms of iron from a wide range of host sources. Pathogenic bacteria often possess iron uptake systems that are also deployed by non-pathogens (siderophore-dependent systems and free metal transporters) but in many cases they rely upon iron transporters that are specific for host iron sources (Figure 1.1). Such mechanisms include:

- the rupture of iron-rich erythrocytes to enable retrieval of iron in the form of haem;
- secretion of high-affinity iron-chelating compounds called siderophores, which allow scavenging of iron from host sources such as transferrin;
- direct binding of host iron-proteins (e.g. transferrin, lactoferrin, haemoglobin, haemopexin and haptoglobin), using specific surface receptors, to allow acquisition of the iron that they hold;
- utilisation of free iron within host niches where free iron is sufficiently available (e.g. low oxygen, low pH or reducing conditions such as the gut, the cytosol and the phagosome); and
- release of iron from cytosolic ferritin.

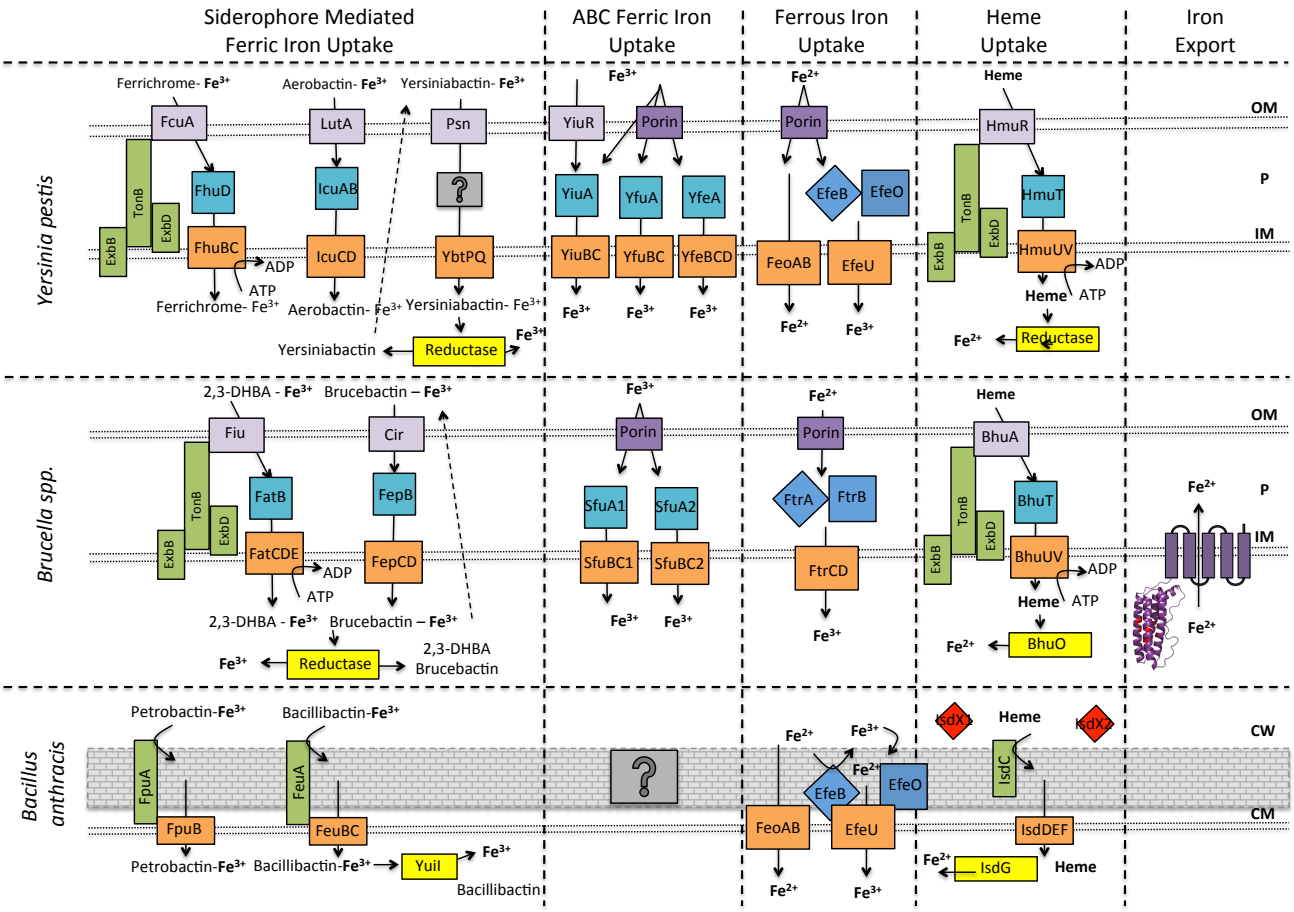

Figure 1.1: Schematic representation of iron transport in Bacteria.

Iron transport systems in selected pathogenic Gram-negative (*Yersinia pestis* and *Brucella suis*) and Gram-positive bacteria (*Bacillus anthracis*). Purple - outer membrane transport proteins, blue – periplasmic binding proteins, orange – inner membrane transport proteins, green – TonB complex, yellow – cytoplasmic reductase.

Table 1.1: Iron transport systems in *Yersinia pestis*, *Brucella suis* and *Bacillus anthracis*.

	Iron Import System			
Organism	**Siderophore**	**Fe^{3+}**	**Fe^{2+}**	**Haem**
Yersinia pestis	FhuBCD	YiuABC	FeoABC	HmuRTUV
	IcuABCD	YfuABC	EfeUOB	
	YbtPQ	YfeABCD		
Brucella suis	FatBCDE	SfuABCD1	FtrABCD	BhuTUV
	FepBCD	SfuABCD2		
Bacillus anthracis	FpuAB		FeoAB	IsdCDEFG
	FeuABC		EfeUOB	

1.3: Introduction to *Brucella* and Brucellosis

Brucellosis is a zoonotic infection caused by the bacterial genus *Brucella*; a small (0.5 x 0.6 μm) Gram-negative, facultatively intracellular aerobic cocco-bacilli. The disease has been known by numerous names, including Mediterranean fever, Malta fever, Bang's disease, gastric remittent fever, and undulant fever. The bacteria are transmitted from animals to humans by ingestion of contaminated food products (unpasteurized milk and related dairy products), direct contact with an infected material (e.g. percutaneous needlestick), or inhalation of aerosols. Slaughterhouse workers are at most risk of contracting Brucellosis where aerosolization of fluids, contamination of skin abrasions, and splashing of mucous membranes can occur.

Fever is the most common symptom of Brucellosis, occurring in 80-100% of cases, alongside additional symptoms including malaise and weight loss (>90% of cases). Death from Brucellosis is rare, occurring in approx. 2% of cases, but the economic loss associated with *Brucella* infection is substantial. This unfortunately, has resulted in *Brucella* spp. being incorporated into bioweapons, first developed by the United States military in the 1950's (Franz et al. 1997). It is estimated that the economic impact of a bioterrorist attack with *Brucella* spp. would cost hundreds of millions of dollars per 100,000 people exposed (Kaufmann et al. 1997).

To date, 10 *Brucella* species have been identified: *B. melitensis* (goat), *B. suis* (swine), *B. abortus* (cattle), *B. canis* (dog), *B. ovis* (sheep), *B. ceti* (porpoise), *B. pinipedialis* (seal), *B. neotomae* (desert woodrat), *B. microti* (common vole) and *B. inopinata* (unknown). The genomes of *B. melitensis* (DelVecchio et al. 2002), *B. abortus* (Halling et al. 2005), and *B. suis* (Paulsen et al. 2002) were the first to be sequenced and highlighted a high degree of similarity between biovars. Each species is named primarily from their source animal, with classical smooth O-lipopolysaccharide expressing *B. melitensis*, *B. suis* and *B. abortus* presenting with the highest human pathogenicity.

Brucellosis remains a major public health concern worldwide and is the most common zoonotic infection with more than 500,000 infections per year worldwide. Effective public and animal health programs limit the geographic distribution of *Brucella* infections, and the prevalence of the disease varies widely between countries. The heaviest disease burden lies in countries of the Mediterranean basin and Arabian

Peninsula, but the disease is also common in India, Mexico, and South and Central America.

Brucellosis can be effectively managed with long-course (6 weeks plus) treatments with antibiotics. Mono-antibiotic therapies with doxycycline can be effective in clearance of infection, but relapse rates approach 40%, therefore the World Health Organization (WHO) recommend a combination treatment of doxycycline for 6 weeks alongside IM streptomycin for 2-3 weeks.

Brucella organisms localise in the reproductive organs of host animals, causing abortions and sterility. This is caused by replication within intracellular compartments associated with the rough endoplasmic reticulum of trophoblasts (Anderson et al. 1986), a layer of cells at the outer surface of the blastocyst, which develops into a large percentage of the placenta. Infection of this tissue and subsequent accumulation of extremely large numbers (10^{13}) of bacteria (Alexander et al. 1981) promotes abortion. Bacterial replication to such extreme concentrations has been linked to the growth stimulatory factor erythritol (Smith et al. 1962), a four-carbon sugar found in the placenta and fetal tissues of *Brucella* hosts. The affinity of *Brucella* for erythritol is such that *in vitro* experimentation determined that *Brucella abortus* would preferentially utilize erythriol over glucose (Sperry and Robertson 1975).

Brucellae are shed in large numbers in the animal's urine, milk, placental fluid as well as other fluids. However, humans experience limited risk of contracting Brucellosis from wild animals, due to a lack of proximity, contact and infrequent use of milk and meat products from these animals. Instead infection is mainly acquired from domestic animals. It is likely that humans are accidental hosts of *Brucella* infection, due to the fact that humans are unable to transmit the disease either vertically or horizontally.

1.4: *Brucella* Intracellular Lifestyle

In incidences of human infection with *Brucella*, entry is gained to the body through breaks in the skin, mucous membranes, conjunctivae, and the respiratory and gastrointestinal tract. Once in the bloodstream, the organisms quickly become internalized by circulating polymorphonuclear cells (PMNs) and macrophages, which results in a large reduction of viable bacteria but replication and survival within host phagocytic cells is possible (Smith and Ficht 1990). It is of note that *Brucella* have a relatively low pyrogenicity, making them poor inducers of some inflammatory cytokines and the adaptive immune response and do not activate the alternative complement system. Phagocytosed Brucellae are first located within an early endosomal vacuole termed the **e**arly **B**rucella **c**ontaining **v**acuole (eBCV) (Celli et al. 2003), characterised by the acquisition of RAB5, its effector EEA1 and the transferrin receptor (Pizarro-Cerda et al. 1998, Celli et al. 2003, Bellaire et al. 2005) before acidification and maturation into late endosomes, characterised by the additional acquisition of late endocytic markers (LAMP1 and CD63), making the endosome competent for fusion with lysosomes (Pizarro-Cerda et al. 1998, Celli et al. 2003, Bellaire et al. 2005). The maturation of the eBCV along the endocytic pathway is deleterious to Brucellae cellular viability; the viable bacterial load within the macrophage is reduced throughout this period. Up to 90% of ingested bacteria are killed rapidly by the macrophage within the first 4 hours of infection (Celli et al. 2003). Fusion with the lysosome serves to further acidify the eBCV; Brucellae adapt to the lowering pH and reduce carbon anabolism to counter nutrient deprivation. Both stimuli activate expression of the VirB, Type 4 Secretion System (T4SS), of which maximal expression is achieved after 5 h post infection (Sieira et al. 2004). The VirB operon is *Brucella's* major virulence determinant (O'Callaghan et al. 1999, Boschiroli et al. 2002) and the encoded VirB apparatus is essential for escape from the endocytic pathway and trafficking towards the replicative BCV (rBVC) (Lestrate et al. 2000, Delrue et al. 2001, Celli et al. 2003) (Figure 1.2).

During transit through the eBCV, when *Brucella* spp. have a reduced replication capacity and are exposed to oxidative stress (Jiang et al. 1993) it is expected that the *Brucella* cell is rich in intracellular iron, acquired during systemic circulation, prior to phagocytosis by the macrophage (Baldwin et al. 1993). The combination of high iron concentrations within an oxidising environment presents a major risk of loss of bacterial viability through acquiring ROS mediated damage. To combat this, *Brucella* encode

two superoxide dismutases (SodA and SodC), a catalase (KatE) and an alkyl hydroperoxidease (AhpC) (Gee et al. 2005, Steele et al. 2010, Martin et al. 2012), all functioning to reduce ROS associated damage.

In contrast to the high iron concentrations observed within the *Brucella* cell, the phagosome is considered a low-iron compartment due to the activity of NRAMP1 (natural-resistance against macrophage pathogens), which is present within the phagosomal membrane, and exports di-valent metal cations from the phagosome, including ferrous iron. Imposition of iron-restriction functions to prevent bacterial iron acquisition, a process called nutritional immunity, preventing replication and growth of intracellular pathogens. Mutation, specifically a $G_{169}D$ point mutation, in the NRAMP1 gene is associated with enhanced susceptibility to infection by intracellular pathogens (Garcia-del Portillo et al. 1992, Pope et al. 1996, Blackwell 2001), through the inability of the phagolysosome to become iron limited. Failure to remove iron from this lumenal space makes availble a source of iron for bacterial aquistion. A second key mechanism for limiting the replication of intracellular pathogens is mitigated through interferon gamma (IFN-γ), which also acts to reduce intracellular iron concentrations (Byrd and Horwitz 1989). IFN-γ causes a reduction in macrophage iron uptake by decreasing expression of the transferrin receptor 1 (a major cellular iron importer) and increasing the expression of iron efflux proteins such as ferroportin 1. This results in decreased free iron availability in the macrophage, which, in turn, leads to decreased phagosomal iron concentrations (Nairz et al. 2008).

Additional features of the innate immune response which function to prevent bacteria colonization of the host and which are specific to *Brucella* infection include the oxidative burst mechanism of macrophages mediated by NADPH oxidase. The presence of NRAMP1 within the phagolysosomal membrane, nitric oxide synthase, NADPH oxidase and superoxide dismutase function to generate reactive oxygen species within the phagolysosome. Nitric oxide synthase catalyses the generation of nitric oxide from L-arginine, NADPH oxidase (nicotinamide adenine dinucleotide phosphate-oxidase) acts to generate superoxide from molecular oxygen, whilst super oxide dismutase dismutates superoxide to hydrogen peroxide. The sole purpose of these activities is to generate a bactericidal concentration of oxygen radicals, to prevent bacterial colonisation. In addition to these mechanisms, neutrophils produce myeloperoxidase (MPO) which functions to generate hypochlorous acid from hydrogen

peroxide and the chloride anion, and is the most potent mediator of redox stress in biological systems. It should be noted however, that *Brucella* species are not thought to colonise neutrophils.

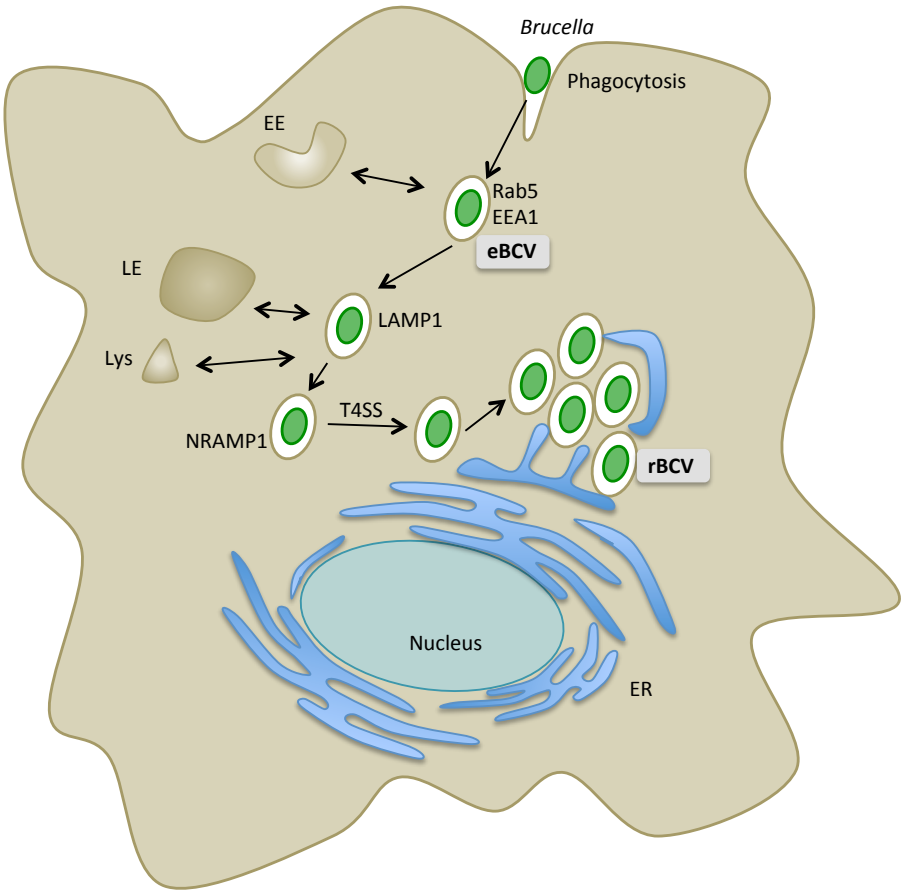

Figure 1.2: Model of *Brucella* intracellular trafficking in mammalian cells.

Brucella spp. reside within a vacuole termed the *Brucella* containing vacuole (BCV) which traffics along the endocytic pathway interacting with early endosome (EE), late endosomes (LE) and lysosomes (Lys). Interaction with the lysosome provides cues for induction of the VirB T4SS, from which VirB type IV effector proteins redirect the BCV to fuse with the endoplasmic reticulum (ER) creating the rBCV.

1.5: *Brucella* iron acquisition

Establishment of the rBCV sees replication of intracellular Brucellae that have adapted to a reduced oxygen respiratory system (Carrica Mdel et al. 2013), with an increased dependency in the use of amino acids as carbon sources (Roop et al. 2009). It is only within the rBCV that genes involved in iron acquisition are activated (Roop et al. 2009); *Brucella* species encode two TonB-dependent outer-membrane protein homologues that transport siderophore-iron complexes (2,3-dihydroxybenzoic acid (2,3-DHBA) (Lopez-Goni et al. 1992) and brucebactin (Gonzalez Carrero et al. 2002)) across the outer membrane; membrane protein functionality is based upon sequence homology to the *E. coli* outer membrane proteins Cir (Griggs et al. 1987) and Fiu (Hantke 1990). Siderophore iron complexes are internalised by two periplasmic binding protein dependent ABC transporters, FatBCDE and FepBCD, homologues of which are present in *Escherichia* and *Vibrio* species (Koster et al. 1991) (Shea and McIntosh 1991, Stephens et al. 1995). A further two ferric-chelate uptake systems, SfuABC1/2 homologues of the *Serratia marcescens* SfuABC complex (Angerer et al. 1992), import ferric iron. Ferrous iron is imported via a haem uptake system, BhuATUV; BhuA is a TonB dependant outer membrane haem transporter and homologue of the *Shigella* ShuA (Mills and Payne 1997) and *Yersinia* HmuA (Thompson et al. 1999) proteins whilst the BhuTUV proteins are homologues of the *Shigella dysenteriae* ShuTUV proteins (Wyckoff et al. 1998) which allow passage of haem across the cytoplasmic membrane. Once haem is internalised, ferrous iron can be liberated via degradation of haem into biliverdin and carbon monoxide via the haem oxygenase BhuQ (Ojeda et al. 2012). Finally, ferrous iron is also acquired via a ferrous-iron uptake system, FtrABCD (Elhassanny et al. 2013) which has functional similarities to the *Escherichia coli* O157:H7 EfeUOB system (Cao et al. 2007). Of these four distinct systems, the heam and ferrous iron transporters are the only systems shown to be essential during infection of both macrophage and mice (Paulley et al. 2007, Elhassanny et al. 2013). Schematic representation of these iron transport systems is displayed in Figure 1.1.

1.6: Novel redox stress resistance mechanisms in *Brucella*

Although multiple routes for iron import have been identified, two of which are crucial for in vivo mouse infection, no iron export system, that might ameliorate iron-induced redox stress in the phagosome, has been described to date. Interestingly, *Brucella* species possess an uncharacterised gene '**m**embrane-**b**ound bacterio**f**erritin', *mbfA (Brucella melitensis:* BMEI0354*, Brucella abortus:* BAB1_1691, *Brucella suis*: BS1330_I1673) that might specify a system fulfilling such a function.

The MbfA protein consists of two predicted domains: a cytosolic, N-terminal, diiron erythrin; and a C-terminal, **v**acuolar **i**ron **t**ransporter (VIT1) domain that is integral to the inner-membrane. The diiron erythrin domain is related to rubrerythrins of anaerobic bacteria. Rubrerythrins consist of two domains, a diiron erythrin and a Cys_4-Fe rubredoxin domain, and act as peroxide reductases affording resistance against exposure to redox stress. Reduction of peroxide is coupled to oxidation of the diiron centre, which is subsequently re-reduced by a rubredoxin-NAD^+ reductase system that employs NADH as the reducing source (Lumppio et al. 2001). A reducing system is expected to be required for MbfA for the N-terminal erythrin domain of MbfA, which re-reduces the diiron centre allowing for continual reduction of hydrogen peroxide. The VIT1 domain is homologous with the VIT1 protein of *Arabidopsis* and '**c**alcium **c**ross-**c**omplementor 1' (CCC1) of *Saccharomyces cerevisiae*. VIT1 and CCC1 are located in vacuolar compartments and are involved in the intracellular trafficking of Fe^{2+} and/or Mn^{2+} (Li et al. 2001, Kim et al. 2006). However, it is speculation that these transport systems are truly importing ferrous iron into the vacuole; the experimentation conducted relied upon inductively coupled plasma – optical emission spectroscopy (ISP-OES) to quantitate vacuolar metal contents. This technique is not specific to either the ferric or ferrous ion and instead quantitates a combined concentration of iron.

It is suggested that the functions of the erythrin and VIT1 domains are combined in MbfA such that reduction of peroxide is coupled to the oxidation and export of ferric iron in order to minimise iron-induced peroxide stress (Andrews 2010). With regards to the influence that MbfA has upon *Brucella* spp. survival within their intra-macrophage niche, it is proposed that MbfA is utilised to minimise ROS and iron-induced oxidative stress (Andrews 2010) during passage of Brucellae towards the rBCV.

The first phenotypic analysis of MbfA was conducted by Ruangkiattikul et al. 2012 in *Agrobacterium tumefaciens*. *mbfA* mutants were found to be more sensitive to hydrogen peroxide and iron stress, and have greater cellular iron contents than their respective wild types, as determined by ICP-OES, suggesting that MbfA is involved in decomposition of H_2O_2 and iron export. Structural work expanding on this was conducted by Bhubhanil et al. (Bhubhanil et al. 2014), confirming the presumed orientation of MbfA within the *A. tumerfaciens* inner membrane. Work by Sankari and O'Brian (Sankari and O'Brian 2014) examined functional and biochemical aspects of MbfA from *Bradyrhizobium japonicum*. The apo-form of the erythrin domain of *B. japonicum* was purified as a homo-dimer and found to exhibit ferroxidase activity, but is restricted to two molar equivalents of ferrous iron, indicating that a di-ferric iron site is formed by the erythrin domain.

1.7: Regulation of Iron Genes in *Brucella* species

The iron response regulator (Irr) is the predominant regulator of iron metabolism, acquisition and storage genes in α-proteobacteria including *Brucella* (Martinez et al. 2005) rather than the Fur (ferric uptake regulator) transcriptional repressor protein (Rodionov et al. 2006), observed in many other proteobacteria. Irr was first identified in *Bradyrhizobium japonicum* (Hamza et al. 1998) where it acts as a repressor of the haem biosynthesis gene, *hemB,* when cellular iron concentrations are low. Upon high intracellular iron conditions, Irr is degraded via ferrochelatase (Qi and O'Brian 2002) resulting in *hemB* repression being relieved. This regulation mechanism has been shown to control *mbfA* expression, *mbfA* is induced in response to high intracellular iron concentrations as well as through hydrogen peroxide stress mediated through Irr-dependent repression control (Ruangkiattikul et al. 2012, Bhubhanil et al. 2014, Sankari and O'Brian 2014). *mbfA* mutants are more sensitive to hydrogen peroxide and iron stress, and have greater cellular iron contents than their respective wild types, suggesting that MbfA is involved in decomposition of H_2O_2 and iron export.Recent research also shows that Irr is an activator of iron acquisition genes. Irr has been shown to up-regulate siderophore production (Martinez et al. 2006), the haem transporter BhuA (Anderson et al. 2011), the haem oxygenase BhuQ (Ojeda et al. 2012) and the ferrous iron uptake operon FtrABCD (Elhassanny et al. 2013) when cellular iron levels are low. In this way, Irr acts to both activate iron acquisition genes and repress iron metabolism and the iron storage gene in low iron conditions, allowing for regulation of iron homeostasis. The positive or negative regulation of genes by Irr is dependent upon

the location of the ICE-box (iron control element), the DNA binding site for Irr. The consensus motif of the ICE-box is: TTTAGAA–N_3–TTCTAAA, a 21 base pair, A/T rich, inverted repeat sequence which is shown to be highly conserved within the *mbfA* promoter region (Rudolph et al. 2006a, Rudolph et al. 2006b).

1.8: Aims and Objectives

Studying the MbfA system from *Brucella* spp. will provide insight into a novel mechanism of iron transport across biological membranes. In particular, not only is the MbfA system unique in terms of sequence and arrangement, but also in terms of the proposed direction and mechanism of iron transport with respects to other systems known in prokaryotes. If substantiated, MbfA would represent the first dedicated iron export system described in bacteria.

The primary aim of this project is to investigate the role that MbfA plays in terms of iron transport within *Brucella* spp. and how this may influence survival within the *Brucella* containing vacuole (BCV). To understand this, the mechanism by which iron is transported across the membrane will be determined through analyzing phenotypic effects that the expression of *mbfA* has upon *E. coli* mutants, as well as by measuring the export of iron from the bacterial cell, and the effect of mutations and environment on this activity.

To add context to the role that MbfA plays in *Brucella* virulence and survival, and the impact that nutritional immunity may play upon *Brucella*, an assessment of the ability *B. melitensis*, *B. suis* and corresponding *mbfA* deletion mutants to withstand exposure to hydrogen peroxide and ferrous iron will be conducted. Additionally, the survival *in vitro* within cultured murine macrophages ($NRAMP1^{+/-}$) as well as *in vivo* within a murine model of wildtype *Brucella* and *mbfA* mutants will be examined. The effect of *mbfA* inactivation in *Burkholderia multivorans* iron export capacity will also be tested, and the mechanism of iron export for a VIT1 system (from plant) will also be analysed as a comparator to MbfA.

Furthermore, experimentation will be undertaken to overexpress, purify and perform biochemical analysis, including metal content analysis, mass spectroscopy and crystallization trials upon the N terminal erythrin domain of MbfA. Spectroscopic measurements of the erythrin domain will provide insight into the iron binding capability of the domain and its ability to reduce hydrogen peroxide. Crystallization of the domain will enable structure solution by x-ray diffraction allowing models to be generated of the erythrin's structure. Together, these experiments will aid in the understanding of the biochemistry occurring at the erythrin domain during iron export.

Chapter 2: Methods

2.1: Bacterial Propagation

2.1.1: Bacterial Strains and Growth Conditions

Escherichia coli strains were grown on Lysogeny broth agar (LA) or in Lysogeny broth (LB) or minimal medium. *Brucella suis* bv.1 str. 1330 and *Brucella melitensis* bv. 1 str. 16M and derivative strains were grown on Brucella agar, Tryptone soya agar or in Brucella broth. All cultures were maintained at 37 °C with continual shaking at 200 rpm when required. Bacterial strains and plasmids used in this study are detailed in Table 1.

All bacteriological media were prepared with distilled (18.2 Ω) water and sterilised by autoclaving at 121 °C at 15 psi for 15 min. Heat labile substances were filter sterilised using a 0.2 μm filter (Millipore). Additions to molten media were made at 55 °C.

- LB: 10 g l^{-1} tryptone, 5 g l^{-1} yeast extract and 5 g l^{-1} NaCl.
    - LA was prepared by addition 1.5% agar to LB.
- Defined minimal media: M9 salts 0.2% v/v glycerol, 2 mM $MgCl_2$, 100 μM $CaCl_2$ and 1 mM thiamine
- Brucella broth: 10 g l^{-1} pancreatic digest of casein, 10 g l^{-1} peptic digest of animal tissue, 2 g l^{-1} yeast extract, 5 g l^{-1} NaCl, 0.1 g l^{-1} sodium bisulfite ($NaHSO_3$) and 1 g l^{-1} dextrose
    - Brucella agar was prepared by addition 1.5% agar to Brucella broth.
- Typtone soy agar (TSA): 15 g l^{-1} pancreatic digest of casein, 5 g l^{-1} enzymatic digest of soya bean, 5 g l^{-1} NaCl and 15 g l^{-1} agar.

2.1.2: Antibiotics

The antibiotics used routinely during experimentation with *E. coli* and *Brucella* spp. are described in Table 2.1, ampicillin, kanamycin and gentamycin are dissolved in water; chloramphenicol is dissolved in ethanol. All dissolved antibiotics are filter sterilised through a 0.2 μm filter (Millipore) and stored at -20 °C.

Table 2.1.: Concentrations of antibiotics.

Antibiotic	Abbreviation	Stock concentration	Working concentration (Brucella spp.)
Ampicillin	Amp	100 mg ml^{-1}	100 µg ml^{-1}
Chloramphenicol	Cm	50 mg ml^{-1}	50 µg ml^{-1}
Kanamycin	Km	50 mg ml^{-1}	25 µg ml^{-1} (45 µg ml^{-1})
Gentamycin	Gm	50 mg ml^{-1}	50 µg ml^{-1}

2.1.3: Bacterial growth curve

An overnight culture form a single isolated *E. coli* or *Brucella* spp. colony was washed once with phosphate buffered saline pH 7.2 and adjusted to a final OD of 1. A micro-titre plate was prepared with 200 µl of media per well and the standardised bacterial cultures used to inoculate individual wells to a starting OD of 0.01. *E. coli* and *Brucella* growth curves were monitored every 30 minutes for up to 48 h using a Bioscreen C (Labsystems) or MultiSkan FC (Thermo-Fisher) incubated spectrophotometer, respectively.

2.2: Cell Culture

2.2.1: Macrophage Cell Lines and Growth Conditions

J774.A1 and RAW264.7 murine macrophages were used for intracellular survival assays of *Brucella* spp. and were passaged and maintained in Dulbecco's modified Eagle's medium (DMEM) with addition of 5% fetal calf serum and 2 mM L-glutamate and incubated at 37 °C with 5% CO_2. In the absence of an increased CO_2 atmosphere (infection assays with *Brucella* within containment level 3 laboratory). Leibovitz's L-15 medium was used to maintain infected macrophages.

2.2.2: Thawing cryo-preserved cells

Liquid-nitrogen-stored cells were thawed at room temperature and immediately added to warm (37 °C) DMEM in a 75 cm^2 flask. After 6 h incubation at 37 °C with 5% CO_2, once cells had adhered to the flask, spent medium was aspirated and replaced with 15 ml fresh media.

2.2.3: Cellular Passage

Cells were observed under the light microscope to determine confluence and passaged at 70-80% confluence (once every 2/3 days). Spent medium was aspirated and cells washed twice with 1x DPBS. Adherent cells were scraped from the flask and re-suspended in 5 ml of DMEM with FCS and glutamate. The number of live cells was determined via addition of 10 µl trypan blue to 10 µl of cell suspension and enumeration of live white cells was achieved with a hemacytometer. Then, $2.5x10^6$ cells were dispensed into 75 cm^2 flasks with 10 ml of supplemented DMEM and incubated at 37 °C with 5% CO_2.

2.2.4: Cyro-preservation

A total of $1x10^6$ of 70% confluent cells were detached and collected by centrifuged at 1000 rpm for 5 min, spent medium was removed and the cells were re-suspended in 3.6 ml FCS. Then, 400 µl of DMSO were added dropwise and 1 ml aliquots were frozen to -80 °C overnight before being transferred to liquid nitrogen for long term storage.

2.3: Molecular Cloning

2.3.1: Polymerase Chain Reaction (PCR)

Primers were purchased from Eurofins MWG Operon, and were supplied as lyophilised oligonucleotides, which were re-hydrated with sterile ultrapure H_2O to give a stock concentration of 100 pmol/µl. Stock primers were diluted 1:10 to produce a working stock of 10 pmol/µl. Once re-hydrated, primers were stored at -20 °C.

2.3.2: PCR reactions

For high-fidelity cloning of genes from plasmid and chromosomal DNA and generation of Gibson assembly components, Q5 or Phusion (New England Biolabs) DNA polymerases were used. Reaction mixtures of 25 µl were assembled on ice and comprised of 5 µl 5x reaction buffer, 0.5 µl of 10 mM dNTPs, 1.25 µl of forward and reverse primers, 1 ng-1 µg of template DNA and 0.25 µl (0.2 U/µl) of DNA polymerase, made to the final volume with sterile ultrapure H_2O. The reaction mix was gently mixed and briefly pulse centrifuged before being transferred to a pre-heated thermocycler (98 °C; BioRad T100). Typical thermocycling parameters are outlined below:

Step	Cycles	Temperature	Time
Initial denature	1	98 °C	30 s
Denature	30	98 °C	10 s
Anneal		50-72 °C	30 s
Extension		72 °C	30 s/kb of plasmid length
Final extension	1	72 °C	2 min

For screening of recombinant DNA, colony PCR was employed with the use of low-fidelity thermostable DNA polymerases (Taq/DreamTaq; New England Biolabs). Putative recombinant DNA containing colonies were taken from an agar plate with a 10 µl pipette tip and inoculated into 50 µl of sterile ultrapure water in a 0.5 ml centrifuge tube. Remaining bacterial suspension was used to subculture into fresh LB with appropriate antibiotic, colonies that presented with a positive PCR result when analysed by agarose gel electrophoresis. A 20 µl reaction mix was assembled on ice comprising of 2.5 µl 10x buffer, 2.5 µl of 2 mM dNTPs, 1 µl of forward and reverse primers, 1 µl of DNA and 0.125 µl (1.25 U/µl) DNA polymerase, made to the final volume with sterile ultrapure H_2O. The reaction mix was gently mixed and briefly pulse centrifuged before

being transferred to a pre-heated thermocycler (95 °C). Typical thermocycling parameters are outlined below:

Step	Cycles	Temperature	Time
Initial denature	1	95 °C	3 min
Denature	30	95 °C	30 s
Anneal		Tm –5 °C	30 s
Extension		72 °C	1 min/kb of plasmid length
Final extension	1	72 °C	10 min

2.3.3: Site-directed mutagenesis

(Agilent QuikChange II Site-Directed Mutagenesis kit)

Mutagenic primers were designed with the aid of the QuikChange primer design program (www.agilent.com/genomics/qcpd), with the following properties: 25 to 45 bp in length, with the desired mutation base in the middle of the primer and a T_m of ≥78 ˚C. The PCR reaction mix was set up on ice to a final volume of 25 µl, comprised of 2.5 µl of 10x reaction buffer, 10 ng of template dsDNA, 31.25 ng of forward and reverse primers, 0.5 µl of deoxyribonucleotide triphosphates (dNTPs), 1.5 µl QuikSolution and 1 µl of *PfuUltra* HF DNA polymerase (2.5 U/µl). The thermocycler was pre-heated to 95 °C before samples were added. Thermocycling parameters are outlined below:

Step	Cycles	Temperature	Time
Initial denature	1	95 °C	30 s
Denature	18	95 °C	30 s
Anneal		55 °C	1 min
Extension		68 °C	1 min/kb of plasmid length
Final extension	1	68 °C	7 min

Following thermocycling, reaction mixtures were placed on ice to cool the reaction. A 0.5 µl volume of *Dpn*I (10 U/µl) was added per reaction mix, the solution was gently vortexed and pulse centrifuged, and was then incubated at 37 °C for 1 h to digest parental, non-mutated template DNA. XL-10 Gold ultra-competent cells (45 µl) where used to transform 1 µl of the *Dpn*I-treated DNA, with the addition of 2 µl of β-mercaptoethanol, with a heat shock time of 30 s.

2.3.4: Plasmid and PCR digestion

Digestion of plasmids with one or two restriction endonucleases (New England Biolabs) was conducted in a final volume of 20 µl. Restriction endonuclease digestions were prepared with the required volume of ultrapure water first, followed by 2 µl of digestion buffer, 1 µl of plasmid DNA and 1 µl of each restriction endonuclease. The reaction mixtures were briefly vortexed and pulse centrifuged to pool the reaction mixture to the base of the reaction vessel, before incubation at 37 °C for 15 min. For digestion of PCR products, a final reaction volume of 30 µl was used. In each case, 10 µl of PCR product were added to 16 µl of sterile ultrapure water, 2 µl of digestion buffer and 1 µl of each restriction endonuclease. The reaction mixture was briefly vortexed and pulse centrifuged before incubation at 37 °C for 1 h. Addition of fast alkaline phosphatase was included in some reactions to prevent unwanted self-ligation of the digested plasmid. The alkaline phosphatase (1 µl) was added to the final reaction after incubation at 37 °C; an additional 5 min incubation step at 75 °C was included to inactive the alkaline phosphatase.

2.3.5: Blunting reaction

To blunt the sticky ends of a digestion reaction (for use in a blunt-end ligation reactions), the Fermentas blunting enzyme was used (enzyme removes 3' overhangs and fills in 5' overhangs). Following the digestion of the plasmid, a 20 µl final volume reaction mixture comprising of 10 µl of reaction buffer, 0.15 pmols of sticky-end DNA fragment and 1 µl DNA-blunting enzyme were briefly vortexed and centrifuged. The reaction mixture was incubated at 70 °C for 5 min and used directly in the ligation reaction.

2.3.6: Agarose gel electrophoresis

Typically, 0.8% agarose gels were used for visualising 500 bp – 10 kb fragments after electrophoretic separation with addition of GelRed (Biotin) or ethidium bromide (Sigma) in 0.5x TBE buffer (5x: 445 mM Tris base, 217 mM borate, 10 mM ethylenediaminetetraacetic acid (EDTA) pH 8.0). DNA samples were prepared in 6 or 12 µl volumes (dependent upon the number of wells used in the gel) with 6x loading buffer (30% glycerol, 0.25% bromophenol blue, 0.25% xylene cyanol), sterile ultra-pure water and 0.5-2 µl of DNA (supercoiled or digested DNA, respectively) per

sample. Gels were submerged in 0.5x TBE buffer and subjected to electrophoresis with a constant 60 V for approx. 2 h in a horizontal gel tank. DNA fragments were visualised with a UV transluminator (G-Box, Syngene).

2.3.7: Molecular weight markers - DNA marker

GeneRuler 1kb and Roche X DNA molecular weight markers (Appendix 9.1) were used to estimate the size and quantity of DNA following agarose gel electrophoresis, using either UV-induced fluorescence of Gel-Red (Biotin) or ethidium bromide at a concentration of 0.5 mg/ml.

2.3.8: Gel extraction and PCR purification

(Thermo GeneJET/Qiagen QIAquick gel extraction/PCR purification kit)

Gel extraction was used to excise a specific band from an agarose gel after digestion with a restriction endonuclease. The fragment of agarose gel containing the DNA fragment was excised using a clean, sterile scalpel blade and placed into a pre-weighed 1.5 ml centrifuge tube. Binding buffer was added in a 100 µl:100 mg ratio and incubated at 55 °C for 10 min to dissolve the agarose gel fragment, releasing the enclosed DNA. Up to 800 µl of DNA containing solution were then added to the centre of a centrifugation column and centrifuged for 1 min at 12000 x g (Eppendorf 5453) and the flow-through discarded. The column was washed with an ethanol-based wash solution and centrifuged for an addition minute to remove residual ethanol, before 20-50 µl of elution solution were added to the centre of the column and centrifuged again for 1 min. The eluent containing the linear DNA fragments was stored at -20 °C.

PCR purification was used to remove residual oligonucleotides, polymerases or restriction endonucleases after PCR or digestion reactions. Equivalent volumes of binding buffer were added to the PCR or digestion reaction in a 1:1 ratio, up to 800 µl was then added to the centre of the centrifugation column. Washing and eluting of bound DNA follows the protocol described above for gel-extracted fragments.

2.3.9: Ligation

All ligation reactions were conducted with the T4 ligase (New England BioLabs), in a final volume of 20 µl comprising of 2 µl T4 ligase buffer, 1:3 vector:insert, DNA ratio and 1 µl of T4 ligase. Sticky end ligations were incubated at room temperature for 10 min whereas blunt end ligations were incubated at room temperature for 1 h. In both cases the entire 20 µl reaction was used for transformation into 200 µl of chemically competent cells.

2.3.10: Gibson Assembly

(ClonTech In-Fusion HD cloning kit)

The In-Fusion cloning procedure was used with gel extracted purified products. Between 50 and 200 ng of each fragment were used with no parental DNA or non-specific background bands present, when analysed by agarose gel electrophoresis. Purified insert fragment (10-200 ng) and 50-200 ng of the linearised vector were added to 2 µl of 5x In-Fusion HD enzyme premix (containing a T5 exonuclease, DNA polymerase and a T4 ligase), made up to a 10 µl total reaction volume. The assembled reaction was incubated for 15 min at 50 °C in a BioRad T100 thermocycler (to allow reliable incubation temperature and rapid cooling to 4 °C when reaction was complete), which was then placed on ice. A 2.5 µl volume of the reaction mix was then used to transform competent cells; Stellar ultra-competent cells were used to ensure high-transformation efficiencies (>1x10^8 cfu/µg). Method 2.27 was followed for transformation.

2.3.11: Chemically competent cells

For preparation of 20 aliquots of 200 µl of competent cells, a 5 ml overnight culture, inoculated with the required strain, was added to pre-warmed, pre-shaken 50 ml LB in a 250 ml Erlenmeyer flask. The culture was monitor until an OD_{600} of 0.4 to 0.5 was achieved at which point the entire 50 ml culture was centrifuged at 3250 x g for 10 mins at 4 °C (Eppendorf 5804R with A-4-44 rotor). The supernatant was removed and the cell pellet resuspended in 30 ml ice cold 0.1 M $MgCl_2$ and incubated on ice for 10 min. The solution was centrifuged (same conditions), the supernatant removed and the pellet resuspended in 30 ml ice cold 0.1 M $CaCl_2$ and incubated on ice for 30 min. The cells were centrifuged for a final time (same conditions), the supernatant removed and the pellet resuspended in 4 ml ice cold 0.1 M $CaCl_2$ and 20% glycerol. Aliquots of 200 µl

were made, flash frozen in liquid nitrogen and stored at -80 °C.

2.3.12: Transformation

Typically 1-2 µl of plasmid DNA (approximately 100 ng/µl) was used in transformation reactions, unless the transformed DNA was from a ligation reaction, in which case the entire reaction mix was transformed into 200 µl of chemically competent cells. Competent cells were defrosted on ice and plasmid DNA added, mixed gently and incubated on ice for 30 min before being heat shocked at 42 °C for 1 min. Heat-shocked cells were incubated on ice for 5 min then 900 µl of pre-warmed LB were added followed by incubation at 37 °C with 250 rpm shaking for 90 min. Cells were centrifuged at 12000 x g (Eppendorf 5453) for 5 min and 1 ml of supernatant removed. The pellet was resuspended in the remaining 100 µl of supernatant and plated onto LA with appropriate antibiotic(s).

2.3.13: Electroporation

Electroporation was used to introduce plasmid DNA into *Brucella* spp. Competent *Brucella* cells were prepared by harvesting *Brucella* from a Brucella agar plate into 1 ml H_2O. The cells were washed three times with 1 ml H_2O via centrifugation (3 min, 20°C, 13,000 rpm), re-suspended in 200 µl of water before dividing into 50 µl aliquots. Up to 5 µl of plasmid DNA (~ 1 µg) were added to 50 µl of competent *Brucella* cells in a cooled 0.2 mm electroporation cuvette and electroporated (BioRad XCell electroporation system) at 400 Ω, 25 µF and 2.5 kV for 10 ms. Electroporated cells were allowed to recover in 1 ml SOC-B at 37 °C overnight before plating onto TSA with appropriate antibiotics and incubated at 37°C for up to 5 days.

2.3.14: Plasmid extraction

(Thermo GeneJET mini prep kit; Qiagen QIAprep Spin Miniprep kit)

A 5 ml liquid culture (LB), with appropriate antibiotic, of *E. coli* harbouring the plasmid required for extraction was grown for a maximum of 16 h at 37 °C with 250 rpm shaking. Following incubation, the entire culture was centrifuged at 3250 x g (Eppendorf 5804R with A-4-44 rotor) for 10 min at 4 °C. The supernatant was removed and the pellet re-suspended in 250 µl resuspension solution, (QIAprep includes addition of 10 µl alkaline phosphatase with incubation at room temperature for 5 mins) 250 µl

lysis solution and 350 µl of neutralisation solution were added and the centrifuged for 5 min at 12000 x g (Eppendorf 5453). A 850 µl volume of supernatant was added to the centrifugation column and centrifuged for 1 min at 12000 x g (Eppendorf 5453), the flow-through was discarded and the column washed twice with an ethanol-containing wash solution. The column was centrifuged for an additional 1 min at 12000 x g (Eppendorf 5453) to remove residual ethanol, before 50 µl of elution solution were added to the centre of the column, incubated at room temperature for 2 min and centrifuged at 12000 x g (Eppendorf 5453) for 2 min. The eluent containing the plasmid was stored at -20 °C.

2.3.15: Estimation of DNA concentration

Prior to ligation and sequencing reactions the concentration of the plasmid DNA was estimated using the Nanodrop spectrophotometer. Plasmid DNA (2 µl) was placed onto the spectrophotometer's pedestal and the absorbance of the sample at 260 nm was determined, with a read out of DNA concentration in ng/µl given. Considerations to the purity of the DNA were undertaken though the ratio of 260/280 nm absorbance.

2.4: Recombinant protein manipulation

2.4.1: Induction of recombinant protein

A single isolated colony of *E. coli* BL21 (DE3) harbouring an overexpression plasmid (pET series) engineered to express a 6xHis tagged recombinant protein was inoculated into LB with ampicillin and incubated overnight at 37 °C with 250 rpm shaking (starter culture). This starter culture was used to inoculate pre-warmed and pre-shaken LB with ampicillin at a ratio of 1:100 (starter culture; fresh LB). The optical density of the culture was monitored until an OD_{600} of 0.5 was achieved, at which point 0.5 mM IPTG was added to induce protein expression. During preliminary expression experiments, 0.5 OD units of cells were collected by centrifugation (7 min at 12000 x g; Eppendorf 5453) every hour for 5 h after induction, with an additional sample taken after overnight growth. The supernatant was removed and dry pellets stored temporarily on ice or overnight at -20 °C. For larger scale overexpression 5 L of culture were harvested by centrifugation at 6000 x g (Sorval RC5B+ with SLA-3000 rotor) for 30 min at 4 °C, 5 h after induction. The resulting pellet was re-suspended in 25 ml ice-cold PBS and centrifuged for 20 min at 4000 x g (Sorval RC5B+ with SS-34 rotor), the supernatant was removed and the pellet frozen to -80 °C prior to lysis (Method 2.5).

2.4.2: Protein solubility

To determine the solubility of expressed recombinant protein, samples of whole cells were solubilized with BugBuster (5 ml/g of cells) and incubated at room temperature for 20 min with gentle shaking. Lysed cells were centrifuged at 12000 x g (Eppendorf 5453) for 20 min at 4 °C, the supernatant was removed and stored in a sterile 1.5 ml centrifuge tube (soluble fraction), the cell debris was resuspended in SDS-sample loading buffer (insoluble fraction). Samples of each soluble and insoluble fraction were applied alongside each other during separation by SDS-PAGE and the relative concentration of the protein in each band determined.

2.4.3: Sodium dodecyl sulphate - polyacrylamide gel electrophoresis (SDS-PAGE)

Pelleted whole cells were re-suspended in 100 µl of 1x SDS sample loading buffer whilst solutions containing protein required the addition of one volume of 2x SDS sample loading buffer (1x sample loading buffer: 50 mM Tris-HCl pH 6.8, 2% SDS, 10% glycerol, 1% β-mercaptoethanol or dithiothreitol, 12.5 mM EDTA and 0.02% bromophenol blue) and denatured by heating at 100 °C for 10 min. To disrupt cell membranes to isolate integral membrane proteins an addition of 8 M urea was made to 1x SDS sample-loading buffer (urea sample loading buffer), whole cell samples were resuspended in urea sample loading buffer and incubated at 37 °C for 1 h.

A 10 µl volume of denatured protein sample was loaded per well of a polymerized polyacrylamide gel (12 or 16% acrylamide concentration) which was subjected to electrophoresis for approx. 1 h with a constant 30 mA per gel in SDS-PAGE running buffer (25 mM Tris base, 192 mM glycine and 0.1% (w/v) SDS, pH 8.3) or until the loading dye had migrated to the bottom of the gel. For visualisation of total protein Coomassie blue stain (1.2 mM Coomassie Brilliant Blue R-250, 50% (v/v) methanol, 10% (v/v) glacial acetic acid) was applied for 2 h, the stain was removed and the gel washed with cold water to remove excess stain. The gel was then submerged in de-stain (10% (v/v) acetic acid, 30% (v/v) methanol) initially for 30 min and then for an additional 2 h minimum, until the gel had little or no blue background staining. Upon complete de-staining, the gel was equilibrated in water, and visualised with the G-Box (Syngene).

2.4.4: Molecular weight markers - Protein marker

PageRuler plus prestained protein ladder and BioRad precision plus kaleidoscope marker (Appendix 9.1) were used to estimate the size and quantity of protein following gel electrophoresis.

2.4.5: Western Blotting

Samples for Western blotting follow Method 2.25 but are not stained with Coomassie blue, after gel electrophoresis the gel with separated protein was removed from the glass plates, equilibrated in 1x Tris-glycine transfer buffer (Novex – Invitrogen) for 15 min and transferred to a polyvinylidene fluoride (PVDF) membrane. The PVDF membrane was prepared by soaking in methanol for 10 s, followed by distilled water for 2 min and 15 min in 1x Tris-glycine transfer buffer. A Bio-Rad Trans Blot SD semi-dry transfer cell was used to transfer protein from the SDS-PAGE gel to the PVDF membrane. A transfer buffer soaked sheet of filter paper was applied to the anode of the transfer cell, ensuring that all air bubbles were removed, followed by the prepared PVDF membrane, the equilibrated SDS-PAGE gel and a final sheet of transfer buffer soaked filter paper. The cathode was attached and proteins transferred for 1-2 h with a continuous 400 mA.

Following transfer, the PVDF membrane and the SDS-PAGE gel were removed from the transfer apparatus. The PVDF membrane was stained with Ponceau S (0.1% (w/v) Ponceau S in 1% (v/v) acetic acid) to ensure that proteins had been transferred to the membrane. Ponceau S was applied directly to the membrane and shaken for 5 min; excess stain was removed by washing with 5% acetic acid or water. The stain is reversible and blocking of the membrane commenced after visualisation of bound proteins to the membrane. In addition, the post-transfer polyacrylmide gel was stained with Coomassie blue to determine the efficiency of the transfer.

The PVDF membrane was blocked with 5% dried skimmed milk powder in Tris-buffered saline (TBS: 50 mM Tris-Cl pH 7.5 and 150 mM NaCl) for 1 h at room temperature with shaking or over-night at 4 °C. Blocking reagent was removed through washing three times for 5 min each with 0.01% skimmed milk powder and 0.05% Tween 20 in TBS. After washing, primary polyclonal antibody was applied at 1:1000 dilution to the membrane and shaken at room temperature for 1 h. The wash step was repeated and secondary antibody (anti-rabbit horse-radish peroxidase) was applied for 45 min with shaking. The wash step was repeated and 10 ml of DAB (50 μM 3,3′-diaminobenzidine tetrahydrochloride in H_2O) with metal enhancer is applied to the membrane and left to develop for 5-10 min. Following development, the membrane was washed with PBS and dried at 50 °C.

2.4.6: Cell lysis by sonication

Frozen, pelleted cells harvested from a large scale overexpression (Method 2.15) were defrosted overnight at 4 °C and re-suspended in 14 ml buffer A1 (50 mM Tris, 15 mM mannitol and 15 mM imidazole, pH 8.0). Cell lysis was initiated by addition of 1 mg/ml lysozyme which was incubated at 22 °C for 1 h. The cells were cooled on ice for 30 min before sonication at 60% amplitude with a 6 mm diameter tip for 15 min (Sonics Libra Cell). The resulting cell lysate was centrifuged three times at 3250 x g (Eppendorf 5810R with A-4-81 rotor) for 20 min at 4 °C and the supernatant filtered through a 0.45 μm sterile filter.

2.4.7: Chromatography

Nickel affinity chromatography

Prior to separation of recombinant protein the nickel-affinity chromatography column was washed with two column volumes (CV) of degassed 30% ethanol, all solutions to be applied to all chromatography columns are degassed via exposure to a negative pressure achieved through vacuum pressure. The column was stripped of bound nickel via washing with 2 CV of 0.5 M EDTA (pH 8.0) followed by a 2 CV wash with ultrapure H_2O. The stripped column was re-charged with nickel via washing with 2 CV 0.5 M $NiSO_4$ followed by a 2 CV wash with H_2O to remove unbound nickel. The column was then equilibrated by washing first with 1 CV of buffer B1 (buffer A1 with 1 M imidazole) then 3 CV of buffer A1. Filtered cell lysate (Method 2.5) in buffer A1 was then loaded onto the buffer-A1-equilibrated nickel-affinity column. Excess un-bound protein was removed from the column by washing with 2 CV of buffer A1, and the flow-through was collected for subsequent SDS-PAGE analysis. All subsequent eluant was collected into plastic test tubes containing 7 ml fractions, and the UV absorbance at 280 nm was measured throughout. A further 2 CV of buffer A1 was used to wash residual unbound protein from the column; the UV reading of the eluent was to 0 and a linear gradient of 0-100% of buffer B1 was applied over 8 CVs. To ensure all protein was eluted, a further 2 CV of buffer B1 was applied followed by 2 CV of buffer A1 and 2 CV of 30% ethanol to preserve the column. A 10 μl volume of all collected fractions displaying elevated UV absorbance (suggesting presence of purified recombinant protein) were analysed by SDS-PAGE through solubilisation with 2x SDS-PAGE loading buffer.

Diethylaminoethanol (DEAE) anion-exchange chromatography

DEAE anion exchange chromatography was used as a secondary purification technique, further purifying recombinant protein from nickel-affinity chromatography. Prior to loading the semi-purified recombinant protein from the nickel-affinity chromatography column, fractions with a high concentration of protein (as determined by SDS-PAGE) were pooled together. The anion-exchange column was washed with 2 CV of degassed H_2O to removed preservative ethanol, the column was then equilibrated with 4 CV of buffer B2 (50 mM Tris, 1 mM dithiothreitol and 1 M NaCl) followed by 8 CV of buffer A2 (50 mM Tris and 1 mM dithiothreitol). Semi-purified pooled protein fractions were loaded onto the column and excess un-bound protein was removed via washing with 2 CV buffer A2, and the flow through was collected. All subsequent eluant was collected into 7 ml fractions; a further 4 CV of buffer A1 was run through the column, the A_{280nm} of the eluent from the column was set to 0 and a linear gradient of 0-100% of buffer B2 was applied over 4 CVs. To ensure all protein was eluted, a further 2 CV of buffer B2 was applied followed by 2 CV of buffer A2 and 2 CV of 30% ethanol to preserve the column. A 10 µl aliquot of all collected fractions displaying elevated UV absorbance suggesting presence of purified recombinant protein was analysed by SDS-PAGE through solubilisation with 2x SDS-PAGE loading buffer.

2.4.8: Dialysis

To exchange the buffer for the pooled fractions after purification (Method 2.9), dialysis using 33 mm diameter cellulose membrane dialysis tubing (Sigma Aldrich) was performed. The solution to be dialysed was enclosed within the dialysis tubing, the sealed tube was placed into the required, pre-chilled, buffer and allowed to exchange by diffusion for 6 h with continuous stirring. Typically, the volume of solution required to ensure complete exchange of solute was 1:1000. The buffer was exchanged three times during the procedure (18 h total dialysis time), after the third change, the protein containing solution was removed from the dialysis tubing and stored at -20/80 °C.

2.4.9: Estimation of protein concentration

UV absorbance

The concentration of recombinant protein was determined using the Nanodrop ND-1000 spectrophotometer. A 2 µl sample of protein was placed onto the spectrophotometer's pedestal and the absorbance of the sample at 280 nm was determined, with a read out of protein concentration in mg/ml was reported. Considerations to the purity of the protein was undertaken though the ratio of 260/280 nm absorbance.

Bradford Assay

A standard curve of known concentrations of bovine serum albumin (BSA) was prepared in PBS, 10 µl of standard and 10 µl of un-diluted, 5x and 10x diluted protein were aliquoted into a 96 well plate. A 200 µl volume of 1:4 diluted Bradford reagent (Bio-Rad) was added to each well and left to enable colour development for 5 min. The absorbance of each well was measured at 595 nm using the Molecular Devices Spectramax 190 spectrophotometer. The concentration of the unknown protein was then be calculated from the standard curve.

2.4.10: Centrifugal concentration

The eluent containing purified recombinant protein from liquid chromatography (Method 2.9) was concentrated using a Vivaspin 20 (30,000 MWCO) (Satorius Stedim Biotech) centrifugal concentrator. Chromatography eluent was loaded into the top of the concentrator and centrifuged at 3250 x g for 20 min at 4 °C (Eppendorf 5804R with A-4-44 rotor), the flow through from the column was kept and analysed by SDS-PAGE to ensure the absence of the recombinant protein. Eluent can be continually applied to the top of the concentrator until the required concentration of protein is achieved.

2.4.11: Reconstitution of recombinant protein with iron

To remove bound metal from the as-isolated erythrin domain to create apo-erythrin, 1 ml aliquots of 2 mg/ml protein solutions were incubated on ice for 1 h with addition of 1 µM diethylenetriaminepentaacetic acid (DTPA), 1 µM 2,2'-dipyridyl and 2 µM sodium dithionite. Metal chelates were subsequently removed through thorough dialysis against 20 mM (4-(2-hydroxyethyl)-1-piperazineethanesulfonic acid) (HEPES) pH 7.0, generating apo-erythrin. Adventitiously bound iron was removed by dialysis of the protein-metal complex through thorough dialysis against 20 mM HEPES pH 7.0.

Typically the UV-visible spectrum of 500 µl of 10 µM apo-protein, anaerobically prepared (N_2 purged) 20 mM HEPES pH 7.0, was measured pre and post addition of anaerobically prepared 20 µM ferrous ammonium sulphate, to ensure reconstitution with iron.

2.4.12: Thermal shift assay method:

A 1 mg/ml solution of apo-erythrin was prepared in 20 mM HEPES pH 7.0, to which, SYPRO orange was diluted to a final x2 concentration. A 10 µl volume of the desired screening reagent (for screening assay 1 and 2 profiles see appendix 9.5) was added to each well of a 96-well PCR plate before 10 µl of the SYPRO orange-erythrin solution. The fluorescence emission signal data (567–596 nm) was collected with an Applied Biosystems 7500 FAST RealTime PCR System (excitation range: 510–530 nm), whilst the temperature was increased from 24 to 94 °C at a rate of 1°C/min. The temperature of hydrophobic exposure at which half of the protein population was unfolded, T_h, was determined with NAMI algorithm (Groftehauge et al. 2015).

2.5: Assays

2.5.1: ^{55}Fe Transport Assay:

A transformant *E. coli* MG1655 colony was grown overnight in 5 ml LB, from which 1 ml was used to inoculate 25 ml of fresh LB with addition of 10 µl $^{55}Fe^{3+}$ (0.185 mBq). Cells were allowed to grow until mid-log phase (2 h), at which time cells were induced with 0.1 mM rhamnose and incubated for a further 1 h. Induced cells were harvested by centrifugation (5000 x g 4 °C 10 min) and the supernatant discarded, the cells were washed three times with 10 ml cold transport buffer (TB: 50 mM MES, 50 mM TAPS pH 7.0, 0.4% glucose, 0.2 mM $CaCl_2$, 2 mM $MgCl_2$). The cell pellet was re-suspended in 1.5 ml ice cold TB and 300 µl aliquots created. One aliquot at a time was diluted in to 3 ml pre-warmed (37 ^oC) TB in the reaction cell, maintained with continual stirring. A 250 µl aliquot of cells was removed from the reaction cell for every time point taken and filtered through a 0.22 µm syringe driven filter, followed by washing with 2.5 ml cold wash buffer (WB: 10 mM EDTA, pH 8.0). then, 2 ml of filtrate were added to 4 ml Ultima Gold XR scintillant (Perkin Elmer) and inverted until mixed. All samples were left for 24 h to allow for a reduction in background chemi-luminescence, before liquid

scintillation counting (0.2 – 6.2 KeV) with the Beckman LS-6500 multi-purpose scintillation counter for 3 min per sample. Results were standardised per mg of protein determined via a Bradford assay. Additions of hydrogen peroxide, catalase (*Micrococcus lysodeikticus*) and CCCP (3.3 mM stock; DMSO) were made immediately prior to addition of cells to the reaction chamber.

2.5.1.1: Principles for using radio-labelled iron for iron export experimentation

Iron-55 (^{55}Fe) is a synthetic radioactive isotope of iron and has a half-life of 2.7 years. The nucleus of ^{55}Fe contains 26 protons and 29 neutrons (compared to the stable ^{56}Fe atom which contains 26 protons and 30 neutrons) and decays by electron capture to stable manganese-55 (25 protons and 30 neutrons). Decay via electron capture (k-electron capture) is a process by which a proton rich nucleus of an electrically neutral atom absorbs an electron from the k electron shell. This process changes the nuclear proton to a neutron as well as emitting an electron neutrino (v_e).

$$p + e^- = n + v_e$$

$$^{26}_{29}Fe + e^- \rightarrow {}^{25}_{30}Mn + v_e$$

If the daughter nuclide is in an excited state, it transitions to its ground state, usually through emission of a gamma ray. After capture of an inner electron into the nucleus, an outer electron replaces it and one or more X-ray photons are emitted in the process. Alternatively, electron capture can result in the Auger effect; the energy released when the outer electron replaces the inner electron is transferred to another outer electron, resulting in this electron's ejection from the atom, leaving a positive ion.

The decay energy of the transition of ^{55}Fe to ^{55}Mn is 2.31 keV (kilo-electronvolts); generated by both X-rays and Auger electrons, and is detected by liquid scintillation counting (LSC). The collected samples containing the radioactive isotope are suspended in a scintillation 'cocktail' (Ultima Gold XR – Perkin Elmer) containing a solvent, surfactant and scintillator, within a translucent plastic scintillation vial. Emitted energy during the radioactive decay is transferred to the aromatic ring of the solvent; the energized solvent molecules transfer the captured energy to other solvent molecules, until the energy is transferred to the primary scintillator. The primary scintillator emits photons, following the absorption of the transferred energy, which are detected by two

photo-multiplier tubes allowing the measurement of the radioactive decay in counts per minute (CPM/DPM). Analysis of a sample of ^{55}Fe via liquid scintillation counting shows the decay energy of 2.31 KeV (Figure 2.1), this allows adjustment of the Beckman LS-6500 multi-purpose scintillation counter to observe photon emissions within defined channels (Figure 2.2). To facilitate conversion of DPM into pmol ^{55}Fe first a conversion to Becquerels (Bq) is performed (1 Bq = 60 DPM), followed by multiplication by the specific activity of the ^{55}Fe source (1.8703). Additionally, through the analysis of known quantities of ^{55}ferric citrate and discrepancies in the determined DPM, a quench factor of 1.58 was included (Figure 2.3).

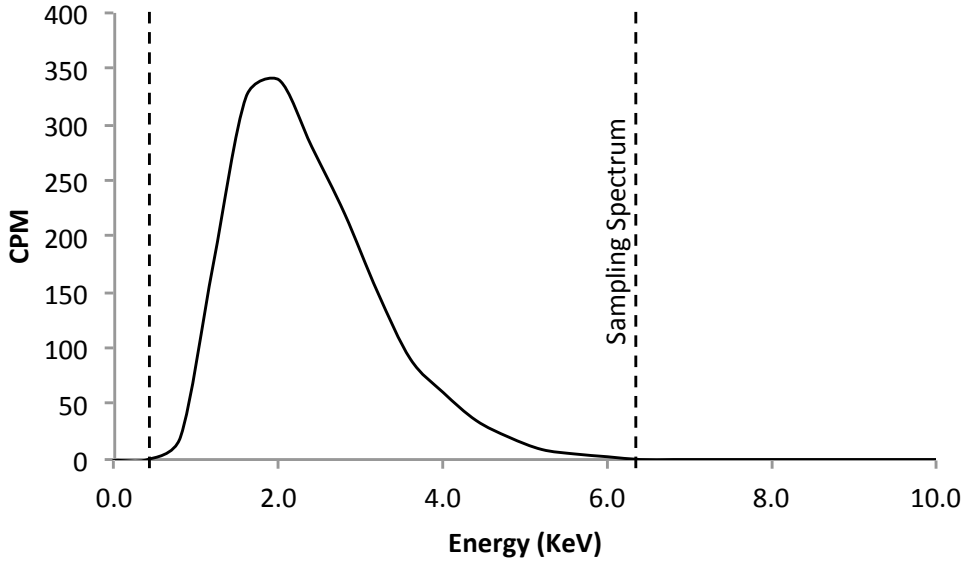

Figure 2.1: Energy emission of ^{55}Fe decay.

Measurement of ^{55}Fe energy emission via liquid scintillation counting as determined by counts per minute (CPM). Horizontal dashed lines represent the predefined high and low limits of detection. Beckman LS-6500 multi-purpose scintillation counter.

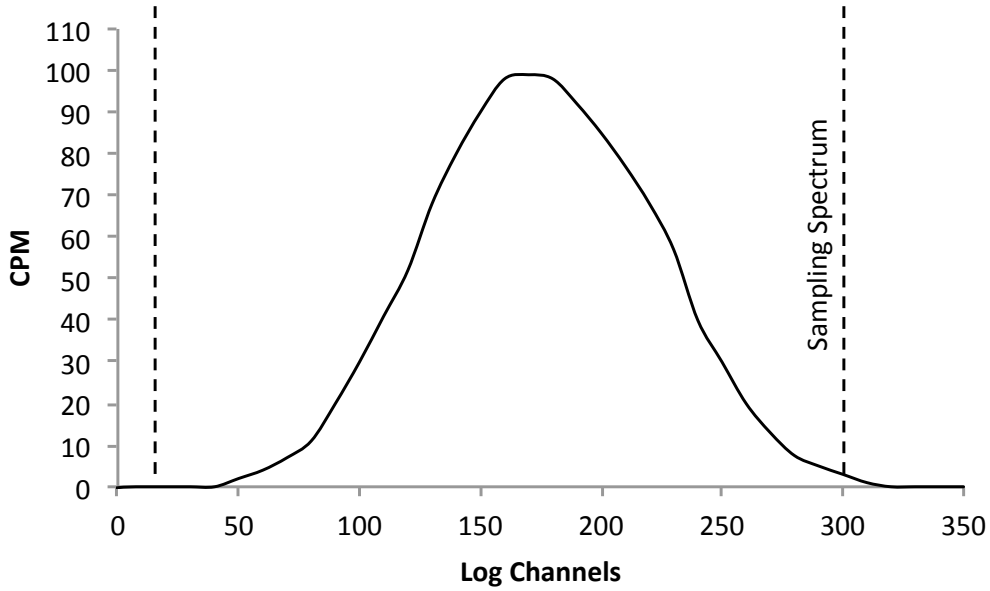

Figure 2.2: Channel range of energy emission from ^{55}Fe decay.

Measurement of ^{55}Fe energy emission via liquid scintillation counting as determined by counts per minute (CPM). Horizontal dashed lines represent the predefined high and low limits of detection. Beckman LS-6500 multi-purpose scintillation counter.

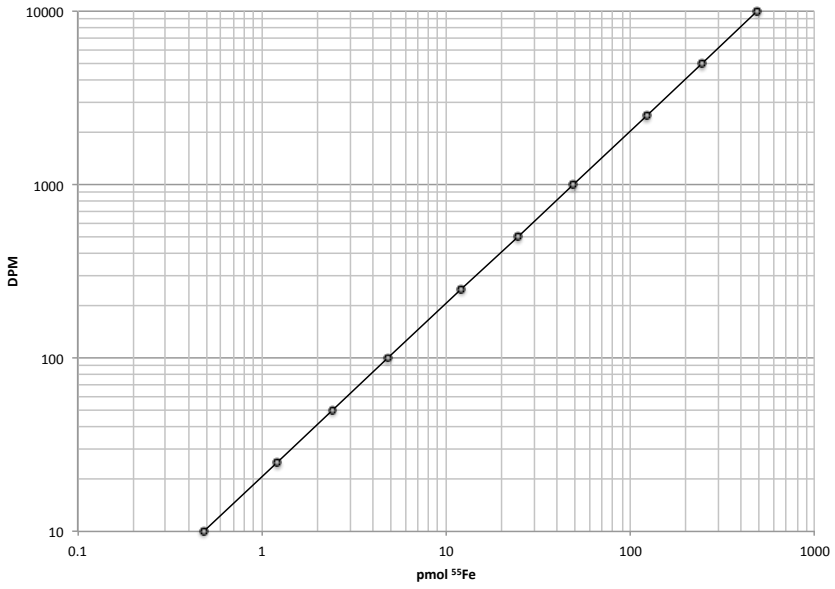

Figure 2.3: Calibration curve of ^{55}Fe disintergrations per minute (DPM) to pmol ^{55}Fe.

2.5.2: Ferrozine assay

A culture of 1 L was propagated and induced as for ^{55}Fe transport assay, then cells were washed and re-suspended to a final 30 ml volume in TB. 10 ml of washed cells were diluted into 60 ml warm TB and 10 ml samples taken per time point. Cellular supernatants were collected by centrifugation before 0.22 μm syringe driven filtration to remove residual cells. Ferric iron concentration was determined with addition of a 1:1 (v/v) ratio of supernatant to 1% ferrozine solution followed by measurement of absorbance at 562 nm. Detection of ferrous iron included addition of 10% acetic acid and 750 mM sodium sulphite to the ferrozine solution to promote reduction to ferrous iron. For determination of whole cell iron concentrations, the ferrous iron protocol was used, preparations were heated to 90 °C for 1 h to allow lysis of cells.

2.5.3: Hydrogen peroxide assay

Measurements of hydrogen peroxide concentrations were made with Amplex Red (Thermo). Transformant *E. coli* MG1655 was inoculated into 5 ml LB (starting OD: 0.05), induced for 1 h at OD_{600nm} 0.5 with 100 μM rhamnose, washed once with 10 ml cold WB, then twice with TB followed by dilution to 1 OD unit ml^{-1}. For each measurement of H_2O_2 concentration, 100 μl of cell-free solution were added to 100 μl Amplex Red reagent and absorbance at 560 nm determined, then compared to a standard curve generated with known concentrations of H_2O_2. For each assay, a measurement prior to addition (Pre) of 15 μM H_2O_2 (T_0) was made to ensure endogenous H_2O_2 concentrations were minimal, then every 2 min after H_2O_2 addition during the assay. When used, desferrioxamine was added prior to addition of cells or iron. The pH of TB was adjusted as required.

2.5.4: Streptonigrin assay

Transformant *E. coli* strains were inoculated into 200 μl LB (starting at OD 0.05) containing up to 4 μg/ml streptonigrin (1 mg/ml stock in DMSO) and 75 μM diethylamine NONOate (nitric oxide liberator; PBS pH 7.4). Bacterial growth was monitored every 30 min by Labsystems Bioscreen C incubated spectrophotometer.

2.5.5: Macrophage survival assay

Macrophages were seeded at a concentration of $1x10^5$ in 24 well plates in Dulbecco's modified Eagle's medium with 5% fetal bovine serum and 2 mM L-glutamate and incubated at 37 °C with 5% CO_2. After 24 h, macrophages were infected with *Brucella* at a multiplicity of infection (MOI) of 100:1 and incubated at 37 °C for 1.5 h to allow phagocytosis. Extracellular bacteria were killed by treatment with gentamicin (50 μg/ml) for 1 h and maintained in Leibovitz's L-15 medium with gentamicin (2 μg/ml) thereafter. At 0, 4, 24 and 48 h after infection, macrophages were washed with PBS and lysed with 0.1% (v:v) Triton X-100 in H_2O. The number of intracellular bacteria was determined by serial dilutions of macrophage lysates and plated on Brucella agar.

2.5.6: Cellular fractionation

A single isolated *E. coli* colony transformed with a controllable expression plasmid (pSU or pBAD) capable of expressing an a *mbfA* isoform was inoculated into 5 ml LB containing appropriate antibiotic and incubated over-night at 37 °C with 250 rpm shaking. The over-night culture was diluted 1:10 into fresh LB with appropriate antibiotic; the OD_{600nm} was measured until a value of 0.5 was achieved, upon which, the culture was induced (0.5 mM IPTG or 0.1 mM rhamnose). The cells were harvested by centrifugation at 4000 x g (Sorval RC5B+ with SS-34 rotor) at 4 °C for 10 min after 2 h a growth post-induction and the supernatant removed. One OD unit of cells was taken and kept as whole cells. The periplasm was extracted via osmotic shock through resuspending the remaining cells in 20% w/v sucrose, 30 mM Tris (pH 8.0) and 1 mM EDTA and incubated on ice for 30 min, after which the cells were pelleted via centrifugation at 3250 x g for 20 min (Eppendorf 5810R with A-4-81 rotor). The supernatant was kept as the sucrose fraction and the pellet resuspended in 10 mM $MgCl_2$ and incubated on ice for 30 min. The cells were pelleted via centrifugation at 3250 x g for 20 min (Eppendorf 5810R with A-4-81 rotor) and the resulting supernatant kept as the $MgCl_2$ fraction. The resulting pellet was resuspended in PBS and the spheroblasts were lysed by sonication using a 6mm diameter tip at 60% amplitude for 15mins (Method 2.5). Unlysed cells were removed through multiple centrifugations at 4500 x g at 4°C for 10 mins (Sorval RC5B+ with SS-34 rotor), the resulting supernatant was kept as spheroplasts lysate. The lysed spheroplasts were subjected to ultracentrifugation at 130,000 x g at 4 °C for 1 h (Beckman Coulter L-90K with SW40 Ti rotor and 14x89 ml centrifuge tubes) to separate the cytoplasm (supernatant) from the cellular membranes (pellet). The pelleted membranes were resuspended in PBS, 3

mM EDTA and 0.5% sarcosyl and incubated at room temperature for 30 min. The total membrane fraction was centrifuged again at 130,000 x g at 4 °C for 1 h to separate the outer-membrane (supernatant) from the inner membranes (pellet), the pellet was resuspended in 50 mM Tris (pH 8.0) with 10 mM EDTA. The resulting membrane fractions were analysed by SDS-PAGE and Western blotting.

2.6: Removal of Biological Materials from Containment Level 3 Facilities

2.6.1: Removal of PCR amplified DNA

To conduct agarose gel electrophoresis on PCR amplified DNA at containment level 2 from DNA samples originating at containment level 3 the following protocol was followed (DSTL-DOC-30515: The Growth, Manipulation and Inactivation of *Brucella* spp.) to ensure the complete inactivation of *Brucella* cells.

A single *Brucella melitensis* colony was resuspended in 100 µl of H_2O and heated to 96 °C for 10 min (demonstrated previously to inactivate 100% of *Brucella melitensis* cells - February 2010 lab book 33/2009). The PCR reaction was prepared with 2 µl of the *Brucella* boilate within a class III safety cabinet which was wiped out of the cabinet using a 10% Chloros soaked cloth before being subjected to the required PCR cycling conditions outside of primary containment. For PCR reactions using genomic DNA an extended 10 min initial denaturation step at 96° C must be included and witnessed by an independent observer, to further ensure sterility of the PCR sample. Upon completion of the thermocycling, the PCR vessels were wiped again with a 10% chloros soaked cloth, removed from the containment suite and analysed immediately at containment level 2 within a class II safety cabinet.

NOTE: 96 °C for 10 min heat inactivation of *Brucella suis* strains had not been previously demonstrated, thus prevented the removal of *B. suis* PCR samples from the containment level 3 facility.

2.6.2: Removal of heat inactivated cells

To remove heat inactivated *Brucella* samples for downstream processes such as SDS-PAGE and Western blotting the heat inactivation and sterility / inactivation checks were conducted as described in DSTL-DOC-30515: The Growth, Manipulation and Inactivation of *Brucella* spp.

A 5 ml *Brucella* sample in a 30 ml container was placed in a 60 °C water bath within a class III microbiological safety cabinet for at least 2 hours to ensure complete inactivation. On completion, the water will be allowed to cool, decanted into a Duran bottle and added to Chloros to give a final concentration of 10% v/v.

To determine sterility of the inactivated material 10% of the inactivated bacterial suspension was inoculated into Brucella broth, the broth volume being in excess, at least 10x that of the inoculum, and incubated for a minimum of seven days at 37 ºC. 10% of the broth was plated out onto Brucella agar (250 µl per plate) and the plates incubated for a further seven days at 37 ºC in sealed containers. Preparations cleared by this method were released upon completion of a 'production and issue of biological materials' form and used at containment level 2. Every sterility check included a positive control to show that the media supports growth of *Brucella* spp.

Table 2.2: Bacterial Strains.

***E. coli* Strains**	**Genotype**	**Reference/Source**
MG1655	F⁻ wild-type	Lab Stock
LC106	MG1655: Δ*ahpCF' kan*::*'ahpF* Δ(*katG17*::Tn*10*)1 Δ(*katE12*::Tn*10*)1	L.Seaver (2004)
W3110	F⁻ λ⁻ *IN(rrnD-rrnE)1 rph-1*	Lab Stock
JC28	W3110 Δ*fecABCDE* Δ*zupT* Δ*mntH* Δ*entC* Δ*feoABC*	J. Cao (2007)
MC4100	F-, *(araD139)$_{B/r}$, Δ(argF-lac)169, λ⁻, e14-, flhD5301, Δ(fruK-yeiR)725(fruA25), relA1, rpsL150(strR), rbsR22, Δ(fimB-fimE)632(::IS1), deoC1*	Lab Stock
H1941	MC4100 Δ*fur*	K. Hantke (2001)
BW25113	*lacI rrnB* Δ*lacZ hsdK* Δ*araBAD* Δ*rhaBAD*	Datsenko and Wanner (2000)
AS01	BW25113 Δ*bfr*	A. Salman (2016)
AS02	BW25113 Δ*dps*	A. Salman (2016)
AS03	BW25113 Δ*ftnA*	A. Salman (2016)
AS04	BW25113 Δ*dps* Δ*ftnA*	A. Salman (2016)
AS05	BW25113 Δ*bfr* Δ*ftnA*	A. Salman (2016)
AS06	BW25113 Δdps Δbfr	A. Salman (2016)
AS07	BW25113 Δ*dps* Δ*bfr* Δ*ftnA*	A. Salman (2016)
	BW25113 Δ*bfd*	Lab stock
	BW25113 Δ*bfr* Δ*bfd*	Lab stock
EM1055	MG1655Δ(*lacI-ZYA*)X74	E. Masse (2002)
EM1256	MG1655 - Δ*fur::kan*	E. Masse (2002)
EM1238	MG1655 - Δ*ryhB::cat*	E. Masse (2002)
EM1257	MG1655 - Δ*fur::kan* Δ*ryhB::cat*	E. Masse (2002)
BL21(DE3)	F⁻ *omp*T *hsd*S_B(r_B^-, m_B^-) *gal dcm*(λDE3)	Invitrogen
BL21(DE3) Star	F⁻ *omp*T *hsd*S_B(r_B^-, m_B^-) *gal dcm rne131* (λDE3)	Invitrogen
BL21(DE3) Rosetta	F⁻ *ompT hsd*S_B(r_B^-, m_B^-) *gal dcm* (λDE3) pRARE2 (Cam^R)	Novagen

***Brucella* Strains**	**Genotype**	**Reference/Source**
B. suis 1330	WT	Laboratory Stock
B. suis Δ*mbfA*	*B. suis* 1330 Δ*mbfA*	This study
B. suis p*mbfA*	*B. suis* Δ*mbfA* carrying pBBR4$mbfA_{suis}$	This study
B. suis p$mbfA_{mel}$	*B. suis* Δ*mbfA* carrying pBBR4$mbfA_{melitensis}$	This study
B. melitensis 16M	WT	Laboratory Stock
B. melitensis Δ*mbfA*	*B. melitensis 16M* Δ*mbfA*	This study
B. melitensis p*mbfA*	*B. melitensis* Δ*mbfA* carrying pBBR4$mbfA_{suis}$	This study
B. melitensis p$mbfA_{mel}$	*B. melitensis* Δ*mbfA* carrying pBBR4$mbfA_{melitensis}$	This study

***Burkholderia* Strains**	**Genotype**	**Reference/Source**
B. multivorans ATCC 17616	WT	Laboratory Stock
B. multivorans Δ*mbfA*	*B. multivorans* Δ*mbfA*	F. Izza (2015)
B. multivorans p*mbfA*	*B. multivorans* Δ*mbfA* carrying pBBR4*mbfA*	F. Izza (2015)

Table 2.3: Plasmids.

Plasmid name	Genotype	Antibiotic resistance	Source
pJET1.2blunt	Cloning vector from which DNA fragments are inserted into Eco32I site within the *eco47IR* gene	Amp	Fermentas
pJET*mbfA271*	*B. melitensis* 16M *mbfA* with 0.5kb 5'/3' flanking sequence	Amp	This work
pJET*mbfA306*	*B. melitensis* 16M *mbfA* with 0.5kb 5'/3' flanking sequence. SDM - c64a to create MbfA306	Amp	This work
pJET*mbfA327*	*B. melitensis* 16M *mbfA* with 0.5kb 5'/3' flanking sequence. SDM - t55c to create wild-type *Brucella* MbfA*327*	Amp	This work
pJET*mbfA*	*B. melitensis* 16M *mbfA* with 1kb 5'/3' flanking sequence	Amp	This work
pJETΔ*mbfA*::kn	*B. melitensis* 16M *mbfA* with 1kb 5'/3' flanking sequence. *mbfA* coding sequence removed, Kn cassette insertion.	Amp/Kn	This work
pCR2.1	Cloning vector	Amp	ThermoFisher
pCR16M	*B. melitensis* 16M *mbfA* with 0.5kb 5'/3' flanking sequence	Amp	This work
pCR16MΔ*mbfA*	*B. melitensis* 16M Δ*mbfA* with 0.5kb 5'/3' flanking sequence	Amp/Kn	This work
pCR1330	*B. suis* 1330 *mbfA* with 0.5kb 5'/3' flanking sequence	Amp	This work
pCR1330Δ*mbfA*	*B. suis* 1330 Δ*mbfA* with 0.5kb 5'/3' flanking sequence	Amp/Kn	This work
pEX100T	Suicide vector, *sacB* negative selection gene	Amp	Martin Roop
pEXΔ*mbfA*::kn	Δ*mbfA* with 1kb 5'/3' flanking sequence	Amp/Kn	This work
pBBR1-MSC4	Broad host range vector, MCS, *lac* promoter and *lacZa*	Amp	Michael Kovach
pBBR4*mbfA*271	*mbfA271* with 0.5kb 5'/3' flanking sequence	Amp	This work
pBBR4*mbfA*327	*mbfA327* with 0.5kb 5'/3' flanking sequence	Amp	This work
pSU18	High copy number vector, MCS, *lac* promoter and *lacZa*	Cm	Lab Stock
pSU*mbfA*271	*mbfA271* cloned into MCS site	Cm	This work
pSU*mbfA*306	*mbfA306* cloned into MCS site	Cm	This work
pSU*mbfA*327	*mbfA327* cloned into MCS site	Cm	This work
$pBAD_{rham}$	Low copy number vector, MCS, rhamnose promoter	Cm	Ford, Ireland 2014
pBAD*mbfA*271	*mbfA271* cloned into MCS	Cm	This work
pBAD*mbfA*306	*mbfA306* cloned into MCS	Cm	This work
pBAD*mbfA*327	*mbfA327* cloned into MCS	Cm	This work
pBAD*mbfA*327D191	*mbfA327* cloned into MCS - SDM D191G	Cm	This work
pBAD*mbfA*327M228	*mbfA327* cloned into MCS - SDM M228G	Cm	This work
pBAD*mbfA*327E232	*mbfA327* cloned into MCS - SDM E232G	Cm	This work
pBAD*mbfA*327Y268	*mbfA327* cloned into MCS - SDM Y268G	Cm	This work
pBADAT_VIT	Synthetic AT_VIT cloned into MCS	Cm	This work
pBADery	*mbfA* - erythrin domain cloned into MCS	Cm	This work
pBADVIT	*mbfA* - Vit domain cloned into MCS	Cm	This work
pBADHisA	Cloning vector, arabinose promoter	Amp	Invitrogen
pARA*mbfA*	*mbfA327* cloned into MCS	Amp	This work

Plasmid name	Genotype	Antibiotic resistance	Source
pET21a	T7 promoter and terminator, MCS, N terminal 6xHis	Amp	Novagen
pET*ery*271	*ery*271cloned into MCS site	Amp	This work
pET*ery*306	*ery*306 cloned into MCS site	Amp	This work
pET*ery*327	*ery*327 cloned into MCS site	Amp	This work
pETeryCO	*ery*CO cloned into MCS site of pET21a	Amp	This work
pHP45ΩKn	High copy number vector, x2 MCS	Amp/Kn	Fellay 1987
pMA-*mbfA*	Synthetic, codon optimised *mbfA*327	Amp	Invitrogen
pMA-AT_VIT	Synthetic, codon optimised *Arabidopsis thaliana* VIT1	Amp	Invitrogen

Table 2.4: PCR primers.

Name	Sequence 5'-3'	GC (%)	Length	T_m (^oC)
Knockout construction				
mbfA0.5kb F	ACACGAAGATGATGAAATCGTAA	35	23	51
mbfA0.5kb R	CGACAACGATCCCGTGCTGGCCT	65	23	68
mbfA1kb F	GTGCCGAACATCAGGAACAATGT	48	23	66
mbfA1kb R	ACCTATTTCGAGCATATGGCCTTTG	44	25	65
mbfAKn F	CACCGCGCAGCACTGCCGGAATTGCCAGCTGGG	70	33	68
mbfAKn R	CGCCGCCAGGACGAGTCAGAAGAACTCGTCAAGAA	57	35	58
ΔmbfA F	CTC GTC CTG GCG GCG GGC ATA	67	21	74
ΔmbfA R	CAG TGC TGC GCG GTG GTC GTG	71	21	75
Site directed mutagenesis				
t55c F	CTCTTTCGATTCGCTTTCTGAACAGGAAATTCTGGCGC	47	38	79
t55c R	GCGCCAGAATTTCCTGTTCAGAAAGCGAATCGAAAGAG	47	38	79
c64a F	CGATTCGCTTTCTGAATAGGAAATTATGGCGCTTGCCAT	44	39	80
c64a R	ATGGCAAGCGCCATAATTTCCTATTCAGAAAGCGAATCG	44	39	80
D191G F	CTTGCGGGCCTGATGGGCGGCTCCGTCTCGAC	72	32	88
D191G R	GTCGAGACGGAGCCGCCCATCAGGCCCGCAAG	72	32	88
M228G F	GCCGGTATTTCGGGGGGCTTTACAGAAGC	59	29	81
M228G R	GCTTCTGTAAAGCCCCCCGAAATACCGGC	59	29	81
E232G F	CGATGGGCTTTACAGGAGCCGTGCATGACG	60	30	83
E232G R	CGTCATGCACGGCTCCTGTAAAGCCCATCG	60	30	83
Y268G F	GGTCACAGCCTGCCCGGTCTGATCAAGGATTTC	58	33	84
Y268G R	GAAATCCTTGATCAGACCGGGCAGGCTGTGACC	58	33	84
pSU18 cloning				
mbfA271 F	GACGAATTCAGGAGGATCTAGATGGCCGCAGAGGAA	53	36	61
mbfA306 F	GACGAATTCAGGAGGATCTAGATGGCGCTTGCCATA	50	36	58
mbfA327 F	GACGAATTCAGGAGGATCTAGATGTTCAGCCGATTC	47	36	52
mbfA R	GTCGGATCCTCAGGCGCTGCCGATCAA	63	27	68
$pBAD_{rham}$ cloning				
mbfA271 F2	GTGCATATGGCCGCAGAGGAACACG	60	25	61
mbfA306 F2	GTGCATATGGCGCTTGCCATATCCTC	54	26	60
mbfA327 F2	GTGCATATGTTCAGCCGATTCTTCC	48	25	55
$pBAD_{ara}$ cloning				
mbfA For	GGAATTAACCATGGGATGTTCAGCCGATTC	47	30	67
mbfA Rev	TGATGATGAGAACCCTCAGGCGCTGCCGATC	58	30	74
Vector For	GAATCGGCTGAACATCCCATGGTTAATTCC	47	30	67
Vector Rev	GATCGGCAGCGCCTGAGGGTTCTCATCATCA	58	30	74

Name	Sequence 5'-3'	GC (%)	Length	T_m (^oC)
pET cloning				
ery271 F	CACCATATGGCCGCAGAGGAA	57	21	61
ery306 F	CACCATATGGCGCTTGCCATATC	52	23	60
ery327 F	CACCATATGTTCAGCCGATTCTTC	46	24	57
ery R	GTGAAGCTTCTTGCGCTCGGC	62	21	57
eryCO F	CACCATATGTTTAGCCGCTTT	43	21	51
eryCO R	GTGAAGCTTTTTGCGTTCTGCTGCACG	52	27	65
Sequencing				
T7 F	TAATACGACTCACTATAGG	37	19	47
pJET R	AAGAACATCGATTTTCCATGGCAG	42	24	69
pBADrha F	GAAGGTCGCGAATTCAGG	56	18	56
pBAD R	GATTTAATCTGTATCAGG	33	18	45
colony PCR				
KnF	GATCGTTTCGCATGATTGAACAAG	42	24	60
KnR	CAAGAAGGCGATAGAAGGCG	55	20	60
mbfAOutF	GCGACGCCGAAGAAAATG	56	18	56
mbfAOutR	AGTATTTCCAATGACGACACGC	46	22	58

Chapter 3: Bioinformatics analysis of *mbfA* of *Brucella*

3.1: Analysis of the coding sequence of *mbfA* in *Brucella suis* bv. 1 str. 1330

Analysis of the *mbfA* gene (BS1330_I1673) and translated amino acid sequence from *Brucella suis* 1330 revealed information regarding the potential activity and mechanism of function of the MbfA protein (the nucleotide and amino acid sequences, and amino acid frequency are in Appendix 9.2 and iron related gene locations in Appendix 9.4).

The N-terminal erythrin domain of MbfA contains four iron-binding motifs, two ExxH and two E-6-Y motifs (Figure 3.1), which are predicted (on the basis of homology to rubrerythrin) to co-ordinate two iron atoms. These iron-binding motifs are well conserved within di-iron carboxylate proteins (Nordlund and Eklund 1995) (Figure 3.1). Substitution of the glutamic acid residues of the E-6-Y motifs to alanine in MbfA of *B. japonicum* (Sankari and O'Brian 2014) results in loss of ferrioxdase activity and failure to form a di-iron centre.

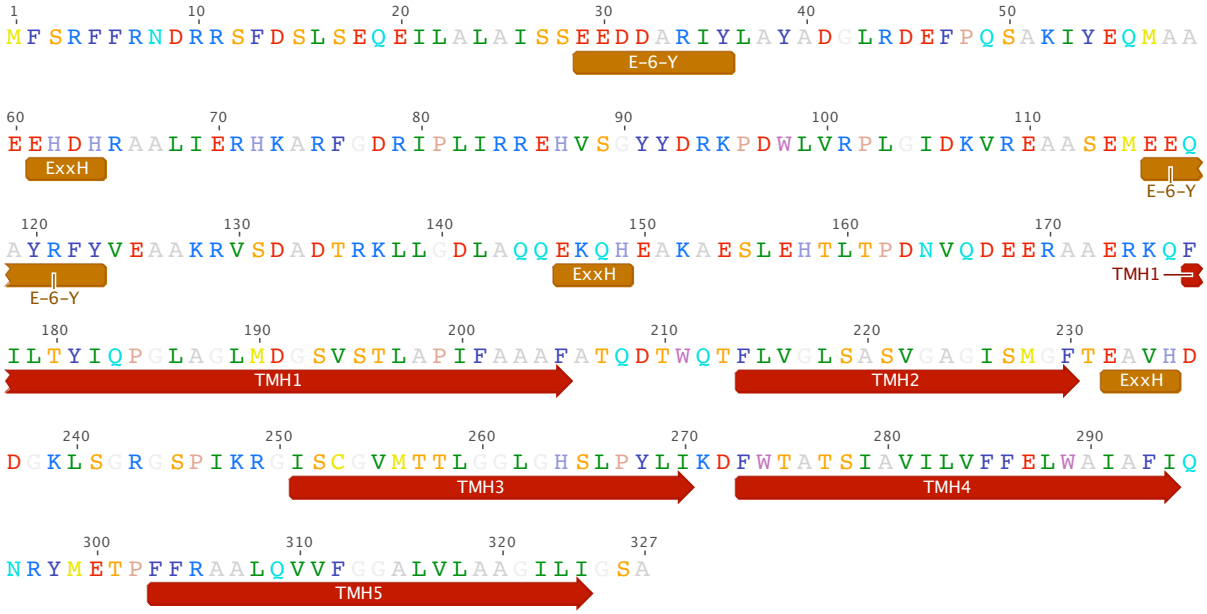

Figure 3.1: Amino acid sequence of *B. suis* MbfA.

Location of iron-binding motifs (orange) and predicted transmembrane helices (red) in *Brucella suis* MbfA. Annotation conducted in Geneious 7.0.6.

Figure 3.2: Di-iron carboxylate protein binding sites

Co-ordination of iron atoms by the two E-6-Y (green and yellow) and two ExxH (red and blue) iron-binding motifs in di-iron carboxylate proteins. The Tyr residues do not act as iron ligands but are highly conserved in the superfamily.

The N-terminal erythrin domain bares similarity to the rubrerythrin protein of anaerobic bacteria. Rubrerythrins consist of two domains, a diiron erythrin and a Cys_4-Fe rubredoxin domain, and act as peroxide reductases affording resistance against exposure to redox stress (Lumppio et al. 2001). Multiple sequence alignment of the conserved N-terminal erythrin domains displays the conservation of the iron binding motifs within the erythrin domain (Figure 3.3a). Differences in the respective C-terminal domain organizations are shown schematically in Figure 3.3b.

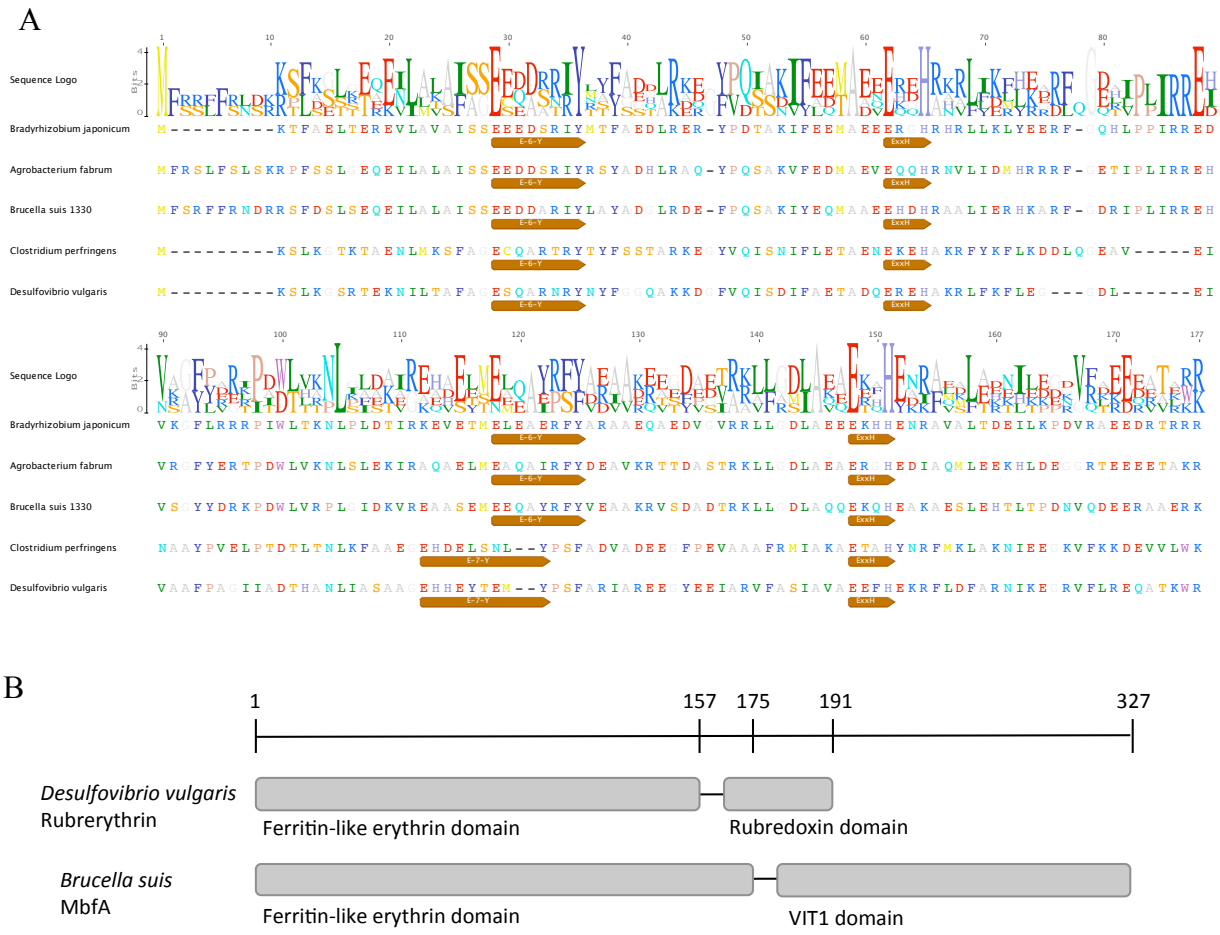

Figure 3.3: Alignment of the amino acid sequences of the erythrin domains of MbfA and rubrerythrin proteins from selected bacterial species

A: Multiple sequence alignment of *Brucella suis* 1330 MbfA and rubrerythrin from selected anaerobic bacteria (*Desulfovibrio vulgaris* and *Clostridium perfringens*) displaying conservation of E-6-Y (AA: 29-36 and 115-123) and ExxH (AA: 62-65 and 148-152) iron binding motifs. Alignment performed and displayed using MUSCLE option of Geneious 7.0.6. B: Schematic representation of domain organisation in *Desulfovibrio vulgaris* rubrerythrin and *Brucella suis* MbfA.

The C-terminal Vit1 domain of MbfA is predicted to be embedded in the inner membrane based upon sequence similarity to *Saccharomyces cerevisiae* CCC1 and *Arabidopsis thaliana* VIT1 (Figure 3.4), and membrane prediction tools (see below) (Figure 3.5). CCC1 and VIT1 facilitate the transport of cytosolic free iron into storage vacuoles and hence are located within the vacuolar membrane (Li et al. 2001, Kim et al. 2006). More recently, a VIT1 protein was identified in *Plasmodium* spp. as well as other *Apicomplexa* and *Kinetoplastida* parasites (*Toxoplasma gondii* and *Trypanosoma brucei* respectivly) (Slavic and Krishna 2016), and has been reported to be located in the vacuole for *P. falciparum*.

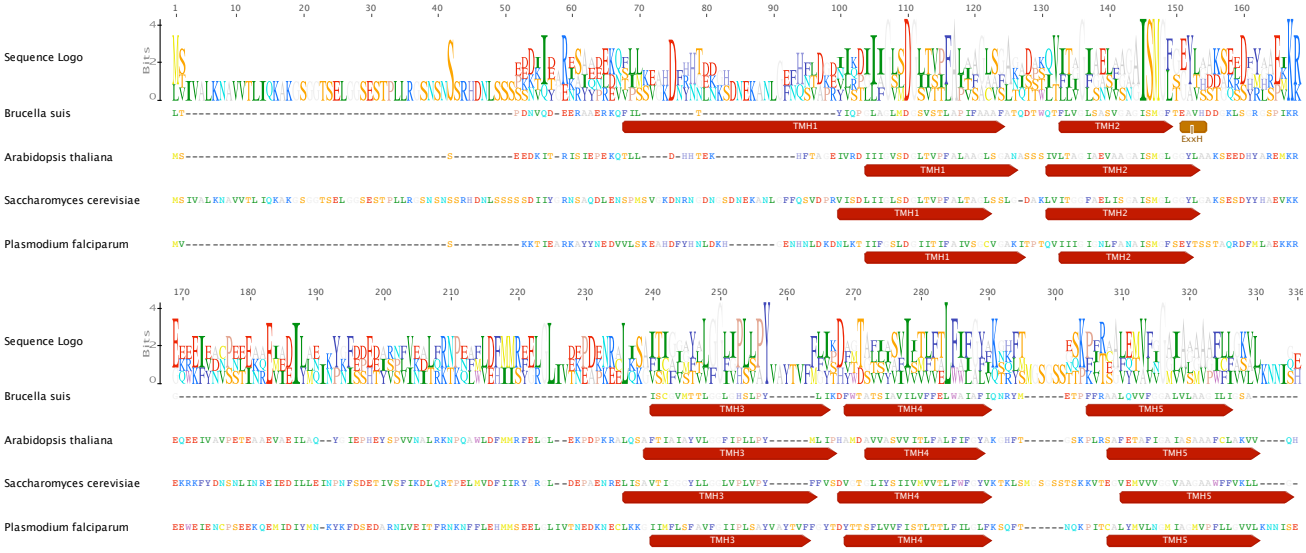

Figure 3.4: Alignment of *Brucella suis* MbfA Vit domain with eukaryotic VIT1 proteins

Multiple sequence alignment of *Brucella suis* MbfA Vit domain with VIT1/CCC1 proteins from *A. thaliana*, *S. cerevisiae* and *P. falciparum*, conserved five transmembrane helices are marked in red.

The localization of MbfA to the bacterial inner membrane is further evidenced by the examination of the membrane topology of MbfA in *Agrobacterium tumefaciens* (Bhubhanil et al. 2014). LacZ and PhoA fusions identified that amino acid 180, located after the erythrin domain but before the Vit1 domain, is located cytoplasmically, whereas the terminal amino acid 327 is located periplasmically. Analysis of the *B. suis* MbfA protein sequence with Phobius - a combined transmembrane topology and signal peptide predictor (Kall et al. 2004) predicts five transmembrane helices with the N-terminal erythrin domain locating within the bacterial cytosol (Figure 3.5). The average

length of the predicted transmembrane helices is 20 amino acid residues and periplasmic regions is 5 amino acids. Whilst the predicted cytoplasmic loops are variable form 20 to 11 amino acids.

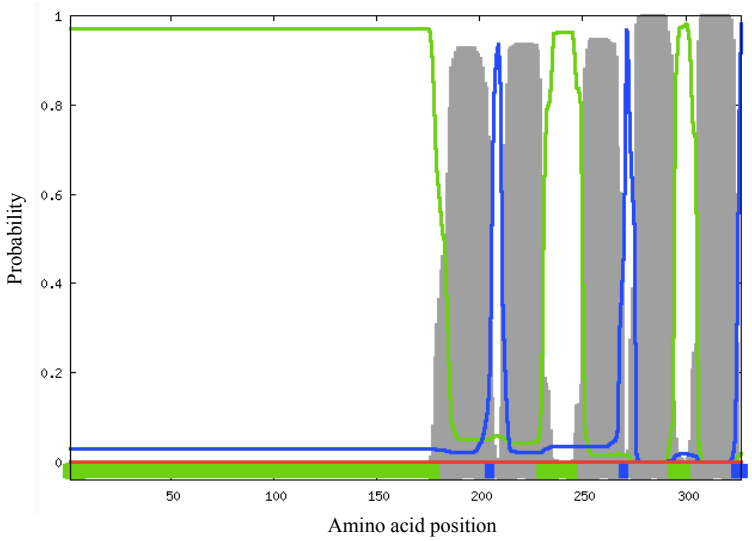

Amino acid position	Cellular location	Length (AA)
1 – 183	Cytoplasmic	183
184 – 205	Transmembrane	22
206 – 210	Periplasmic	5
211 - 230	Transmembrane	20
231 – 250	Cytoplasmic	20
251 – 270	Transmembrane	20
271 - 275	Periplasmic	5
276 – 294	Transmembrane	19
295 – 305	Cytoplasmic	11
306 – 325	Transmembrane	20
326 - 327	Periplasmic	1

Figure 3.5: Trans-membrane helix prediction of *B. suis* MbfA

Prediction of membrane spanning regions of *Brucella suis* MbfA with Phobius transmembrane topology prediction. Grey bars: transmembrane, green line: cytoplasmic, blue line periplasmic, red line signal peptide.

3.2: Examples of MbfA and MbfA-like proteins

It is of note that the eukaryotic VIT1 proteins examined in Figure 3.4 possess an elongated cytoplasmic loop (approx. 70 AA in length). Alignment of 70 MbfA/VIT1 sequences (52 prokaryotic and 18 eukaryotic) (Figure 3.6) displays that this feature is not unique to eukaryotes, but select prokaryotes also exhibit a conserved cytoplasmic loop between transmembrane helices 2 and 3. (More detailed alignments of erythrin, Vit and loop segments in Appendix 9.3). This multiple species alignment allows for the determination of the complete conservation of an aspartic acid within transmembrane helix 1 and that five TMH are present in all cases. In addition, the alignment allows the differentiation of MbfA-like sequences into 5 discrete sub-families denoted: Ia, Ib, Ic, IIp and IIe.

Sub-families Ia-c represent MbfA-like sequences, these proteins contain 2 domains, with the VIT1 domain located downstream from the erythrin domain. Sub-family Ia comprises sequences with uncharacterised N terminal domains, solely *Bartonella* spp.. Subfamily Ib represents the MbfA sequence present within *Brucella* spp. and is characterized by the absence of a cytoplasmic loop between TMH2 and 3. Subfamily Ic represents MbfA sequences characterized by the presence of a cytoplasmic loop between TMH2 and 3) (Location of loop shown schematically in Figure 3.7). Both of these sub-families comprise proteins with two pairs of highly conserved iron binding motifs – ExxH and E-6-Y – which are present within the N-terminal cytoplasmic erythrin domain of all MbfA proteins, allowing co-ordination of two iron atoms. One notable exception is the *Burkholderia cepacia* spp., which possess a unique 41 AA truncation at the N terminus of erythrin domain resulting in one of the four iron binding motifs being absent, potentially compromising the di-iron site and peroxide reductase activity of this domain. In addition, *mbfA* in *Burkholderia* spp. is limited to the *Burkholderia cepacia* complex strains, as it is encoded on the non-essential virulence plasmid C3 (Agnoli et al. 2012).

Type II subfamilies can be differentiated into either prokaryotic or eukaryotic grouping, but in either case they lack an N-terminal domain, therefore only consist of a VIT1 domain. All examples contain the cytoplasmic loop insertion between TMH2 and 3.

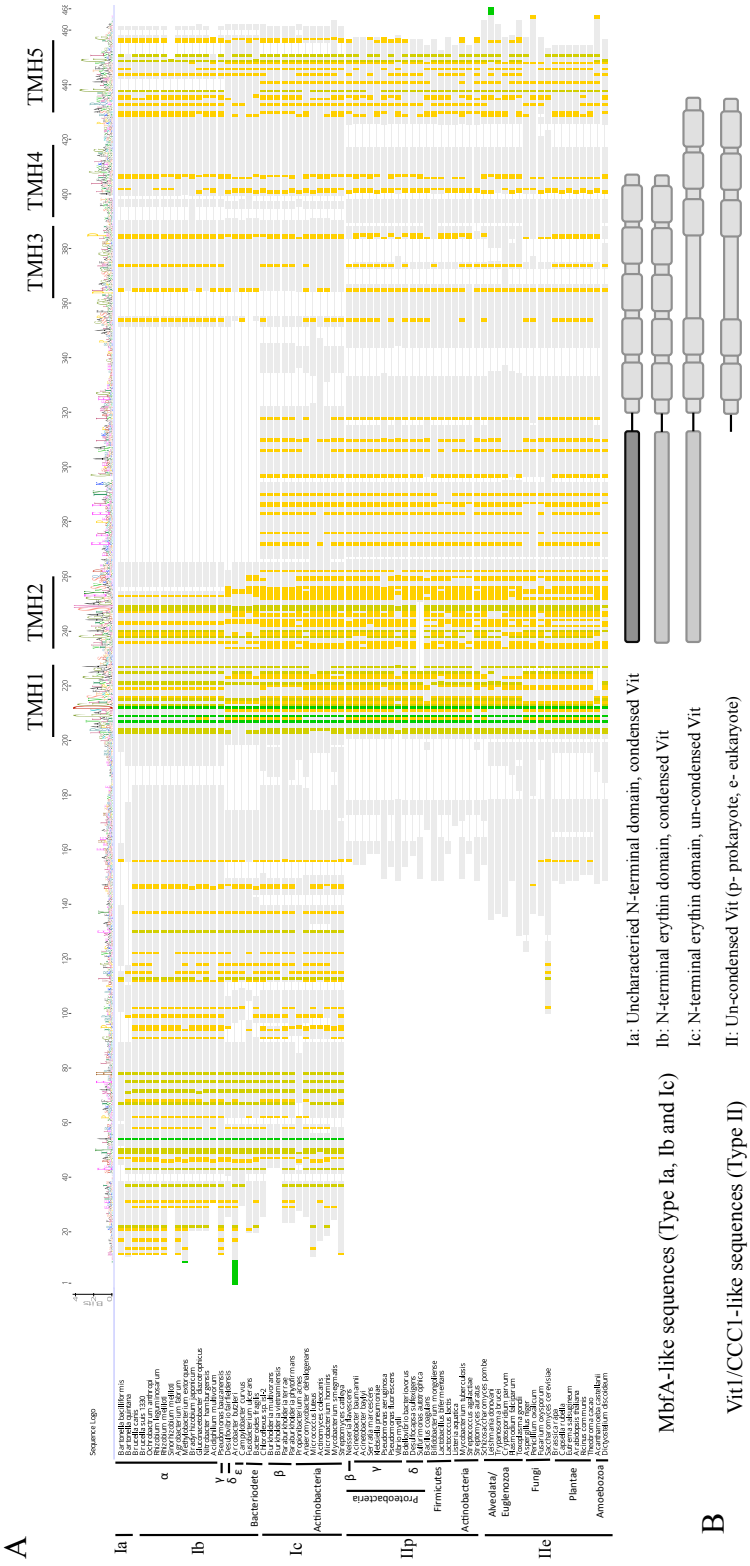

Figure 3.6: Alignment of prokaryotic and eukaryotic MbfA and VIT1-like proteins

A: Multiple sequence alignment of prokaryotic and eukaryotic MbfA and VIT1-like proteins displaying conservation of five transmembrane helices and aspartic acid (green TMH1). B: Schematic representation of the separation of mbfA-like sequences into sub-families denoted: Ia, Ib, Ic, IIp and IIe. TMH and cytoplasmic loop locations indiucted with boxes within the Vit domain.

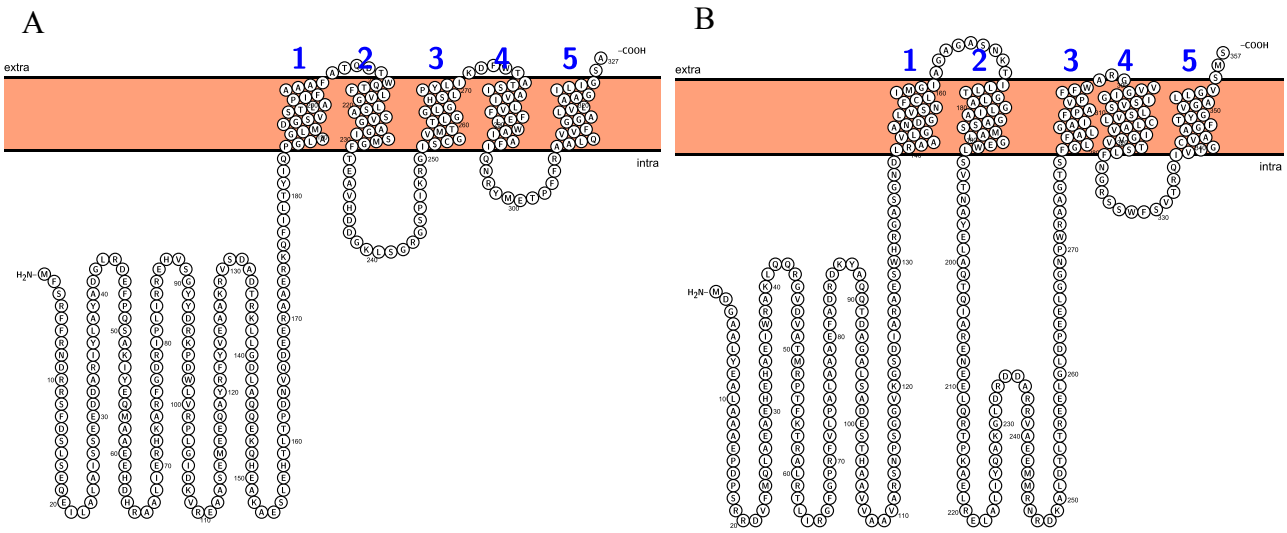

Figure 3.7: 2D plot of *Brucella suis* and *Burkholderia multivorans* MbfA membrane topology.

Brucella suis (A) and *Burkholderia multivorans* (B) MbfA membrane topology. Bacterial membrane (pink), TMH number (blue). Transmembrane helix location determined by Phobius prediction.

To examine the relationship and evolution of the MbfA-like proteins phylogenetic analysis (Geneious) was conducted on the conserved trans-membrane helix regions from the 70 MbfA/VIT1 sequences analysed previously (Figure 3.8). The phylogenetic arrangement of the MbfA proteins displays a distinct separation into previously denoted MbfA subfamilies, suggesting evolution of the protein to facilitate a common function within these bacterial species.

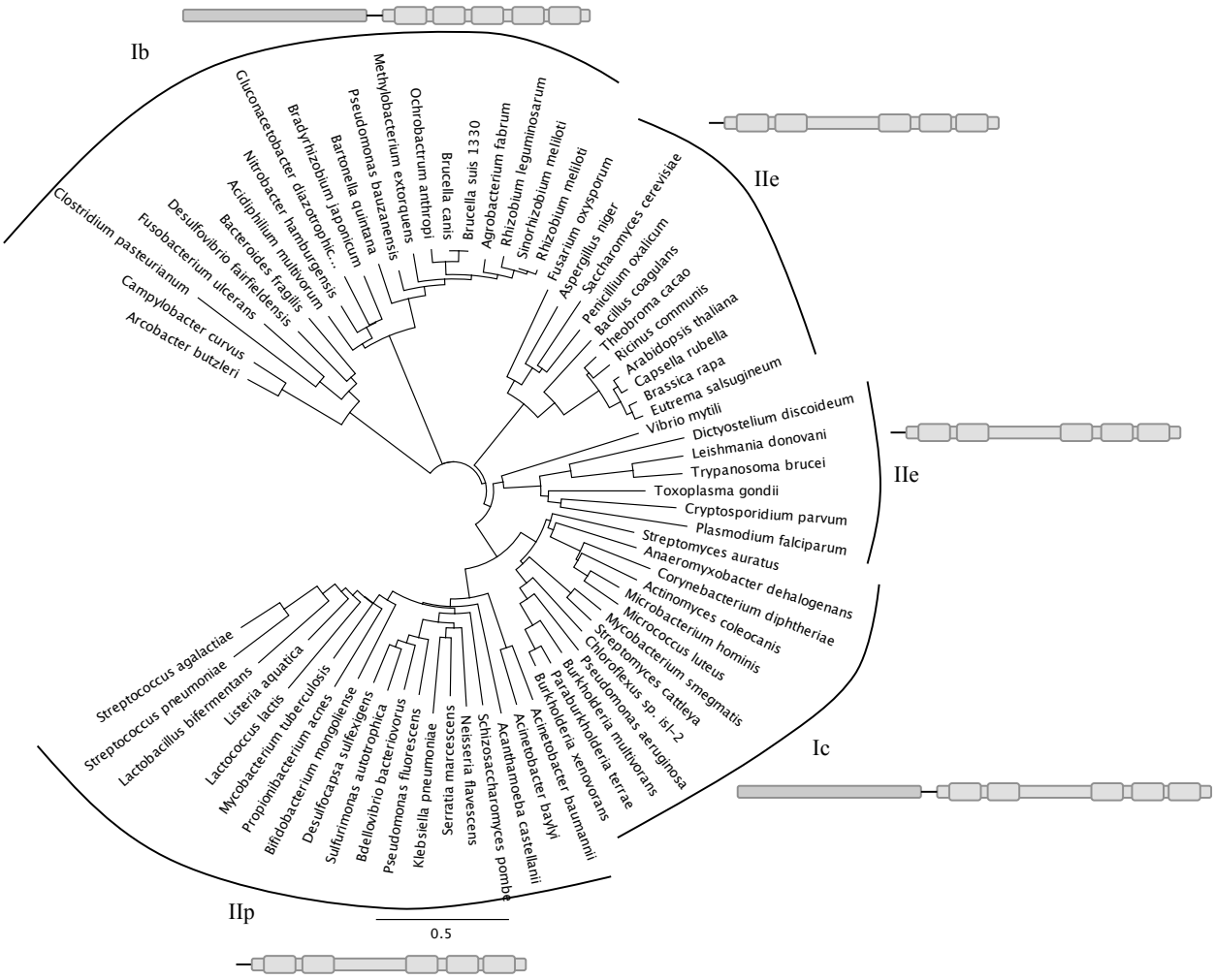

Figure 3.8: Phylogenetic analysis of prokaryotic and eukaryotic MbfA and VIT1-like proteins

Phylogenetic analysis of prokaryotic and eukaryotic MbfA and VIT1-like proteins displaying corresponding assignment to MbfA sub-families.

Multiple sequence alignment and phylogenetic analysis show that type Ib/c MbfA-like proteins are widely spread across bacterial phyla. Attention should be drawn to the high number of sequences observed within the alpha-proteobacteria, in particular, *mbfA* sequences are present within all *Brucella* spp., both classical (*B. suis*, *B. melitensis* and *B. abortus*) as well as non-classical strains (*B. ovis* and *B. microti*) and display a high sequence similarity (321/327 AA – 98.2% identical sites). However, the *mbfA* coding sequence of *Brucella melitensis* bv.1 str. 16M and *Brucella melitensis* bv. 3 str. Ether display a C→T point mutation at nucleotide 55 resulting in an amber stop codon (UAG) in place of a glutamate codon (CAG) at the 18th codon (Figure 3.9). The inclusion of this stop codon is predicted to result in a cryptic version of the gene resulting in no translation of the MbfA protein. In addition, a second glutamate to amber stop codon SNP ($C_{634}T$) is present in the C terminal end of all clade I *B. melitensis* strains (*B. melitensis* UK31/99, *B. melitensis* Ether, *B. melitensis* F15/06-7 and *B. melitensis* F5/07-239A), suggesting that the *mbfA* gene has accumulated nullifying mutation in *B. melitensis*.

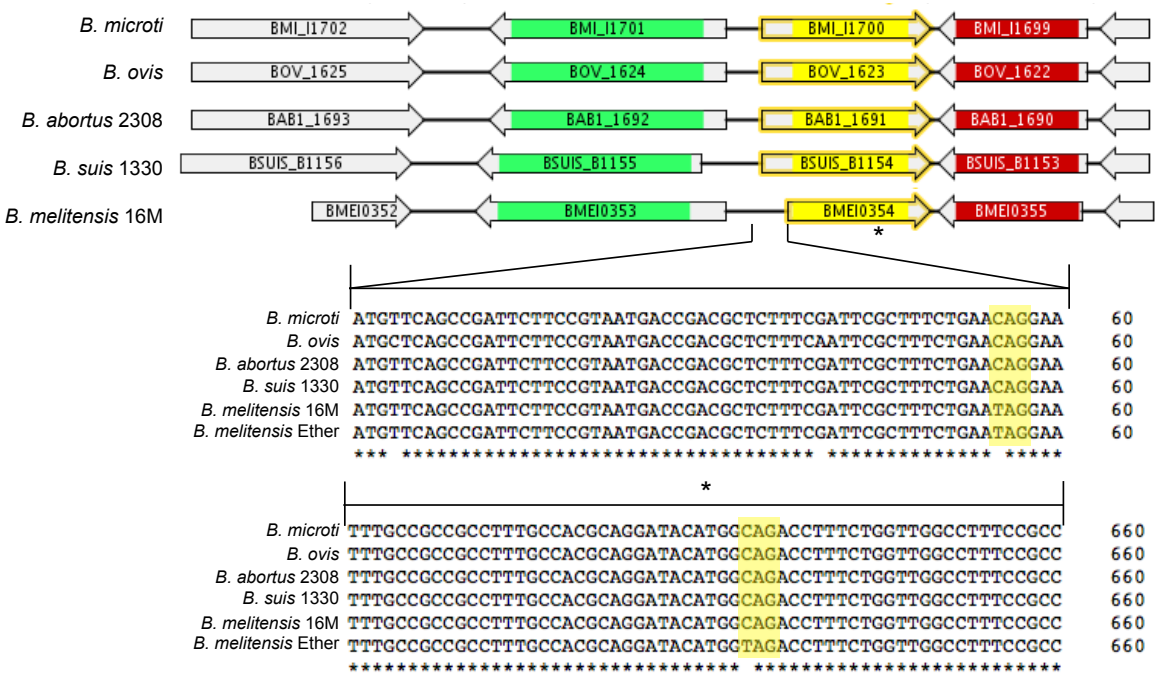

Figure 3.9: Cryptic *mbfA* in *Brucella melitensis* strains.

Gene context tool analysis (GeConT 3 - (Martinez-Guerrero et al. 2008)) of *mbfA* from *B. microti* (BMI_I1700), *B. ovis* (BOV_1623), *B. abortus* 2308 (BAB1_1691), *B. suis* 1330 (BSUIS_B1154) and *B. melitensis* 16M (BMEI0354) and multiple sequence alignment of *Brucella mbfA* highlighting disruptive SNP locations in *B. melitensis* 16M and *B. melitensis* Ether (*) compared to classical and non-classical *Brucella* isolates.

It is of additional interest that there are just two *B. melitensis* strains that lack the SNP at nucleotide 55 and thus encode non-cryptic versions of *mfA*. *B. melitensis* bv. 1 str. 16M13W and *B. melitensis* S66 both possess a T at position 55 of the *mbfA* gene, restoring the wildtype sequence of the gene. *B. melitensis* bv. 1 str. 16M13W is experimentally derived from *B. melitensis* bv. 1 str. 16M following a 13-week period of mouse infection (Ke et al. 2012), whilst, *B. melitensis* S66 was isolated from the blood of a human patient suffering from Brucellosis (Ke et al. 2012). However, the validity of these observations is questionable as analysis of the genomes of these two isolates (Tan et al. 2015) suggests that both segregate into a group that does not belong to other *B. melitensis* strains raising concern that the Chinese *Brucella melitensis* 16M strain may not be the same *B. melitensis* strain used worldwide isolates.

A wider analysis of the sequence identity of MbfA outside of the *Brucella* spp., but remaining within the rhizobiale α-proteobacteria reveals maintenance of conservation. As described previously, MbfA has been studied in *Agrobacterium tumefaciens* (ATCR1_17048) (Ruangkiattikul et al. 2012, Bhubhanil et al. 2014) but also within *Bradyrhizobium japonicum* (BJ6T_85830) (Sankari and O'Brian 2014). The sequence identity of these two organisms with *Brucella suis* MbfA are displayed in Table 3.1.

	A. tumefaciens	***B. japonicum***
B. suis	224 AA (68.5%)	186 AA (57.6%)
A. tumefaciens		191 AA (59.1%)

Table 3.1: Sequence identity of *B. suis*, *A. tumefaciens* and *B. japonicum*

As highlighted previously, MbfA sub-family Ia comprises sequences with uncharacterised N terminal domains, which solely comprises *Bartonella* spp.. *Bartonella* are closely related to *Brucella* spp. phylogentically and inhabit a similar intracellular niche, from which the requirement of MbfA might originate. Although *Bartonella* spp. encode an N-terminal domain, it shares no sequence identity to the *B. suis* erythrin domain or any other sequences in protein databases, however, the C-terminal VIT domain is highly conserved (Figure 3.10). The loss of the erythrin domain in *Bartonella* spp. may represent an iron export system that is not dependent on the reduction of hydrogen peroxide to facilitate the export or iron via the VIT domain, although examination of the *Bartonella* N-terminal domain would be required to test this hypothesis.

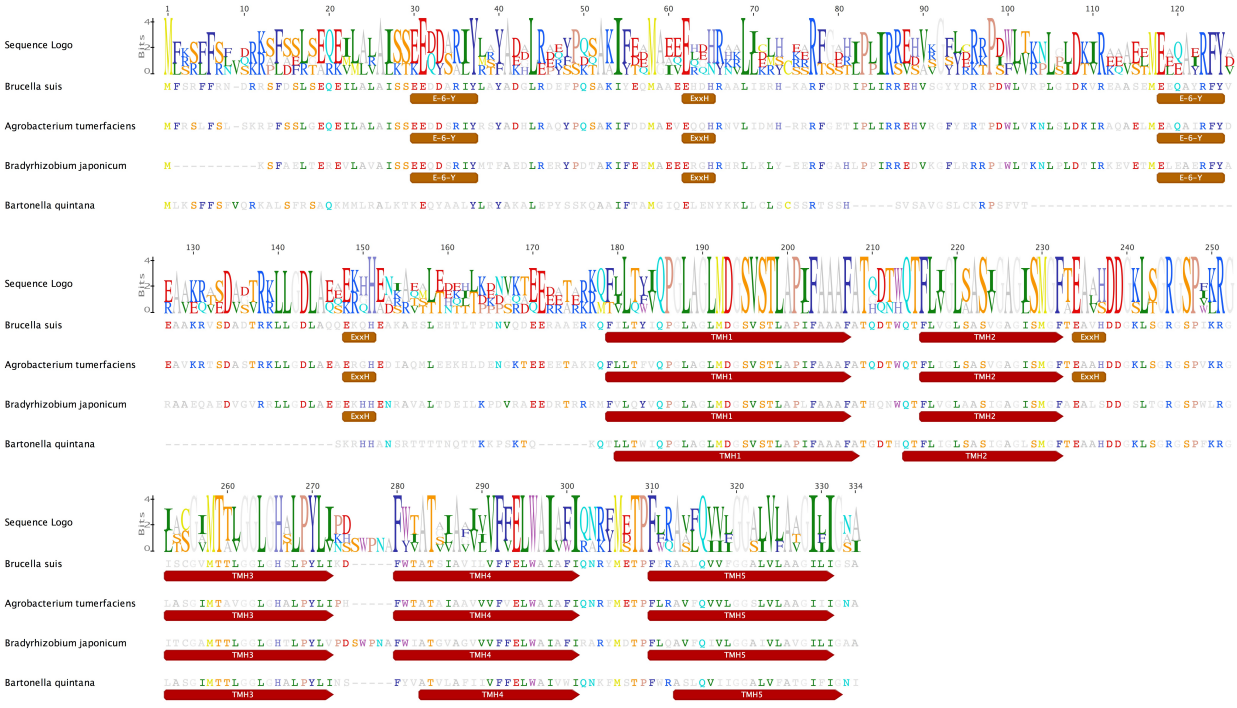

Figure 3.10: Sequence alignment of α-proteobacteria *mbfA*

Multiple sequence alignment of *B. suis, A. tumefaciens, B. japonicum* and *B. quintana* MbfA. Orange: iron binding motifs, Red: transmembrane helices.

3.3: Prediction of *B. suis* MbfA tertiary Structure

A prediction of tertiary structure of the erythrin domain was generated using the protein homology/analogy recognition engine (Phyre 2) (Kelley and Sternberg 2009). Alignment of the erythrin domain to the ferritin of *Magnetospirillum magnetotacticum* (PDB: d2oh3a1) reveals 145 residues from amino acid 18 to 165 (44% of the total MbfA protein, 83% of the erythrin domain) can be modelled with 89.7% confidence to the ferritin protein. This prediction further suggests that the erythrin domain assembles into a four alpha helical bundle, with each helix similar in length and carrying a single di-iron motif (E-6-Y or ExxH) located at the centre of the helix. In addition, the amino acid side chains predicted to coordinate the di-iron centre are orientated inwards towards the expected location of the di-iron species (Figure 3.11).

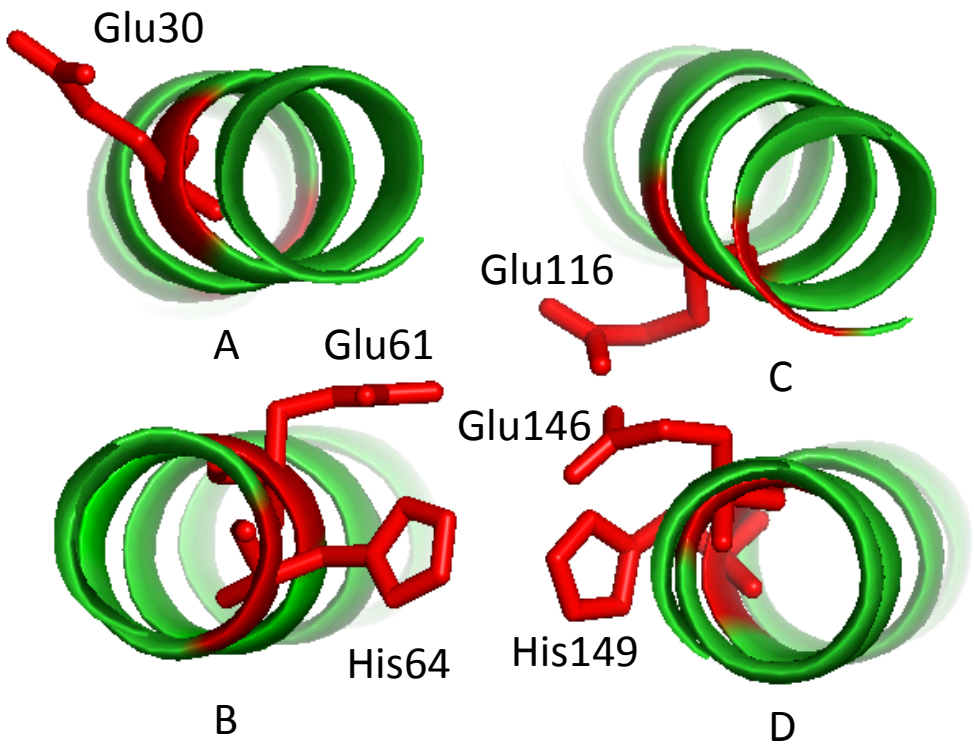

Figure 3.11: *B. suis* MbfA tertiary structure prediction

Prediction of tertiary structure of the MbfA erythrin domain displaying 4 alpha helices, labeled A-D, (green) and di-iron binding motifs E-6-Y and ExxH (red) from Phyre 2, image annotation with Pymol.

3.4: Regulation of *mbfA*

Analysis of the upstream DNA sequence from the *mbfA* gene has led to insight into its regulation. A region of DNA highly homologous to the consensus ICE-box is found located directly overlapping the transcription initiation site (-10 promoter region) (Figure 3.10). The location of the ICE-box suggests that Irr is negatively regulating *mbfA* transcription under low iron conditions and repression will be relieved under high iron conditions, this fits with the assumption that MbfA is acting as an iron efflux protein as the trigger of increased iron concentration would thus drive export of iron.

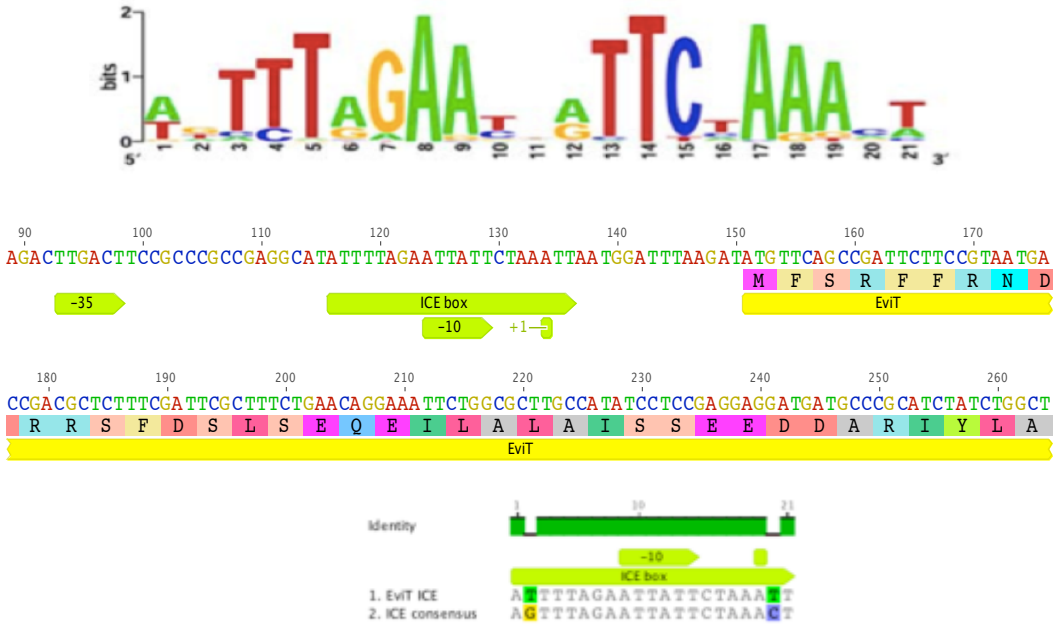

Figure 3.10: ICE box location - regulation of *mbfA*.

A: ICE-box location covering -10 box that would be expected to mediate negative regulation of *mbfA* under low iron concentrations through Irr control. B: ICE consensus aligned with *mbfA* ICE – 19/21 bp match, mismatch is within the least conserved region with respect to the ICE Box consensus sequence. -10 and -35 sites identified through sequence conservation.

Rudolph et al. (2006) showed that in *B. japonicum's* ICE-like motifs are located upstream of bll6680 (bacterioferritin) and blr7895 (rubrerythrin) genes, at the respective -10 boxes and that these sites mediate negative regulation by Irr. These findings provide precedence for the impact of an ICE box at the -10 site. Furthermore, Ruangkiattikul et al. (2012) showed that *mbfA* is regulated by Irr in *A. tumerfaciens*. With Irr present, *mbfA* expression was repressed at low iron concentrations, whilst expression was increased under high iron concentrations and also in an isogenic *irr* mutant. These findings demonstrate that Irr represses *mbfA* in this α-proteobacterium, which supports the likelihood that Irr also controls *mbfA* in *Brucella* species. Further details of relevant *B. suis* 1330 iron metabolism and redox stress genes supplied in appendix 9.4.

3.5: Discussion

To summarize, bioinformatical analysis of the MbfA sequence from *Brucella suis* 1330 has enabled a detailed hypothesis of the mechanism of action of MbfA. The presence of 4 iron-binding motifs within the erythrin domain suggests it has the capability of binding 2 iron atoms per protein monomer. This, along with the similarity of the erythrin domain to the rubrerythrin protein suggests that an involvement in hydrogen peroxide reduction may occur at the di-iron center. In addition, the membrane topology, 5 conserved TMH and single aspartic acid residue within TMH1 suggest that the C terminal VIT1 domain of MbfA is likely to function in a similar manner to examples of VIT1/CCC1 observed in *A. thaliana*, *S. cerevisiae* and *P. falciparum*. In addition, analysis of the region of DNA upstream of the coding sequence has allowed hypothesis that Irr regulates MbfA in response to intracellular iron and hydrogen peroxide concentrations through the conservation of the ICE-box spanning the -10 transcription initiation site.

Multiple sequence alignment enabled the in depth evaluation of the distribution of MbfA and MbfA-like genes within nature. The MbfA variant observed within *B. suis* is well conserved across the alpha-proteobacteria, but is also present in wider phyla. It is possible to sub-divide the MbfA-like sequences observed into 4 distinct sub-families based upon the presence of an N-terminal erythrin domain, as well as the presence or absence of a 70 AA cytoplasmic loop between TMH2 and 3.

Despite MbfA being widespread across both prokaryotes and eukaryotes suggesting that the expression of MbfA affords a distinct advantage, presumably during periods of redox stress, *B. melitensis* strains may present a differing view. The observation that *B. melitensis strains* have accumulated possible nullifying mutations throughout the *mbfA* gene, promotes questions to be asked as to the importance of a potential iron export protein. Although export of potentially toxic iron, during residence within a redox active environment presents as a valid mechanism of cellular preservation; the process of iron export nonetheless depletes stores of an essential micronutrient. The acquisition of nullifying mutations, thus preventing iron export may be evidence of the adaption of *B. melitensis* strains to their host species, but would require specific experimentation to prove.

Chapter 4: Construction of Genetic Reagents

4.1: Introduction

MbfA has not yet been studied in *Brucella* although characterisation in other bacteria has shown a role in resistance to iron toxicity and hydrogen peroxide (Ruangkiattikul et al. 2012, Bhubhanil et al. 2014, Sankari and O'Brian 2014). MbfA is suggested to function as an iron exporter, although this has yet to be proven. Thus, to study the mechanism of iron export by MbfA, and to understand how this confers resistance to oxidative stress and might aid intracellular survival of *Brucella* spp., the *mbfA* gene was cloned from *Brucella melitensis*. The *mbfA* gene is 984 bp in length in all *Brucella* spp.; the small size of this gene and monocistronic nature of the transcribed mRNA product allow for straightforward manipulations of the DNA sequence. *mbfA* DNA sequences from *Brucella suis* 1330 (functional) and *Brucella melitensis* 16M (cryptic – non-functional) were ulitised during this project. During initial experimentation, only *B. melitensis* 16M gDNA was available, from which the *B. suis* 1330 *mbfA* variant was constructed through SDM.

In summary, the *mbfA* sequence was amplified from *B. melitensis* 16M genomic DNA by PCR and ligated into the pJET1.2 plasmid, permitting propagation in *E. coli* and allowing the subsequent construction of engineered plasmids for specific purposes. From the pJET1.2 plasmid, the *mbfA* sequence was manipulated to represent the coding sequence observed in *Brucella suis* and other *mbfA* expressing *Brucella* spp.. This modified *mbfA* gene was then used as a source for cloning into inducible expression plasmids (pSU18, pBADrham and pBADara) as well as an over-expression (pET), suicide (pEX100T) and complementation plasmids (pBBR1-MSC4), all designed specifically to allow investigation into precise aspects of *Brucella* and *mbfA* function. Details of the constructions generated are provided below.

4.2: Cloning of *mbfA* from *Brucella melitensis* bv.1 str. 16M

The *mbfA* gene with 0.5 kb of up and downstream flanking sequence was amplified by PCR (primers mbfA0.5kbF/R; Table 2.4) from a preparation of genomic DNA isolated from *B. melitensis* bv. 1 str. 16M. The single, blunt-end PCR product (Figure 4.1A) was ligated into pre-linearized pJET1.2 (ThermoFisher) with T4 DNA ligase in a 3:1 molar ratio (insert:vector), in order to generate pJET*mbfA* (Figure 4.1C). The ligation reaction

was transformed into *E. coli* Top10 chemically competent cells and recombinant colonies selected for via resistance to ampicillin (additional selection is achieved when using pJET1.2 due to inserts disrupting the lethal restriction enzyme gene, *eco47IR*, enabling positive selection of recombinants). Plasmids from presumptive recombinant colonies were extracted and digested with *Xho*I and *Xba*I, unique restriction sites outside of the inserted *mbfA* fragment, and *Sac*I, which is unique to the inserted fragment (Figure 4.1B). Upon confirmation of *mbfA* insertion into pJET1.2 through release of the *mbfA*-containing fragment, Sanger sequencing (Primers T7F and pJETR; Table 2.4) was used to confirm the *mbfA* sequence within the pJET1.2 vector. Sanger sequencing additionally confirmed the presence of the C to T SNP within the *B. melitensis* nucleotide sequence.

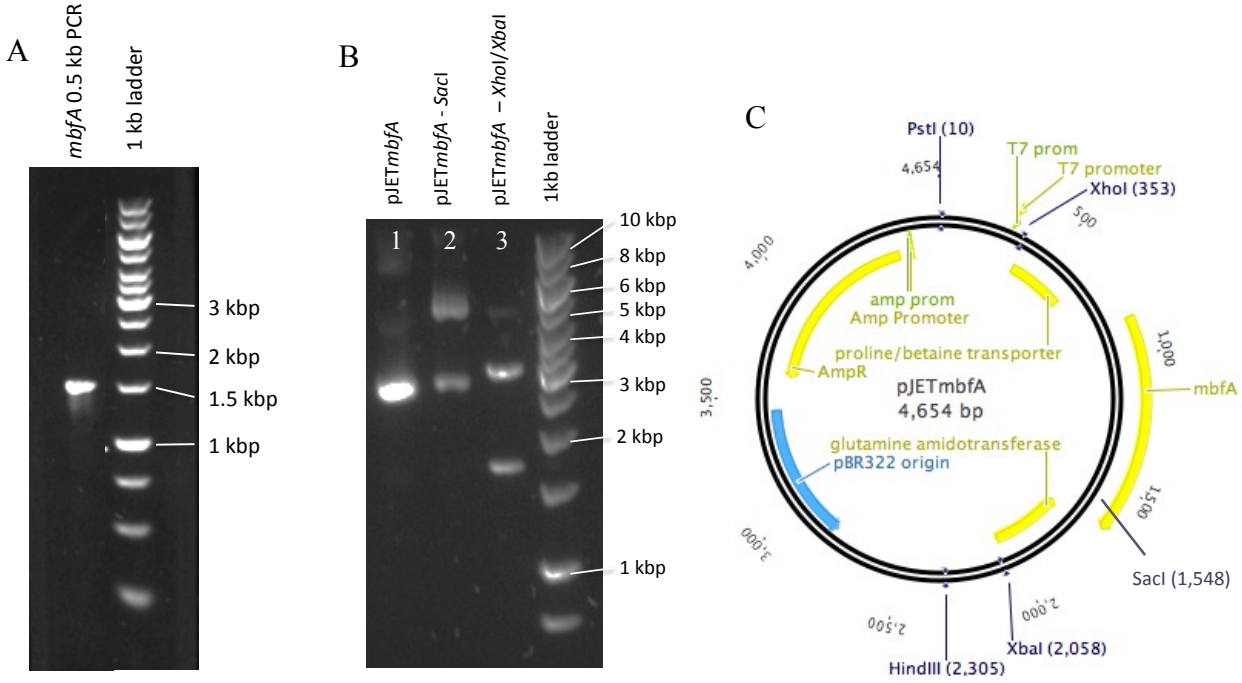

Figure 4.1: Cloning of *mbfA* into pJET

A: 0.8% agarose gel of the PCR product (1680 bp). B: Restriction confirmation of the pJET*mbfA* plasmid. Tracks left to right: 1, undigested plasmid; 2, *Sac*I digested plasmid (incomplete digestion) resulted in an approx. 4.5 kb linear fragment, together with uncut plasmid; 3, *Xho*I and *Xba*I double digestion plasmid resulted in two linear fragments of approx. 1.7 and 3 kb,. C: Vector map of pJET*mbfA*.

4.3: Correction of SNP in *Brucella melitensis mbfA* sequence

From bioinformatic analysis, it is expected that the C to T nucleotide substitution at position 55 of the *mbfA* gene in *B. melitensis* strains (that results in a stop codon in place of glutamate) will prevent translation of *mbfA*, rendering *mbfA* cryptic in *B. melitensis*. It is however; possible that translation may occur at a downstream start codon to give a truncated MbfA polypeptide. Downstream of the C to T point mutation, there are two potential alternate start codons that would permit translation of polypeptides of 271 and 306 amino acids respectively ($MbfA_{271}$ and $MbfA_{306}$) (Figure 4.2). $MbfA_{271}$ would be translated from mRNA at the next available, in-frame ATG. It is unlikely that $MbfA_{271}$ would be fully functional as one of the four di-iron binding motifs would not be present in the polypeptide sequence, preventing iron binding to the protein and thus failure to generate a catalytic centre capable of peroxide reductase activity. Alternatively, a translation product yielding $MbfA_{306}$ may result if translation initiated from the uncommon start CTG codon (O'Donnell and Janssen 2001). If this peptide were produced, the first di-iron site would be present within the amino acid sequence affording the ability to bind iron at the di-iron centre.

These suggested alternate *mbfA* translation products for *B. melitensis* strains are speculative; thus, to determine if *mbfA* is indeed rendered cryptic by the SNP at position 55 in *B. melitensis*, site directed mutagenesis (SDM) was used to repair the mutation. This would then allow comparison of the 'cryptic' and 'non-cryptic' versions of *mbfA*. SDM was used to correct the C to T point mutation (primers t55cF/R; Table 2.4) in the *B. melitensis mbfA* sequence *(*pJET*mbfA*), converting it to the sequence observed in *B. suis* and other *Brucella* spp.. Reversion of the point mutation was confirmed by Sanger sequencing (primers: T7F and pJETR) and the resulting plasmid named pJET$mbfA_{suis}$. In addition, a second point mutation (C64A) was introduced to the *B. melitensis mbfA* (pJET*mbfA*) sequence by SDM (primers: c64aF/R), changing the potential start CTG to ATG. This mutation would allow for the subsequent generation of a cloned construct able to efficiently express the $MbfA_{306}$ polypeptide. The presumptively mutated plasmid was isolated from transformants, confirmed by Sanger sequencing and named pJET$mbfA_{306}$.

The original cloned *mbfA* sequence, pJET*mbfA*, was subsequently used to generate the MbfA271 polypeptide and was thus re-named pJET$mbfA_{271}$.

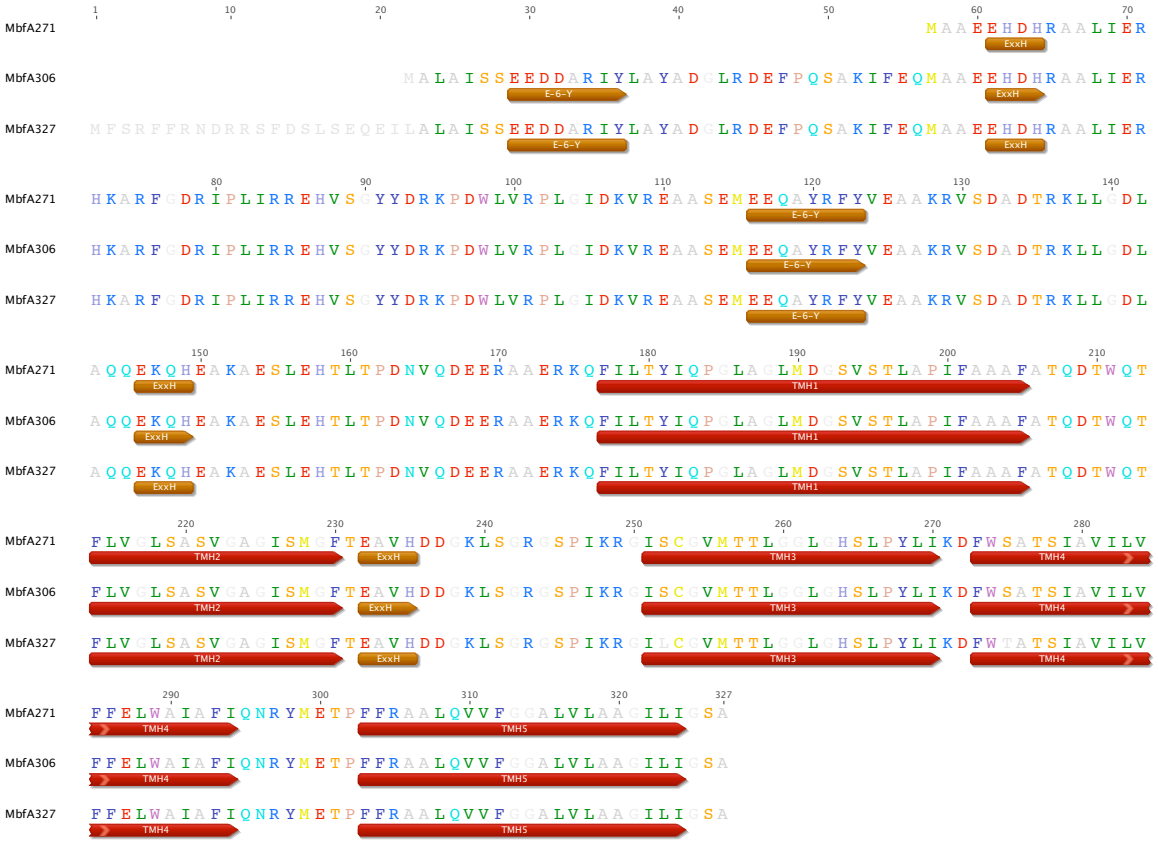

Figure 4.2: Translations from Sanger sequencing reads of MbfA isoforms.
Alignment of translated mbfA nucleotide Sanger sequencing reads from pJETmbfA271, pJETmbfA306 and pJETmbfAsuis (pJETmbfA327), showing differences in gene length though truncations from the N terminus.

The *mbfA* genes encoding the two potential MbfA polypeptides will be cloned into inducible expression vectors, alongside the corrected *B. suis* variant, to allow assessment of their ability to functionally complement specified *E. coli* mutants. It is of note that even if a phenotype is observed with expression of a truncated MbfA peptide when expressed in *E. coli*, that these isoforms may not be expressed in *B. melitensis* strains due to the lack of an apparent corresponding Shine-Dalgarno sequence.

4.4: Construction of controllable expression plasmids

To enable the determination of the functional effects of MbfA, the *mbfA* gene from each pJET*mbfA* variant was cloned into the pSU18 (p15A origin, ~10 copies per cell, *lac* promoter) and $pBAD_{rham}$ (p15A origin, ~10 copies per cell, rhamnose promoter) plasmids to enable the controllable induction of *mbfA* within specific *E. coli* mutant strains.

To enable effective transcription of the *mbfA* gene from the *lac* promoter in pSU18, a ribosome-binding site (RBS) was introduced 7 bp upstream of each *mbfA* isoform start codon. The RBS, *Eco*RI and *Bam*HI restriction sites required for cloning into pSU18 were introduced by PCR (primers $mbfA_{271}F$, $mbfA_{306}F$, $mbfA_{327}F$ and mbfAR; Table 2.4) using the high fidelity Q5 DNA polymerase. The vector and PCR fragments were digested with *Eco*RI and *Bam*HI, and ligated with T4 DNA ligase in a 3:1 molar ratio (insert:vector). The ligation mix was transformed into chemically competent Top10 cells, and recombinant colonies were selected on LA with chloramphenicol with blue/white screening using 5-bromo-4-chloro-3-indolyl-β-D-galactopyranoside (XGal) and isopropyl β-D-1-thiogalactopyranoside (IPTG). Confirmation of Lac^- colonies was achieved by plasmid extraction and digestion with *Eco*RI and *Bam*HI to excise the inserted fragment (Figure 4.3). The nucleotide sequence confirmed *mbfA* containing plasmids were then used for phenotypic analysis. The constructs created were designated pSU$mbfA_{271}$, pSU$mbfA_{306}$ and pSU$mbfA_{327}$, respectively. Similarly, *mbfA* variants were cloned into the $pBAD_{rham}$ plasmid through PCR amplification (primers $mbfA_{271}F2$, $mbfA_{306}F2$, $mbfA_{327}F2$ and mbfAR; Table 2.4) of the target gene sequence with addition of *Nde*I and *Bam*HI restriction sites (addition of RBS not required as located on plasmid). Ligation of digested DNA fragments, selection and confirmation of transformants was achieved using the same procedure as described for pSU18 cloning (XGal selection omitted) (Figure 4.3). The constructs created were designated pBAD$mbfA_{271}$, pBAD$mbfA_{306}$ and pBAD$mbfA_{327}$, respectively.

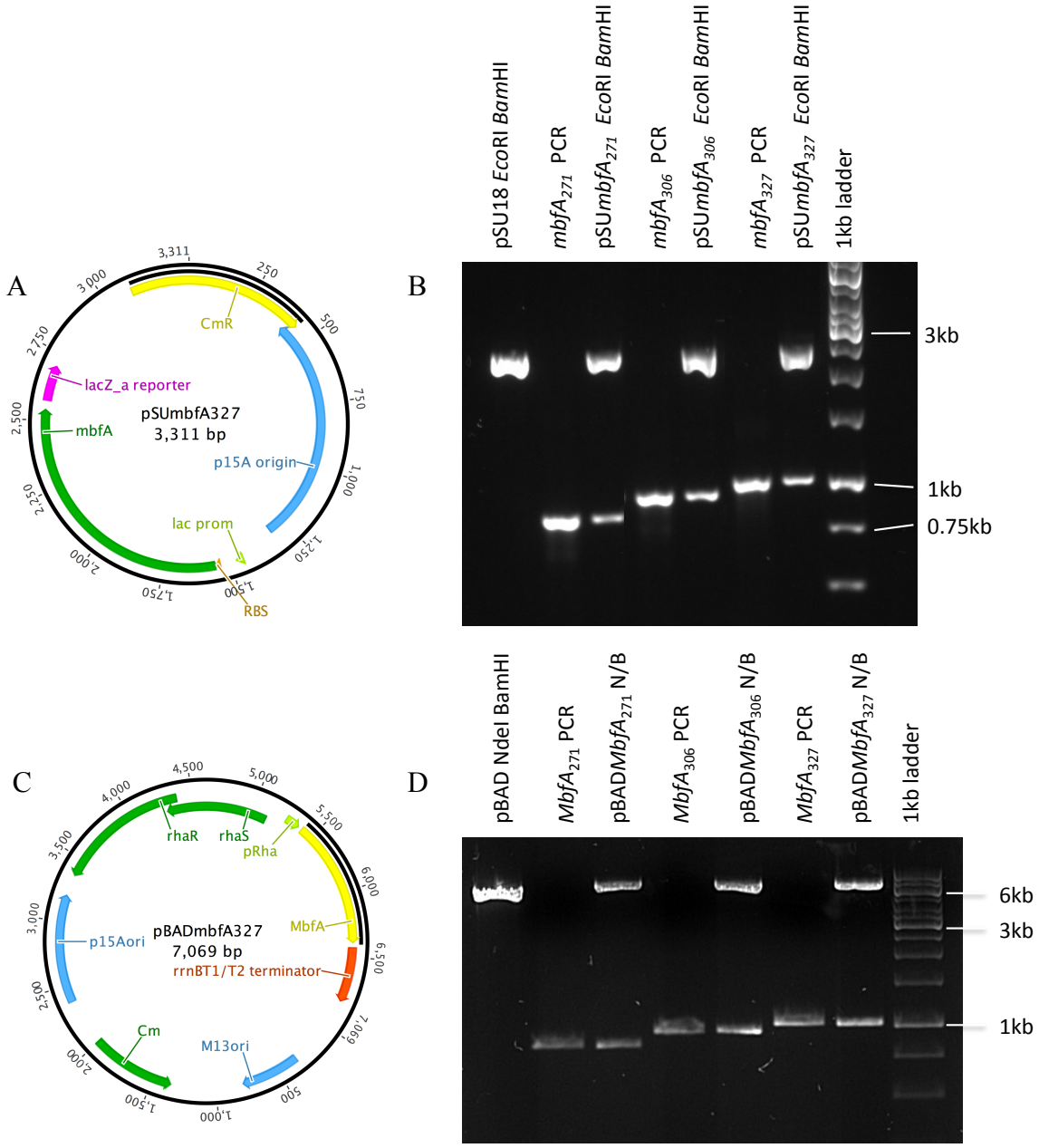

Figure 4.3: Cloning of *mbfA*271, *mbfA*306 and *mbfA*327 into pSU18 and pBADrham.

A: Vector map of pSU*mbfA*$_{327}$. B: 0.8% agarose gel of restriction confirmation of the pSU*mbfA* variant plasmids. Tracks contain *Eco*RI and *Bam*HI digested pSU18, the three *Eco*RI and *Bam*HI digested *mbfA* variant PCR products (816, 921 and 984 bp, respectively), the *Eco*RI and *Bam*HI digested pSU*mbfA* constructs showing the released insert and vector backbone fragments of equal size to the pre-ligation products and the molecular weight marker. C: Vector map of pBAD*mbfA*$_{327}$. D: As B but for pBAD*mbfA* variant constructs digested with *Nde*I and *Bam*HI.

To clone the *B. suis mbfA* sequence into $pBAD_{ara}$, Gibson assembly was used due to the lack of restriction endonuclease sites available to clone the *mbfA* gene in context with the arabinose promoter and RBS. This technique allows for assembly of multiple DNA fragments, regardless of fragment length or end compatibility (Gibson et al. 2009). The method includes three different enzymatic reactions: a T5 exonuclease that removes nucleotides from the 5' end to create single-stranded 3' overhangs that facilitate the annealing of fragments that share complementarity at one end (overlap region approx. 15-80 bp); a DNA polymerase that fills in gaps within each annealed fragment; and the *Taq* DNA ligase that covalently seals the nicks in the assembled DNA. First, PCR (primers araF, araR, mbfAaraF and mbfAaraR; Table 2.4) was used to introduce 15 bp regions of complementary DNA onto the 5' and 3' ends of the inserted *mbfA* fragment and linearized vector. The amplified DNA fragments were separated via agarose gel electrophoresis and excised from the gel before combining 50 ng of *mbfA* insert with 200 ng linearized $pBAD_{ara}$ vector with Gibson assembly reagents, and ligation was promoted through incubation at 50 °C for 15 min. Reaction products were then transformed into Top10 competent cells. Colony PCR (primers mbfAaraF and mbfAaraR) was used as a first line screen for the identification of presumptive *mbfA* containing transformants (77% false positive transformants present as pJET*mbfA* template DNA and pBADara plasmids are both Amp^R). PCR positive isolates were further confirmed to contain the *mbfA* insert via restriction digestions and Sanger sequencing.

4.5: Construction of over-expression plasmids

To enable examination of the biochemistry of the N-terminal erythrin domain, specifically formation of the di-iron centre and resulting reactivity, this domain is required to be expressed in high concentrations to allow the purification of sufficient quantities of the protein for analysis. This was achieved by cloning the erythrin domain into a vector containing the T7 RNA polymerase promoter (pET21a). This vector, when transformed into an *E. coli* strain containing a prophage harboring the T7 RNA polymerase (BL21/DE3) under the control of the *lac* promoter allows the strong expression of the target gene in the presence of the inducer, IPTG.

The gene fragment encoding the N-terminal erythrin domain of each variant of the *mbfA* gene (*mbfA*$_{271}$*:* 1-524 bp, *mbfA*$_{306}$*:* 1-356 bp and *mbfA*$_{327}$*:* 1-461 bp) was amplified by PCR (primers ery$_{271}$F, ery$_{306}$F, ery$_{327}$F and eryR; Table 2.4) designed to incorporate *Nde*I and *Hin*dIII restriction endonuclease sites. The amplified fragments were gel extracted to avoid carryover of parental DNA when cloning into *Nde*I and *Hin*dIII digested pET21a as both parental and insertion vectors are ampicillin resistant. The pET21a vector and erythrin domain inserts were digested with *Nde*I and *Hin*dIII, and ligated with T4 ligase in a 3:1 molar ratio (insert:vector) before transformation into chemically competent Top10 cells. Selection for recombinants was achieved with resistance to ampicillin. Sanger sequencing (primers T7F and pJETR) confirmed that the erythrin domain was present in the recombinant colonies. Further confirmation was achieved through *Nde*I and *Hin*dIII digestion of the extracted plasmid DNA releasing the desired inserted fragment (Figure 4.4). Confirmed constructs were named pET*ery*$_{271}$, pET*ery*$_{306}$ and pET*ery*$_{327}$, respectively.

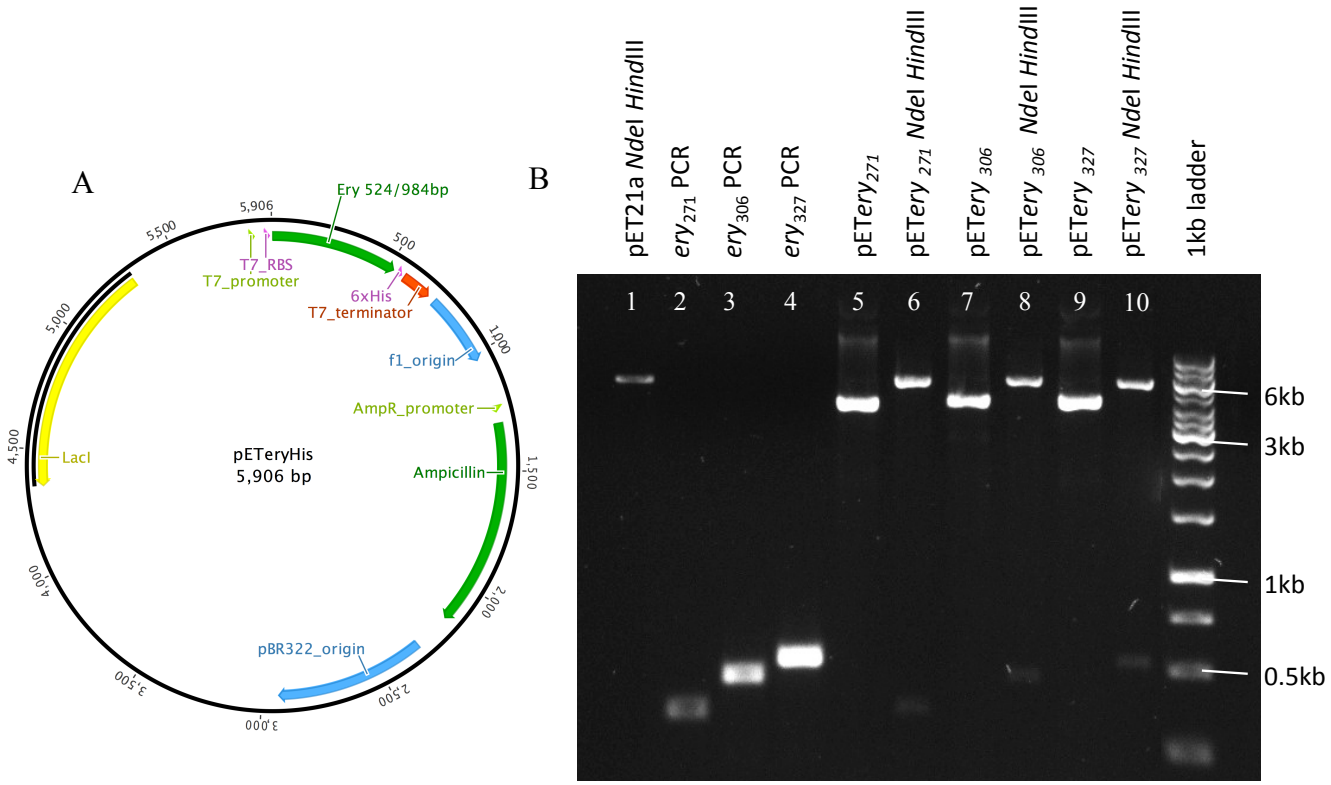

Figure 4.4: Cloning of erythrin variants into pET21a

A: Representative vector map of the pET*ery*$_{327}$ construct. B: 0.8% agarose gel of digested pET*ery* vector variants. Tracks from left to right: 1, gel extracted *Nde*I and *Hin*dIII digested pET21a (~4.6 kb); 2, 3 and 4, gel extracted *Nde*I and *Hin*dIII digested ery PCR products 356, 461 and 524 bp; 5, 7 and 9, undigested pETery constructs (supercoiled); 6, 8 and 10 *Nde*I and *Hin*dIII digested pETery constructs showing the released insert and vector backbone fragments of equal size to the pre ligation products.

4.6: Construction of *Brucella mbfA* knockout vector

To allow the function of *mbfA* in resistance to oxidative stress to be determined and its role in *Brucella suis* and *B. melitensis* survival within the macrophage to be deduced, a suicide vector was designed to generate a non-polar gene excision of the *mbfA* gene in *B. suis* 1330 and *B. melitensis* 16M and replacement with a kanamycin resistance determinant. The pEX100T suicide plasmid was utilized to remove the *mbfA* coding sequence from the *Brucella* genome as it encodes *sacB* (levansucrase) which, when expressed in the presence of sucrose, generates a toxic phenotype to the transformed cell allowing negative selection. This function can be used to force a recombination event from the suicide plasmid to the bacterial genome, enabling the removal of the target gene.

To construct the suicide vector, first, the *mbfA* gene with 1 kb of up- and down-stream flanking sequence was amplified from the genomic DNA of *Brucella melitensis* bv. 1 str. 16M by PCR (primers mbfA1kbF/R; Table 2.4). 1 kb of flanking DNA sequence is used as standard within the published *Brucella* literature to provide sufficient base pair overlap to allow for successful recombination into the chromosome of *Brucella* spp (Elhassanny et al. 2013). The size of the PCR product (3172 bp) was confirmed by agarose gel electrophoresis (Figure 4.6). The purified PCR fragment was blunt-end ligated into the pJET1.2 with T4 DNA ligase in a 3:1 molar ratio (insert:vector) and transformed into chemically competent Top10 cells. The plasmid DNA of ampicillin resistant colonies was extracted; presumptive pJET*mbfA* plasmids were digested with *Hin*dIII, *Pst*I and *Sac*I restriction endonucleases (Figure 4.5). The resulting separation of DNA fragments by agarose gel electrophoresis allowed determination and confirmation of the insertion of the *mbfA* into the pJET1.2 vector. Sanger sequencing (primers T7F and pJETR) confirmed the sequence and polarity of the inserted fragments.

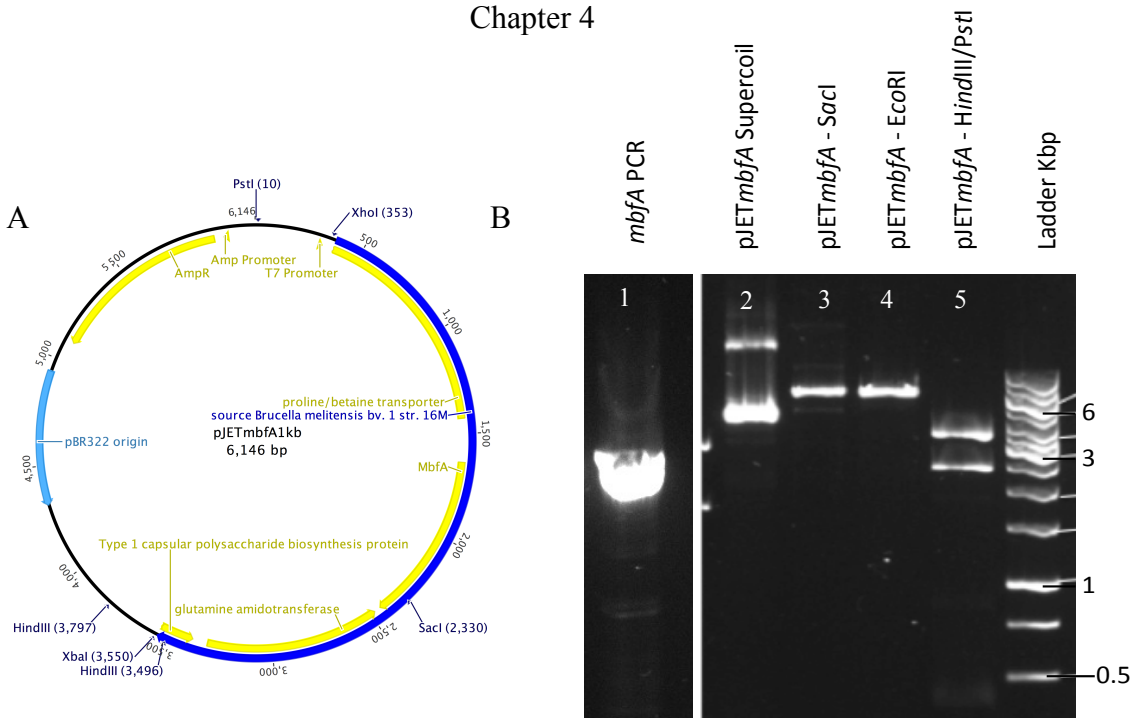

Figure 4.5: Cloning of *Brucella melitensis* bv.1 str.16M *mbfA* into pJET

A: Vector map of pJET*mbfA*1kb. B: 0.8% agarose gel of restriction digest confirmation of pJET*mbfA*1kb. Tracks left to right: 1, PCR amplification of *mbfA* with 1 kb flanking DNA from the *Brucella melitensis* genome, 2, Supercoiled pJET*mbfA*1kb, 3, *Sac*I digested pJET*mbfA*1kb (unique restriction site to inserted *mbfA* sequence), 4, *Eco*RI digested pJET*mbfA*1kb (unique restriction site to inserted pJET1.2 vector) 5, *Hin*dIII and *Pst*I digested pJET*mbfA*1kb (release of inserted *mbfA*1kb 3486 and 301 bp fragments).

To introduce the kanamycin resistance gene into the coding sequence of the *mbfA* gene, at the same time as removing the coding nucleotides, to create a non-polar gene excision, the Gibson assembly technique of molecular cloning was employed. Inverse PCR (primers ΔmbfAF/R; Table 2.4) was used to amplify the flanking sequences of *mbfA* with the pJET vector backbone, excising the coding sequence of *mbfA*. The resulting PCR product was excised from an agarose gel after electrophoretic separation, centrifugation column purified and estimates of the DNA concentration made through absorption measurement made at 260nm with a Nanodrop spectrophotometer. The DNA fragment was designated pJETΔ*mbfA*. The kanamycin resistance gene and its promoter (Kan^R cassette) were amplified from pHP45ΩKn (Fellay et al. 1987) (kanamycin cassette originates from the *E. coli* Tn*5* transposon). Primers (mbfAKnF/R) were designed to amplify the Kan^R cassette from pHP45ΩKn whilst incorporating additional DNA sequence complementary to the regions of DNA at the

up- and down-stream ends of the linearized pJETΔ*mbfA* PCR fragment. As the additional regions of complementary DNA provided by the primers would not anneal to the pHP45ΩKn template DNA in the first round of PCR a two-step PCR reaction was used (Methods 2.3.2). The resulting PCR product was prepared as above and designated *mbfA*Kn^R.

50 ng of the *mbfA*Kn^R insert and 200 ng of the pJETΔ*mbfA* backbone vector were combined with the Gibson assembly enzymes and ligated at 50 °C for 15 mins. The ligation mixtures were directly transformed into chemically competent *E. coli* and desired transformants were selected through ampicillin and kanamycin resistance. Restriction endonuclease digestion with *Pst*I (an additional *Pst*I restriction site was introduced into the plasmid within the inserted kanamycin cassette, allowing further confirmation of the plasmid) of the isolated plasmid DNA allowed confirmation of the construct, designated pJETΔ*mbfA*::Kn (Figure 4.6).

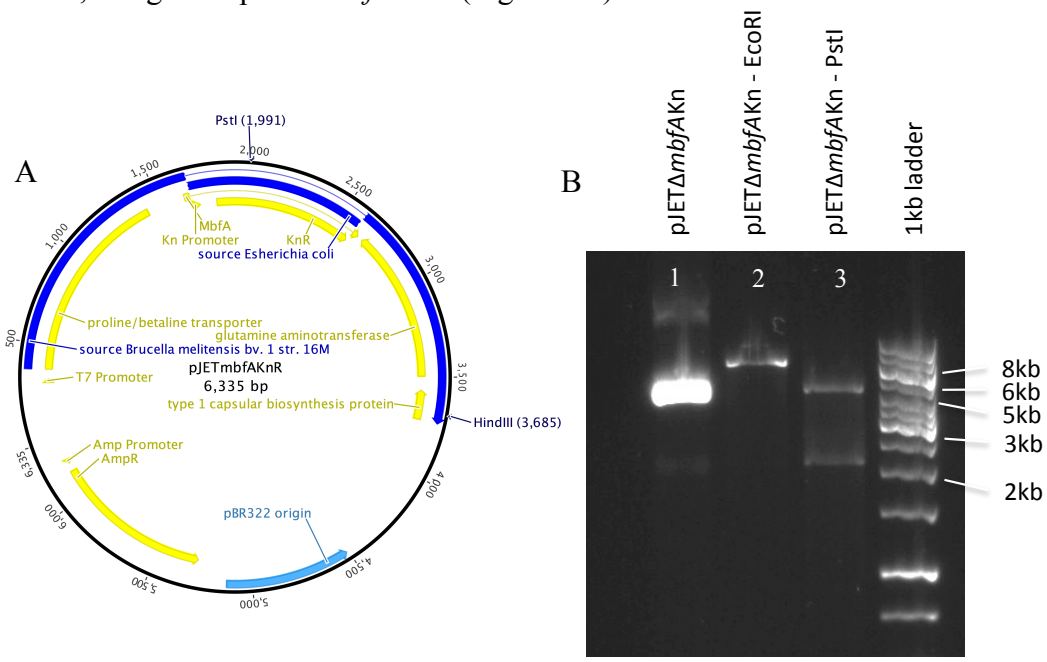

Figure 4.6: Insertion of kanamycin resistance cassette into the coding sequence of *mbfA*

A: Vector map of pJETΔ*mbfA*Kn. B: 0.8% agarose gel of restriction digest confirmation of pJETΔ*mbfA*Kn. Tracks left to right: 1, Supercoiled pJETΔ*mbfA*Kn; 2, *Eco*RI digested pJETΔ*mbfA*Kn (unique restriction site to inserted pJET vector); 3, *Pst*I digested pJETΔ*mbfA*Kn (release of 4353 and 1982 bp fragments).

The next step involved PCR amplification of the Δ*mbfA*::Kn^R fragment of pJETΔ*mbfA*::Kn using the same primers (mbfA1kbF/R) used to clone the 1 kb flanking regions from the *B. melitensis* chromosome. The resulting PCR products were excised from an agarose gel after electrophoretic separation and centrifugation column purified. pEX100T (Amp^R) was prepared to accept the Δ*mbfA*::Kn^R PCR fragment through digestion with *Sma*I (blunt end restriction endonuclease) and the linearised DNA was then excised from an agarose gel after electrophoretic separation, and was centrifugation column purified. The DNA fragments were ligated with T4 DNA ligase, creating pEXΔ*mbfA*::Kn^R. The resulting ligation mixture was transformed into chemically competent Top10 cells and plated onto LA with ampicillin and kanamycin. To ensure that transformants were pEX100T constructs and not carryover pJET constructs (both plasmid constructs are ampicillin and kanamycin resistance) the toxic activity required for a second recombination event in *Brucella* associated with SacB (levansucrase) was accessed (specific to pEX100T constructs). Transformant Kn^R, Amp^R colonies were screened for sensitivity to sucrose through replica plating onto LA (with 100 μg/ml Amp, 50 μg/ml Kn) with and without 20% sucrose (Figure 4.8). Plasmid DNA was isolated from colonies that presented with the correct phenotypic profile (Amp^R, Kn^R, Suc^S) and were digested with *Xho*I to confirm the size of the plasmid (Figure 4.7).

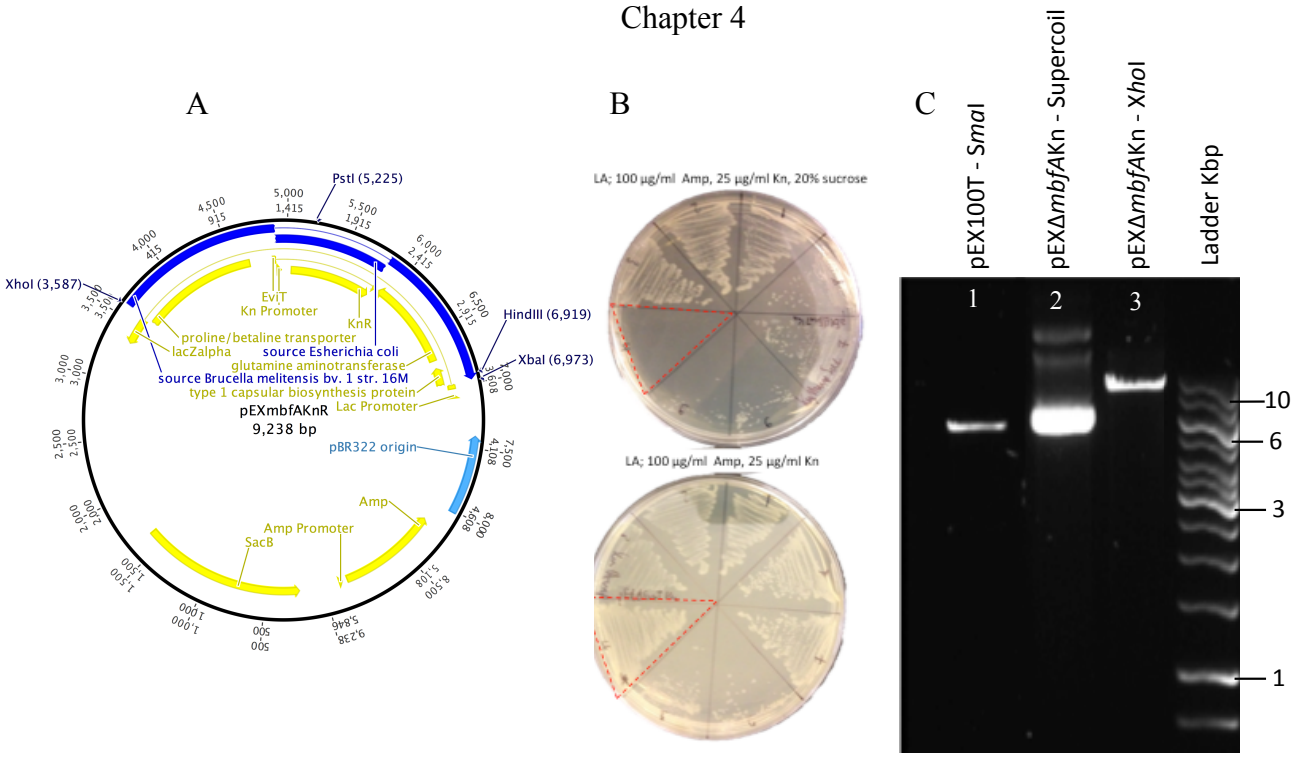

Figure 4.7: Cloning of Δ*mbfA*::*Kn*^{R} fragment into pEX100T suicide plasmid.

A: Vector map of pEXΔ*mbfA*Kn. B. Representative LA plate displaying the phenotypic characteristics of pEXΔ*mbfA*Kn transformant *E. coli* (Amp^R, Kn^R, Suc^S) highlighted in red. C: 0.8% agarose gel of restriction digest confirmation of pEXΔ*mbfA*Kn. Tracks left to right: 1, *Sma*I linearised pEX100T (5846 bp); 2, supercoiled pEXΔ*mbfA*Kn; 3, *Xho*I linearised pEXΔ*mbfA*Kn (9238 bp).

4.7: Construction of complementation vectors

To confirm that phenotypes observed in the *B. suis* and *melitensis* mutants are truly a result of the deletion of the target gene, wild type activity must be shown to be restored with the target gene expressed in *trans* on a complementation plasmid. Expression of genes in *trans* was conducted with the broad host range plasmid pBBR1MCS-4 (ampicillin resistant). Two constructs, representing the *mbfA* gene sequence observed in *B. suis* and *B. melitensis* strains, were created. The pattern of expression of these genes in *trans* from the complementation plasmid should match that of the wild type as they remain under control of their native promoter. An increase in expression level through the multi-copy nature of plasmids will be limited due to the low copy number (10 copies per cell) of pBBR1MCS-4 in *Brucella* spp (Elzer et al. 1995).

Construction of the described complementation plasmids was achieved by digesting the pJET*mbfA* (*B. suis* and *B. melitensis* derived, with 0.5 kb of up- and down-stream flanking sequence) and pBBR1MCS-4 plasmid with *Xho*I and *Xba*I restriction enzymes. The resulting *mbfA* encoding 1680 bp fragments were excised from an agarose gel after electrophoretic separation, then centrifugation column purified and ligated with T4 DNA ligase in a 3:1 molar ratio (insert:vector). The ligation reactions were transformed into chemically competent Top10 cells and transformants screened for ampicillin resistance on LA. Additional screening with XGal was used to differentiate from pBBR1MCS-4 with no insert (Lac^+) and pBBR4*mbfA* (Lac^-). The pBBR4*mbfA* plasmids were extracted, digested with *Xho*I and *Xba*I to excise the inserted fragments (Figure 4.8) and Sanger sequenced to confirm the presence/presence of the c55t SNP within the respective *B. melitensis* and *B. suis* sequences.

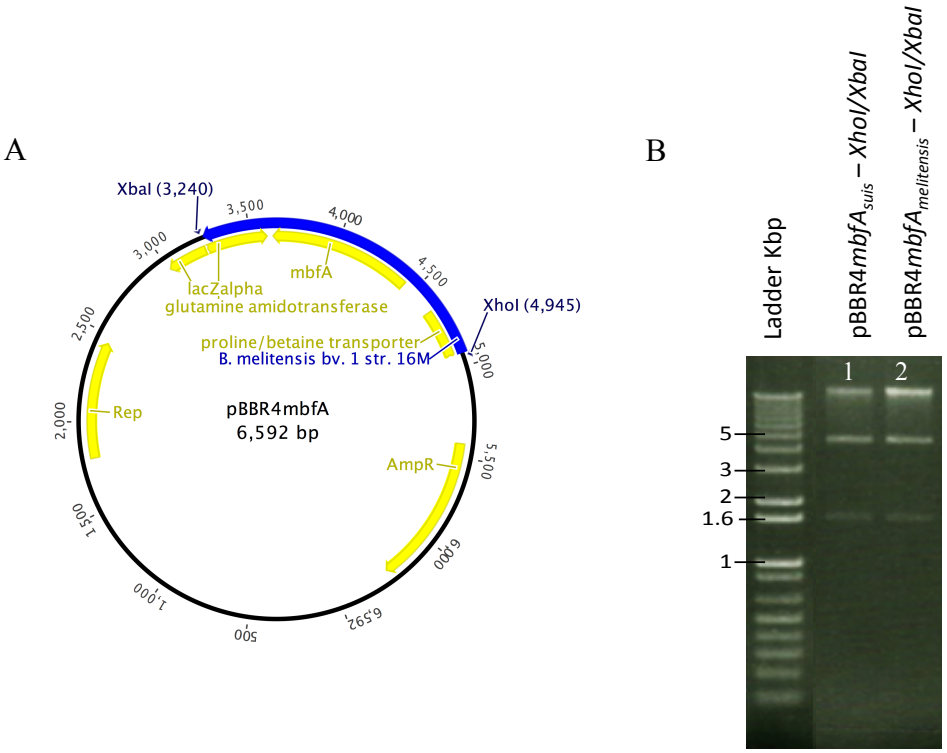

Figure 4.8: Cloning of *mbfA*$_{suis}$ and *mbfA*$_{melitensis}$ into pBBR4 complementation plasmid.

A: Vector map of pBBR4*mbfA*$_{mel}$. B: 0.8% agarose gel of restriction digest confirmation of pBBR4*mbfA*. Tracks left to right, *Xho*I and *Xba*I digested: 1, pBBR4*mbfA*$_{suis}$ (released fragment 1680 bp); and 2, pBBR4*mbfA*$_{melitensis}$ (released fragment 1680 bp).

Chapter 5: Investigation of MbfA erythrin domain biochemistry

5.1: Rationale - Generation and analysis of recombinant erythrin protein

To enable investigation of the biochemistry mediated by the cytoplasmically located N-terminal erythrin domain of the MbfA protein; the encoding sequence was expressed with tight control to allow the purification of sufficient quantities of the protein. This was achieved by cloning the erythrin domain into a vector containing the T7 RNA polymerase promoter (pET21a) – detailed in Chapter 4. In addition to maximizing expression, ideally, the protein should remain soluble in the cytoplasm of the expression strain, as the accumulation of insoluble polypeptides within inclusion bodies presents extra complications during subsequent purification steps. To extract and purify the target protein from the bacterial cytosol, a x6 His tag was incorporated at the C-terminal end of the erythrin domain (engineered into the pET21a vector). The affinity that histidine residues have for transition metals, especially nickel, was then used to retain the polyhistidine tagged protein to a nitrilotriacetic acid (NTA) agarose chromatography column saturated with Ni^{2+}. The NTA side chain binds nickel (II), forming an Ni-NTA complex, which has high affinity for polyhistidine-tagged proteins. When a concentration gradient of imidazole is subsequently applied, polyhistidine binding to Ni-NTA is displaced, allowing elution of purified protein.

Once the desired protein had been overexpressed and purified, biochemical analysis of the interactions of the protein with iron and hydrogen peroxide could be made, specifically the binding of iron to the erythrin as well as redox reactions at the di-iron centre. In addition, techniques such as mass spectroscopy, protein crystallisation and generation of polyclonal antibodies can be conducted to enable more in-depth knowledge of MbfA.

5.2: Small-scale recombinant protein expression trials

Three variants of the erythrin domain were cloned into the pET21a vector (detailed in Chapter 4) and were confirmed by Sanger sequencing to contain the desired nucleotide sequence. Each construct was transformed into BL21(DE3) chemically competent cells and transformants selected for by resistance to ampicillin. Before progressing to large-scale production of the recombinant proteins, a preliminary study was conducted to ensure that each pET21a construct was generating His-tagged recombinant erythrin protein of the expected molecular weight. For this purpose, the expression profile of each pET21a transformant was examined in 50 ml of growth medium for a small-scale overexpression experiment.

The growth of each strain was monitored to mid-log phase (0.5 OD units) whereupon the culture was induced with 0.5 mM IPTG. A total of 0.5 optical density units of whole cells were harvested every hour for 5 h as well as after overnight incubation. Pelleted whole cells were solubilized in SDS loading buffer (50 mM Tris-HCl pH 6.8, 2% SDS, 10% glycerol, 12.5 mM EDTA, 1% dithiothreitol and 0.02 % bromophenol blue), heated to 100 °C for 10 min, centrifuged for 5 min at 12000 x g (Eppendorf 5452) and separated by SDS-PAGE. The resulting polyacrylamide gel was stained with Coomassie blue, fixed with acetic acid (10%) and destained with ethanol (30%) (Figure 5.1). No expression of recombinant protein was observed for any of the *E. coli* BL21(DE3) pET-*ery* transformants. The predicted molecular weights for each recombinant protein are; ery_{271}: 15.5 kDa, ery_{306}: 19.5 kDa and ery_{327}: 21.9 kDa.

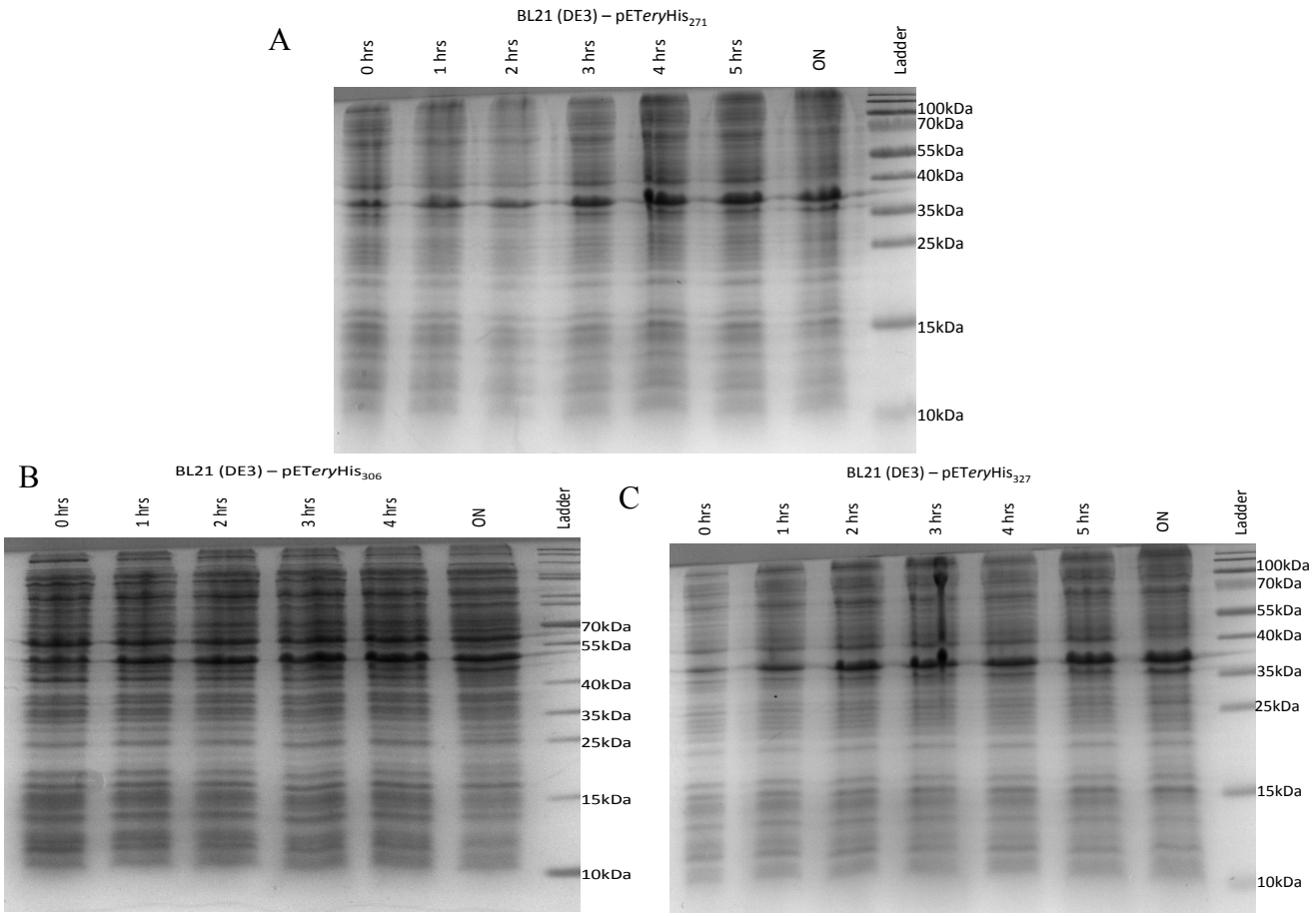

Figure 5.1: SDS-PAGE resolution of erythrin domain overexpression from pETery constructs in BL21(DE3).

16% SDS-PAGE analysis of pET*ery*$_{271}$ (A), pETery$_{306}$ (B) and pET*ery*$_{327}$ (C) expression in BL21(DE3), time after induction from which cells were harvested indicated. Induced proteins expected at 15.5, 19.5 and 21.9 kDa, respectively.

The lack of recombinant protein expression is predicted to be a result of codon bias (differences in tRNA usage) between *Brucella* and *E. coli*. Two approaches were taken to address the lack of expression of recombinant protein. First, a synthetic, codon optimized, *mbfA* was synthesized which would eliminate those *Brucella* codons that are employed rarely by *E. coli*. Secondly, alternate *E. coli* cell types, which provide rare *E. coli* tRNA's to increase translational efficiency, where used as expression host.

5.3: Codon optimisation of *Brucella suis mbfA*

The nucleotide sequence of *mbfA* from *B. suis* was optimized for expression in *E. coli* by Gene Art, Life Technologies, Invitrogen. The codon optimization manipulates the DNA sequence of the target gene, but preserves the encoded amino acids, therefore maintaining the amino acid sequence. This methodology is employed to utilize the alternative codons that are used most frequently in *E. coli* enabling more efficient translation of non-*E.coli* originating genes in *E. coli*. The native *mbfA* sequence was predicted to have less than optimal parameters for expression in *E. coli;* the average frequency of optimal codons for *E. coli* was 40%, suggesting that translation might stall during expression. After optimization of each codon of the *mbfA* sequence, the use of optimal codons was predicted to be increased to 80%. In addition, optimization reduced the average GC content from 59.39 to 47.52%, which closely matches that of the *E. coli* chromosome (Figure 5.2).

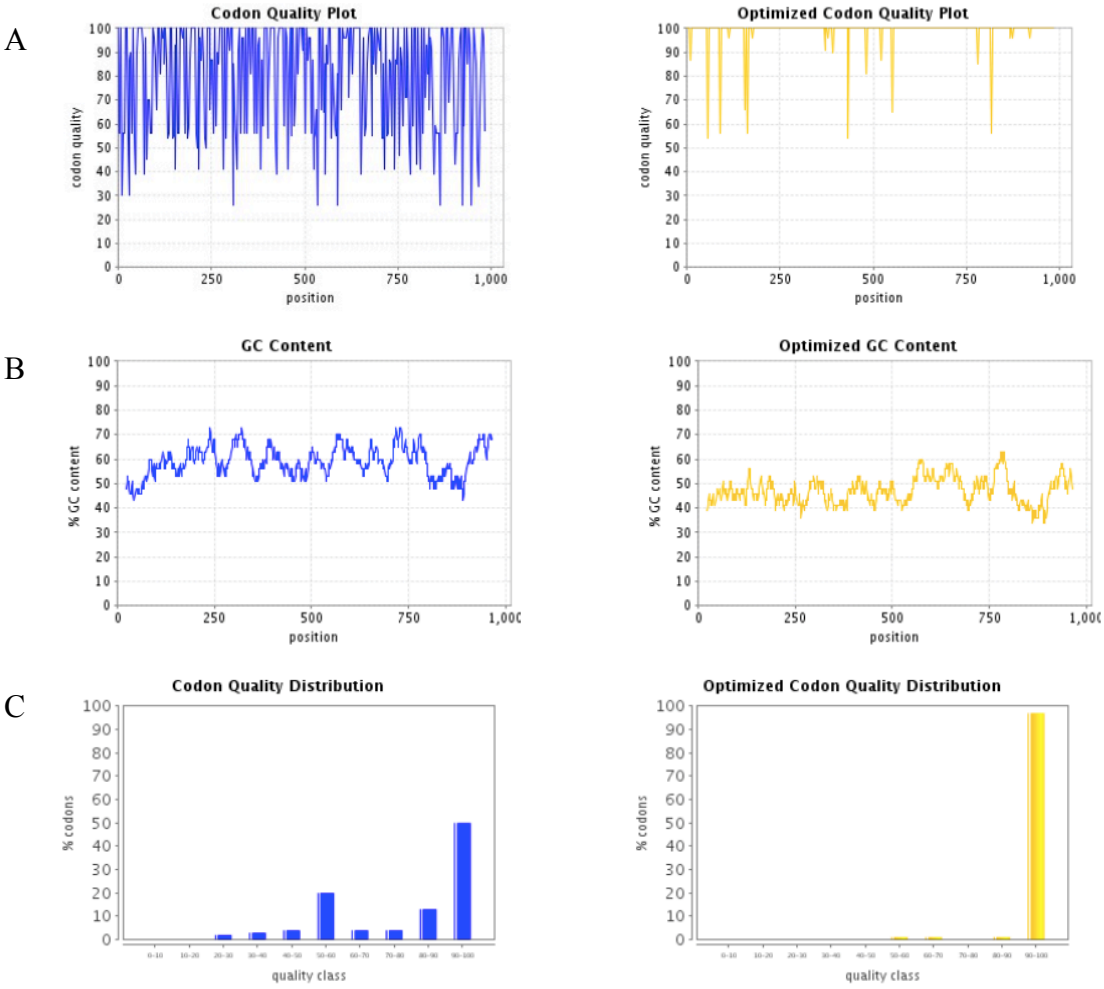

Figure 5.2: Impact of codon optimisation on the nucleotide sequence and expression of mbfA. A: Quality of used codons B: Percentage GC content C: Codon quality distribution. Native (blue) and synthetic (yellow) mbfA gene.

The synthetic *B. suis mbfA* gene was designed with *Nde*I and *Hin*dIII restriction endonuclease sites at the up- and down-stream ends, respectively, allowing excision from the pMA-T plasmid backbone (Figure 5.3A). The excised fragment was ligated into *Nde*I and *Hin*dIII digested pET21a generating pET*ery*CO. The pET*ery*CO construct was confirmed by comparison of the released eryCO fragment size by *Nde*I and *Hin*dIII digestion to that of the gel extracted *Nde*I and *Hin*dIII pMATeryCO fragment (Figure 5.3B). The confirmed pET*ery*CO construct was then transformed into chemically competent BL21(DE3) cells and transformants were selected through resistance to ampicillin.

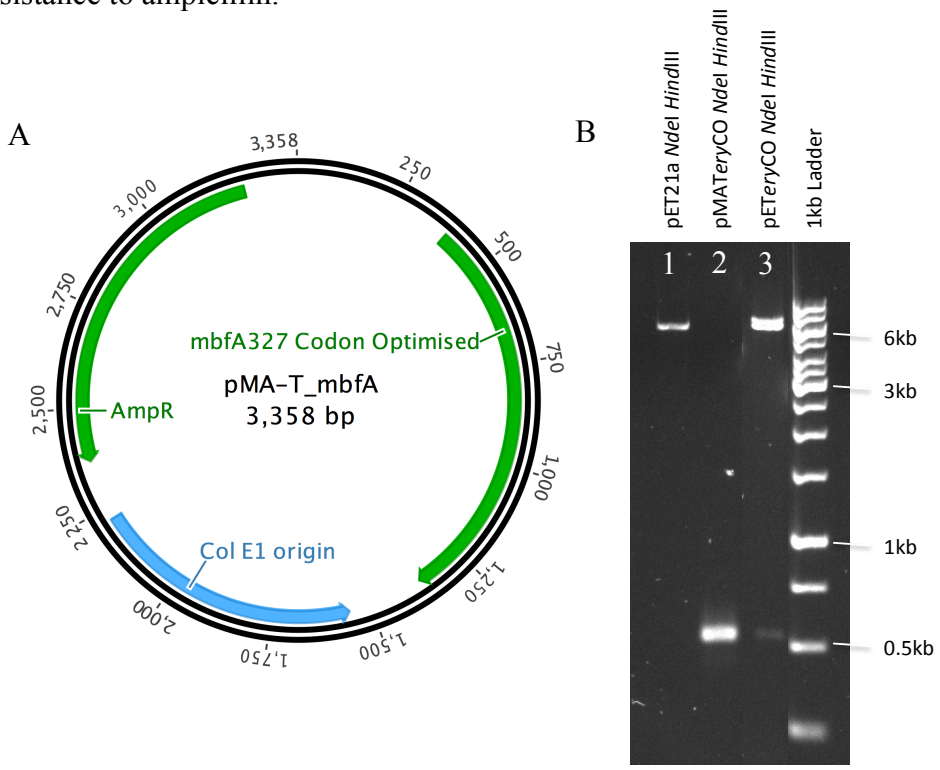

Figure 5.3: Cloning of the codon optimized erythrin domain from *B. suis mbfA* into pET21a.

A: Vector map of pMA-T*mbfA*$_{327}$. B: 0.8% agarose gel of pET*ery*CO cloning substrates and products. Tracks from left to right: 1, gel extracted *Nde*I and *Hin*dIII digested pET21a (~4.6 kb); 2, gel extracted *eryCO* PCR product 524 bp; 3, undigested pET*ery*CO (supercoiled DNA); and 4, *Nde*I and *Hin*dIII digested pET*ery*CO construct showing the released inserted fragment of equal size to the PCR product whilst the second fragment aligns with that of linearised pET21a.

The small-scale over-expression through induction with 0.5 mM IPTG was repeated and expression of recombinant protein was observed when 0.5 optical density units of solublised cell extracts were separated by SDS-PAGE and stained with Coomassie blue (Figure 5.4).

The successful overexpression of recombinant protein through codon optimization of the erythrin coding sequence suggests that the lack of expression observed from the native *Brucella* constructs in *E. coli* BL21(DE3) was due to suboptimal codon usage.

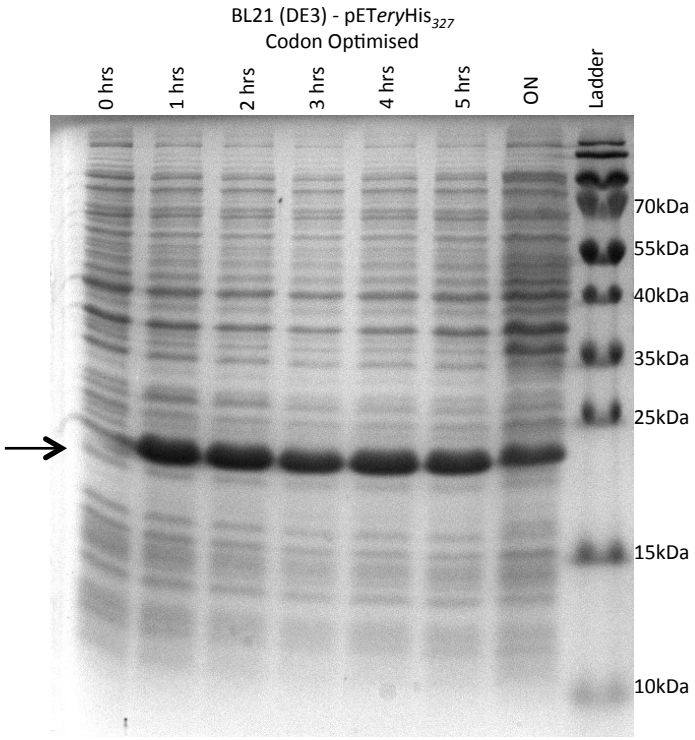

Figure 5.4: SDS-PAGE analysis of codon optimized erythrin domain overexpression from the pETeryCO construct.

16% SDS-PAGE of whole-cell extracts of BL21(DE3) transformed with pET*ery*CO and induced with IPTG at the time intervals indicated. Induced protein expected mass of 21.9 kDa, indicated with arrow.

5.4: Expression of *mbfA* in *E. coli* BL21(DE3) Rosetta

The second approach used to promote expression of *mbfA* from the T7 promoter, conducted alongside the codon optimization approach, was to transform the pET21a constructs into two genetically engineered *E. coli* strains designed to optimise protein expression. These strains were: *E. coli* BL21(DE3)Star, which carries a mutated *rne* gene (*rne131*) that encodes a truncated RNase E enzyme that lacks the ability to degrade mRNA, resulting in an increase in mRNA stability; and BL21(DE3)Rosetta which encodes tRNAs for the codons AUA, AGG, AGA, CUA, CCC, GGA and CGG on a chloramphenicol-resistant pRARE2 plasmid, in *E. coli* BL21(DE3). Small-scale over-expression was repeated and expression of erythrin was observed for all constructs in both *E. coli* BL21(DE3)Rosetta and *E. coli* BL21(DE3)Star (Figure 5.5).

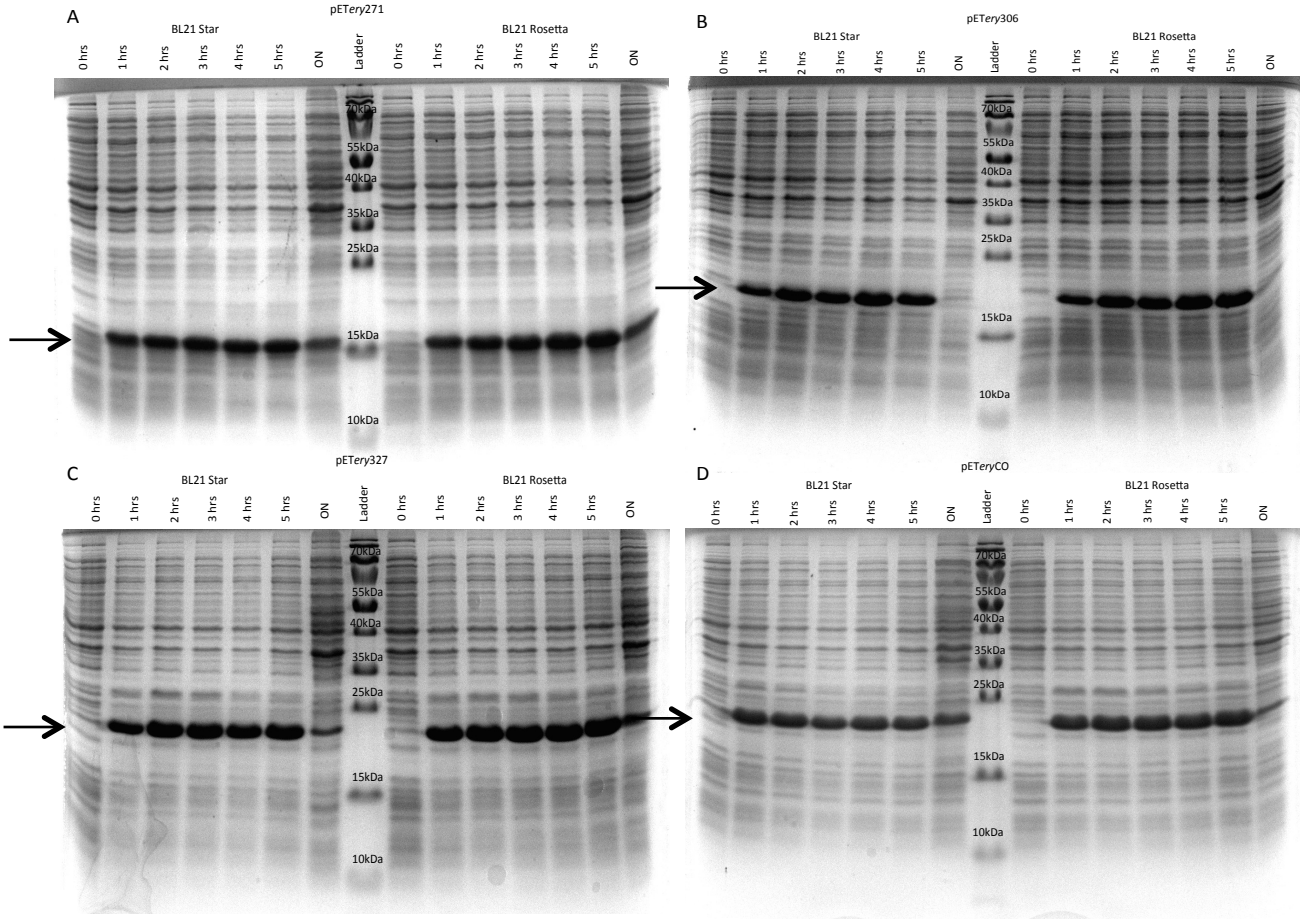

Figure 5.5: SDS-PAGE analysis of erythrin overexpression in *E. coli* BL21(DE3)Star/Rosetta.

16% SDS-PAGE of whole-cell extracts of pET*ery*$_{271}$ (A), pET*ery*$_{306}$ (B), pET*ery*$_{327}$ (C) and pET*ery*CO (D) transformants of *E. coli* BL21(DE3)Star/Rosetta following induction with IPTG for the time periods indicated. Overproduced proteins expected at 14.1, 17.9 and 21.9 kDa, respectively, indicated with arrow.

With confirmation of expression of all erythrin constructs via small-scale over-expression experimentation, through either codon optimization or alteration of *E. coli* expression strain, an estimation of the molecular weight (kDa) of the corresponding protein bands was conducted against a molecular weight marker. A digital image of a Coomassie stained polyacrylamide gel was used to calculate the retention values of each molecular weight marker and the recombinant protein bands, allowing calculation of the approximate molecular weights of the expressed protein (GeneSystem - GBox) (Figure 5.6 and Table 5.1). The approximated molecular weight of each recombinant protein was within a maximum of 1.6 kDa of the predicted molecular weight, suggesting that the observed bands are those of the desired protein.

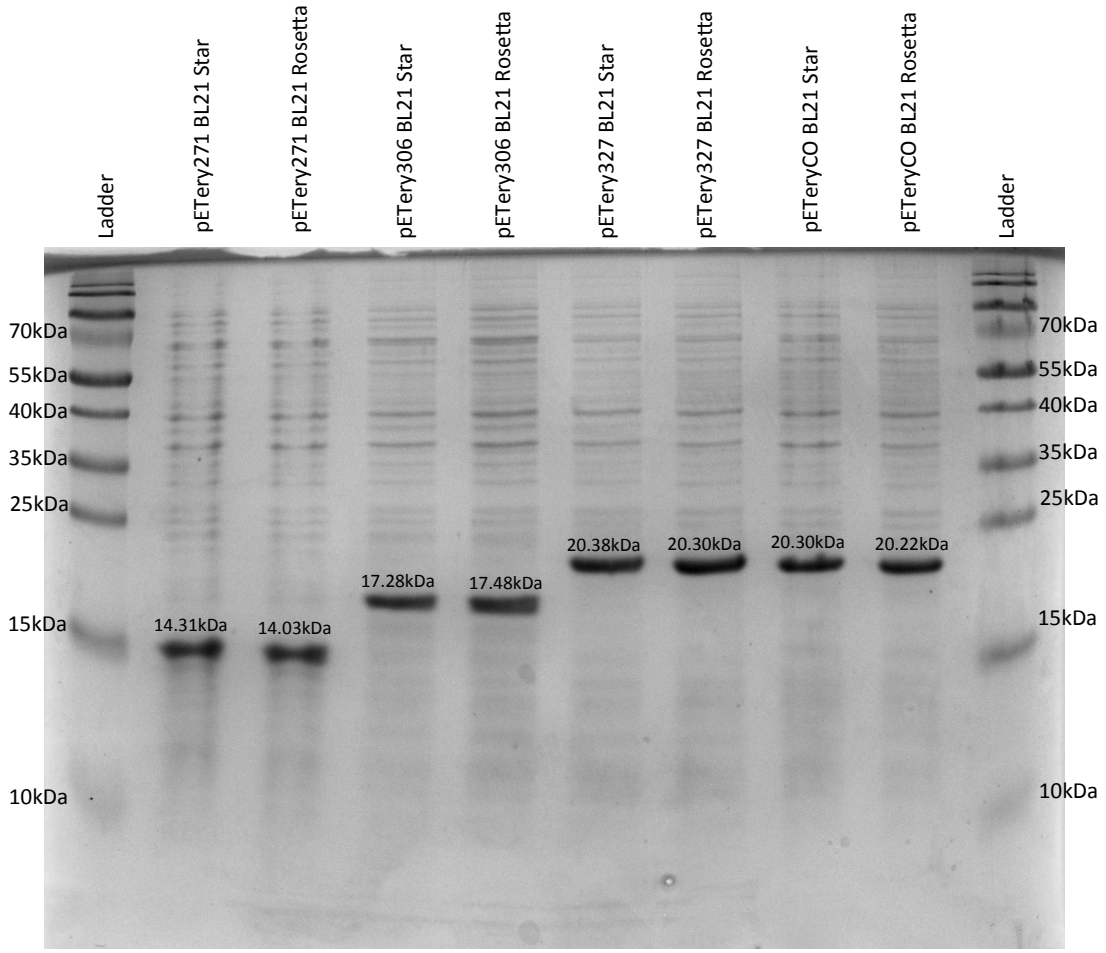

Figure 5.6: SDS-PAGE analysis of erythrin overexpression from native and codon optimized pETery constructs.

16% SDS-PAGE of whole-cell extracts of pET*ery*$_{271}$, pET*ery*$_{306}$, pET*ery*$_{327}$ and pET*ery*CO transformants of *E. coli* BL21(DE3)Star/Rosetta following induction with IPTG. Estimated protein molecular weights displayed.

Table 5.1: Comparison of calculated molecular weights of recombinant protein to predicted molecular weight (kDa).

Erythrin length (AA)	Predicted MW (kDa)	Average calculated MW (kDa)
132	14.1	14.17
167	17.9	17.38
187	21.9	20.34
187	21.9	20.30

5.5: Solubility of recombinant erythrin domain proteins

Before commitment to large-scale overexpression and purification of the erythrin domain variants, the solubility of each was determined. A mild cell lysis reagent (BugBuster - Novagen) was used to rupture the cells, releasing the cytoplasmic contents, whilst not solubilising inclusion bodies. The supernatant (soluble fraction) and pelleted cell debris (insoluble fraction) were collected for each pET*ery* variant expressed in both *E. coli* BL21(DE3)Star and *E. coli* BL21(DE3)Rosetta strains (and *E. coli* BL21/DE3) for the codon optimized construct) after 5 h post induction with 0.5 mM IPTG. The samples were fractionated by SDS-PAGE and compared to whole-cell lysates of the respective transformant strains to compare the relative percentage of soluble and insoluble protein (Figure 5.7).

The truncated erythrin proteins were present almost exclusively in the supernatant of the corresponding over-expressing *E. coli* BL21(DE3) strains, whereas the full length, non-truncated, constructs presented with ~30% of the protein in the insoluble fractions. The proportion of soluble protein obtained was considered acceptable for the purposes of purification.

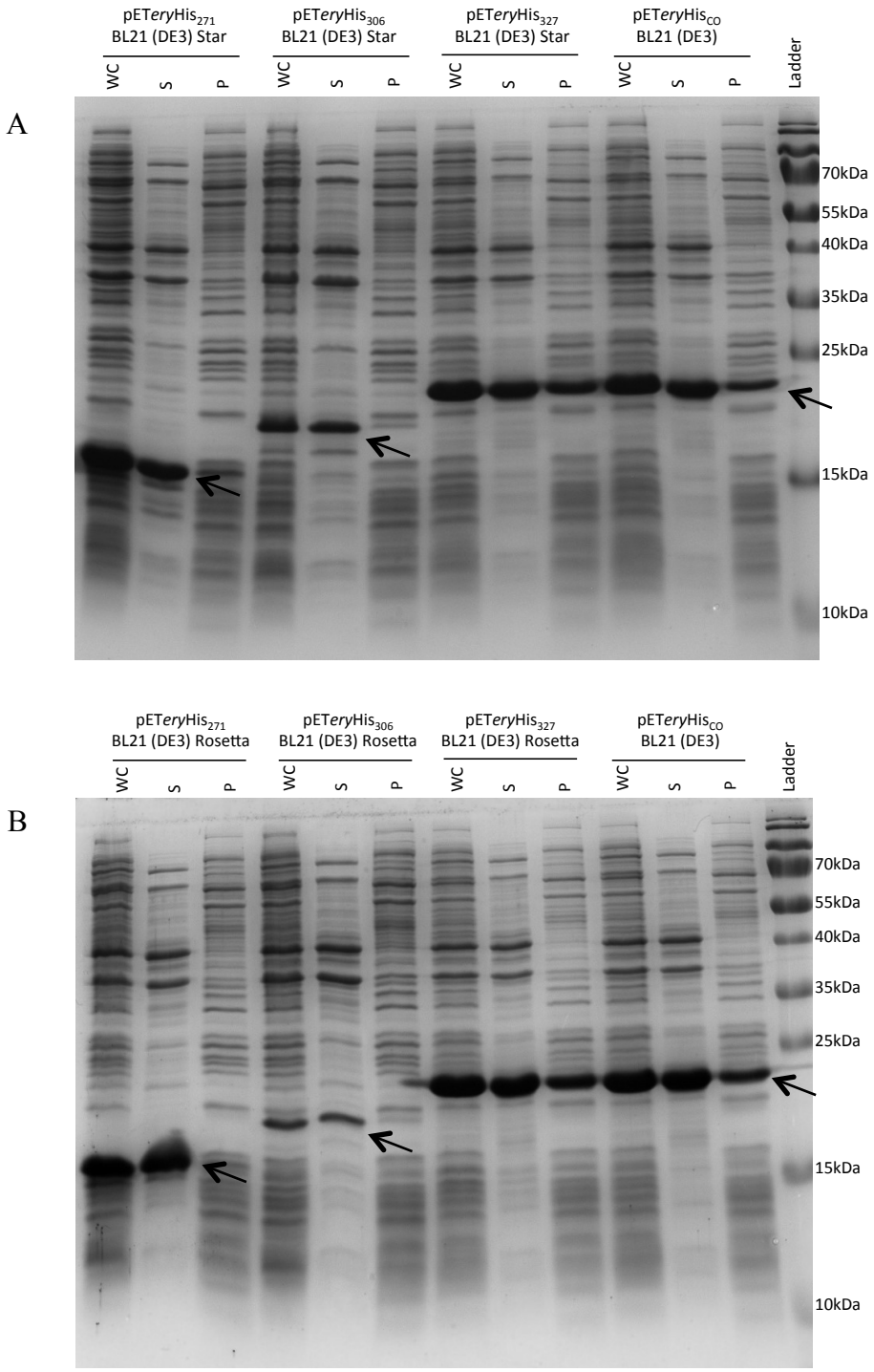

Figure 5.7: SDS-PAGE analysis of relative solubility of recombinant erythrin domain proteins from native and codon optimized pETery constructs.

16% SDS-PAGE of supernatant and pellet fractions of lysed *E. coli* BL21(DE3) strains transformed with pET-BM1*ery*, pET-BM2e*ry*, pET-BS*ery* and pET-BS*ery*CO 5 h post induction. Proteins expected at 14.1, 17.9 and 21.9 kDa, respectively, indicated with arrow.

5.6: Large-scale overexpression of recombinant protein

Upon confirmation of recombinant protein expression and solubility, expression of the 187 amino acid, full length erythrin construct was conducted at a larger scale. Five litres of LB (50 ml in previous experiments) was inoculated with *E. coli* BL21(DE3)Rosetta transformed with pET*ery327*. Cells were harvested by centrifugation at 6000 x g (Sorval RC5B+ with SLA-3000 rotor) for 30 min at 4 °C, 5 h post induction with 0.5 mM IPTG. Pelleted cells were re-suspended in buffer A1 (50 mM Tris and 15 mM imidazole pH 8.0) with 1 mg/ml lysozyme then incubated at room temperature for 1 h with 200 rpm shaking to enable degradation of peptidoglycan by lysozyme. Cells were subsequently cooled on ice for 30 min before sonication (60% amplitude with a 6 mm diameter tip for 15 min) to lyse cells. The cell lysate was centrifuged at 3250 x g (Eppendorf 5810r with A-4-81 rotor) for 20 min at 4 °C three times, collecting clear lysate between each centrifugation step, to remove unlysed cells. The collected lysate was filtered (0.45 μm pore size) before loading onto an equilibrated nickel affinity chromatography column. Washing with buffer A1 facilitated removal of un-tagged proteins until the UV-absorbance of the flow-though had reached a minimal plateau. After maximal removal of non-specific proteins, a linear gradient of buffer A2 (50 mM Tris and 1.0 M imidazole pH 8.0) was applied to the column and 7 ml fractions collected. The eluted fractions displaying a high UV absorption, as displayed by the chromatogram from the nickel affinity column, were separated by SDS-PAGE and stained for total protein with Coomassie blue (Figure 5.8A).

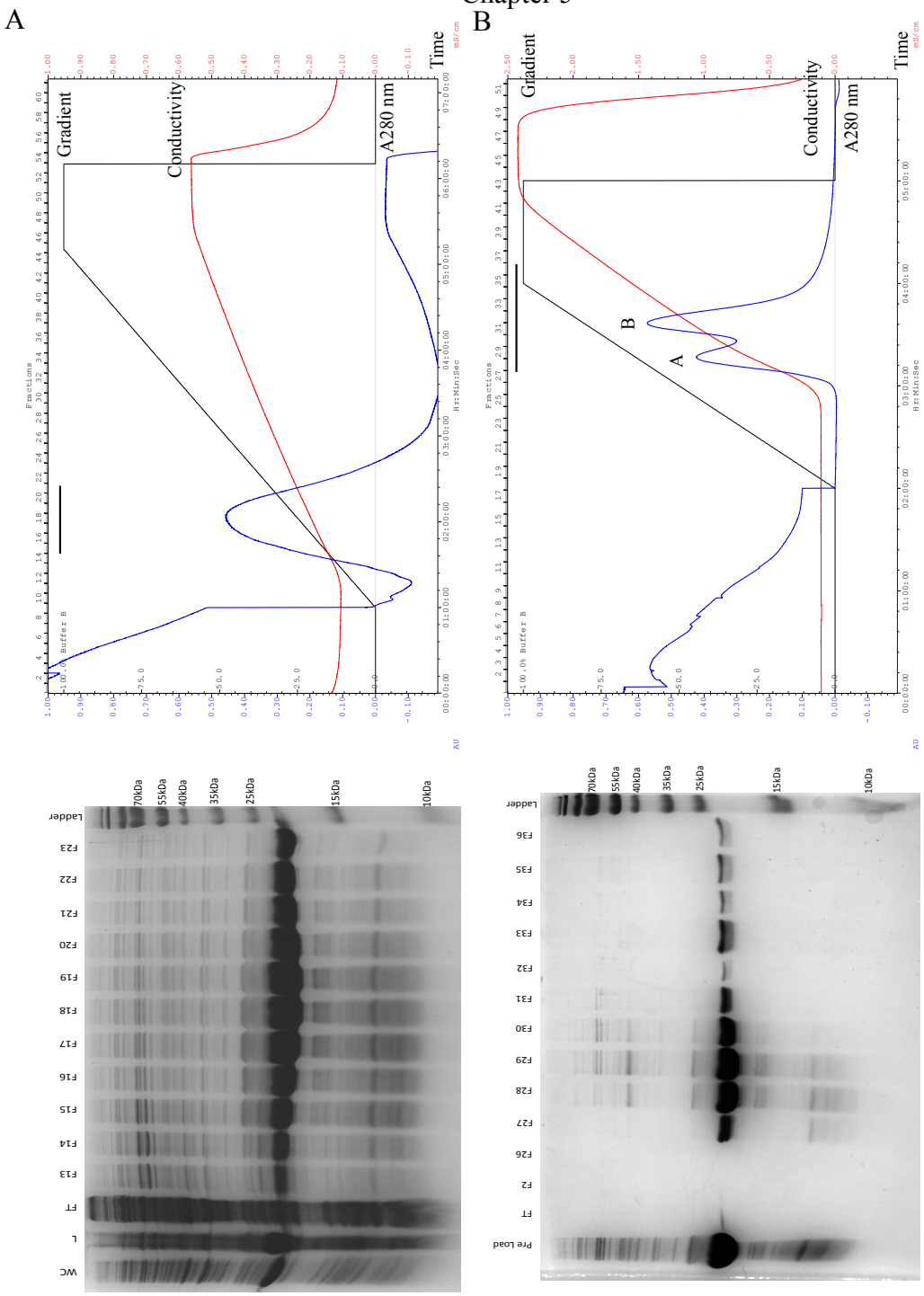

Figure 5.8: Chromatograms and SDS-PAGE analysis of eluted fractions from nickel affinity and anion exchange chromatography.

A: Chromatogram and 16% SDS-PAGE of nickel affinity chromatography purification of erythrin. SDS-PAGE of 0.5 optical density units of whole cells (WC) and cell lysate (L), and 10 µl of flow-through (FT) and fractions 15 to 21. B: Chromatogram and 16% SDS-PAGE of anion exchange chromatography purification of erythrin. SDS-PAGE of 10 µl of pooled fractions 15-21 (the loaded sample), flow-through (FT) and fractions 27 to 36. Buffer gradient (black line), conductivity (mS/cm) (red line), A_{280} nm (blue line). Erythrin peak A/B labeled, pooled fractions indicate by black bar.

5.7: Differential separation of erythrin by anion-exchange chromatography

Eluted fractions 15 to 21 from the nickel affinity column, which displayed a high recombinant protein content when analysed by SDS-PAGE, were pooled together to give a final volume of 49 ml. The semi-purified sample was loaded onto an equilibrated diethylaminoethyl (DEAE) anion-exchange chromatography column (25 x 140 mm). The column was washed (buffer B1 – 50 mM Tris pH 8.0) and a linear gradient of buffer B2 (50 mM Tris and 1.0 M NaCl pH 8.0) was applied to the column over a volume of 240 ml, and 7 ml fractions collected. The chromatogram displayed a differential separation of the recombinant protein. The first minor absorption peak corresponded to a larger quantity of eluted protein, as assessed by SDS-PAGE and Coomassie blue staining, whereas, the second, larger absorption peak surprising displayed a lower quantity of protein (Figure 5.8B). The separated eluted proteins were pooled according to their respective peaks; peak A, fractions 27-31 (35 ml) and peak B, fractions 32-36 (35 ml).

One explanation for the differential separation of the erythrin domain is that holo-erythrin (metal bound) may result in alterations to the tertiary structure and/or surface charge of the protein due to metal binding, exposing more positively charged residues to the stationary phase of the anion-exchange column. This would result in a higher ionic strength of eluent being required to dissociate the protein from the stationary phase, resulting in a delayed elution time from the DEAE column. This hypothesis predicts that the high UV absorbance observed in peak B from DEAE chromatography is due to the binding of metals to the erythrin domain. Transition metals, including iron and zinc, strongly absorb UV light (Table 5.2), and would therefore give artificially increased approximations to protein concentrations when calculated from 280 nm absorbance using spectroscopic analysis with a Nanodrop spectrophotometer. Therefore, calculations of metal-bound erythrin concentrations were made via Bradford assay to approximate protein concentration dependent on the amino acid composition.

Table 5.2: UV absorption of Group four transition metals (provided by University of Reading, Department of Soil Sciences)

Group 4 Transition Metal	λmax (nm)
Manganese (Mn)	257.610
Iron (Fe)	238.204
Cobalt (Co)	230.786
Nickel (Ni)	231.604
Copper (Cu)	324.752
Zinc (Zn)	213.857

Analysis of the protein concentration of each sample when determined spectroscopically with the Nanodrop ND-1000 or via a Bradford assay (BSA standard curve), before and after concentration using a Vivaspin-20 (3,000 MWCO, erythrin domain 21,989 MW) centrifugal concentrator (Satorius Stedim Biotech) (Table 5.3), demonstrated the excessively high estimations of peak B protein concentration by 280 nm absorption. The concentration of protein in peak A (expected low metal content) displayed a difference of 3.8- and 2.9-fold, pre and post concentration, between Nanodrop and Bradford assays. In contrast, the concentration of peak B protein (expected high metal content) displayed a difference of 8.5- and 12.75-fold, pre and post concentration, between the Nanodrop and Bradford assays.

Table 5.3: Concentration of recombinant protein before and after centrifugal concentration

	Pre-concentration			Post-concentration		
	Volume ml	**ND mg/ml**	**Bradford mg/ml**	**Volume ml**	**ND mg/ml**	**Bradford mg/ml**
Ery Peak A	70	0.5	1.9	15	3.1	9.0
Ery Peak B	70	0.34	0.04	15	2.55	0.2

*ND – Nanodrop

5.8: Amino acid analysis (AAA) of His-tagged erythrin

To add additional confirmation that the purified protein was His-tagged erythrin, amino acid analysis (Alta Bioscience) of the pooled fractions post nickel affinity and anion exchange chromatography was conducted. Amino acid analysis is considered to be the golden standard analysis for accurate quantitation of proteins and can be used to very accurately determine the quantity of purified proteins in a manner that is not biased by differences in amino acid composition.

A 5 ml aliquot of erythrin was dialysed into 20 mM HEPES pH 7.0 to allow removal of NaCl added during the anion exchange chromatography step and the concentration was then estimated via Bradford assay at 2.87 mg/ml. To determine the amino acid composition of the sample, hydrolysis with 5.7 N HCl and a small amount of phenol under vacuum was conducted for 22-24 h at 110 °C. Hydrolysis can have varying effects on different amino acids: asparagine and glutamine are converted to their corresponding acids (aspartic acid and glutamic acid), therefore cannot be measured independently within the sample, whereas tryptophan is completely destroyed by the hydrolysis process. The sample was then dissolved in distilled water containing EDTA (to chelate metal ions) before commitment to derivatisation and high performance liquid chromatography (HPLC) by the amino acid analyzer. Derivatisation reacts the free amino acids, under basic conditions, with phenylisothiocyanate (PITC) to produce phenylthiocarbamyl (PTC) amino acid derivatives that can be separated by HPLC; a reverse phase C18 silica column allows detection of the PTC chromophore at 254 nm. Chromatographic peaks are identified and quantitated allowing determination of the amount of amino acid (in nmole/ml) in the sample.

The quantity of each amino acid in the sample was used to determine the percentage frequency of that amino acid as a percentage of the sum of the total protein concentration. The quantity of each amino acid was subsequently used to calculate the molecular weight it contributes to the total molecular weight of the protein (Table 5.4). The concentration of protein in the submitted sample was 0.927 mg/ml, 3.1 fold lower than the estimate obtained by Bradford assay. This discrepancy will be used in future parts of this thesis to correct protein concentrations obtained by Bradford assays to give a true estimate of protein concentration. The calculated MW of the erythrin protein was 21.829 kDa, 122 Da less than the expected molecular weight (21.951 kDa).

Table 5.4: Amino acid analysis. Supplied data from amino acid analysis highlighted in grey.

	Theoretical			AAA Calculation				
	Freq (AA)	MW (Da)	Sum MW (KDa)	nmole/ml	ug/ml	Freq (%)	Freq (AA)	MW (KDa)
Alanine	22	71.0779	1.564	988	70.22	12.35	23.09	1.641
Asp/Asn	18	115.0874	2.072	762	87.70	9.52	17.81	2.050
Glu/Gln	30	128.1292	3.844	1220	156.32	15.25	28.52	3.654
Phenylalanine	8	147.1739	1.177	313	46.07	3.91	7.32	1.077
Glycine	5	57.0513	0.285	259	14.78	3.24	6.05	0.345
Histidine	12	137.1393	1.646	607	83.24	7.59	14.19	1.946
Isoleucine	8	113.1576	0.905	534	60.43	6.67	12.48	1.412
Lysine	9	128.1723	1.154	404	51.78	5.05	9.44	1.210
Leucine	15	113.1576	1.697	737	83.40	9.21	17.23	1.949
Methionine	3	131.1961	0.394	91.2	11.97	1.14	2.13	0.280
Arginine	22	156.1857	3.436	802	125.26	10.02	18.75	2.928
Proline	6	97.1152	0.583	210	20.39	2.62	4.91	0.477
Serine	13	87.0773	1.132	424	36.92	5.30	9.91	0.863
Threonine	3	101.1039	0.303	146	14.76	1.82	3.41	0.345
Valine	6	99.1311	0.595	303	30.04	3.79	7.08	0.702
Tyrosine	6	163.1733	0.979	200	32.63	2.50	4.67	0.763
Tryptophan	1	186.2099	0.186	0	0	0	0.00	0.186
Total	187		21.951	8000.2	925.90	100.00	187	21.829

5.9: Identification and quantification of metals bound to erythrin and recreation of di-iron centred erythrin

To determine the stoichiometric concentrations of metals bound to the purified erythrin domain, aliquots of peak A, peak B and apo-erythrin (metal free) were analysed by inductively-coupled plasma optical-emission spectroscopy (ICP-OES) and electrospray-ionisation-coupled mass spectroscopy (ESI-MS). Apo-erythrin was generated by the removal of bound metals via chelation from peak A erythrin by treatment with 1 mM diethylenetriaminepentaacetic acid (DTPA - non-specific transition metal chelator), 1 mM 2,2'-dipyridyl (specific ferrous iron chelator) and 2 mM sodium dithionite (reductant). The metal chelates were subsequently removed through dialysis against 20 mM (4-(2-hydroxyethyl)-1-piperazineethanesulfonic acid) (HEPES) pH 7.0.

Di-iron carboxylate proteins, such as the erythrin domain, are able to bind iron atoms (as well as other group four transition metals including; manganese, cobalt, nickel, copper and zinc) with a stoichiometry of two (Nordlund and Eklund 1995). It is therefore expected that divalent metals will associate with the di-iron binding motifs of the recombinant protein during expression in *E. coli.* However, it is unclear whether iron will have been incorporated with the highest stoichiometry into the erythrin domain, due to the low concentration of free iron maintained within *E. coli* (10 μM) and potential binding to other metals. Additional divalent transition metals such as zinc, which, although present at lower concentrations within the cytoplasm compared to iron, are also able to bind metalloproteins when over-expressed in *E. coli*. As indicated by the Irving-Williams series (Irving and Williams 1953), zinc has a higher binding affinity than iron so is able to outcompete iron for iron binding sites within proteins.

ICP-OES analysis was conducted with 0.0125 mg/ml (predicted metal ion concentration of 25 ppm - due to a predicted two metal atoms per protein monomer) of peak A, peak B and an apo-erythrin samples, using a Perkin Elmer Optima 7300 ICP-OES instrument in the School of Soil Sciences at the University of Reading (Figure 5.9).

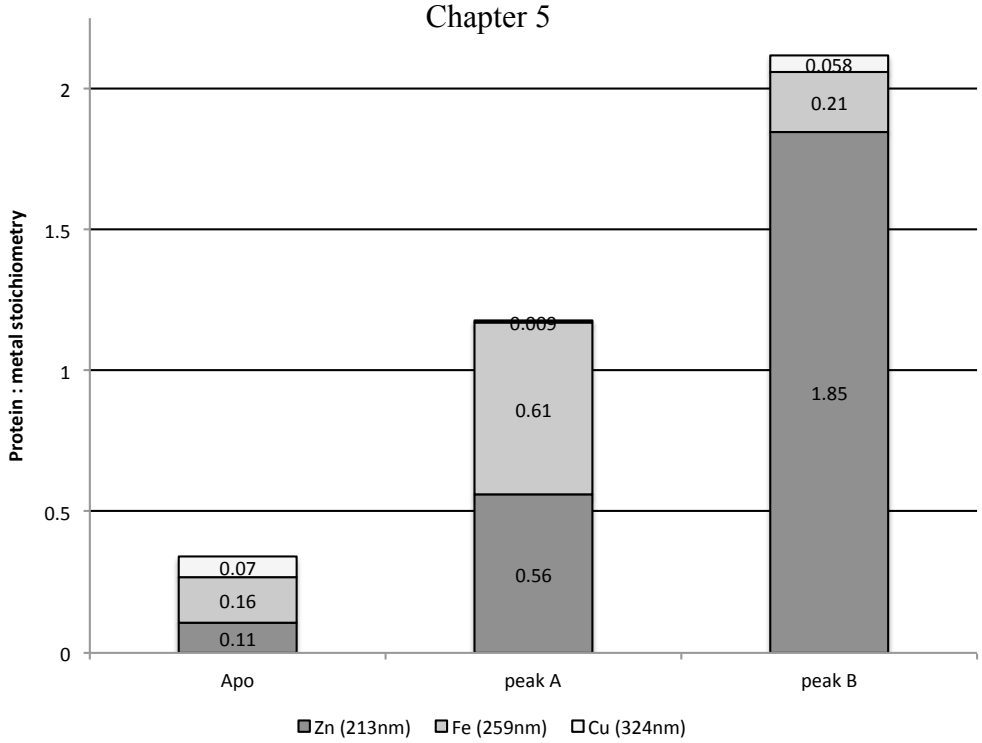

Figure 5.9: ICP-OES analysis of peak A, peak B and apo-erythrin.
Stoichiometric concentrations of transition metals bound to peak A, peak B and apo-erythrin when analyzed via ICP-OES.

Analysis of the three samples revealed that chelation and dialysis effectively removes bound metals from the peak A erythrin sample. Peak A erythrin had a mixed occupancy of zinc and iron in equal stoichiometry (~0.6 and 0.6 per protein molecule), whilst zinc was bound with much higher stoichiometric levels in peak B erythrin with an approximate stoichiometry of two (with very little iron apparent), suggesting the formation of a di-zinc form of erythrin. These data support the suggestion that differential separation observed with DEAE chromatography is based upon metal occupancy and that the erythrin domain binds a maximum of 2 metal atoms per monomer.

Upon creation of the apo-erythrin (originating from peak A) its binding capacity for ferrous iron was then determined. Anaerobically prepared (N_2 purged) 10 mM ferrous ammonium sulphate was titrated against 30 μM of apo-erythrin and measurements of UV-visible absorption (200-500 nm) at sub-stoichiometric iron concentrations were recorded with a Unicam Helios alpha spectrophotmoter (Figure 5.10A). Titration with Fe^{2+} resulted in a linear increase in UV absorbance (λmax ~265 nm) up to two iron atoms per protein monomer (Figure 5.10B/C), suggesting the formation of the di-iron centre.

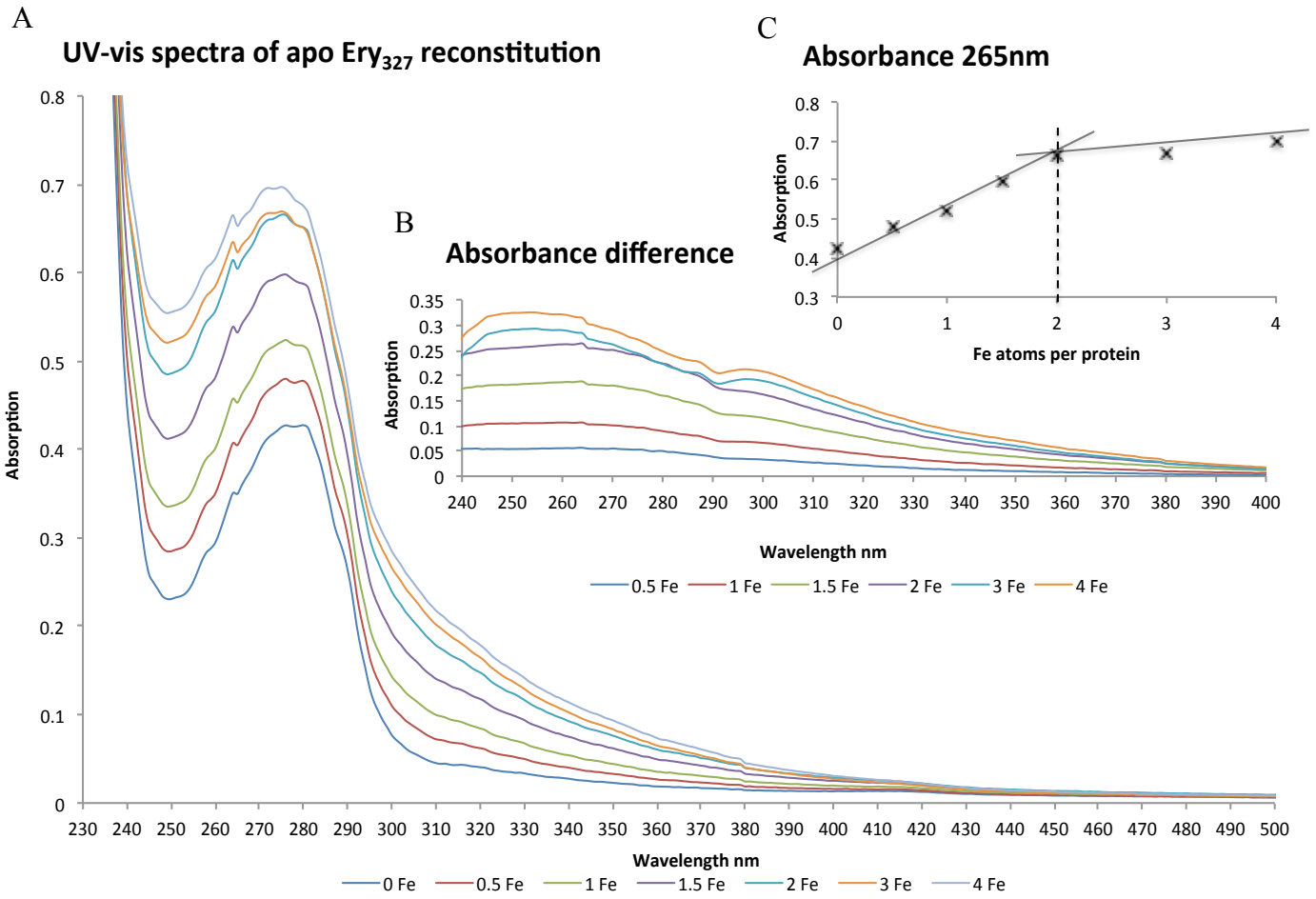

Figure 5.10: UV-visible spectroscopy of titration of apo-EryHis with ferrous iron. A: UV-visible spectrum from 200-500 nm of sub-stoichiometric concentrations of ferrous iron titrated against 30 μM apo-Ery. B: absorbance difference of apo-EryHis following iron addition. C: comparison of absorbance change at 265 nm with addition of ferrous iron. A linear increase in A_{265} of ~0.125 A units per Fe atom equivalent is observed, for up to two atoms per protein, after which the degree of increase is diminished (to just ~0.0125 A unit per Fe atom equivalent) with further iron addition.

To generate substantial quantities of di-iron erythrin, a four-fold excess of ferrous ammounium sulphate was added to 10 ml of the apo-erythrin and incubated on ice for 2 h. Excess, unbound iron was then removed by dialysis against 20 mM HEPES pH 7.0, and to ensure metal stoichiometry, an aliquot was submitted for ICP-OES analysis (Figure 5.11).

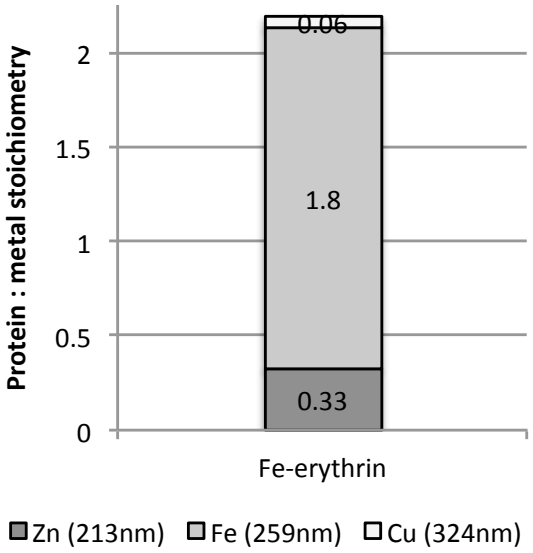

Figure 5.11: ICP-OES analysis of diiron-erythrin.
Stoichiometric concentrations of transition metals bound to Fe-erythrin analyzed by ICP-OES.

A comparison of the UV-visible absorbance spectrum (200-400 nm) of 2 µM apo, diiron and dizinc (peak B) erythrin variants conducted with the Unicam Helios alpha spectrophotometer at room temperature in 20 mM HEPES pH 7.0 (Figure 5.12). Absorbance of apo-erythrin was consistently less than 0.1 absorbance units, whereas, saturation with iron and zinc resulted in increased absorption. Di-Zn erythrin gave maxima of 0.48 at 210 and 0.12 at 260 nm whilst di-Fe erythrin gave maxima of 0.35 at 210 and 0.18 at 260 nm. The absorbance of the iron-saturated erythrin at visible wavelengths was reflected by the observation of a clear yellow-coloured solution.

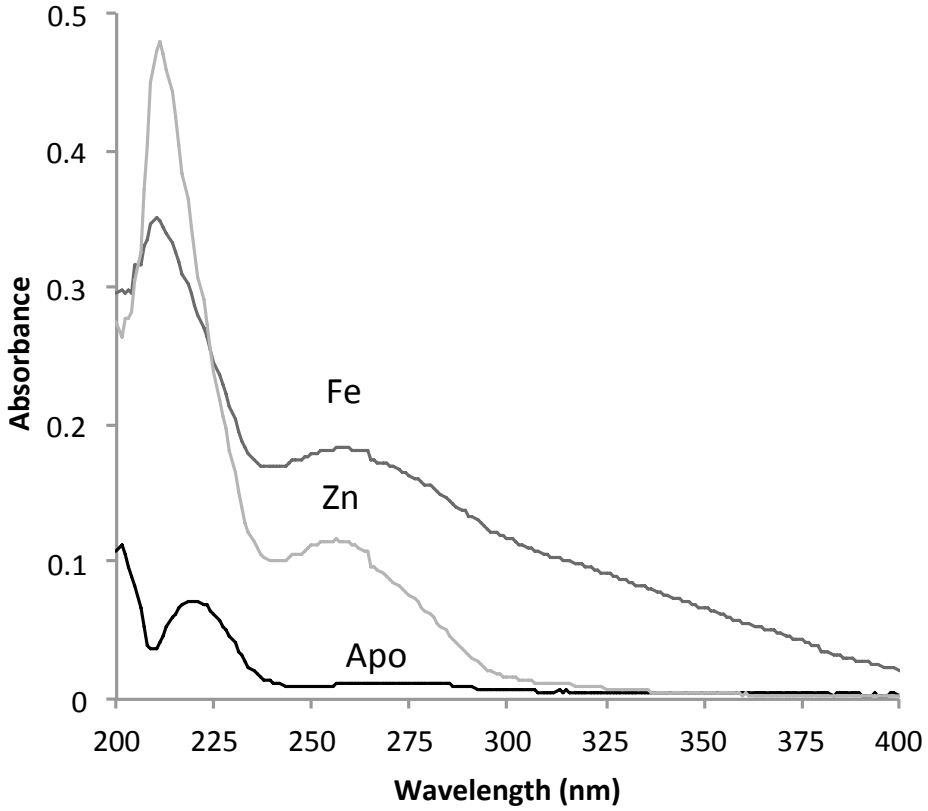

Figure 5.12: UV-visible spectroscopy of apo-, di-Fe- and di-Zn-erythrin (peak B). Spectra were recorded at 200-400 nm, with a 1 nm band width and scan rate of 1 nm/s. Proteins were at 2 μM in 20 mM HEPES pH 7.0.

To accurately determine the intact mass of the peak A, peak B apo, diiron and dizinc forms of the recombinant erythrin protein and to confirm the presence of the bound metals, 50 μg (100 μl) samples of protein dialysed into 50 mM ammonium acetate were submitted for analysis with the Thermo Fisher Velos Orbitrap with Electron Transfer Dissociation at the Advanced Mass Spectroscopy Facility at the University of Birmingham. Samples were analyzed via electro-spray ionization mass spectroscopy (ESI-MS) which allows the mass determination of macromolecules including proteins, as it is a 'soft ionization' technique which prevents the fragmentation of these molecules during ionization.

Analysis of peak A (found to be largely metal free by ICP-OES) revealed three distinct mass/charge peaks, deconvolution of this data allowed determination of their masses as 21988.09, 22052.00 and 22115.91 Da (Figure 5.13A). The smallest mass (21988.08)

represents the apo-protein presenting as 1.56 Da less that the theoretical mass (21989.64 Da) of the 188 amino acid His-tagged erythrin protein. The second mass peak, 22052.00 Da, of 80% relative abundance has a difference of 63.91 Da compared to the apo-protein, which represents the approximate weight of a single zinc atom (65.38 Da). The third mass peak, 2215.91 Da, of 45% relative abundance has a difference of 127.82 Da compared to the apo-protein and represents the approximate weight of two zinc atoms (130.76 Da). The selection of Zn as the metal associated with the erythrin is based upon the ICP-OES data suggests that high concentrations of zinc, and not other metals (such as copper and iron) are present within this sample. Together this data equates to the approximate stoichiometry of one metal atom per protein molecule which is consistent with that observed by ICP-OES.

Mass spectroscopy analysis of peak B (suspected dizinc-erythrin according to the ICP-OES data) indicated a single distinct mass/charge peak which upon deconvolution revealed a mass of 22115.89 Da (Figure 5.13B). This mass is 127.8 Da greater than that of the apo-protein form identified for the peak A sample and again represents the approximate weight of two zinc atoms (0.02 Da difference between respective dizinc erythrins). It should be noted that the MS analysis gave no evidence of a dimeric (or any other multimer) form suggesting that the erythrin domain is monomeric in nature. This is in contrast to the observations made by (Sankari and O'Brian 2014) for the equivalent domain of MbfA from *B. japonicum*, which was found to be dimeric according to gel filtration chromatography analysis.

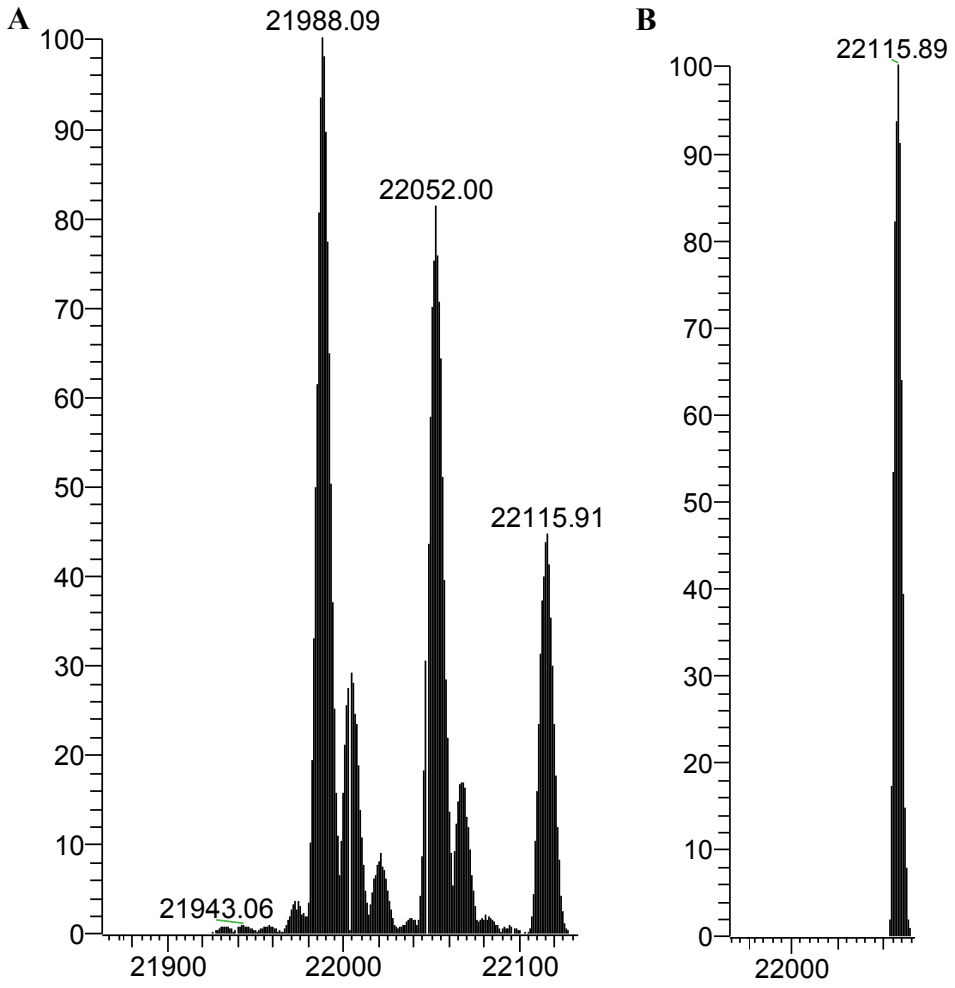

Figure 5.13: ESI-MS analysis of peak A and peak B (dizinc).

Electrospray ionization analysis of whole protein masses of protein-metal species present in peak A (A) and peak B (B).

Lastly analysis of the diiron-reconstituted erythrin (anaerobic ferrous ammonium sulphate addition to previously chelated protein) by ESI-MS revealed a single distinct mass/charge peak, which upon deconvolution reveals a mass of 22101.82 Da (Figure 5.14). This mass is 113.73 Da greater than that of the apo-protein identified in the peak A sample. This difference in mass represents the approximate weight of two iron atoms (Fe: 55.85 Da; 2 Fe: 111.7 Da) and suggests that two iron atoms are bound (matching the ICP-OES data), most likely at the di-iron binding site.

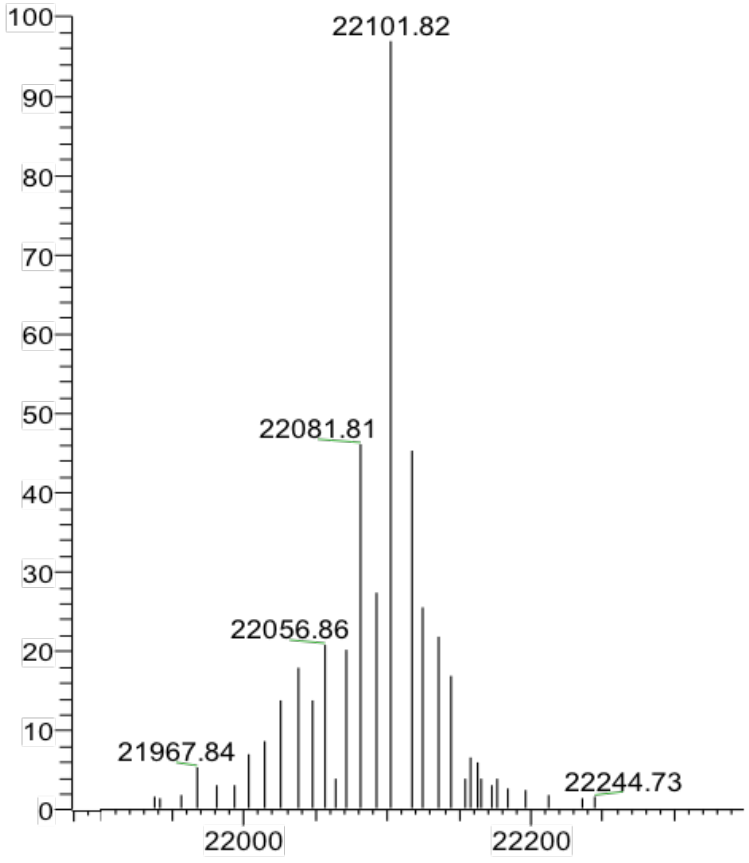

Figure 5.14: ESI-MS analysis of diiron-erythrin.

Electrospray ionization analysis of whole protein masses of protein-metal species present in di-iron reconstituted erythrin.

5.10: Reduction and oxidation of purified diFe-Erythrin

The current model suggests that ferrous iron export from the cytosol of the bacterial cell by MbfA is facilitated by the movement of electrons from the exported iron atoms thus converting the iron to the ferric form. The released electrons are thought to reduce the iron atoms of the diiron centre of the erythrin domain generating a di-ferrous centre. The reduced iron centre can then be oxidized back to the ferric form, in the process reducing harmful cellular peroxides. In an attempt to provide support for this mechanism, the redox activity of the erythrin diiron centre was assessed spectroscopically through reduction with sodium dithionite followed by oxidation by hydrogen peroxide to the erythrin domain (Figure 5.15).

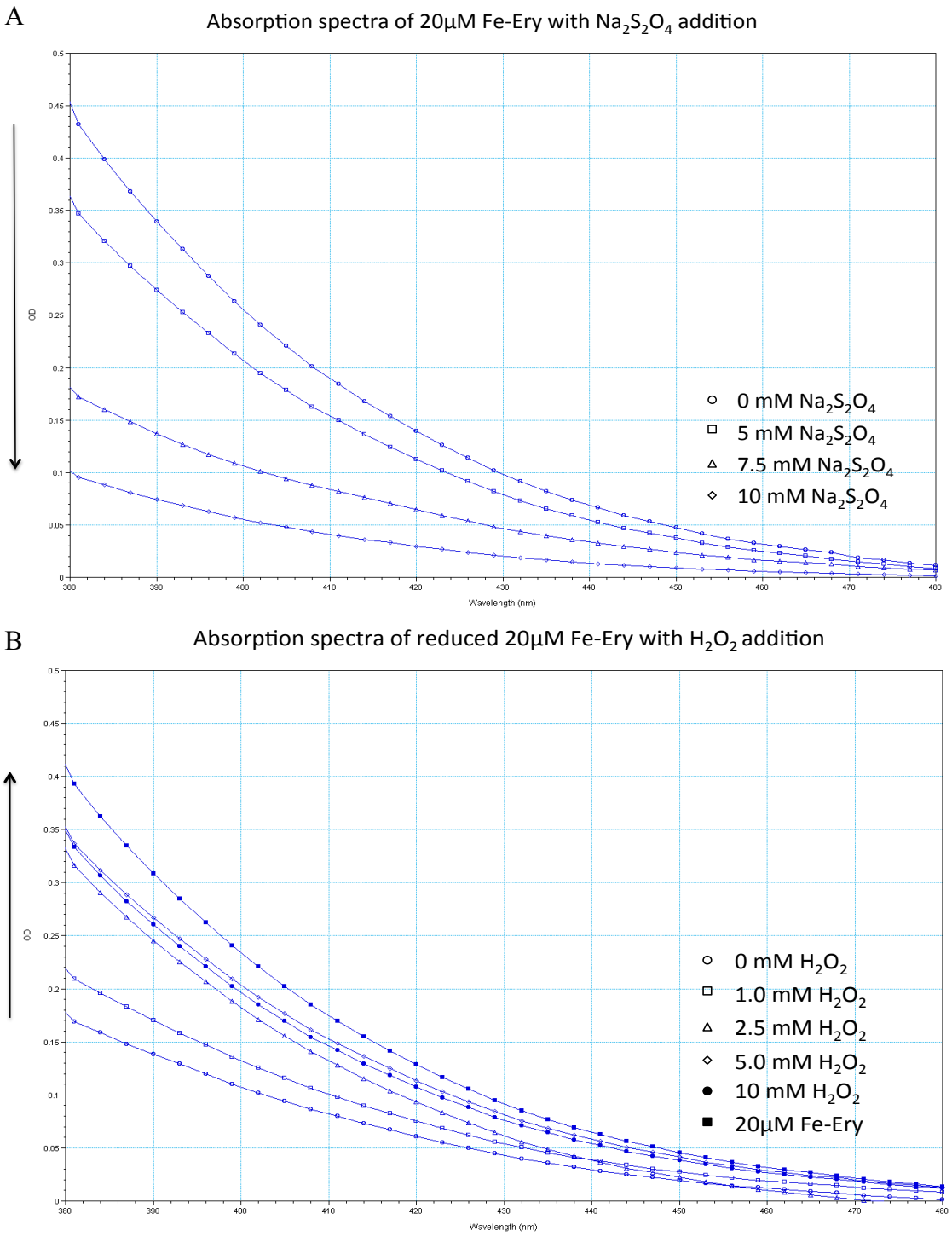

Figure 5.15: Spectroscopic measurement of erythrin reduction and oxidation. UV-visible spectroscopy of reduction (A) and oxidation (B) of 20 µM Fe-erythrin in 20 µM HEPES pH. 7.0 through addition of sodium dithionite followed by addition of hydrogen peroxide respectively. Experimentation conducted at room temperature.

The absorbance of visible light between 380 and 480 nm was observed to decrease for each addition of sodium dithionite, resulting in the yellow protein becoming colourless as the di-ferric centred erythrin domain was presumed to be reduced to a di-ferrous state. The fully reduced protein was then titrated with hydrogen peroxide, which resulted in an increase in absorbance back to the original absorbance of the untreated protein as the di-ferric center was presumed to be re-formed.

Interestingly, oxidation of the di-ferrous centred erythrin was also observed without the addition of hydrogen peroxide. Kinetic spectroscopy at 380 nm over a 10 min time course displayed that oxidation of the di-ferrous centre was possible with atmospheric oxygen as well as hydrogen peroxide (Figure 5.16).

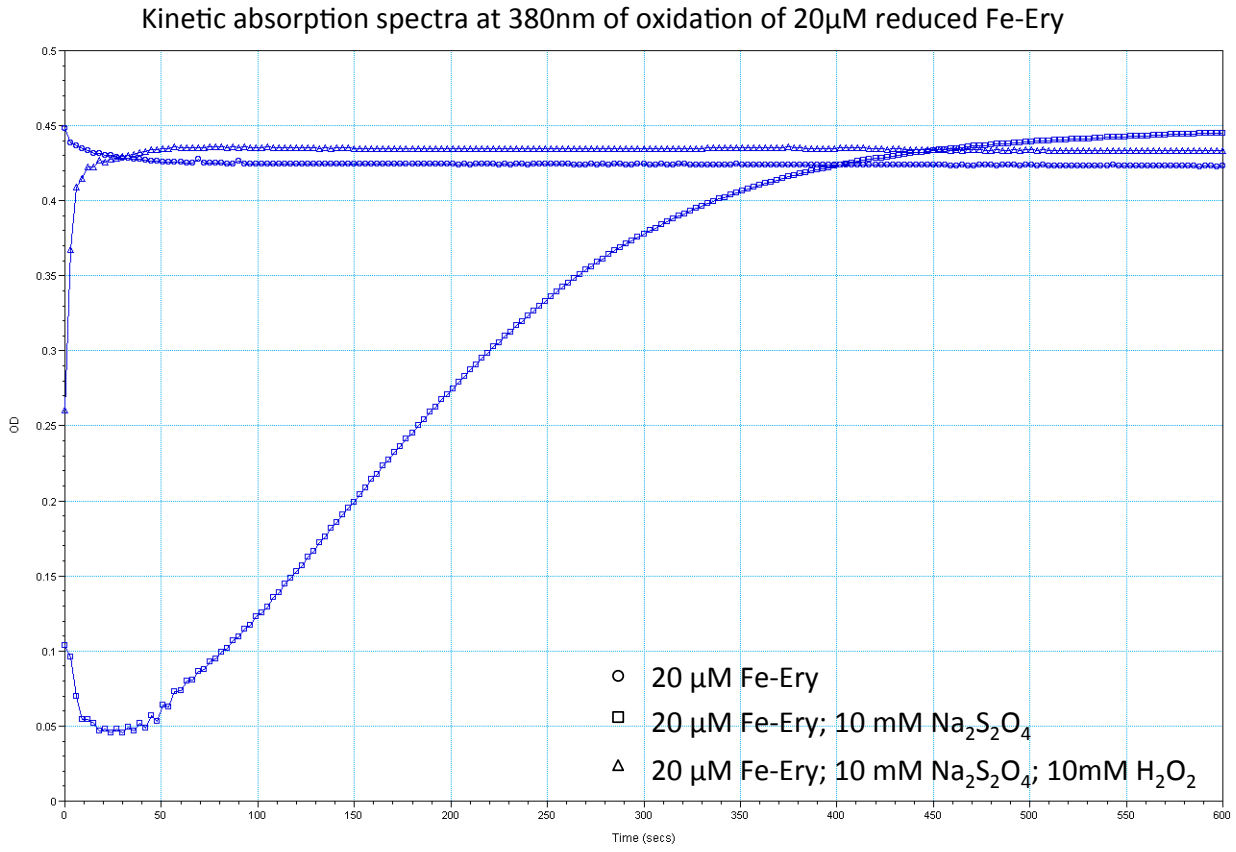

Figure 5.16: Oxidation of reduced erythrin with hydrogen peroxide or molecular oxygen.

Change in absorbance at 380 nm over time arising from the oxidation of 20 µM reduced Fe-erythrin by hydrogen peroxide or oxygen, at room temperature.

The time taken for the fully reduced di-ferrous centre to become oxidized by 10 mM hydrogen peroxide was ~50 s, whereas oxidation via atmospheric oxygen took ~10 min, 12 times slower. In both, cases the absorbance of fully oxidized protein was equivalent to that of the control non-reduced sample which suggests that the di-Fe centre can undergo redox cycling without loss of integrity.

The creation of a redox sensitive di-iron centered erythrin prompted analysis of the proposed peroxide reductase activity that this domain of the MbfA protein possesses and comparison to apo-EryHis and the as-isolated di-zinc erythrin (peak B). Peroxide reductase activity was measured by kinetic UV-vis spectroscopy through reduction in absorbance at 240 nm (wavelength at which hydrogen peroxide strongly absorbs UV light) over time. 10 μM of each protein was exposed to excess (10 mM) hydrogen peroxide but no change in 240 nm absorbance was observed, suggesting that no peroxide reductase activity is present (data not shown).

This *in vitro* examination of peroxide reductase activity was not successful due to the requirement of a source of electrons providing a route for re-reduction of the di-iron center, which would normally be supplied within the *in vivo* environment.

5.11: Additional purifications of recombinant erythrin protein

The erythrin protein was purified a further two times during the course of this project to generate sufficient quantities and concentration of protein to allow for the completion of all conducted biochemical assays, including: recreation of a di-iron centre, UV-visible spectroscopy, ICP-OES studies and ESI-MS, thermal shift assays, crystallization trials and amino acid analysis.

A second purification of the His-tagged erythrin domain of MbfA was conducted using the same methods described previously. After collection of eluted protein from anion exchange chromatography, the as-isolated bound metals were removed from all protein via chelation, and the metal-chelates were removed by dialysis against 20 mM HEPES pH 7.0, as before.

The generated apo-erythrin sample was split into two aliquots, one was left as apo-erythrin the second was committed to generating a di-iron centred form. To generate the di-iron centred erythrin, an estimate of the concentration of the apo-erythrin was determined via a Bradford assay and adjusted based upon variation between Bradford assay and amino acid analysis. Addition of a 10-fold excess of anaerobic ferrous ammonium sulphate was made to the protein solution. An increase in absorbance was apparent within seconds after addition of ferrous iron, with a yellow colour intensifying with incubation over two hours, suggesting oxidation of iron during incorporation into the iron binding site – an indication of ferroxidase activity. Excess unbound iron was removed by dialysis against 20 mM HEPES pH 7.0.

To further facilitate purification and examine differences between the apo and di-iron erythrin; the apo- and diiron-erythrin samples were subjected to a second round of anion exchange chromatography (Figure 5.17).

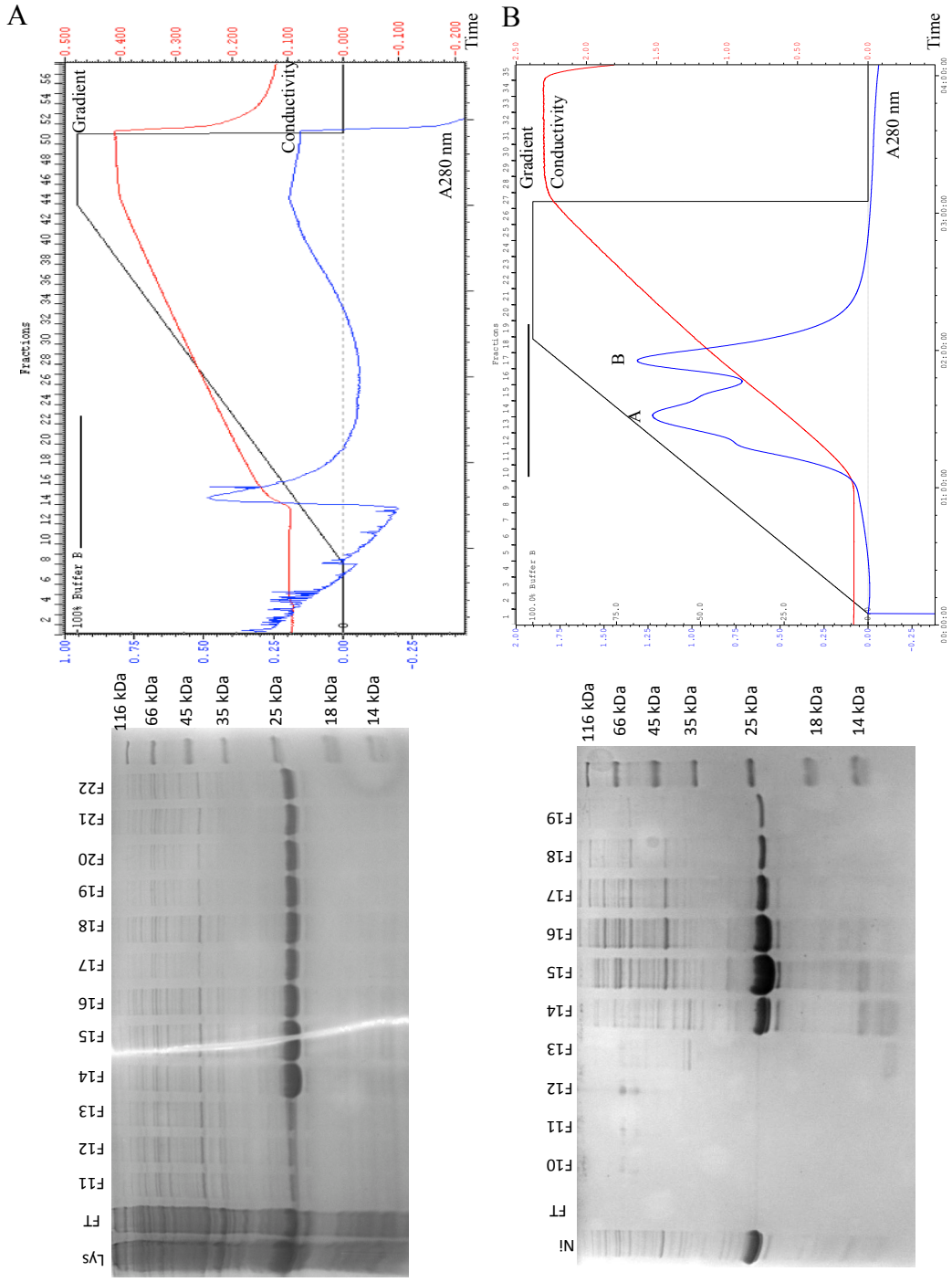

Figure 5.17: Chromatograms and SDS-PAGE analysis of eluted fractions from nickel affinity and anion exchange chromatography.

A: Chromatogram and 16% SDS-PAGE analysis of nickel affinity chromatography purification of erythrin. SDS-PAGE resolution of cell lysate (L), flow-through (FT) and fractions 11 to 22. B: Chromatogram and 16% SDS-PAGE analysis of anion exchange chromatography purification of erythrin. SDS-PAGE of pooled fractions 11-22, flow-through (FT) and eluted fractions 10 to 19. Buffer gradient (black line), conductivity (mS/cm) (red line), A_{280} nm (blue line). Erythrin peak A/B labeled, pooled fractions indicate by black bar.

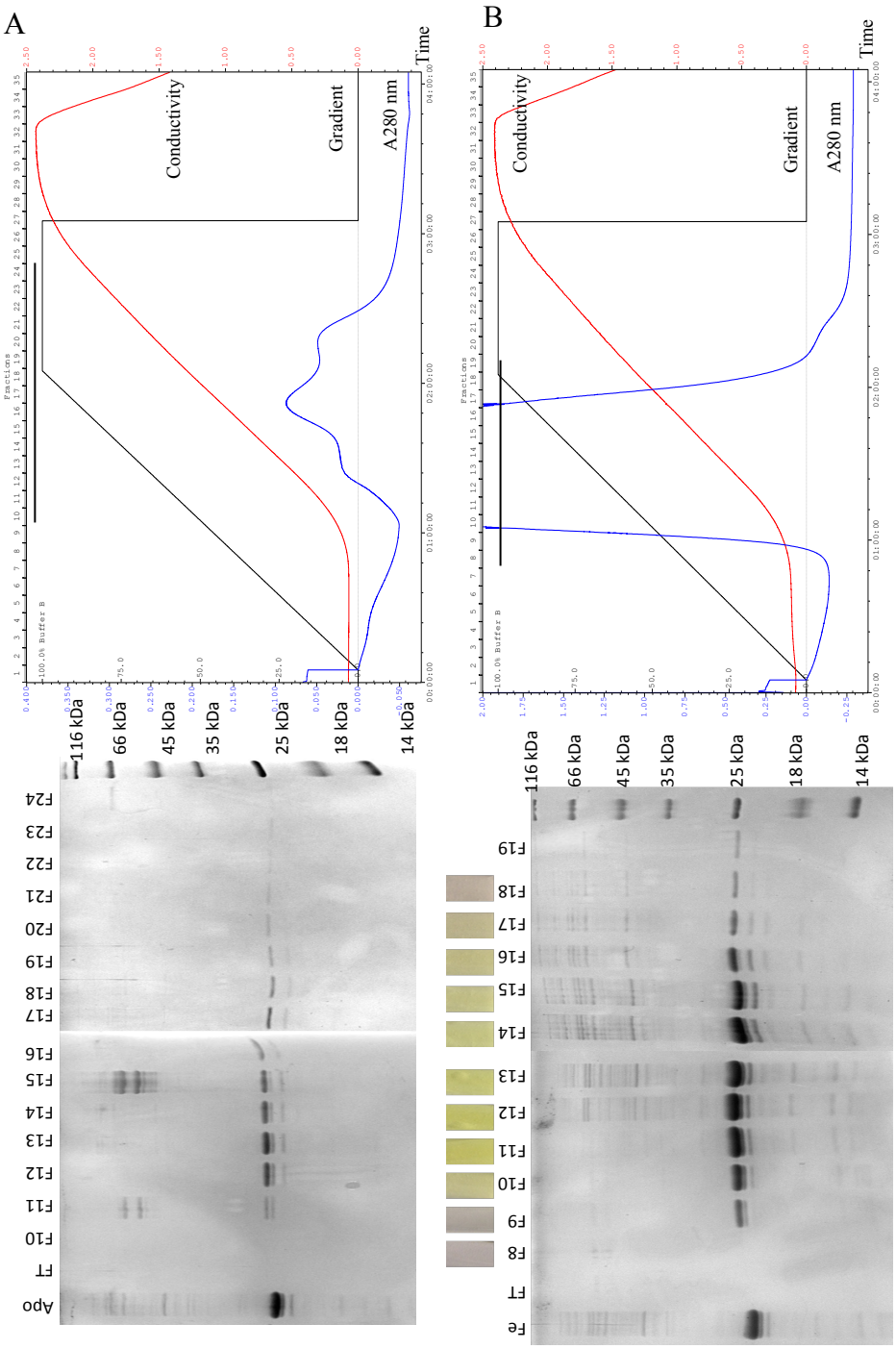

Figure 5.18: Chromatograms of DEAE anion exchange chromatography of apo- and diiron-erythrin.

A: Chromatogram and 16% SDS-PAGE analysis of anion exchange chromatography purification of apo-erythrin. SDS-PAGE of flow-through (FT) and fractions 10 to 24. B: Chromatogram and 16% SDS-PAGE analysis of anion exchange chromatography purification of apo-erythrin. SDS-PAGE of flow-through (FT) and fractions 8 to 29. Photographs of fraction colour are provided. Buffer gradient (black line), conductivity (mS/cm) (red line), A_{280} nm (blue line). Erythrin peak A/B labeled, pooled fractions indicate by black bar.

The relatively low absorbance for the three peaks seen in the chromatogram of apo-erythrin (Figure 5.18A) suggest that all metal centres were removed, although it is unclear why the protein eluted in three peaks. In contrast, the high intensity of Fe-erythrin peak (absorbance at 280) on the chromatogram (Figure 5.18B) suggests that this protein is metallated, as is supported by the brown colouration of the fractions obtained.

5.12: Thermal shift assay

In order to assist crystallization trials with the erythrin domain (in an attempt generate X-ray diffraction data to solve the crystal structure), preliminary studies were conducted, by means of a thermal shift assay, to determine stabilizing conditions that may be beneficial to the generation of protein crystals in solution.

A thermal shift assay (TSA) allows determination of the temperature at which half of the protein population is denatured (T_h). This measurement is useful within procedures designed to identify ligands which are stabilising to the protein's tertiary structure, aiding attempts to generate protein crystals to conduct X-ray diffraction analysis. The principle of the assay involves the addition of SYPRO orange (ThermoFisher) which exhibits a low fluorescence signal in polar environments (aqueous solutions) but a high fluorescence signal in non-polar environments, such as when in contact with the hydrophobic core of proteins (exposed upon denaturation). The assay involves monitoring kinetically the fluorescence emission at 580 nm whilst the protein:SYPRO solution is heated from 24 °C to 94 °C at a rate of 1 °C/min. As the temperature increases and the protein begins to denature; the hydrophobic core is exposed allowing binding of SYPRO orange increasing the fluorescence emission signal. The fluorescence emission data generated was analyzed by the NAMI algorithm (Groftehauge et al. 2015) which identifies the temperature at which the emission data fits a linear regression with a correlation coefficient of r = 0.996. This reading is used to identify a T_h as well as a maximum and minimum melting temperature. The thermal shift assay of erythrin in H_2O (Figure 5.19) demonstrates the rapid linear increase in fluorescence emission upon denaturation of the protein which is used by the NAMI algorithm to determine the T_h.

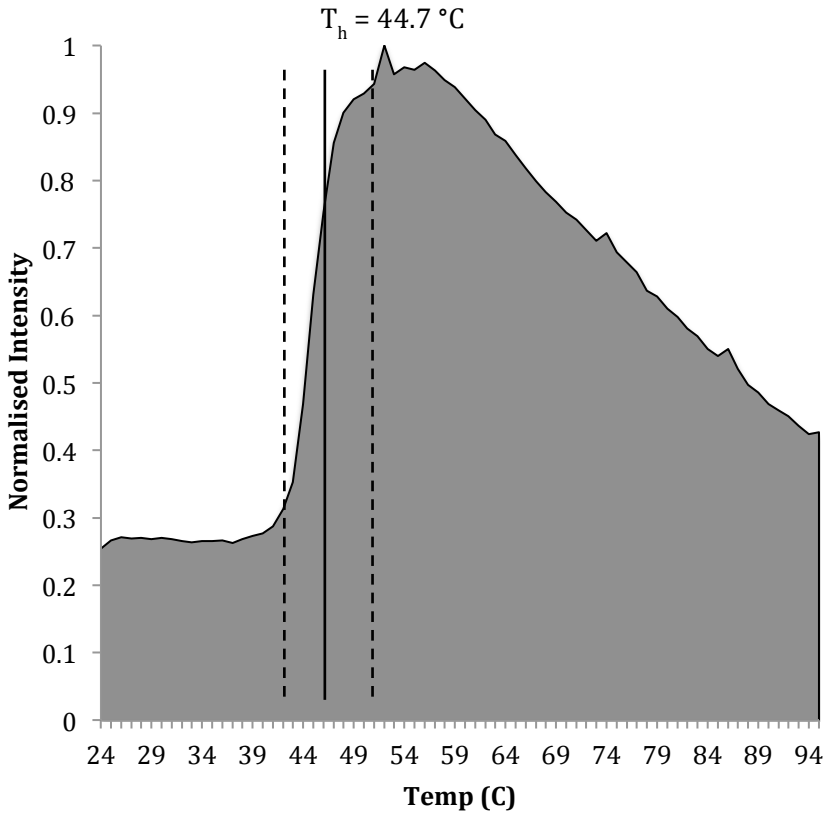

Figure 5.19: Thermal shift assay of apo-erythrin in H_2O.
Normalized fluorescence intensity data collected from 24 to 94 °C for apo-erythrin diluted into H_2O. Dashed line represent minimum and maximum melting temperatures, solid line represents T_h determined by NAMI.

Firstly, an initial study was conducted with 1 mg/ml apo-erythrin to determine an optimal pH range in which apo-erythin is most stable, i.e. the pH at which T_h is greatest. A pH screen matrix was created by Emily Cardew (University of Durham) which comprised 93 different pH conditions, ranging from pH 4.1 to 10.9, through 28 different buffers all at a concentration of 100 mM (Appendix 9.5). The fluorescence emission data collected from the RT-PCR machine was analysed by the NAMI algorithm and is displayed in Figure 5.20.

The data show that the erythrin protein is more stable at acidic pH than at basic pH, with melting temperatures decreasing at a linear rate from approximately pH 6.0 to 9.0, with the lowest T_h (27 °C) achieved when assayed in 100 mM CAPS pH 10.4. The highest melting temperatures were achieved in buffers of pH 5.0 to 6.0, with a maximal T_h of 51.5 °C in 100 mM succinate pH 5.4, a 6.8 °C increase over the same assay conducted in H_2O.

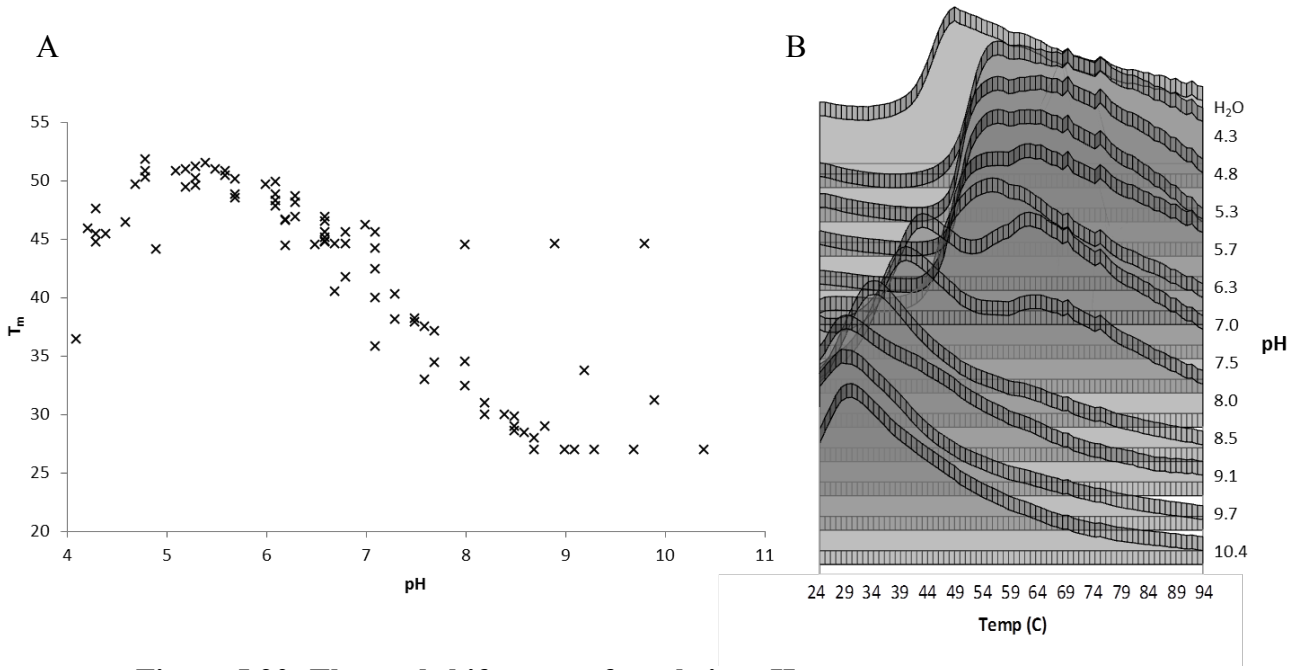

Figure 5.20: Thermal shift assay of erythrin; pH screen.

A: T_h calculated via thermal shift assay for apo-erythrin for all assay conditions in pH screen matrix. B: Normalised intensity fluorescence emission readings of selected pH values of apo-erythrin.

A second study examined the T_h of apo-erythrin with addition of simple salt solutions. A salt screen matrix created by Emily Cardew comprised a titration of concentrations of six different salt solutions: sodium malonate, ammonium sulphate, sodium chloride, ammonium chloride, magnesium sulphate and sodium sulphate. In addition, 200 mM alkali metal chlorides were used in the screen, along with 100 mM sodium halides, 2 mM lanthanide chlorides and 1 mM transition metal salts (Appendix 9.5). The data collected from the RT-PCR machine was analysed by the NAMI algorithm and is displayed in Figure 5.21.

A

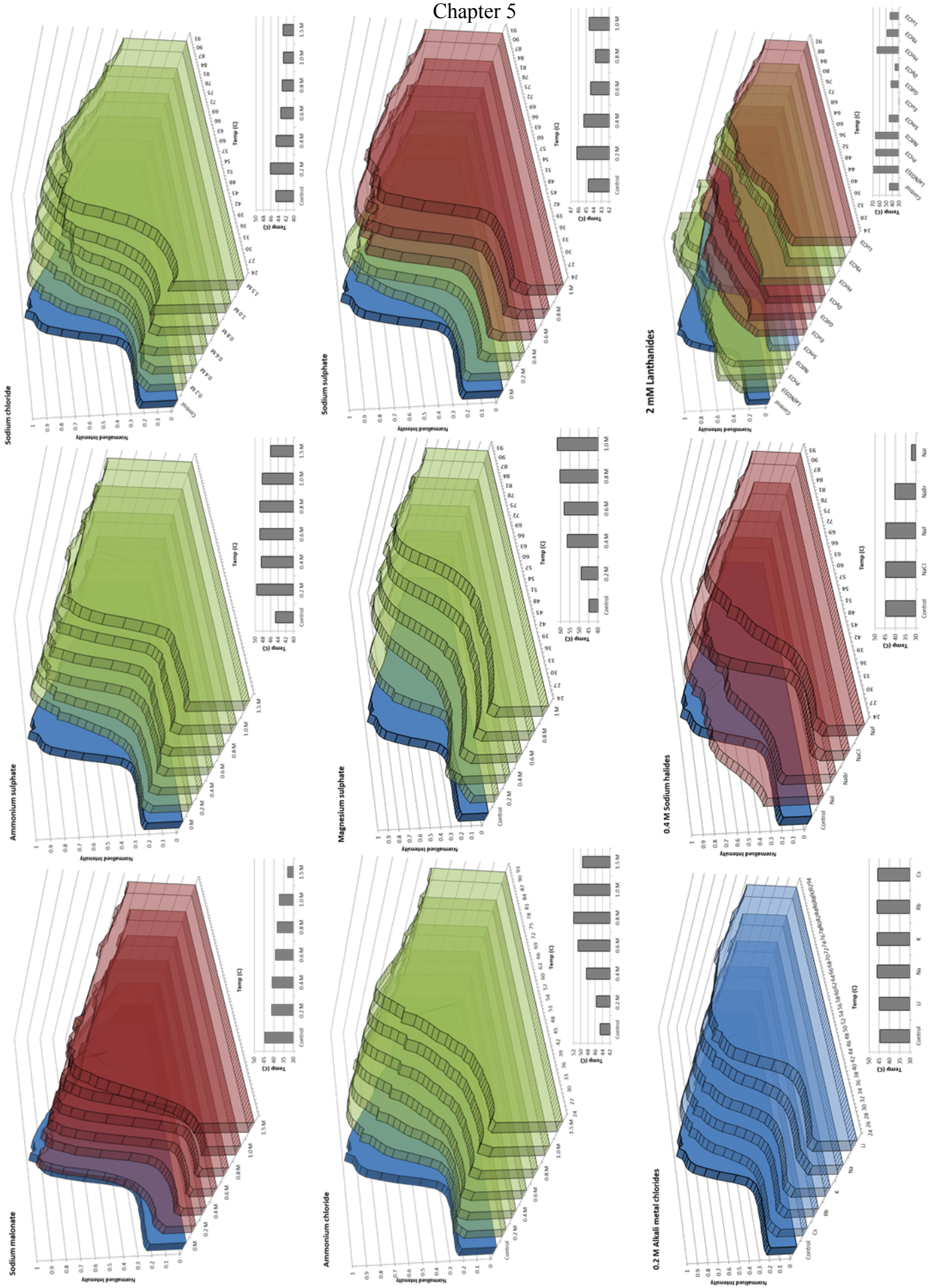
Sodium chloride
Sodium sulphate
2 mM Lanthanides
Ammonium sulphate
Magnesium sulphate
0.4 M Sodium halides
Sodium malonate
Ammonium chloride
0.2 M Alkali metal chlorides
Normalised Intensity
Temp (C)
Control
NaCl
NaF
NaBr
NaI
Li
Na
K
Rb
Cs

B

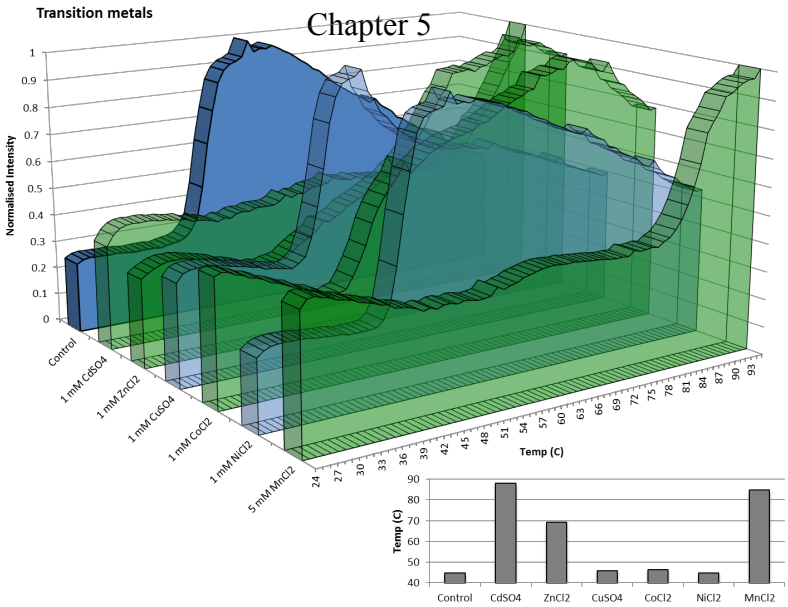

Figure 5.21: Thermal shift assay, salt screen.

A: Normalised intensity fluorescence emission data and T_h bar graph representation of thermal shift assays of 1 mg/ml apo-erythrin with sodium malonate, ammonium sulphate, sodium chloride, ammonium chloride, magnesium sulphate, sodium sulphate, alkali metal chlorides, sodium halides and lanthanide chlorides. B: Normalised intensity fluorescence emission data and T_h bar graph representation of thermal shift assays of 1 mg/ml apo-erythrin with transition metal salts

Titration of sodium malonate to apo-erythrin resulted in a concentration dependent decrease in T_h, from 44.7 °C with no addition (H_2O control) to 33.0 °C with 1.5 M sodium malonate. Titration of ammonium sulphate to apo-erythrin resulted in a concentration independent increase in T_h, 0.2 M ammonium sulphate increased T_h by 4.9 °C over an H_2O control to 49.6 °C, whereas 1.5 M ammonium sulphate only increased T_h by 1.3 °C over an H_2O control to 46.0 °C. Similar, relatively modest, concentration independent increases in T_h, were observed for additions of sodium chloride and sodium sulphate. Titration of ammonium chloride and magnesium sulphate to apo-erythrin resulted in a concentration dependent increase in T_h of 7.1 °C and 17.1 °C at a 1 M respectively, compared to an H_2O control. Thus, Mg^{2+} have a relatively large T_h increase.

Comparison of 200 mM lithium to caesium alkali metal chlorides resulted in no difference in T_h. Whereas, analysis of 400 mM sodium halides resulted in a decrease in T_h as the halide descended in the group of the periodic table. Addition of NaF presented in no difference to the H_2O control, but addition of NaI decrease T_h by 12.6 °C to 32.1 °C. Addition of 2 mM lanthanide chlorides resulted in a both increases and decreases to T_h, with no trend across the series identified. La, Pr, Nd and Ho all increased T_h, on average by 22.0 °C, whereas Sm, Yb and Lu presented no difference compared to a H_2O control, whilst, Eu, Gd and Dy all decreased T_h on average by 9.4 °C.

Addition of transition metal salts resulted in the largest increases in T_h. This is not surprising as the di-iron carboxylate proteins such as erythrin require the binding of iron for their catalytic activity (iron was not included in this preliminary assay). Addition of $CuSO_4$, $CoCl_2$ and $NiCl_2$ resulted in very little difference in T_h when compared to the H_2O control, however, addition of $CdSO_4$, $ZnCl_2$ and $MnCl_2$ increased T_h markedly by 43.3, 24.7 and 40.1 °C, respectively. These large increases in T_h can be observed clearly in the normalised intensity bar charts, where specifically, addition of cadmium and manganese salts results in the complete stabilisation of the protein complex to approximately 78 °C.

In summary, addition of simple salts, alkali metal chlorides, and sodium halides provide marginal effects upon the T_h of erythrin, especially in comparison to the addition of the transition metal salts, of $CdSO_4$, $ZnCl_2$ and $MnCl_2$. This result is not surprising given the evidence that the erythrin protein has the ability to bind two iron or zinc atoms.

With the observation of a large increase in the T_h of apo-erythrin with addition of Mn, Zn and Cd a third TSA was developed to determine the effect on T_h with titration of the transition metals: V, Mn, Fe, Co, Ni, Cu, Zn, Mo, Cd and Pb. Concentrations from 1 μM to 2 mM were assayed which correspond to a protein:metal stoichiometry ranging from 0.01 to 10. The fluorescence emission data of stabilizing salts collected from the RT-PCR machine was analysed by the NAMI algorithm generating T_h values and is displayed against stoichiometry in Figure 5.22. The T_h values of transition metal salts which did not produce a stabilizing effect are displayed in Figure 5.23.

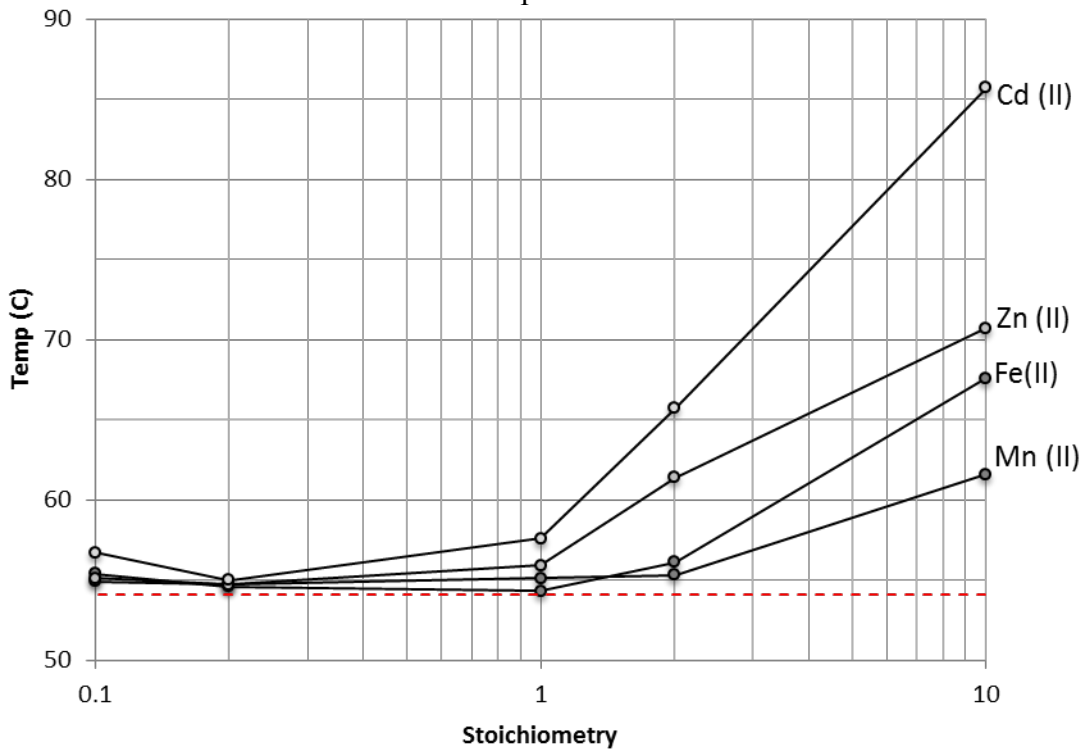

Figure 5.22: Thermal shift assay determination of T_h with titration of transition metals.

T_h calculated via thermal shift assay for erythrin in titrated concentrations (20 µM to 2 mM; 0.1 – 10 fold stoichiometry) of manganese, ferrous iron, zinc and cadmium.

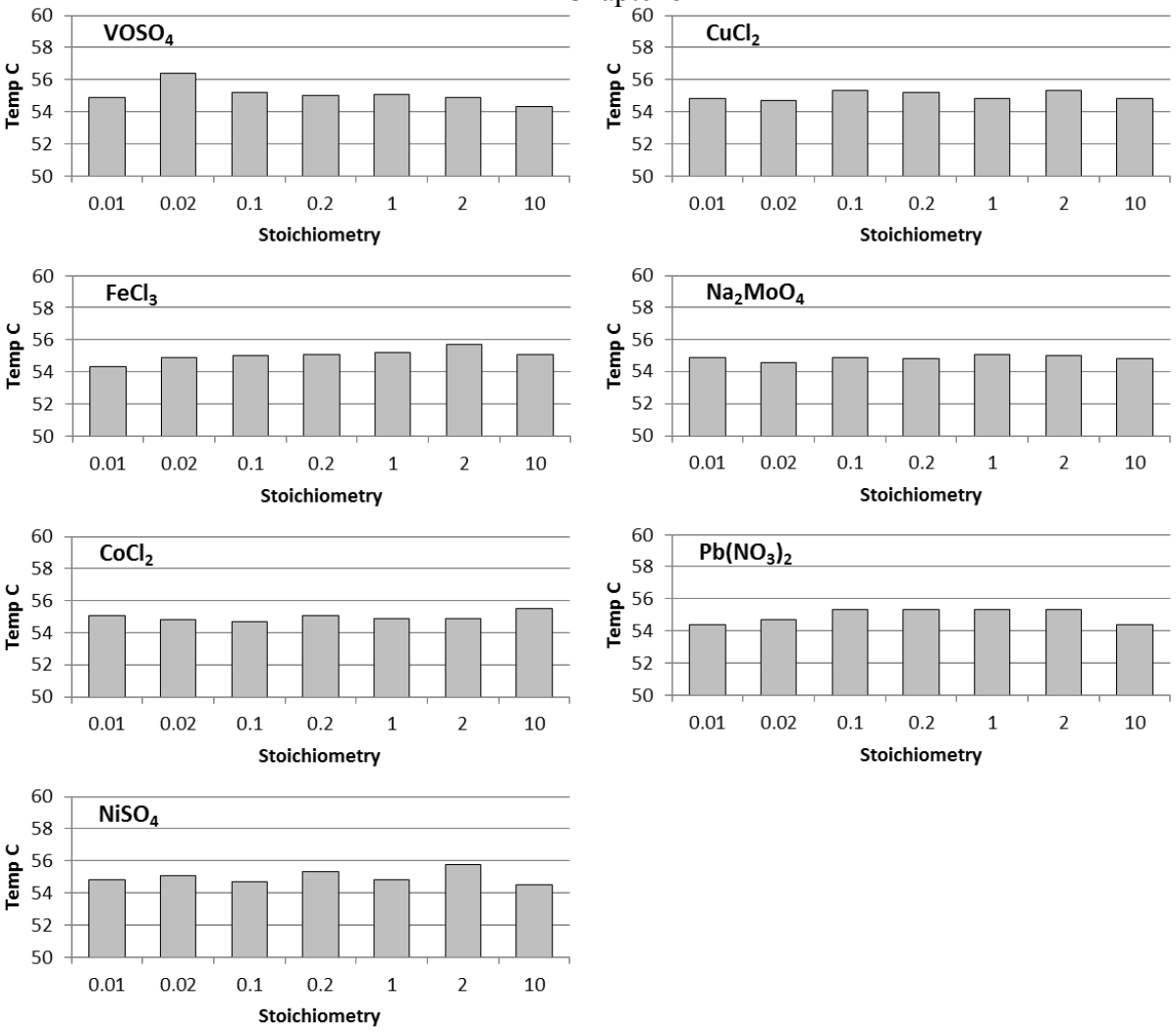

Figure 5.23: Thermal shift assay determination of T_h with titration of transition metals displaying weak effects.

T_h calculated via thermal shift assay for erythrin in titrated concentrations (2 µM to 2 mM; 0.01 – 10 fold stoichiometry) of vanadium, copper, ferric iron, molybdenum, cobalt, lead and nickel.

5.13: Crystallization trials

With the knowledge that the transition metals iron, zinc and manganese generate a stabilizing effect upon the erythrin protein's tertiary structure, attempts were made to generate erythrin crystals in the presence of these three transition metals. Each metal was added in a 10-fold molar excess as a sulphate salt to apo-erythrin (protein concentrations: iron-erythrin: 13.47 mg/ml, zinc-erythrin: 20.49 mg/ml, manganese erythrin: 19.37 mg/ml).

Two crystallization trays were prepared per metal-protein solution; PACT primer and JCSG-plus (Molecular Dimensions) – details of the concentrations of the salts, buffers and precipitants in each well are detailed in Appendix 9.6. Protein-erythrin samples were prepared as two parallel sitting drops (1: 200:200µl, 2: 100:200µl – protein:sample condition) and were left to at room temperature.

Crystallization plates were first examined one month after preparation, iron containing samples presented with multiple brown precipitates suggesting precipitation and oxidation of iron, in contrast the Zn- and Mn-containing plates presented with no colouration and less precipitation. Drops A7 and A8 within the Zn containing PACT primier plate presented with the most promising crystals/precipitation, conditions displayed in Table 5.5.

Table 5.5: Conditions in which most promising precipitate was present for Zn-erythrin.

Well	**Conc**	**Salt**	**Conc**	**Buffer**	**pH**	**Conc**	**Precipitant**
A7	0.2 M	Sodium chloride	0.1 M	Sodium acetate	5.0	20 % (w/v)	PEG 6000
A8	0.2 M	Ammonium chloride	0.1 M	Sodium acetate	5.0	20 % (w/v)	PEG 6000

5.14: Discussion

In summary, the experimentation conducted in this chapter details the optimization of recombinant erythrin protein expressed from a pET21a expression vector in *E. coli* BL21(DE3). Initial problems of achieving overproduction of recombinant erythrin were overcome through either codon optimization of the erythrin DNA coding sequence or transformation of the native *Brucella* sequence into alternate expression vectors; this then allowed purification and a preliminary assessment of the biochemistry of MbfA. Initially, the expression of soluble erythrin at high concentrations facilitated the generation of sufficient quantities of recombinant erythrin protein to enable its purification by chromatographic methods. The incorporation of a C-terminal His-tag enabled initial purification of erythrin by nickel-affinity chromatography, which was followed by anion-exchange chromatography to yield high concentrations and homogeneity of erythrin. Purification by anion-exchange chromatography resulted in a differential separation of erythrin protein into two distinct isomeric forms. The analysis of each form by ICP-OES and ESI-MS revealed differing stoichiometry and type of bound metal to each, a property used in subsequent purifications to generate high yields of di-iron centred erythrin. The differences in results obtained via ICP-OES and ESI-MS techniques for the stoichiometry of iron and zinc bound to the erythrin protein is likely explain through the limitations of each spectroscopic method. The high intensity measurements of di-Z erythrin compared to di-Fe erythrin for ESI-MS suggests that di-Zn erythrin may be more stable (supported by TSA measurements – Figure 5.22) and hence result in better flight and detection by the mass spectrometer quadrupole, with the latter being more difficult to detect. It is also of note that ICP-OES measurements detect total concentrations of metals, not just metal ligands. Additional spectroscopic methods should be used in further examinations of the di-iron centre of erythrin including Mössbauer and electron paramagnetic resonance (EPR) spectroscopy. As ^{57}Fe is a Mössbauer-active isotope, incorporation of ^{57}Fe into the di-iron center of erythrin would allow examination of the redox state of the iron atoms during reactions with hydrogen peroxide (Gupta et al. 1995) and would establish its di-iron status. Additionally, EPR spectrum analysis has been documented on the rubrerythrin from *Desulfovibrio vulgaris* (Ravi et al. 1993, Gupta et al. 1995) and shows that a characteristic spectrum of a di-iron centre is observable despite limitations of the EPR-silent nature of ferrous iron.

The purification to homogeneity of the erythrin protein allowed several subsequent analyses to be performed, including: the generation of polyclonal antibodies to be raised

in rabbits, facilitating the immune-detection of MbfA in *E. coli* and *Brucella*. As well as, the formation of apo-erythrin (metal free) through the chelation of bound metals, which were subsequently removed by dialysis, enabled the recreation of a di-iron centre erythrin through the titration of ferrous iron. Experimentation determined that the di-iron centre is oxidised by hydrogen peroxide, a process which is hypothesized to be linked to the export of a ferric iron atom (Chapter 6). The system could be reduced artificially with strong reductant, but *in vivo,* a cellular reductase is hypothesized to be required to reduce the di-iron centre back to the ferrous form, to allow subsequent export of iron. The requirement of a reductase system *in vivo* represents a challenge for the observation of peroxidase activity *in vitro*. Instead of a biological reductase system, a chemical reductant was employed *in vitro* during this analysis, but this poses difficulties in measuring the peroxide reductase functionality, as the reduction of H_2O_2 by erythrin is outcompeted by the reduction of H_2O_2 by the chemical reductant. To allow monitoring of peroxide reductase by erythrin *in vitro* a biological reductase will be required, this provides a basis for additional experimentation.

The metal-binding capacity of the erythrin domain was examined by thermal shift assay which showed that, in addition to iron, at least three other metals (zinc, manganese and cadmium) are also able to bind the di-iron binding site in a fashion that stabilizes the protein thus increasing its melting temperature. This knowledge facilitated directed attempts to generate protein crystals; crystallization trials were conducted on iron, manganese and zinc centred erythrin.

Experimentation conducted with the *Brucella suis* erythrin protein are largely in agreement with those observed with the erythrin domain of MbfA from *Bradyrhizobium japonicum* (Sankari and O'Brian 2014). The *B. japonicum* erythrin domain (denoted ferritin like domain –FLD) was observed by Western blotting to be located on the cytoplasmic side of the inner membrane, and the FLD had a metal:peptide stoichiometry of two when titrated with ferrous iron. The binding of iron at the di-iron centre was found to be reliant on the glutamic acid residues of the di-iron binding motifs, as mutation of these residues resulted in abolition of iron binding. However, the FLD was purified as a homo-dimer by gel filtration chromatography, this experiment has not been conducted with the *B. suis* erythrin domain to date, but would warrant consideration due to the suggestion made her by MS that the *Brucella* erythrin domain is a homo-dimer which contrasts with the findings made for *B. japonicum*.

In addition to the analysis of the native erythrin domain of *B. suis* MbfA, experimentation was planned to also examine the potential for metal binding and subsequent biochemical activity of truncated erythrin proteins. Truncated variants of the erythrin domain were generated which represented peptides that may have been translated from alternative start sites from the *B. melitensis mbfA* gene due to the location of a disruptive SNP at the proximal end of the gene. This experimentation was not conducted for several reasons: firstly due to time limitations but more significantly, the lack of MbfA or truncated variants detected when probing *B. melitensis* with anti-erythrin antibodies (Chapter 7.4) indicated that such variants are not generated naturally, thus there is little justification for examination of their biological activity. Subsequently, bioinformatic analysis showed that other bacterial species encode MbfA proteins with truncated N-terminal erythrin domains (Chapter 3.2), most notably *Burkholderia multivorans*, but its MbfA remains functional (Chapter 6.5) due to the maintenance of all four iron-binding motifs. Thus, the *mbfA* gene of *B. melitensis* would appear distinct from that of other bacteria since it is apparently cryptic in nature (not expressed).

Chapter 6: Characterization of MbfA function and mechanism of action

6.1: Confirmation of *mbfA* expression in *E. coli* and sub-cellular location by immuno-detection

A series of *E. coli* vectors (pSU18 and pBADrham/ara derived) containing the *Brucella mbfA* coding sequence under control of an inducible promoter was created previously (Chapter 4). However, it remained unclear whether these vectors allowed production of the MbfA polypeptide. Thus, the expression of *mbfA* from these inducible plasmids in *E. coli* was investigated. Given the requirement for codon optimization or specific expression strains to obtain expression of the erythrin domain during recombinant protein overproduction, there was a good possibility that expression would not be easily achieved using the native gene. However, the *mbfA* cloned into the above vectors for exploring the phenotype conferred by *mbfA* expression in *E. coli* was the codon optimized version, which increases the likelihood of successful expression. Thus, expression from the lactose, rhamnose and arabinose promoters was assessed before initiation of the phenotype experiments with *mbfA* expressed in *E. coli*.

Immuno-detection with polyclonal anti-erythrin antibodies, raised in New Zealand white rabbits by Proteogenix (France) using protein generated as in Chapter 5, was conducted on 0.5 OD units of whole cells collected from *E. coli* MG1655 pBAD*mbfA* and pSU*mbfA* before and after induction, of an exponentially growing culture with rhamnose (0.1 mM) or IPTG (0.5 mM). Proteins were analysed by SDS-PAGE and transferred to a PVDF membrane, then immune-stained using anti-erythrin antibodies (Methods 2.4.5). The resulting Western blot showed that MbfA is indeed generated for both the pSU*mbfA* and pBAD*mbfA* transformants but differences are apparent between the two plasmids (Figure 6.1).

The clear increase in MbfA protein post-induction for the pBAD*mbfA* transformant indicates regulation of *mbfA* gene expression from the rhamnose promoter. In contrast, MbfA levels for the pSU*mbfA* transformant show similar levels pre- and post-addition of inducer, suggesting leaky expression from the *lac* promoter. Importantly however, the Western blots demonstrate that MbfA is produced to give its expected mass from each of the two plasmids tested. Thus, these plasmids can be used in future experiments exploring the effect of heterologous expression of *mbfA* in *E. coli.*

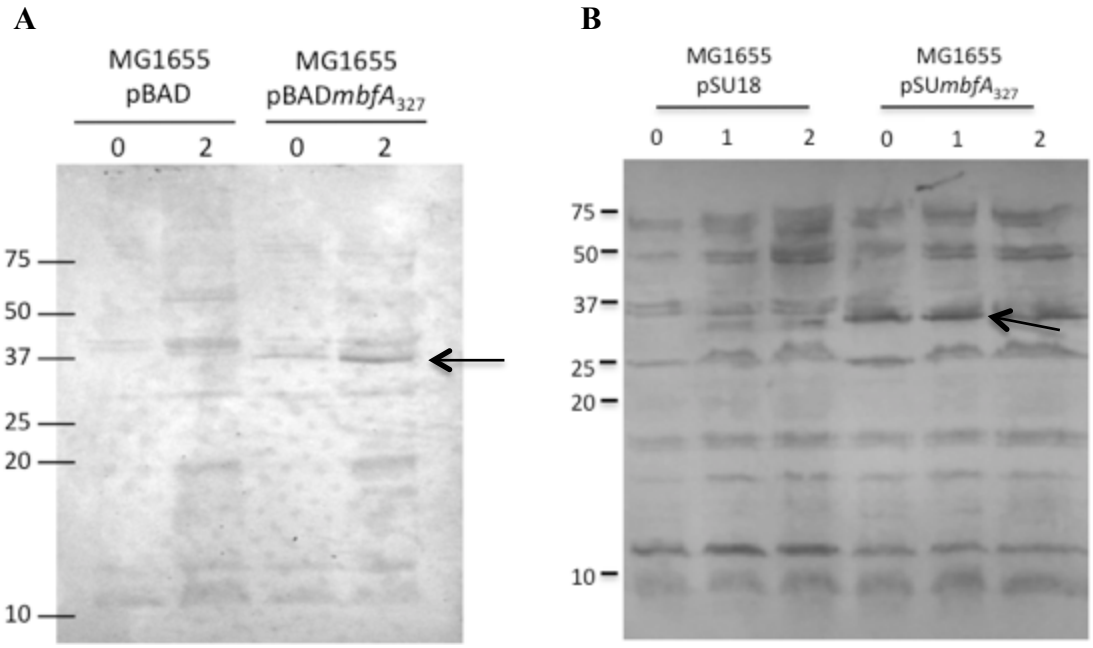

Figure 6.1: Western blot analysis of expression of pBAD*mbfA* and pSU*mbfA*

A: Immuno-detection of expression of *mbfA* from pBAD*mbfA* in *E. coli* MG1655, lanes from left to right: vector control (pBADrha) before (0 h) and after induction (2 h); pBAD*mbfA* before (0 h) and after induction (2 h). B: Immuno-detection of expression of *mbfA* from pSU*mbfA* in *E. coli* MG1655, lanes from left to right: vector control (pBADrha) before (0 h) and after induction (1-2 h); pSU*mbfA* before (0 h) and after induction (1-2 h). MbfA, 36.2 kDa indicated with arrow.

6.2: Cellular localisation of MbfA

To further assess functional status of *mbfA* expression in *E. coli*, it was considered desirable to determine the subcellular location of the heterologously expressed MbfA. On the basis of membrane topology prediction, VIT1 homology and direct experimentation with *mbfA* from *B. japonicum* (Sankari and O'Brian 2014), it is very much anticipated that the *B. suis* MbfA would need to be incorporated into the inner membrane in order to be functional.

Thus, *E. coli* MG1655 was transformed with pSU*mbfA*. Induced cells were harvested and fractionated into the following fractions: whole cells, lysed spheroblasts, cytoplasm, periplasm, total membranes, inner membrane and outer membrane (Methods 2.5.6). The periplasm was extracted via osmotic shock, the resulting spheroplasts were lysed by sonication and the cytoplasm separated from the membranes via ultracentrifugation. Inner and outer membranes were further separated by incubation with sodium lauryl sarcosinate (solubilises inner membranes) and ultracentrifugation. Subcellular fractions were analysed by 16% PAGE and probed for the presence of MbfA with anti-erythrin antibodies via Western blotting (Figure 6.2). MbfA can be seen localized exclusively to the inner membrane (also present in whole cells, lysed spheroblasts, total membranes due to fractions containing inner membrane). Thus, MbfA is associated with the expected subcellular compartment, which suggests that MbfA might exhibit functionality in *E. coli.*

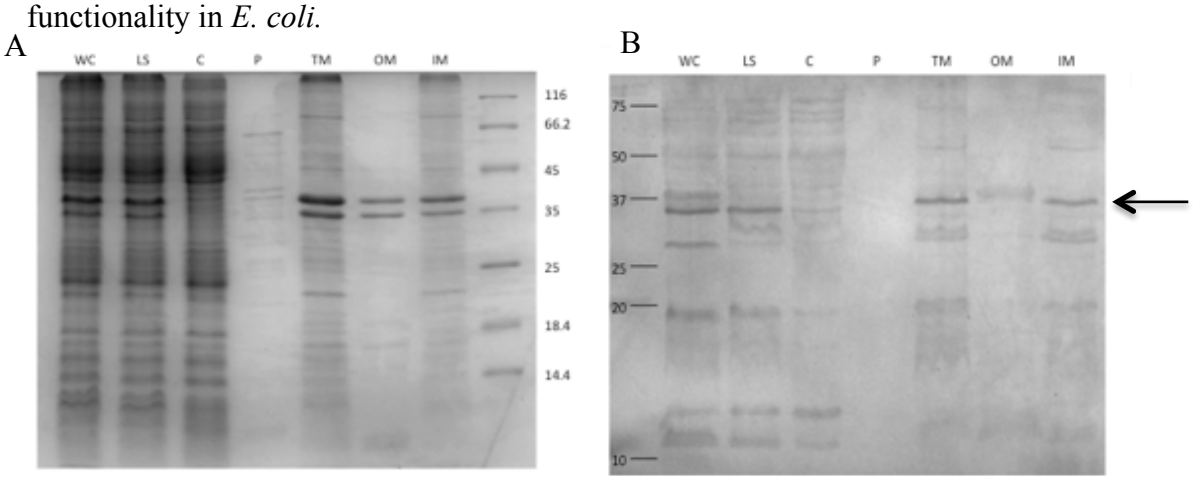

Figure 6.2: SDS-PAGE and Western blot analysis of MbfA subcellular location upon expression in *E. coli.*

A: 16% SDS-PAGE analysis of expression of *mbfA* from pSU*mbfA* in *E. coli* in whole cells (WC), lysed spheroblasts (LS), cytoplasm (C), periplasm (P), total membranes (TM), outer membrane (OM) and inner membrane (IM) fractions. B: As (A) but Immuno-detection of expression MbfA. 36.2 kDa indicated with arrow.

6.3: Complementation of *E. coli* mutants with *mbfA* demonstrates a phenotype consistent with an iron export role for MbfA

To provide evidence for the hypothesized iron export and peroxide reductase activities of MbfA, *E. coli* Δ*fur* (H1941 - deregulated iron uptake), *E. coli* Δ*fecABCDE* Δ*zupT* Δ*mntH* Δ*entC* Δ*feoABC* (JC28 - deficient in all known high affinity iron import systems), *E. coli* Δ*ahpCF' kan*::*'ahpF* Δ(*katG17*::Tn*10*)1 Δ(*katE12*::Tn*10*) (LC106 – oxidative stress sensitive) and corresponding parental wild-type strains were transformed with the *B. suis mbfA* gene (pBAD*mbfA* plasmid) or empty vector control (pBADrham) under the control of an inducible rhamnose promoter and assayed for differences in cellular growth in L broth or minimal medium. Cellular growth was assessed by measurement of OD of bacterial cultures with the LabSystems Bioscreen C.

High cytosolic iron concentrations within the *E. coli* Δ*fur* mutant (H1941), through un-regulated iron uptake and lack of iron storage, render it more susceptible to oxidative stress than the parental *E. coli* stain (MC4100) (McHugh et al. 2003) as is observed by a 0.51 OD unit, 60% reduction in final OD compared to the parent (Figure 6.6A). Complementation of *E. coli* Δ*fur* with pBAD*mbfA* resulted in a minimal increase (0.074 OD units – 9.7%) in growth under oxidative stress conditions (400 μM H_2O_2) after 18 h, but major reduced time in lag phase (by 2 h; Figure 6.3). Although a statistical difference in growth is not observed, as the differences in growth curves between *mbfA* expressing and vector control E. coli H1941 are too small, the slight growth enhancement (reduction in lag phase) of H1941 (pBAD*mbfA*) under condition of oxidative stress is consistent with the notion that MbfA is able to export iron, but presumably not at a rate that exceeds that of iron import in the *fur* mutant where iron uptake is constitutive.

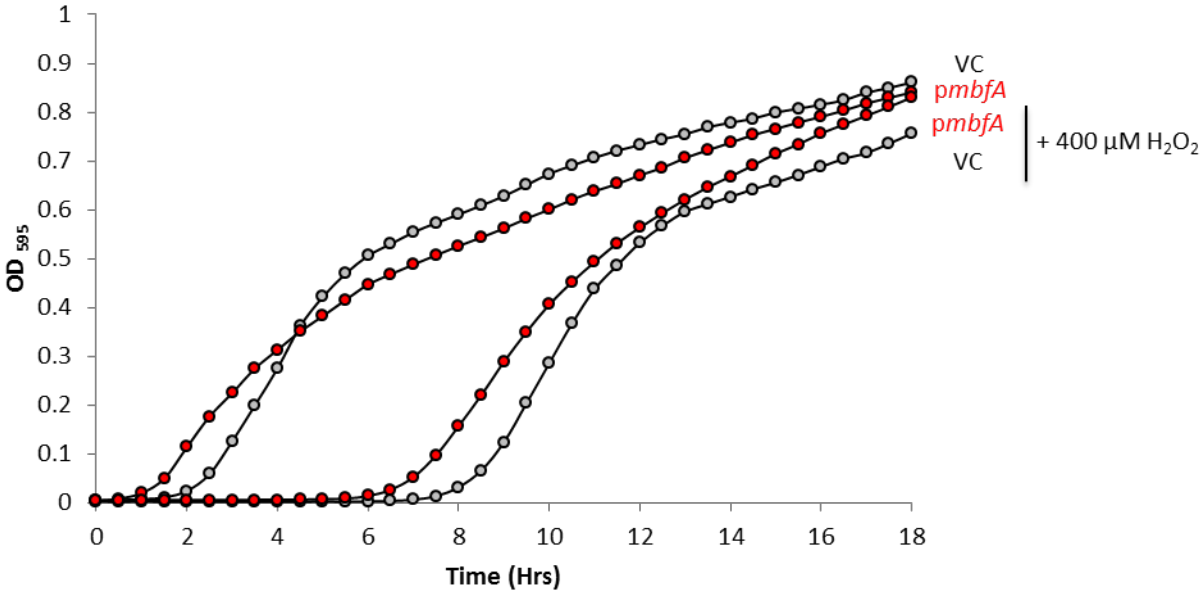

Figure 6.3: Growth of *E. coli* Δ*fur* (H1941) transformed with pBAD*mbfA*.
Growth curve under aerobic conditions in L broth +/- 400 µM H_2O_2 for *E. coli* H1941 transformed with pBAD*mbfA* or vector control (VC, pBADrham). Data shown are the means of three independent experiments conducted in triplicate. Rhamnose was included at 0.1 mM.

An attempt to observe an *E. coli* growth phenotype consistent with iron export was next performed using *E. coli* JC28. This strain harbours deletions to all known high affinity iron import systems (Δ*fecABCDE* Δ*zupT* Δ*mntH* Δ*entC* Δ*feoABC*); the absence of iron import machinery and expression of the iron exporter *mbfA* within *E. coli* is expected to result in reduced growth when available iron is limited.

Transformation of *E. coli* JC28 with pBAD*mbfA* resulted in a decrease in growth in iron supplemented (20 µM ferric citrate) minimal media by 0.453 OD units (94%) after 48 h of aerobic growth in minimal medium (Figure 6.6B). Addition of 1 µM diethylenetriaminepentaacetic acid (DTPA) to the minimal medium, further limiting iron availability, severely hindered the growth of *E. coli* JC28 (Figure 6.4), with pBAD*mbfA* further decreasing the ability of *E. coli* JC28 to grow. These reduced-growth *mbfA*-induced phenotypes are consistent with the removal of cellular iron by MbfA, further reducing cellular iron for *E. coli* JC28.

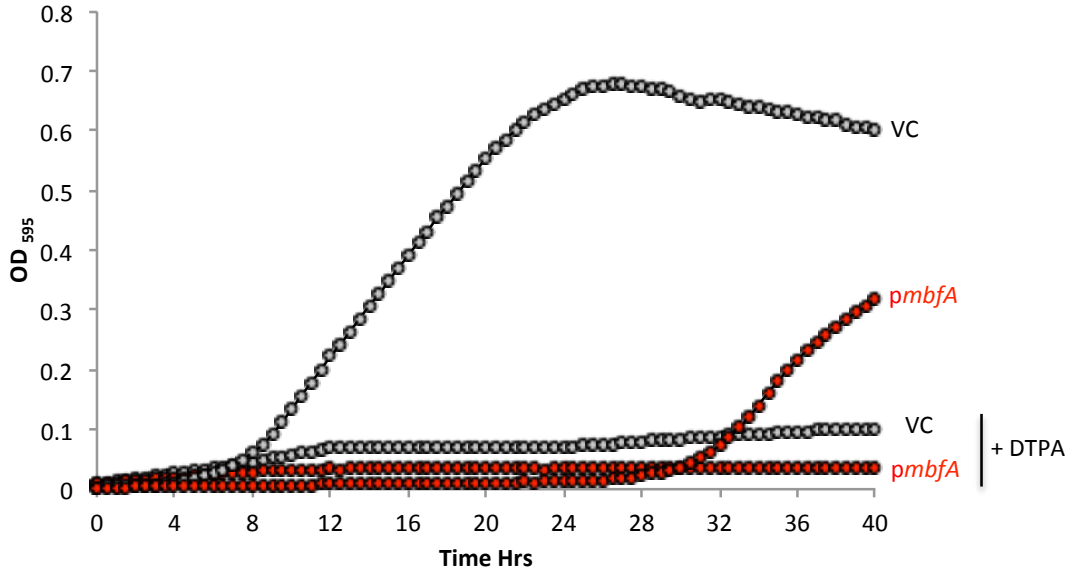

Figure 6.4: Growth of *E. coli* Δ*fecABCDE* Δ*zupT* Δ*mntH* Δ*entC* Δ*feoABC* transformed with pBAD*mbfA*.

Growth under aerobic conditions in minimal medium with 20 µM ferric citrate or 1 µM DTPA for *E. coli* JC28 with p*mbfA* or vector control (pBADrham). Data shown are the means of three independent experiments conducted in triplicate. Rhamnose was included at 0.1 mM.

The next *E. coli* strain used for phenotype analysis was *E. coli* LC106, which lacks catalases and alkyl-hydroperoxide reductases, and thus displays low resistance to oxidative stress (Seaver and Imlay 2004). This strain was indeed observed to be sensitive to addition of 200 µM hydrogen peroxide to LB (Figure 6.6C). Transformation with pBAD*mbfA* resulted in an increase in growth by 0.275 OD units (55%) after 18 h of growth compared to vector control (Figure 6.5). In the presence of H_2O_2, induction of *mbfA* caused a decreased lag phase (~2.5 h) as well as a greater overall growth (~33% increase in OD at 18 h; Fig. 6.5).

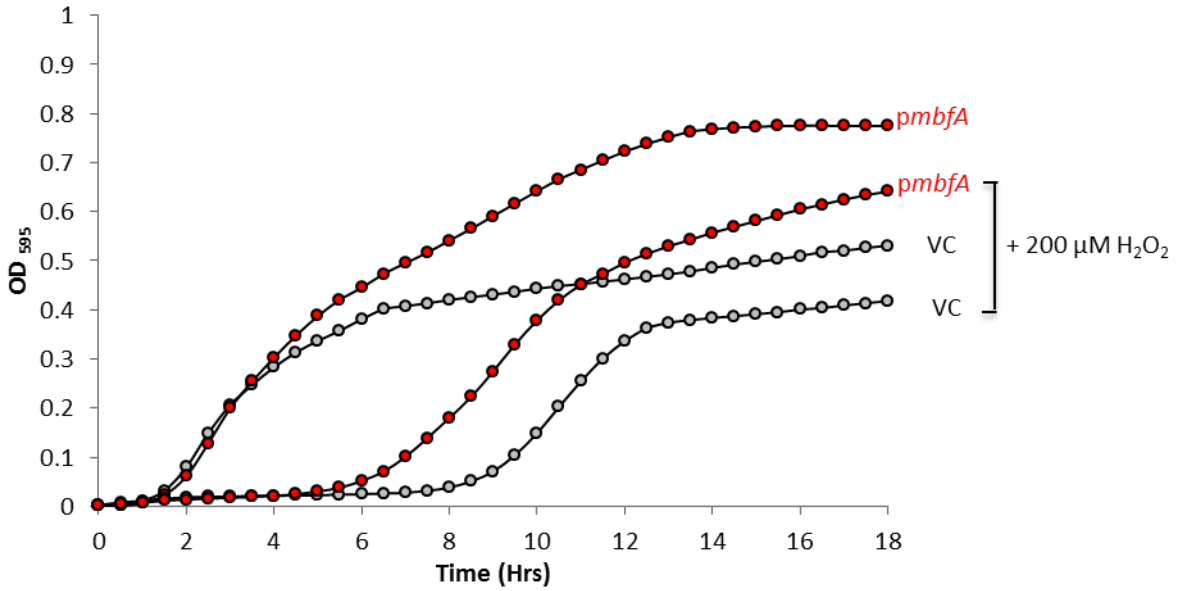

Figure 6.5: Growth of *E. coli* Δ*ahpCF* Δ*katG* Δ*katE* (LC106) transformed with pBAD*mbfA*.

Growth under aerobic conditions in L broth +/- 200 µM H_2O_2 of *E. coli* LC106 with pBADmbfA or vector control (VC). Data shown are the means of three independent experiments conducted in triplicate. Rhamnose was included at 0.1 mM.

Induction of *mbfA* also complemented the low resistance to oxidative stress of *E. coli* LC106 when exposed to organic peroxides and redox (Figure 6.6D). The pBAD*mbfA* LC106 transformant out grew the vector control in the presence of *t*-butyl peroxide, dicumyl peroxide and methyl viologen by 0.44 (40%), 0.49 (49%) and 0.83 OD units (114%), respectively, at 18 h.

The above observations show that MbfA provides resistance to alkyl hydroperoxides, hydrogen peroxide and a redox-cycling agent (superoxide inducer). It is unclear if the predicted peroxide reductase activity of the erythrin domain is specific to hydrogen peroxide, or whether the tested organic peroxides are also able to serve as substrates for MbfA, and thus if such activity plays a role in detoxification of these peroxides.

The resistance to MV provided by MbfA may arise due to its ability to degrade the raised levels of H_2O_2 that would be generated by superoxide dismutase in response to MV exposure. In addition, the proposed ability of MbfA to export cellular iron would be expected to contribute to resistance to both alkylhydroperoxides and superoxide (as well as H_2O_2) through limiting iron-induced Fenton chemistry intracellularly, and possibly by promoting iron-induced peroxide degradation extracellularly.

Concentrations of hydrogen peroxide additions used during the above *in vitro* experiments range from 50- to tenfold higher than those expected to be found in the macrophage phagolysosome or eBCV (1-4 μM; (Slauch 2011), 30 μM; (Winterbourn et al. 2006)). During *in vitro* experiments, H_2O_2 additions were provided as a single bolus, resulting in high level exposure initially followed by an expected gradual decreased exposure as the peroxide is degraded by the culture. This is in contrast to the mode of peroxide exposure in the phagolysosome where hydrogen peroxide generation is continuous and thus concentrations can be expected to be maintained at a steady concentration. In addition, the toxic effect exerted by H_2O_2 is enhanced in the phagolysosome by the generation of NO, leading to production of toxic peroxynitrite. Thus, the *in vitro* exposure of *E. coli* to peroxide applied above does not closely mimic the conditions within the phagolysosome (or early BCV) where MbfA may act to aid colonization of macrophages, but nevertheless clearly display a role for MbfA in redox stress resistance that would be expected to be of relevance during macrophage infection.

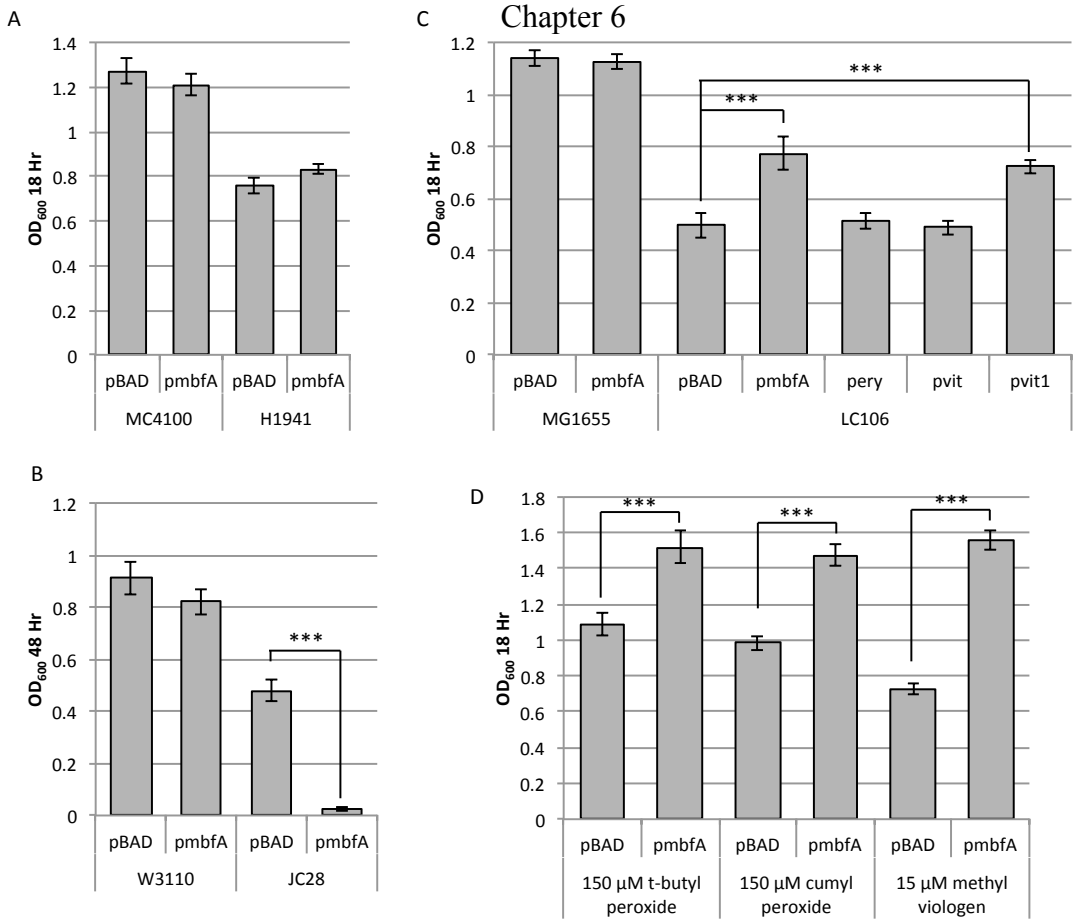

Figure 6.6: Phenotypes conveyed through expression of *B. suis mbfA* and *A. thaliana VIT1*, and the MbfA N-terminal erythrin and C-terminal Vit domains in *E. coli* mutant strains.

A: Aerobic growth after 18 h in 400 µM H_2O_2 supplemented L broth of *E. coli* MC4100 and H1941 transformed with *B. suis mbfA* (pBAD*mbfA*) or vector control (pBAD). B: Aerobic growth after 48 h in 20 µM ferric citrate supplemented minimal medium of *E. coli* W3110 and JC28 transformed as above. C[1]: Aerobic growth after 18 h in 200 µM H_2O_2 supplemented LB of *E. coli* MG1655 and LC106 transformed as above, or with pBAD*ery* (N-terminal erythrin domain; p*ery*), pBAD*vit* (C-terminal Vit domain; p*vit*), pBAD_*AtVIT1* (*Arabidopsis thaliana VIT1*, p*VIT1*). D[2]: Aerobic growth after 18 h in 150 µM t-butyl peroxide, 150 µM cumyl peroxide or 15 µM methyl viologen supplemented LB for *E. coli* LC106 transformed as in A. Data shown are the means ± standard deviation of three independent experiments conducted in triplicate and analysed using an unpaired, two tailed Student's *t*-test; * $P<0.05$, ** $P<0.01$ *** $P<0.001$. Growths included 0.1 mM rhamnose. [1] Figure 6.6C conducted by L. Wynne, under supervision, Final Year Project Student, 2015. [2] Figure 6.6D conducted by J. Lewis, under supervision, Final Year Project Student, 2016.

To determine whether the phenotypes conferred by *mbfA* require coupling of its two domains to allow reduction of hydrogen peroxide at the erythrin domain combined with export of iron via the vit domain, the two domains were cloned separately and introduced into *E. coli* LC106 (Figure 6.6C). Neither domain in isolation was able to restore the increased growth phenotype to *E. coli* LC106 as was seen with *mbfA* expression. For the solo erythrin domain, this is presumably due to lack of iron export and oxidation capacity since the erythrin domain would be expected to lack the reduction pathway provided through Vit-domain-mediated export-oxidation of ferrous iron. For the solo-Vit domain, a lack of a sink for electron transfer during its export of iron, coupled to ferroxidation, might be expected to debilitate its activity through inability to oxidise ferrous iron prior to transport. These findings are consistent with the notion that oxidation of the erythrin domain di-iron-centre by hydrogen peroxide drives the export process and that the two domains must be combined to elicit functionality.

To address the nature of H_2O_2 degradation further (i.e. to determine to what degree iron export, as opposed to erythrin domain H_2O_2 reduction, are responsible for the *mbfA* phenotypes observed above), the vacuolar iron transport 1 (*VIT1*) gene from *Arabidopsis thaliana* was cloned and expressed in *E. coli* LC106 (p*At_VIT1*). VIT1 is a natural solo-Vit domain protein so would be expected to mediate iron export, but not peroxide reduction, when functionally expressed in *E. coli*. Expression of *VIT1* resulted in an increase in culture density of 0.226 OD units (45%) after 18 h growth compared to the vector only control (Figure 6.7), an increase similar to that observed with *mbfA*. VIT1 acts as a transporter of ferrous iron into seed vacuoles (Kim et al. 2006, Cockrell et al. 2014) and the membrane organisation is such that when expressed in *E. coli* VIT1 is expected to be localised to the inner-membrane, as is *mbfA,* where it would act to export iron from the bacterial cell into the periplasm. Due to the lack of a peroxide reducing erythrin domain in the VIT1 protein, it is likely that the observed resistance to H_2O_2 occurs through export of iron which would lower potential for iron-mediated Fenton reactions in the cytosol and might result in enhanced iron-mediated decomposition of extracellular H_2O_2. Therefore, reduction of peroxide at the erythrin domain in MbfA may play a minimal role in peroxide detoxification, indicating importance for the physiological control of iron export in response peroxide exposure.

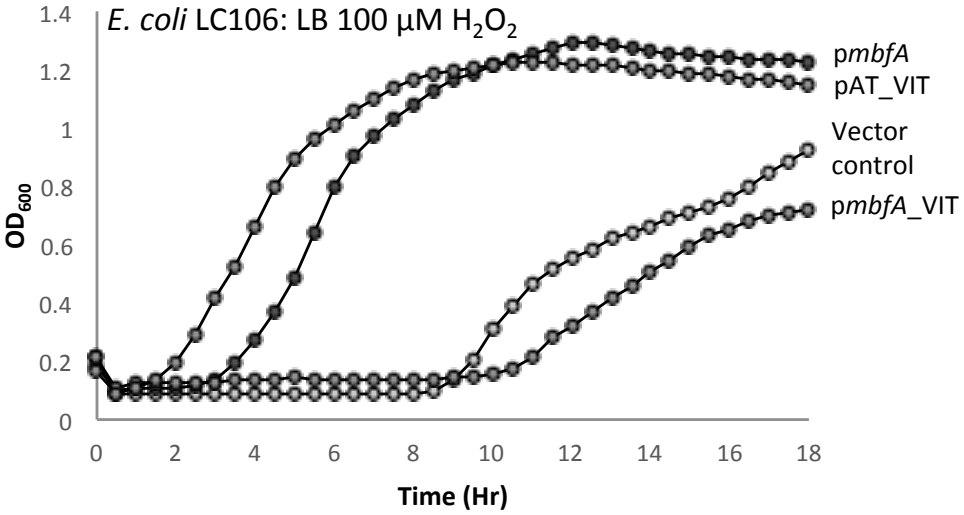

Figure 6.7: *E. coli* Δ*ahpCF* Δ*katG* Δ*katE* transformed with p*At_VIT1* (*A. thaliana* VIT1) exhibits decreased oxidative stress sensitivity.

Growth curve under aerobic conditions in L broth +/- 100 µM H_2O_2 for *E. coli* LC106 transformed with p*mbfA,* p*mbfA*_VIT, p*At_VIT1* or vector control. Data shown are the means of three independent experiments conducted in triplicate. Rhamnose was included at 0.1 mM.

6.4: Expression of *mbfA* is directly related to streptonigrin resistance

Streptonigrin is an aminoquinone antibiotic that induces bacterial killing in a manner that is dependent upon high intracellular iron concentrations. This principle has been used as an assay to determine potential export of iron in *Salmonella* and *Agrobacterium* spp. (Frawley et al. 2013, Bhubhanil et al. 2014). Thus, the effect of MbfA on the viability of *E. coli* upon exposure to streptonigrin was examined, with the expectation that MbfA would provide resistance to this antibiotic.

The resistance to streptonigrin killing of *E. coli* MG1655, H1941, LC106 and JC28 transformed with either empty vector or pSU*mbfA* was assayed through growth against various streptonigrin concentrations (1, 2, 4, 8 and 16 µg/ml dissolved in DMSO). Figure 6.8A/B displays representative growth curves of *E. coli* JC28 pSU18 and pSU*mbfA*. To allow comparison of multiple bacterial strains, final optical densities after 22 h displayed in Figure 6.9.

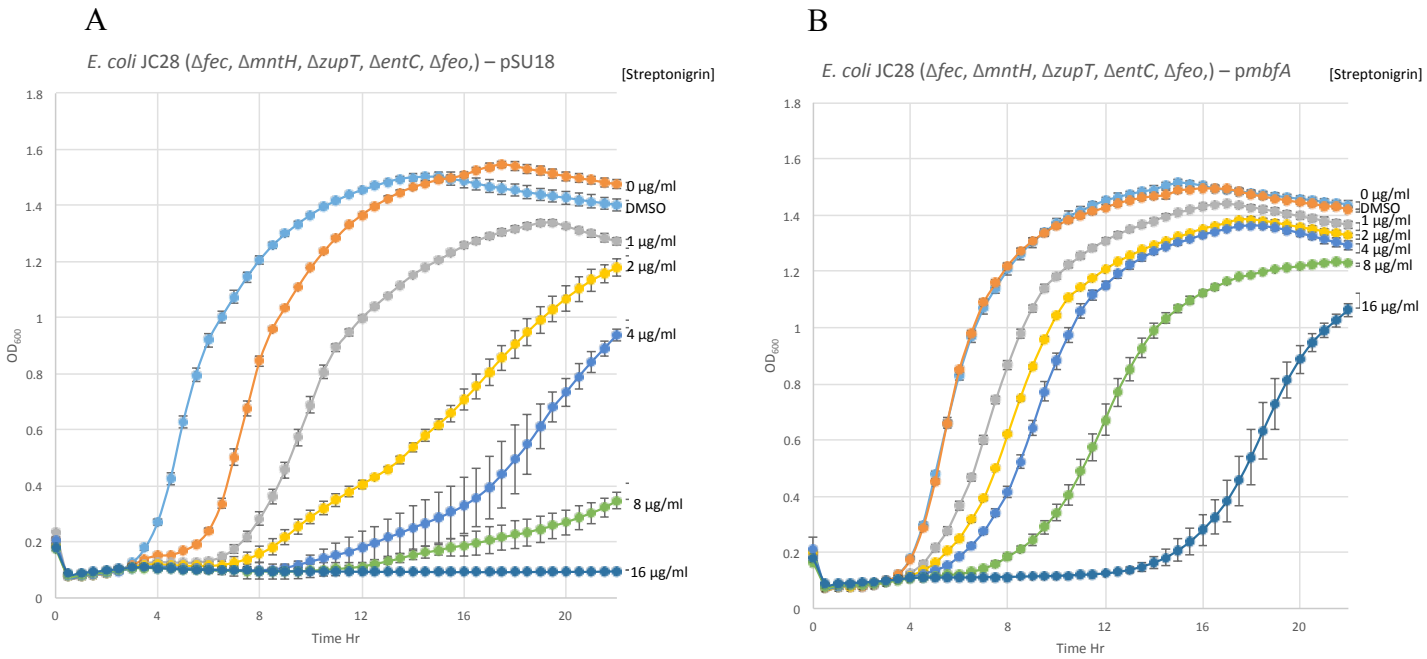

Figure 6.8: Representative growth curves of *E. coli* JC28 resistance to streptonigrin.

Aerobic growth in L broth with various levels of streptonigrin, (as displayed) for *E. coli* JC28 transformed with vector control (A) or pSU*mbfA* (B) or, with 0.5 mM IPTG. Data shown are the means ± standard deviation of three independent experiments conducted in triplicate.

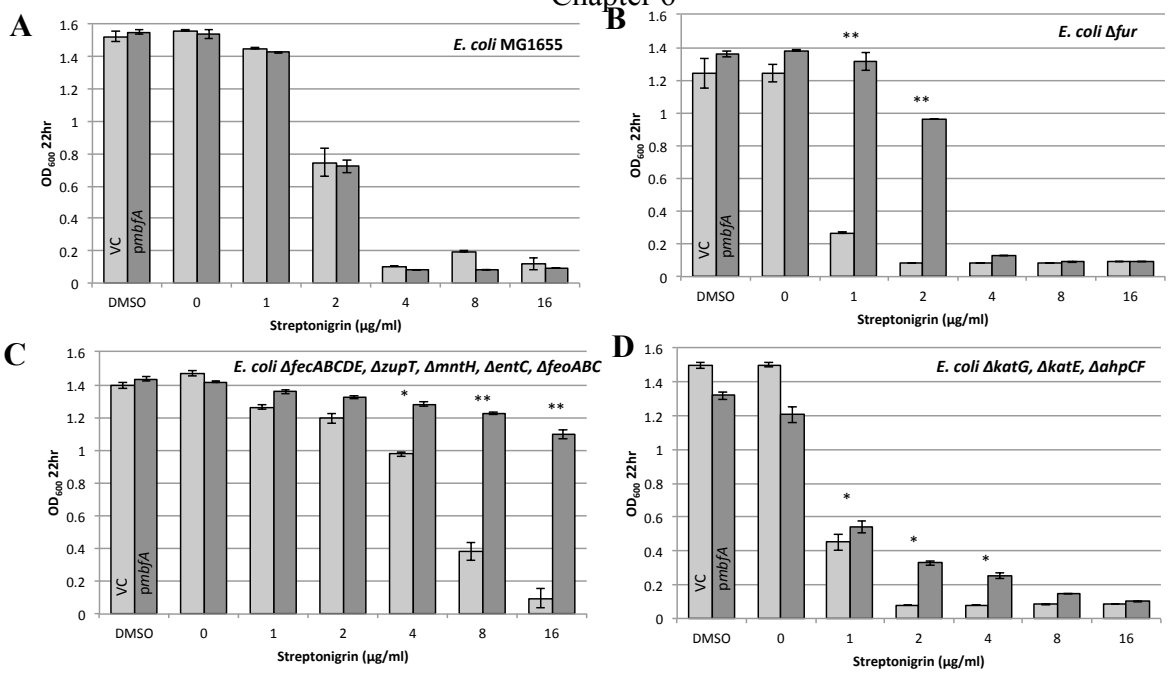

Figure 6.9: Expression of *mbfA* confers resistance to *E. coli* strains against streptonigrin.

Growth of vector control and pSU*mbfA* transformants after 22 h under aerobic conditions in L broth with 0-16 μg/ml of streptonigrin. A: *E. coli* MG1655, B: *E. coli* H1941, C: *E. coli* JC28 and D: *E. coli* LC106. Data shown are the means ± standard deviation of three independent experiments conducted in triplicate and analysed using an unpaired, two tailed Student's *t*-test: * $P<0.05$, ** $P<0.01$ *** $P<0.001$. Rhamnose was included at 0.1 mM.

Exposure of *E. coli* MG1655 (wildtype) to a range of streptonigrin concentrations resulted in an ~50% loss of growth a 2 μg/ml and complete loss at ≥4 μg/ml for both vector control and *mbfA* complemented strains (Figure 6.9A). The OD of the vector control and pSU*mbfA* transformants with addition of 2 μg/ml were reduced by 52.2 and 53.1% compared to those with no addition of streptonigrin, displaying no significant difference in cellular viability with expression of *mbfA*.

In contrast, examination of *E. coli* H1941 (Δ*fur*) using the same assay resulted in a 78.5 and 93.3% reduction in OD with the addition of 1 and 2 μg/ml streptonigrin (respectively) to *E.coli* Δ*fur* (VC) compared to zero addition, but only a 5.0 and 30.4% reduction for *E. coli* Δ*fur* transformed with pSU*mbfA* (Figure 6.9B), thus indicating a significant and major increase in streptonigrin resistance mediated by MbfA. This result extends the minor phenotypic observations of *mbfA* expression displayed previously in *E. coli* Δ*fur*. The results support the view that the deletion of *fur* increases

free, reactive cytosolic iron (Abdul-Tehrani et al. 1999), thus increasing sensitivity to streptonigrin, as indicated by the increased sensitivity for the VC seen at 1 and 2 µg/ml (Figure 6.9A & B). In addition, the results suggest that expression of *mbfA* drives export of cytosolic free iron which protect against the bactericidal action of streptonigrin through lowering concentrations of available iron able to interact with streptonigrin. It is interesting to note that the wildtype strain showed no gain in streptonigrin resistance when provided with *mbfA* which suggests that MbfA provides such an advantage for H1941 due to an ability to reverse the increase in free cytosolic iron caused by the *fur* mutation.

The *E. coli* JC28 strain showed a clear increase in streptonigrin resistance with respect to the wildtype and H1941 (Figure 6.9C). This was particularly apparent at 4 µg/ml where the JC28 vector control showed good growth (OD of 0.97 c.f. 0.10 for MG1655; Figure 6.9C). This marked increase in resistance to streptonigrin is directly related to the genotype of the JC28 strain; removal of iron import machinery would be expected to limit accumulation of iron within the cell for reaction with streptonigrin. It is of note that pSU*mbfA* further increased *E. coli* JC28 resistance to streptonigrin which is particularly evident at 16 µg/ml streptonigrin where MbfA increased growth from 0.10 to 1.1 OD units). These results thus suggest that the combined loss of iron uptake capacity and increase in iron export ability provide resistance to high levels of steptonigrin probably by driving very low intracellular iron concentrations.

Finally, the effect of *mbfA* on resistance of *E. coli* LC106 to streptonigrin was assessed. The deletion of catalase and alkyl hydroperoxidase was expected to have large implications of the resistance to streptonigrin due to raised redox stress sensitivity. The exact mechanism of action of streptonigrin is currently unknown but an involvement of reactive oxygen species is thought to contribute to its bactericidal effect (Lown 1983). The LC106 vector control grew less well than the wildtype by 0.67 OD units upon exposure to 2 µg/ml streptonigrin (Figure 6.9D). Transformation with pSU*mbfA* increased growth by 0.25 OD units, but did not restore growth to wild type levels (requiring an increase of 0.64 OD units). Nevertheless, *mbfA* provided significant protection (~threefold) against 2 and 4 µg/ml streptonigrin, where such protection was not seen in wild type *E. coli*. This indicates that MbfA is able to compensate for lack of redox-stress resistance in LC106, either by provision of peroxide reductase activity or through iron export activity.

6.5: Quantitation of iron export by MbfA using a radioactive isotope of iron

The above results support a role for MbfA in iron export, but provide no direct evidence for removal of iron from *E. coli.* Indeed, no direct evidence has yet been published demonstrating iron export by MbfA in any bacterium. Thus, to determine conclusively that iron is exported by MbfA, current published literature was reviewed to determine a protocol for an iron export assay. However, at the time this work was conducted there was little information in the literature of any methodology for conducting such experiments. Experiments conducted by Siva Sankari and Mark O'Brian (Sankari and O'Brian 2014) show the only "Iron export assay" in current literature. In this assay $^{55}FeCl_3$ was added to an exponentially growing *B. japonicum* culture, in rich broth, before extracellular iron was chelated at 20 min. Samples of cells with internalised ^{55}Fe were then taken at regular time points and the decrease in intracellular ^{55}Fe, as measured by a LBK γ-counter, was reported as evidence of iron export. However, this assay did not determine the export of intracellular iron as such, but instead measured the decrease in internal iron (in pmoles of ^{55}Fe per mg of protein) over a 180 min duration. Due to the fact that the original culture, at T_0, was at mid-log phase, in rich medium, the decrease in internal iron/mg protein is likely be due to growth, in addition, the product of export (i.e. supernatant iron accumulation) was not reported.

Radiolabeled iron transport experiments had also previously been conducted by Grass et al. (Grass et al. 2005) during the investigation of FieF (ferric iron efflux) iron transport in *E. coli*. In this assay, bacterial cultures were propagated in iron deplete medium, *fieF* was induced 30 min prior to the addition of radiolabeled ferrous iron, cells were collected by filtration, analysed by LSC and cellular iron concentrations reported. In similar respects to the experimentation conducted with *B. japonicum*, the effect of FieF expression was reported to prevent the accumulation of iron within the cell, rather than drive iron export from the cell.

Lastly, a different approach to characterizing iron export was conducted by Frawley et al. (Frawley et al. 2013) in the investigation of *Salmonella* Typhimurium IceT (iron citrate efflux transporter). *S.* Typhimurium *ΔiceT* was transformed with a plasmid harbouring the FeoAB ferrous iron transport system under a controllable expression promoter; the total cellular iron contents were determined via ICP-OES for this strain as well as an *iceT* transformant and compared. The cellular iron content of the IceT expressing strain was half that of the non-expressing strain, leading to the deduction the

IceT prevents cellular iron accumulation through exporting iron. Additionally, in the absence of constitutive expression of FeoAB in *S. Typhimurium* a reduction in cellular iron content of 10% was observed with expression of IceT.

To expand upon these studies, a protocol for accurately measuring accumulation of ^{55}Fe in the supernatant through export via MbfA was developed. A transformant *E. coli* MG1655 colony was grown overnight in 5 ml LB, from which 1 ml culture at an OD of 1, was used to inoculate 25 ml of fresh LB (starting OD 0.04) with 10 µl ^{55}Fe (0.185 mBq). The cells were allowed to grow until early-log phase (2 h, OD ~0.5) (Figure 6.10), during which time ^{55}Fe will be imported into the cell. After this, cells were induced with 0.1 mM rhamnose and incubated for a further 1 h. Induced cells were harvested by centrifugation (5000 x g 4 °C 10 min), the supernatant discarded, and the cells were washed three times with 10 ml cold transport buffer (TB: 50 mM MES, 50 mM TAPS pH 7.0, 0.4% glucose, 0.2 mM $CaCl_2$, 2 mM $MgCl_2$), ensuring the removal of extracellular ^{55}Fe. (N.B: transport buffer lacks essential nutrients, preventing growth during subsequent steps, but contains salts, for membrane integrity and glucose as an energy source to maintain cellular metabolism). The cell pellet was re-suspended in 1.5 ml ice cold TB and was then divided into 300 µl aliquots. One aliquot at a time was diluted into 3 ml pre-warmed (37 ^{o}C) TB in the reaction cell, maintained with continual stirring. 250 µl of cells were removed from the reaction cell for every time point taken and filtered through a 0.22 µm syringe driven filter, followed by washing with 2.5 ml cold wash buffer (WB: 10 mM EDTA, pH 8.0). 2 ml of filtrate (cellular supernatant) were added to 4 ml Ultima Gold XR scintillant (Perkin Elmer) and inverted until mixed. All samples were left for 24 h to allow for a reduction in background chemi-luminescence, before liquid scintillation counting for 3 min per sample across the 10–300 nm channels (0.2–6.2 KeV) with a Beckman LS-6500 multi-purpose scintillation counter. Additionally, to provide standardised results, diluted cells were removed from the reaction cell and the total protein concentration determined via a Bradford assay.

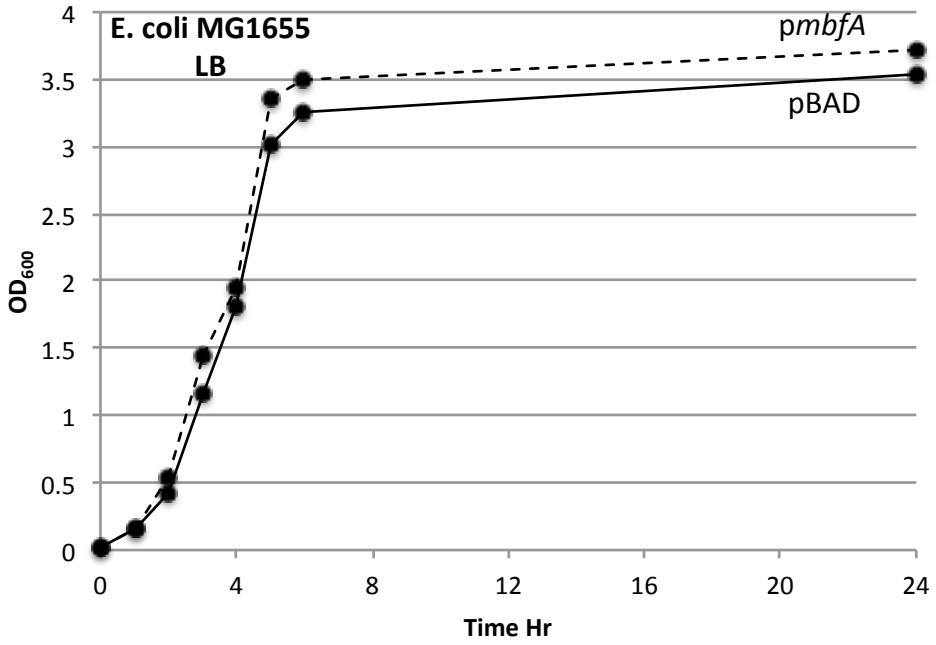

Figure 6.10: Growth of *E. coli* MG1655 in iron supplemented L broth.

Optical density growth curve of 24 h aerobic growth in L. broth of complemented *E. coli* LC106 with pBAD*mbfA,* or vector control. Data shown are the means of three independent experiments conducted in triplicate. Rhamnose was included at 0.1 mM.

6.6: Induction of *mbfA* is required for maximal export of iron

Initially, transformant with pBAD (vector control) and pBAD*mbfA* were assayed for export of ^{55}Fe into the supernatant in response to induction with rhamnose. 100 μM rhamnose was added to a culture of *E. coli* MG1655 transformed with pBAD or pBAD*mbfA* after 2 h growth, but was omitted from two equivalent cultures. Exported ^{55}Fe (pmol/mg) was measured every 5 min for 30 min (Figure 6.11A). Maximum export of ^{55}Fe (704.38 pmol mg^{-1}) was observed for pBAD*mbfA* with addition of rhamnose, resulting in a significant difference (p = 0.0004) at 15 min after initiation of the assay compared to that achieved without addition of rhamnose. ^{55}Fe export was far greater (>14-fold) upon *mbfA* induction, with 700 pmol mg^{-1} total export c.f. <50 pmol mg^{-1} without inducer (and also for the vector control) at 15 min.

Additionally, minimal export of ^{55}Fe was observed p*mbfA* without addition of rhamnose, resulting in a significant difference ($p = 0.003$) at 30 min after initiation of the assay compared to pBAD, which demonstrates no export of ^{55}Fe with and without addition of rhanmose (Figure 6.11B). This observation is supported by a Western blot in which ^{55}Fe was changed to ^{56}Fe allowing manipulation outside the Radiation Laboratory (Figure 6.11C). 1 OD of cells were harvested after 1 hour induction with and without addition of rhamnose; expression of MbfA (36.2 kDa) is observed maximally with addition of rhamnose, however, minimal expression is observed without addition of rhamnose. No expression is observed in the vector control samples, observations that are fitting with those of Figure 6.11.

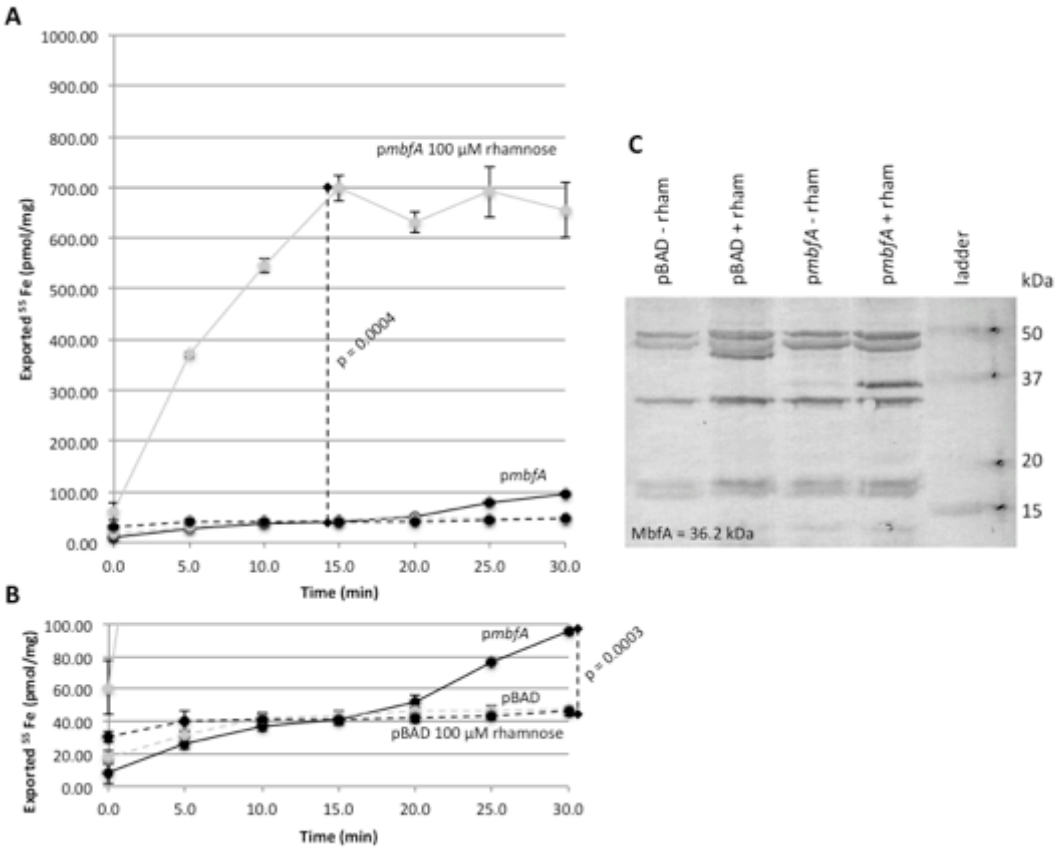

Figure 6.11: Export of iron is dependent upon MbfA expression.

Measurement of ^{55}Fe in cellular supernatant from *E. coli* MG1655 pBAD*mbfA* and pBAD transformants via liquid scintillation counting in the presence and absence of rhamnose. The data presented represents the means ± standard deviations obtained from three separate experiments. A: ^{55}Fe exported by *E. coli* MG1655 pBAD*mbfA* with and without addition of rhamnose (0.1 mM), statistically significant differences as determined by Students *t*-test ($p < 0.01$) at T = 15 min are indicated. B: Expanded view taken from A showing ^{55}Fe exported by *E. coli* MG1655 pBAD*mbfA* without addition of rhamnose and *E. coli* MG1655 pBAD, statistically significant differences as determined by Students *t*-test ($p < 0.01$) at T = 30 min are indicated. C: Western blot showing the presence of the *mbfA* translation product in *E. coli* MG1655(pBAD*mbfA*) with addition of rhamnose for cultures grown as in A. MbfA, 36.2 kDa.

6.7: Provision of hydrogen peroxide enhances export of iron by MbfA

Export of iron by MbfA is hypothesised to be combined with reduction of hydrogen peroxide at the erythrin domain; an electron is taken from ferrous iron prior to export across the inner-membrane, oxidising it to ferric iron, which is then used to reduce hydrogen peroxide at the erythrin domain, driving the export process. To investigate this proposed mechanism, hydrogen peroxide was added exogenously to the reaction cell upon initiating the ^{55}Fe export assay. The expectation was that increased hydrogen peroxide concentrations would increase iron export.

Addition of 100 μM H_2O_2 at T_0 resulted in a significant increase in ^{55}Fe export (629.00 pmol mg^{-1} to 856.25 pmol mg^{-1}– difference of 227.25 pmol mg^{-1}) until T_{20} ($p = 0.0248$) compared to no hydrogen peroxide addition, whereupon, export rate was not significantly different to that with 0 μM H_2O_2 addition (Figure 6.12). To further explore this effect, the converse experiment was conducted; in place of peroxide, an addition of 100 U of a haem catalase from *Micrococcus lysodeikticus* was made to the reaction cell at T_0. Addition of catalase was expected to decrease endogenous hydrogen peroxide concentrations (given the non-polar nature of hydrogen peroxide, concentrations outside the cell are expected to be approximately equal to those within the cell) which would inhibit ^{55}Fe export (presuming that export is peroxide dependent). A significant ~2.5-fold reduction of 392 pmol mg^{-1} ($p = 0.0026$) in exported ^{55}Fe was observed at T_{20} when compared to no addition of catalase. The amount of ^{55}Fe exported did not reach that observed with no addition, over the duration of the assay, but remained ~2.5-fold lower. This effect is presumably due to the catalase-mediated degradation of H_2O_2 which would be expected to maintain very low levels of H_2O_2 within the culture. However, ^{55}Fe export was still significantly (sixfold) more than that of the vector control ($p = 0.0034$) throughout the assay. In combination, these results strongly suggest that MbfA is indeed an iron exporter and that its export activity is promoted biochemically by H_2O_2.

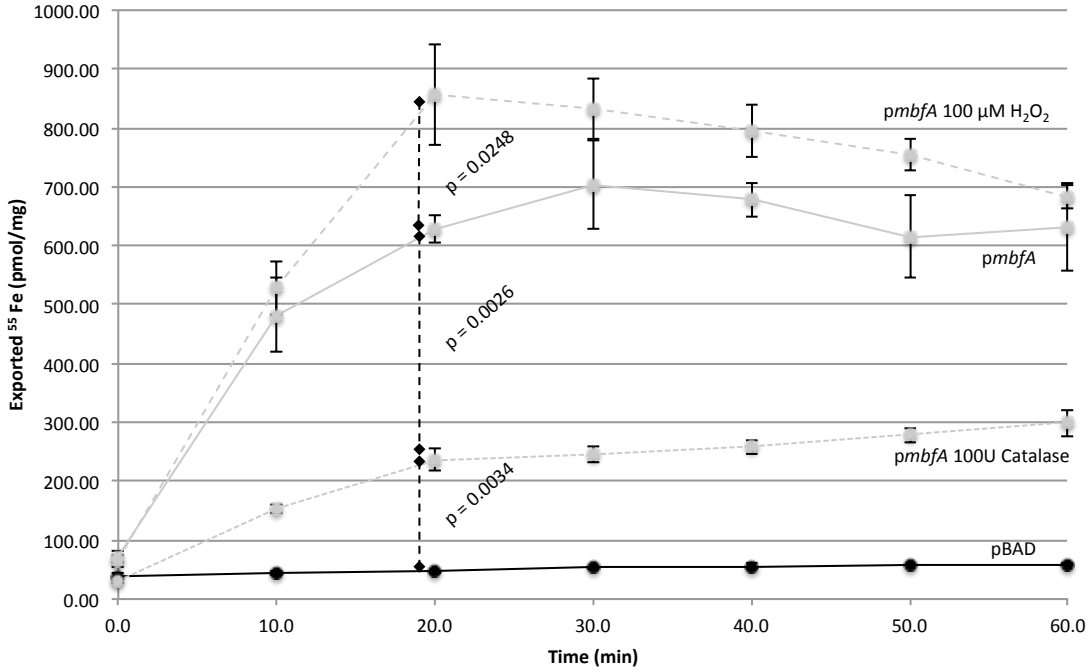

Figure 6.12: Addition of hydrogen peroxide increases export of iron.

Measurement of ^{55}Fe in cellular supernatant of *E. coli* MG1655 pBAD*mbfA* and pBAD transformants via liquid scintillation counting in the presence/absence of hydrogen peroxide or catalase. The data presented represents the means ± standard deviations obtained from three separate experiments. Statistically significant differences as determined by Students *T*-test ($p < 0.01$) at T = 20 min are indicated.

The N-terminal erythrin domain of MbfA is predicted to facilitate the reduction of hydrogen peroxide; previously generated N- and C-terminal mutant constructs of *mbfA* (pBAD*ery* and pBAD*vit*) were compared to ^{55}Fe export by MbfA. Removal of the erythrin domain and expression of the membrane embedded VIT1 domain only, and conversely, expression of only the erythrin (peroxide reductase) domain, without the VIT1 domain, resulted in no significant difference in ^{55}Fe export to that of the vector control (pBAD) (Figure 6.13A/B). This shows that iron export by MbfA requires the combination of both domains and is consistent with the findings made earlier in this chapter showing that redox-stress resistance conferred by MbfA requires both domains (Figure 6.6C). This finding thus further supports the suggested mechanism of iron export by MbfA where hydrogen peroxide reduction is hypothesized to drives iron export.

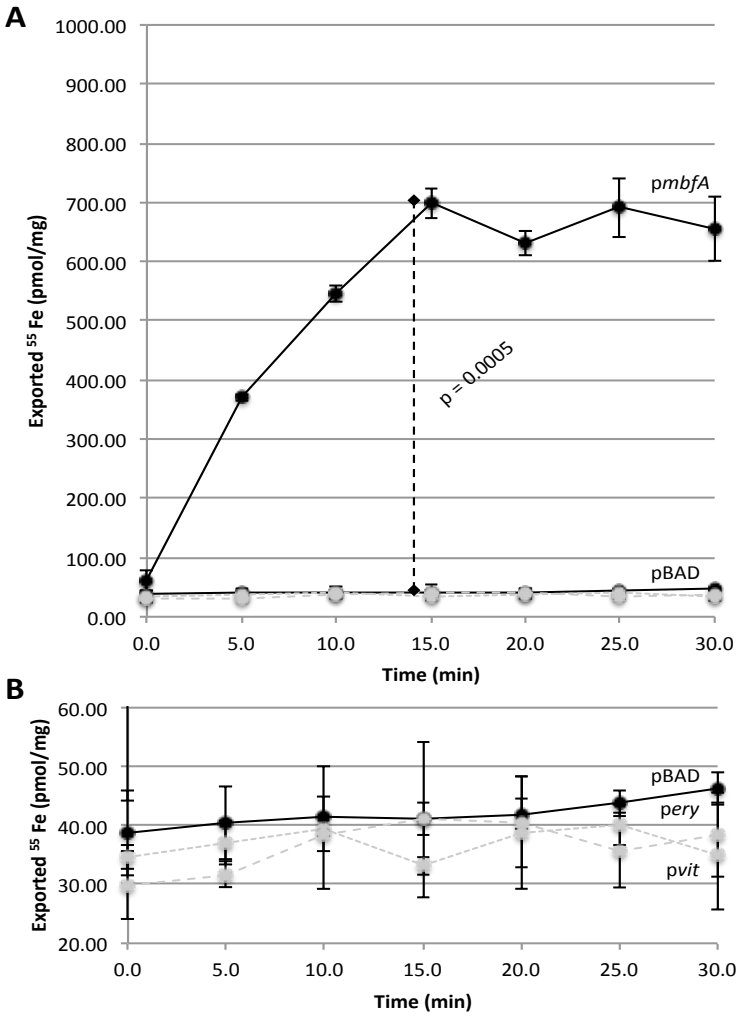

Figure 6.13: Both domains of MbfA are required for export of iron.

Measurement of ^{55}Fe in cellular supernatants from *E. coli* MG1655 pBAD*ery* and pBAD*vit* transformants via liquid scintillation counting. The data presented represent the means ± standard deviations obtained from three separate experiments. A: ^{55}Fe exported by *E. coli* MG1655 pBAD*mbfA* (data from Figure 6.11) compared to *E. coli* MG1655 pBAD*ery*, statistically significant differences as determined by Students *t*-test ($p < 0.01$) at T = 15 min are indicated. B: Expanded view taken from A, ^{55}Fe exported by the vector control, *E. coli* MG1655 pBAD*ery* and *E. coli* MG1655 pBAD*vit,* no statistically significant differences are observed.

An extension to this experiment was conducted in which the erythrin and VIT domains were expressed *in trans* from two separate plasmids within the same cell. In this way, an attempt was made to complement the lack of iron export observed with the domains expressed in isolation, through the supply of both protein domains. Two distinct origins of replication, inducible promoters and antibiotic resistance markers are required on each plasmid to allow compatibility within the same cell. The pBADHisA plasmid (pBR322 origin, Kn^R arabinose inducible) was selected as a suitable system to use

alongside the current pBAD$_{rham}$ plasmid (p15A origin, Cm^R, rhamnose inducible). Initially, experimentation was conducted to ensure that the pBADara plasmid harbouring the *B. suis mbfA* sequence yielded similar observations of iron export to that seen previously with the pBAD*mbfA* (rhamnose) expression plasmid (Figure 6.14).

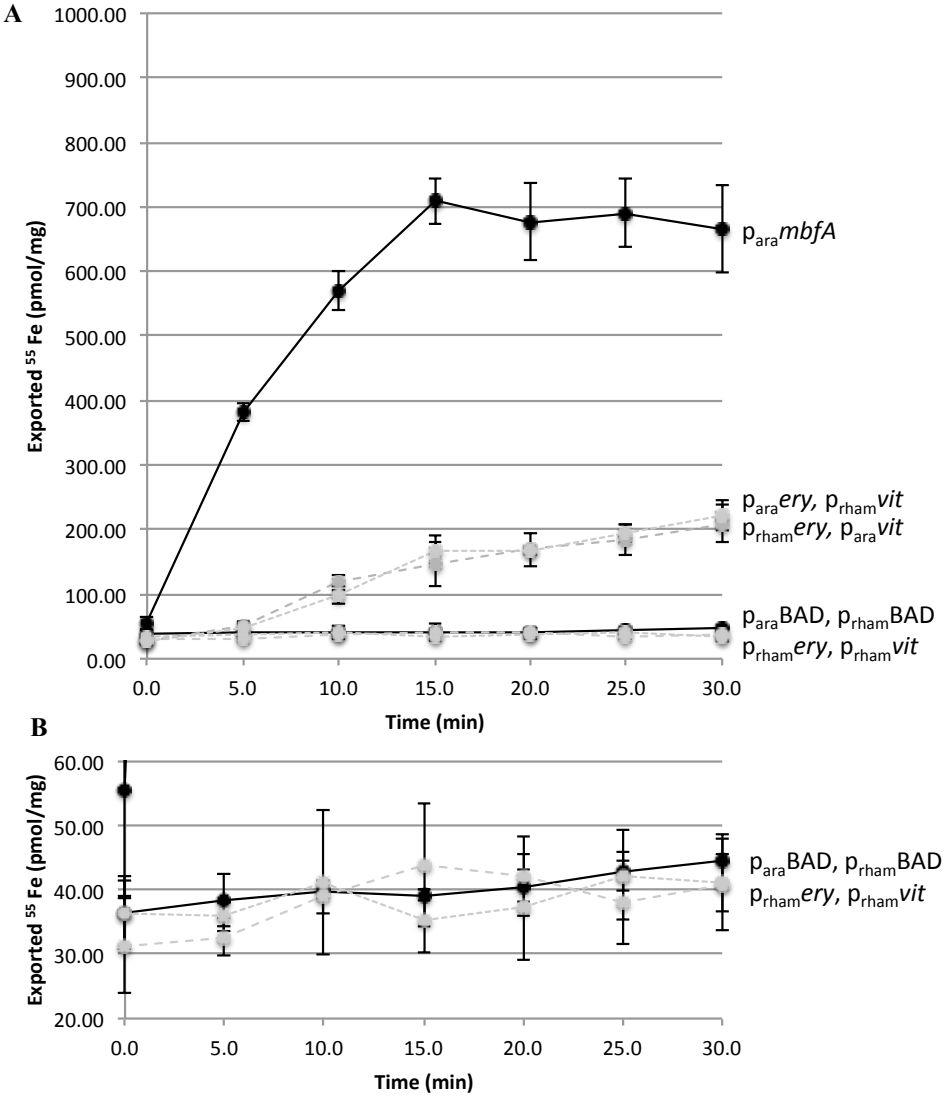

Figure 6.14: Expression of MbfA and erythrin and VIT1 domains *in trans* from arabinose inducible vector results in export of iron.

Measurement of ^{55}Fe in cellular supernatants from *E. coli* MG1655 pBADrham and pBADara transformants. The data presented represent the means ± standard deviations obtained from three separate experiments. A: ^{55}Fe exported by *E. coli* MG1655 pBAD*mbfA*(ara), pBADery(ara)/pBADvit(rham), pBADery(rham)/pBADvit(ara) pBADara and pBADrham, rhamnose and arabinose included at 0.1 mM. B: Expanded view taken from A.

Expression of MbfA from the arabinose inducible plasmid resulted in very similar concentrations of iron export from *E. coli* MG1655, also, as was previously noted, the expression of either the erythrin or Vit domain in isolation resulted in no export of iron. Next, examination of iron export was monitored from *E. coli* MG1655 transformed with a combination of either pBADery(ara) and pBADvit(rham) or pBADery(rham) and pBADvit(ara) (Figure 6.14).

Expression of the two MbfA domains *in trans* resulted in export of iron from *E. coli* MG1655 reaching an average maximum of 216.3 pmol mg^{-1}, however this represented a 67.5% reduction in the amount of iron exported after 30 min compared to the native MbfA system. This result is significant as is shows that interactions between the two MbfA domains are possible, permitting iron export, even when both are supplied inside the cell, despite no physical linkage. Export rate is significantly reduced compared to the native MbfA system; this likely relates to the dilution of interactions between the two domains through the loss of the physical connection.

In line with the experiments described previously, additions of hydrogen peroxide and catalase were conducted with the *in trans* MbfA expression system (Figure 6.15). Addition of 100 μM hydrogen peroxide resulted in a 20.0% increase in export, whilst addition of 100U haem catalase resulted in a 37.3% decrease in export compared to a no addition control.

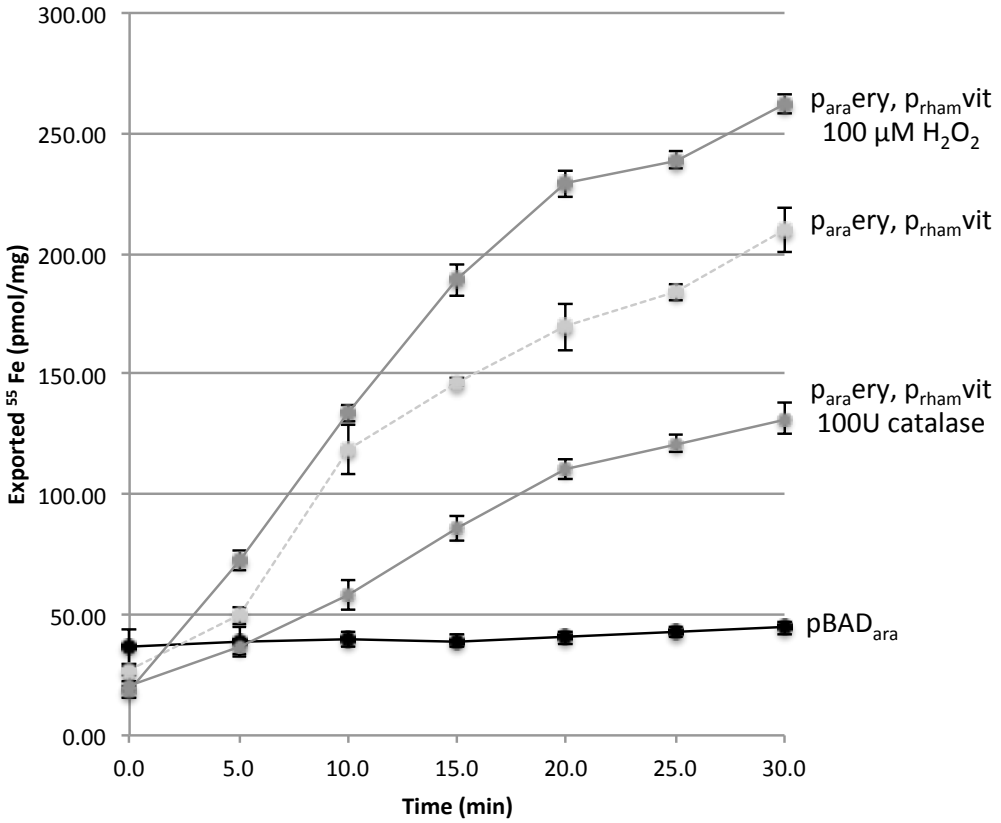

Figure 6.15: Addition of hydrogen peroxide increases *in trans* MbfA iron export rate.

Measurement of ^{55}Fe in cellular supernatants from *E. coli* MG1655 pBADrham and pBADara transformants in the presence/absence of hydrogen peroxide or catalase. The data presented represent the means ± standard deviations obtained from three separate experiments.

Another experiment supporting the involvement of hydrogen peroxide driving iron export by MbfA was conducted by washing cells with degassed transport buffer. De-gassing, removal of dissolved oxygen, was achieved through the bubbling of nitrogen gas through required solutions for 20 min. 3 ml of degassed transport buffer was used within the reaction cell, which was also sealed with an o-ringed plunger to maintain a decreased oxygen environment. The removal of oxygen ensured the cessation of oxidative respiration, therefore preventing hydrogen peroxide generation – thus removing the oxidation substrate thought to be required for iron export. Removal of oxygen resulted in a significant reduction in ^{55}Fe export compared to that seen in aerobic conditions, 84% reduction (115.84 pmol mg^{-1} after 30 min), although export was still present and significantly more than that of the vector control ($p = 0.011$) after 15 min (Figure 6.16A/B). To increase iron export under depleted oxygen conditions, 100 μM hydrogen peroxide (vacuum degassed) was introduced via a hypodermal syringe injection through the O-ringed sealed plunger at T_{15} (Figure 6.16A). At T_{20}, T_{25} and T_{30} (5, 10 and 15 min after H_2O_2 introduction respectively) detection of significantly increased ^{55}Fe (nearly fivefold at T_{30}) in the supernatant was measured compared to no H_2O_2 introduction ($p = 0.015$, $p = 0.004$ and $p = 0.009$ respectively).

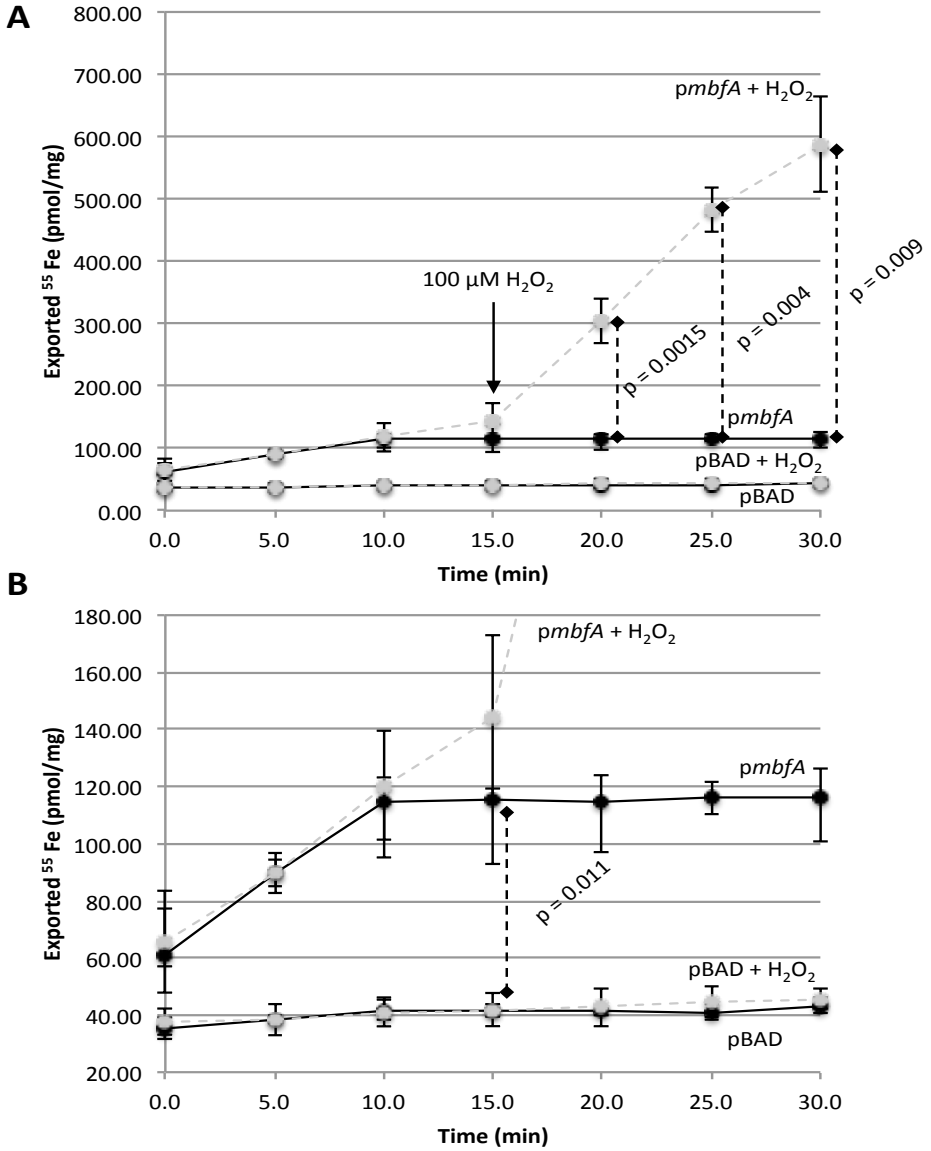

Figure 6.16: Removal of oxygen limits MbfA-mediated export of iron.

Measurement of ^{55}Fe in cellular supernatant from *E. coli* MG1655 pBAD*mbfA* transformants under decreased oxygen conditions. The data presented represents the means ± standard deviations obtained from three separate experiments. A: ^{55}Fe exported by *E. coli* MG1655 pBAD*mbfA* under decreased oxygen conditions with addition of 100 µM hydrogen peroxide at T = 15 min, statistically significant differences as determined by Students *t*-test ($p < 0.01$) at T > 15 min are indicated. B: Expanded view taken from A.

6.8: Identification of conserved amino acids required for iron transport by MbfA.

The VIT1-like domain of the MbfA protein is conserved across both prokaryotes and eukaryotes and can be presumed to act universally to transport iron and/or related metals across a single membrane. To identify conserved residues in the coding sequence of the VIT domain, the amino acid sequence of the *B. suis* 1330 MbfA Vit domain was aligned with VIT1 proteins of plant, yeast and mammalian parasites (Figure 6.17). The location of trans-membrane helices was determined through trans-membrane domain analysis (Phobius - (Kall et al. 2004)) and was over-laid on the alignment data to allow contextual information of amino acid location to be given to conserved residues across species. With respect to iron transport, four amino acids (D_{191}, M_{228}, E_{232} and Y_{268}) were identified as potential iron ligands due to their high conservation, location within membrane helices or cytoplasmic loops and known iron-binding capacity.

Site directed mutagenesis (SDM) was used as an investigative tool to gain insight to the mechanism of iron transport across the inner membrane in Gram-negative bacteria. SDM (Primers D191G F/R, M228G F/R, E232G F/R and Y268G F/R; Table 2.4) was used to change the nucleotide sequence of the D_{191}, M_{228}, E_{232} and Y_{268} codons of *B. suis mbfA* to glycine. In this way, modified pBAD*mbfA* constructs with a targeted mutated residue can be assayed for ability to promote export of iron and thus assess residue involvement in MbfA/VIT1 iron-export function. To ensure that mutation of the *mbfA* nucleotide sequence resulted in efficient expression of the MbfA protein, Western blot analysis was conducted on each variant (Figure 6.18). Immuno-blotting identified that MbfA was present from each mutated variant, allowing valid assessments of iron export potential to be determined.

Impaired iron transport was assessed using two assays: first, via measurement of optical density of *E. coli* JC28 transformants. The essentiality of the amino acid for iron transport will be measured by the relative increase in *E. coli* JC28 growth compared to that of *E. coli* JC28 growth with non-mutated MbfA construct expressed. Secondly, the ability of mutated constructs to facilitate iron export was measured quantitatively via the radioactive iron export assay.

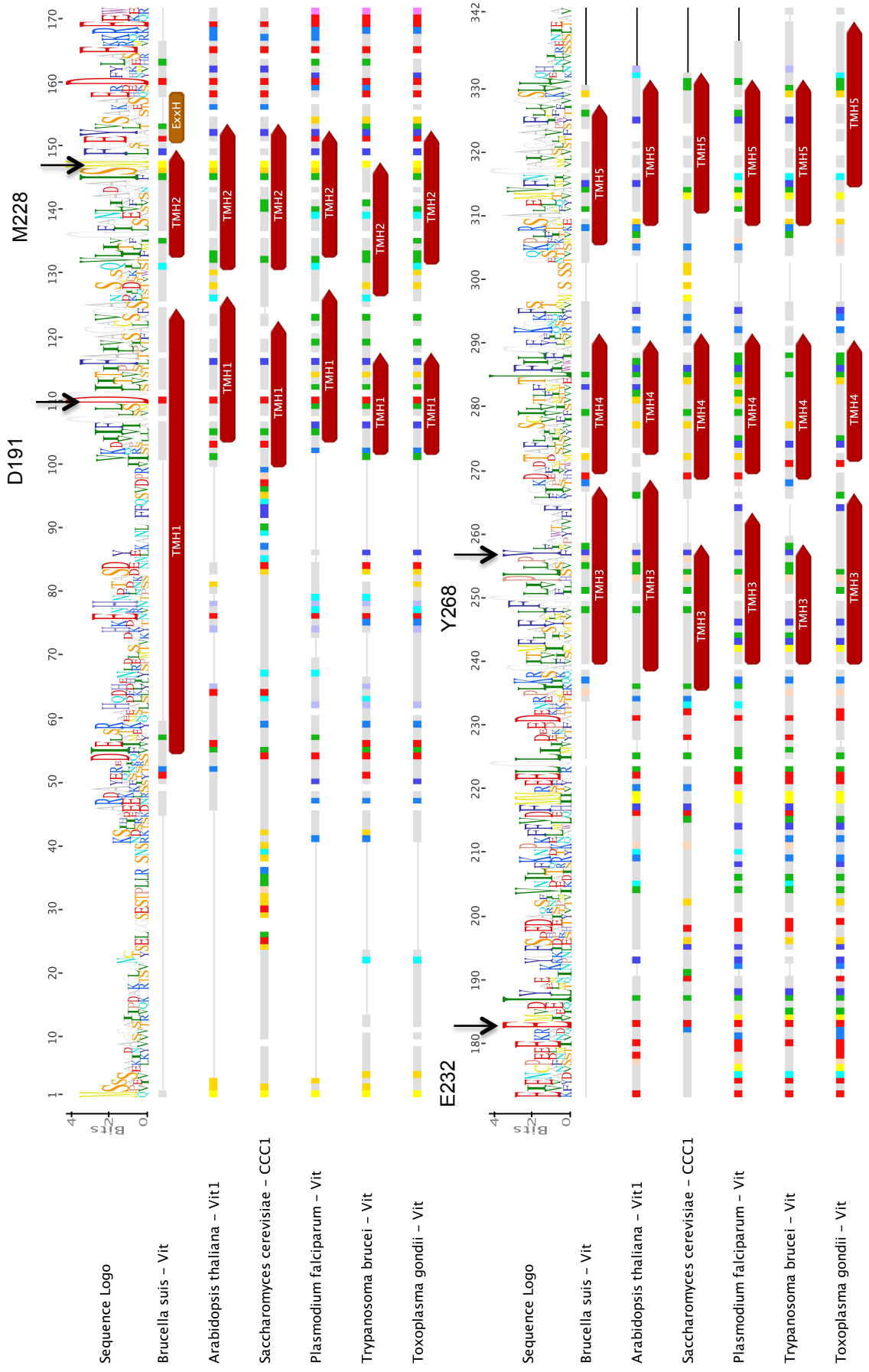

Figure 6.17: Alignment of VIT1 and Vit domain amino acid sequences with over-laid trans-membrane helix locations. Mutated residues indicated with arrow.

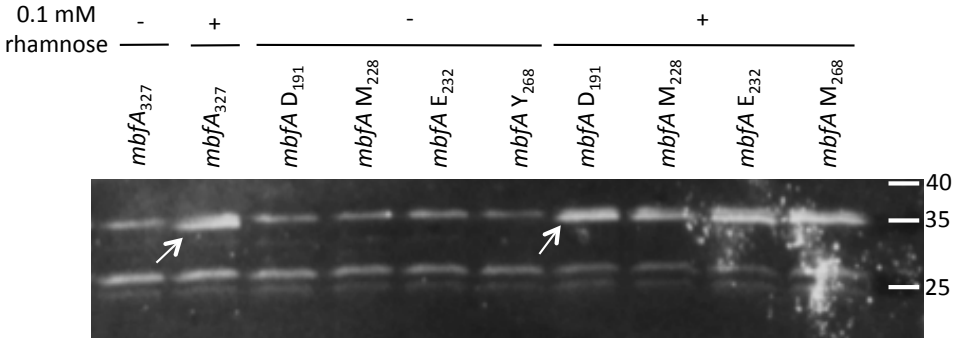

Figure 6.18: Western blot analysis of expression of SDM pBAD*mbfA* variants.
Immuno-detection of expression of *mbfA* from pBAD*mbfA* SDM variants (D_{191}, M_{228}, E_{232} and Y_{268}) in *E. coli* MG1655, lanes from left to right: pBADmbfA without and with induction with 0.1 mM rhamnose. pBAD*mbfA*D_{191}, pBAD*mbfA*M_{228}, pBAD*mbfA*E_{232} and pBAD*mbfA*Y_{268} without then with induction with rhamnose. MbfA 36.4 kDa indicated with arrow.

Bacterial growth curves were generated for a negative and positive control ($pBAD_{rha}$ and pBAD*mbfA*). Transformants carrying putative iron export *mbfA* mutants were then monitored for improvements in growth in iron restricted minimal medium compared to the wild type *mbfA* expressed in JC28 cells (Figure 6.19).

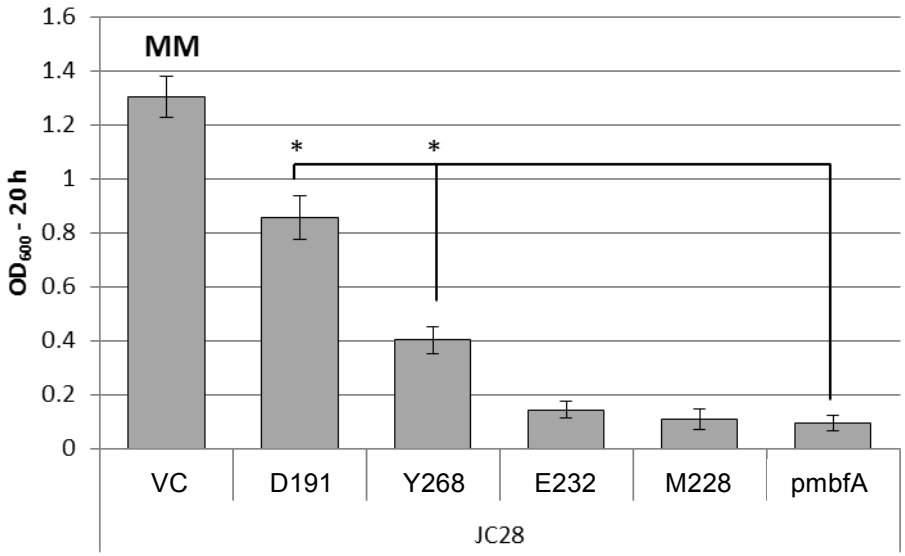

Figure 6.19: Assessment of effect of MbfA SDM variants on growth of *E. coli* JC28.
Growth after 48 h aerobic growth in 10 μM iron citrate supplemented minimal medium of complemented *E. coli* JC28 with pBAD*mbfA,* vector control (pBAD) and the indicated SDM variants of pBAD*mbfA*. Data shown are the means ± standard deviation of three independent experiments conducted in triplicate and analysed using an unpaired, two tailed Student's *t*-test; * $P<0.05$, ** $P<0.01$ *** $P<0.001$.

Expression of the pBAD*mbfA*D_{191} and pBAD*mbfA*Y_{268} MbfA mutant constructs resulted in a significant increase in growth compared to the growth of *E. coli* JC28 with expression of the non-mutated *mbfA* after 48 h. This increase in growth suggests that more iron is available to the cell for these strains due to a detrimental mutation in the VIT domain of MbfA preventing iron removal. The transformant with mutation in the D_{191} *mbfA* codon yielded an optical density after 48 h most similar to *E. coli* JC28 vector control, suggesting a key role in iron transport for this residue. D_{191} is located in the centre of trans-membrane helix 1 (Figure 6.20) and may act as a key binding ligand for iron during passage across the inner membrane. Mutation of Y_{268} provides a significant increase in growth compared to the non-mutated *mbfA*, but less than that of D_{191}. Y_{268} is located in the periplasmic-facing end of trans-membrane helix 3 and act as a binding ligand for iron during release into the periplasm.

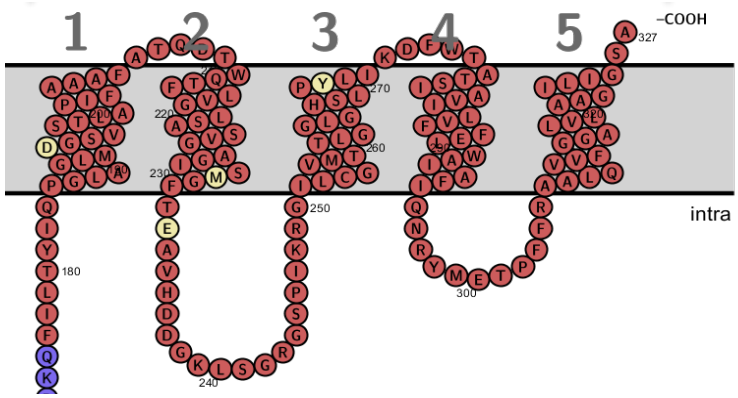

Figure 6.20: Schematic representation of *B. suis* 1330 Vit domain of MbfA.
Schematic representation of the structure of the VIT domain of MbfA. Locations of trans-membrane helices, periplasmic and cytoplasmic loops and SDM targets are displayed (blue residues represent the location of the erythrin domain).

In addition to assessment of *E. coli* JC28 growth, the ability of the *mbfA* SDM variants to export ^{55}Fe from *E. coli* (MG1655) was also determined (Figure 6.21). Mutation of $M_{228}/E_{232}/Y_{268}$ resulted in no significant difference in supernatant accumulation of ^{55}Fe after 15 min compared to the non-mutated *mbfA* construct. Although no significant difference was apparent for $M_{228}/E_{232}/Y_{268}$, the M_{228} and E_{232} variants gave lower export than the Y_{268} variant. However, mutation of D_{191}, located in the centre of trans-membrane helix 1, resulted in 41% less ^{55}Fe export than the positive control. Although the results for exported iron are not in complete agreement with the results obtained

with *E. coli* JC28, regarding mutations which present the greatest attenuation in iron transport, D_{191} presented in both cases as the most important of the four residues tested. This may suggest a central role in D_{191} acting as a transporting ligand during iron efflux through MbfA, as well as VIT1.

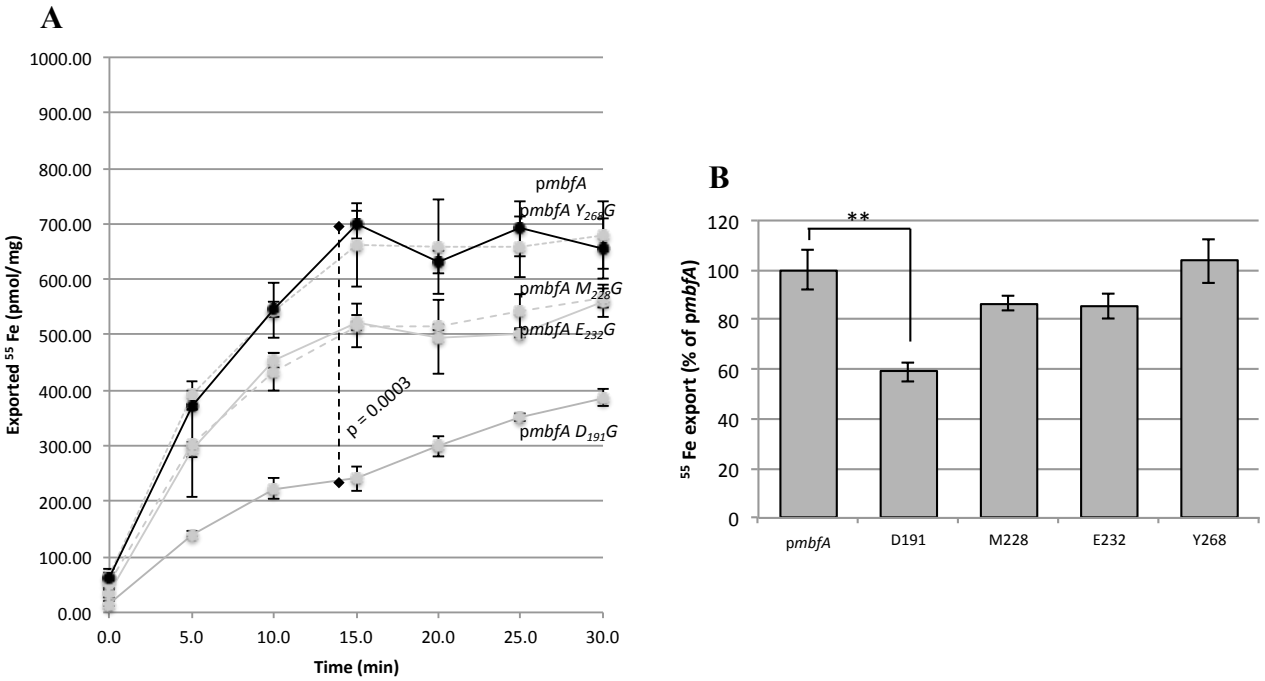

Figure 6.21: Assessment of effect of *mbfA* SDM variants on export of iron from *E. coli* MG1655.

Measurement of ^{55}Fe in cellular supernatants from *E. coli* MG1655 pBAD*mbfA* site directed mutant transformants. The data presented represent the means ± standard deviations obtained from three separate experiments. A: ^{55}Fe exported by *E. coli* MG1655 pBAD*mbfA* compared to *E. coli* MG1655 pBAD*mbfA* SDM variants, statistically significant differences as determined by Students *T*-test ($p < 0.01$) at T = 15 min are indicated. B: Comparison of ^{55}Fe export as a percentage of non-mutated MbfA at 15 min (data from A), statistically significant differences as determined by Student's *t*-test; * $P<0.05$, ** $P<0.01$ *** $P<0.001$.

6.9: Iron export by *Arabidopsis thaliana* vacuolar iron transport 1

With the phenotypic evidence of iron export collected from the complementation of the oxidative stress sensitive *E. coli* LC106 strain with pBAD*At_VIT1*, a more thorough examination of iron export by *Arabidopsis thaliana* vacuolar iron transport 1 was conducted. The ^{55}Fe export assay was repeated as described previously but with replacement of *E. coli* MG1655 p*mbfA* transformants for *E. coli* MG1655 pBAD*At_VIT1* transformants (Figure 6.22).

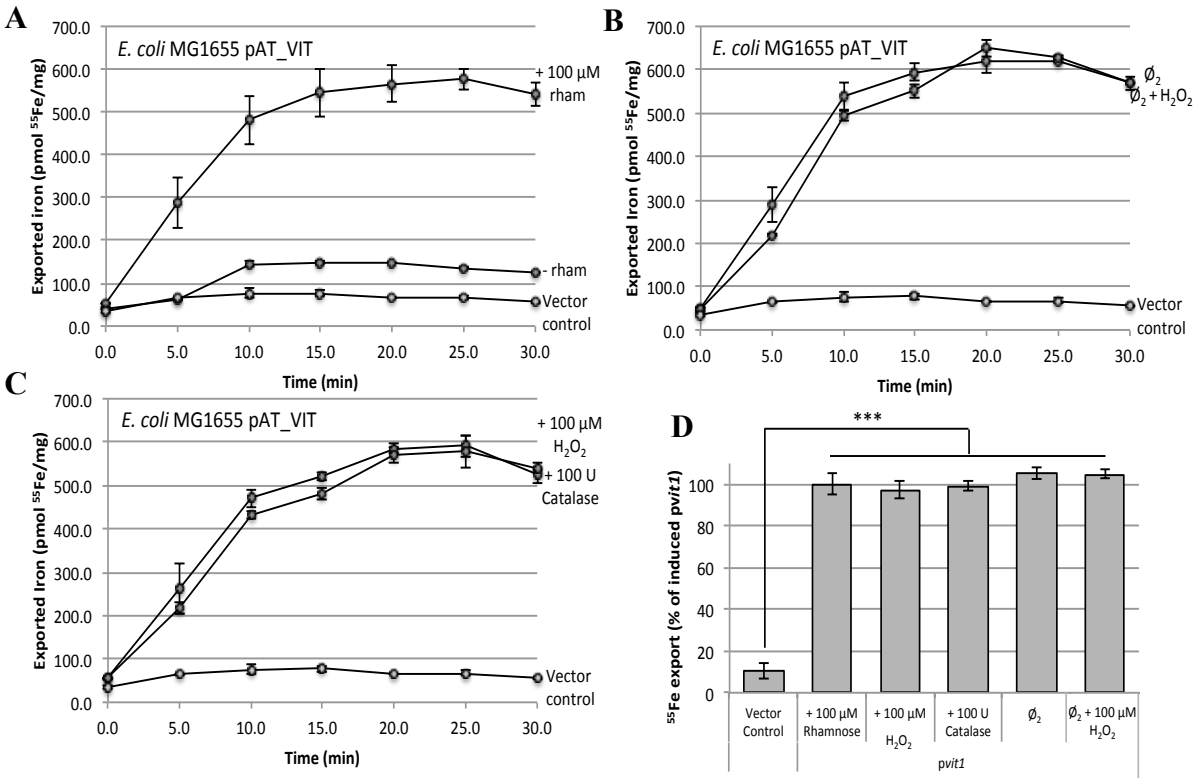

Figure 6.22: Iron export by VIT1 from *A. thaliana*.

^{55}Fe accumulation in *E. coli* MG1655 supernatant during iron export through expression of VIT1 from pBAD*At_VIT1* with no addition (A), 100 µM H_2O_2, 100 U catalase (B), anaerobic propagation or anaerobic propagation followed by 100 µM H_2O_2 injection (C). D: Summary of data expressed as the percentage of ^{55}Fe export. Vector control is also included. Data shown are the means ± standard deviation of three independent experiments conducted in triplicate and analysed using an unpaired, two tailed Student's *t*-test; * P<0.05, ** P<0.01 *** P<0.001. Rhamnose was present at 0.1 mM.

Export of ^{55}Fe by VIT1 was observed to reach a maximum of 542 pmol mg^{-1} after 30 min (162 pmol mg^{-1} lower than form MbfA). Iron accumulation in cellular supernatants only occurred with addition of 100 μM rhamnose, inducing gene expression, during bacterial propagation. This demonstrates that the VIT1 protein, without an N-terminal erythrin domain as present in MbfA, is able to export iron out of *E. coli*.

In contrast to the hydrogen peroxide dependent export of iron observed in MbfA, manipulation of H_2O_2 through addition or removal of H_2O_2, or anaerobic culture, did not influence supernatant accumulation of ^{55}Fe directed by VIT1 (Figure 6.22B/C). This provides evidence to both the hypothesis that the erythrin domain drives the H_2O_2-dependent export of iron in MbfA, and also indicates that a different mechanism of iron transport must be present and functional in Vit1 proteins lacking an erythrin domain.

Due to the location of VIT1 in the vacuole and artificially within the inner membrane of *E.coli*, it is likely that energetically the VIT1 domain is acting as a Fe^{2+}/H^+ antiporter. To elucidate this mechanism of iron translocation across the vacuolar and inner membranes, the effect of addition of the proton ionophore carbonyl cyanide *m*-chlorophenyl hydrazone (CCCP) was examined upon export activity of VIT1 and MbfA (Figure 6.23).

1, 10 and 100 μM concentrations of CCCP all resulted in a decrease in ^{55}Fe export in both VIT1 and MbfA transformant strains. However, disruption of the proton gradient was less marked in terms of iron export for MbfA (10 μM CCCP gave a 74.5% reduction for VIT1 but just a 5.3% reduction for MbfA), presumably because MbfA iron export is peroxide, not proton motive force, dependent. The slight decrease in iron export could be due to disruption of cellular respiration, which might reduce endogenously generated H_2O_2. It is likely that CCCP effectively prevents iron translocation by VIT1 through the disruption of the proton motive force across the inner membrane, which strongly suggests that VIT1 uses a Fe^{2+}/H^+ antiporter mechanism.

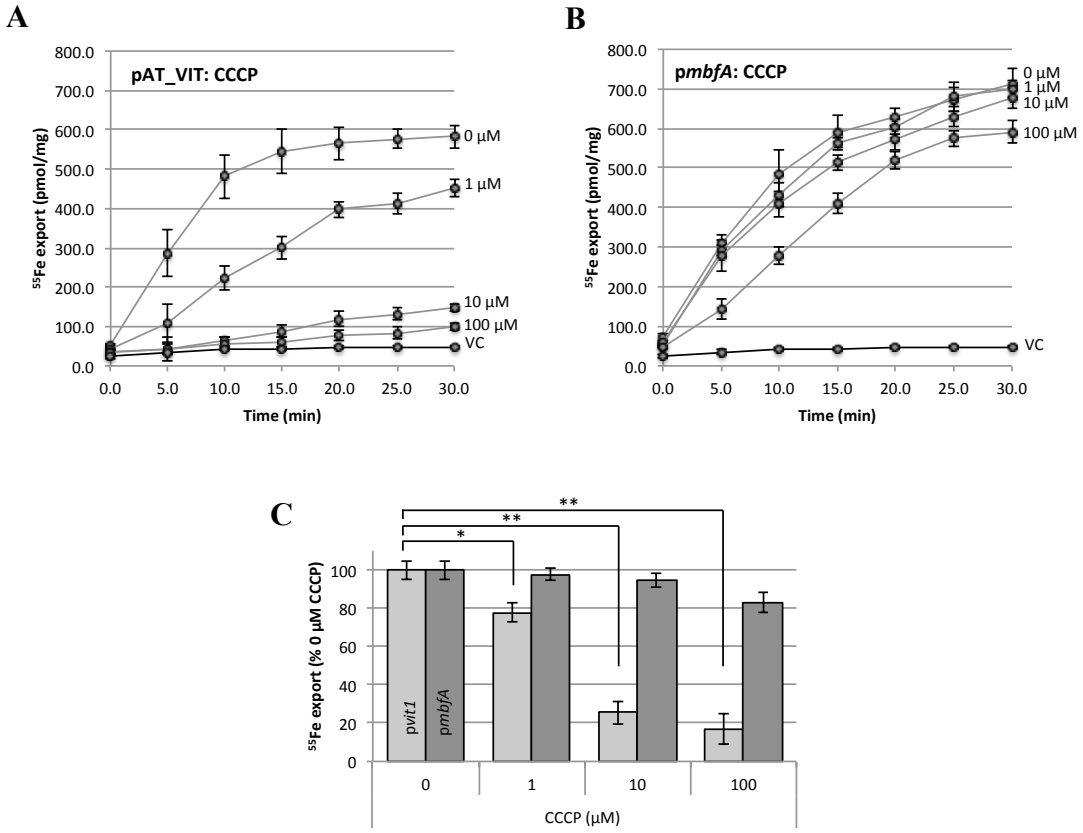

Figure 6.23: Effect of CCCP on iron export by MbfA and VIT1.

^{55}Fe export by *E. coli* MG1655 transformed with p*At_VIT1* (A) or p*mbfA* (B) with 0-100 µM CCCP. C: Summary of data expressed as the percentage of ^{55}Fe export. Data shown are the means ± standard deviation of three independent experiments conducted in triplicate and analysed using an unpaired, two tailed Student's *t*-test; * $P<0.05$, ** $P<0.01$ *** $P<0.001$.

6.10: MbfA exports ferric iron, Vit1 exports ferrous iron.

Given the current hypothesis of iron export by MbfA, where ferrous iron in the cytosol is oxidised to ferric iron during export into the periplasm, exported iron will present in the ferric oxidation state. In contrast, due to the lack of an erythrin domain and capability to reduce ferrous iron, Vit1 systems are thought to export ferrous iron in to the periplasm in the *E. coli* model.

To determine experimentally the oxidation state of the exported iron by MbfA and VIT1, a colorimetric assay using the specific ferrous iron chelator ferrozine was conducted. An adaption was made to a standard ferrozine assay to allow determination of the redox state of the exported iron. Ferrozine specifically binds ferrous iron, the inclusion of acetic acid and 750 mM sodium sulphite within the assay converts all available iron to the ferrous form, allowing the quantitation of total iron from the generation of the colorimetric ferrous-ferrozine complex (extinction coefficient: 27.9 mM^{-1} cm^{-1} at 562 nm). To determine specifically if MbfA/VIT1 export ferric or ferrous iron, first a ferrozine assay with acetic acid and sodium sulphite omitted was conducted, followed by the assay of the same sample with acetic acid and sodium sulphite included. The difference in iron concentration between the two assays will give the concentration of ferric iron in solution. The ^{55}Fe transport assay protocol was used to facilitate collection of cellular supernatant samples (^{55}Fe was substituted for non-radioactive ^{56}Fe).

Preliminary studies collecting supernatant from 3.3 ml and 50 ml of cultured cells after 20 min incubation at 37 °C provided inconclusive evidence of the redox state of the exported iron due to iron concentrations beneath the limit of detection for the assay. Increasing the number of cells within the assay through using 1 litre of culture reduced to a volume of 50 ml, thus increasing the concentration of iron exporting cells, resulted in detectable concentrations of iron.

Minimal detection of either ferric or ferrous iron was observed within the supernatant of *E. coli* MG1655 pBADrham (vector control). The detection of ~25 μM of ferric iron was detected in the supernatant from *E. coli* MG1655 pBAD*mbfA* with induction, whilst ~30 μM of ferrous iron was detected in the supernatant from *E. coli* MG1655 pBAD*At_VIT1* (Figure 6.24).

The cloned *mbfA* construct specifically exported ferric iron supporting the hypothesis that the erythrin domain removes an electron from the exported cytosolic ferrous iron during export. Conversely, due to the lack of an erythrin like domain in the VIT1 system, VIT1 transports specifically ferrous iron. These observations support those made by Cockrell et al (Cockrell et al. 2014) who determine by Mossbauer and EPR spectroscopy that ferrous iron is translocated into the seed vacuole and is subsequently oxidised.

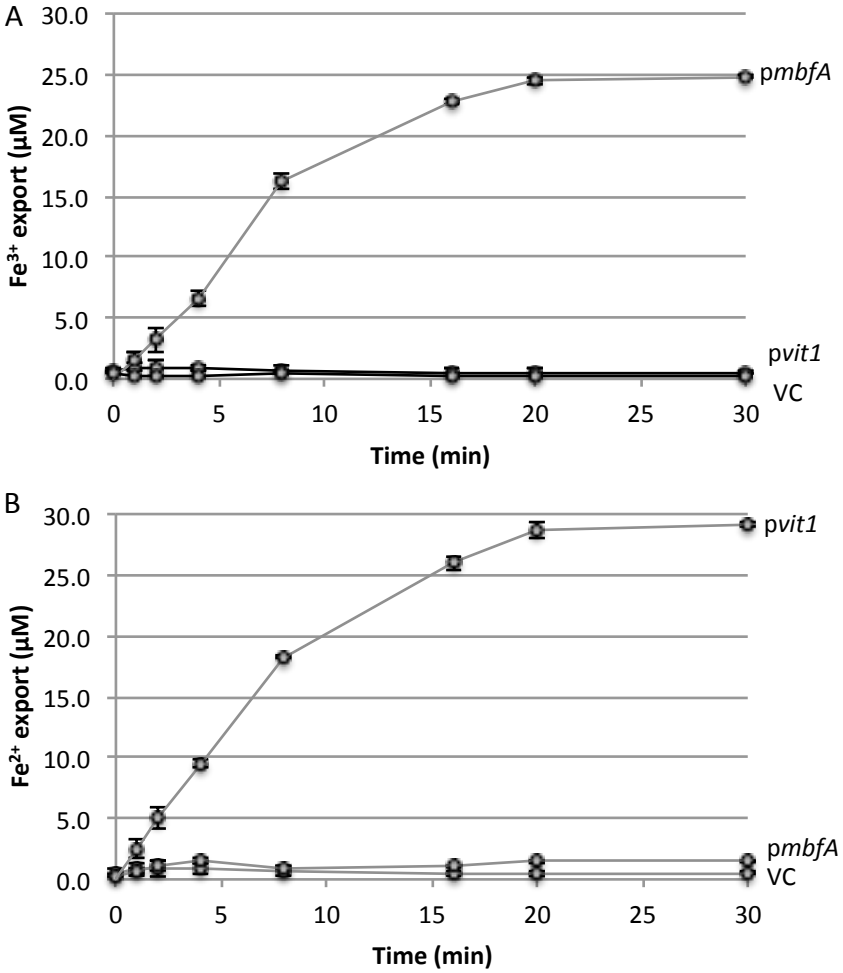

Figure 6.24: Oxidation state of iron exported by MbfA and VIT1.

Accumulation of exported ferric (A) and ferrous iron (B) through colorimetric ferrozine assay from *E. coli* MG1655 pBAD*mbfA* or pBAD*At_VIT1* compared to vector control (VC). Data shown are the means ± standard deviation of three independent experiments conducted in triplicate. Rhamnose was present at 0.1 mM.

6.11: MbfA iron export is up-regulated under high iron conditions.

To examine the mechanisms of regulation of *mbfA* in iron replete and limited conditions the ^{55}Fe export assay was used to measure export of ^{55}Fe by *Burkholderia multivorans*. This organism was employed as it naturally possesses an *mbfA* gene, is a pathogen and can be used under level 2 containment conditions. Experimentation with *mbfA* in *Brucella* is complicated due to the requirement for both containment level three facilities combined with a radiation laboratory. *B. multivorans* is an example of a containment level 2 organism encoding *mbfA* (AA sequence identity 16.2% to *B. suis* MbfA), on which iron export experimentation can be conducted at the University of Reading radiation laboratory. In addition, an *mbfA* mutant in this organism was already available (F. Issa, 2015). There are notable differences in the regulatory regions upstream of the *mbfA* coding sequences in *B. multivorans* and *Brucella* spp.. *mbfA* in *Brucella* is regulated by the iron response regulator (Irr), as evidenced from the location of the iron control element (ICE) box and the observed up-regulated in response to high iron (Figure 3.10). Control of iron related genes in *B. multivorans* could possibly be achieved by the ferric uptake regulator (Fur), but investigation regarding this is required.

To determine if *B. multivorans mbfA* exports ^{55}Fe under conditions of high iron concentrations, and is hence up-regulated (expression or activity levels), wild-type *B. multivorans, B. multivorans* Δ*mbfA* and *B. multivorans* Δ*mbfA* complemented with a pBBR series vector harbouring *mbfA* (generated by F. Issa, 2015) were grown in minimal medium with 1 μM iron. The iron export assay as described previously was conducted with the following modifications, minimal medium with and without 10 μM ferric chloride was used in place of L broth, and rhamnose was omitted. Export of ^{55}Fe was observed with both high (10 μM) and low (1 μM) ferric chloride concentrations, from the wild-type and complemented mutant strains of *B. multivorans*, but not from the *B. multivorans* Δ*mbfA* strain (Figure 6.25A/B). For the strains in which iron export is present, a 2.3 fold increase in export was observed when *B. mulitvorans* was propagated in a high iron environment compared to a minimal iron environment. This suggests that upon exposure to iron, MbfA activity is enhanced allowing the increased removal of toxic iron from the cytosol preventing generation of ROS and associated redox stress.

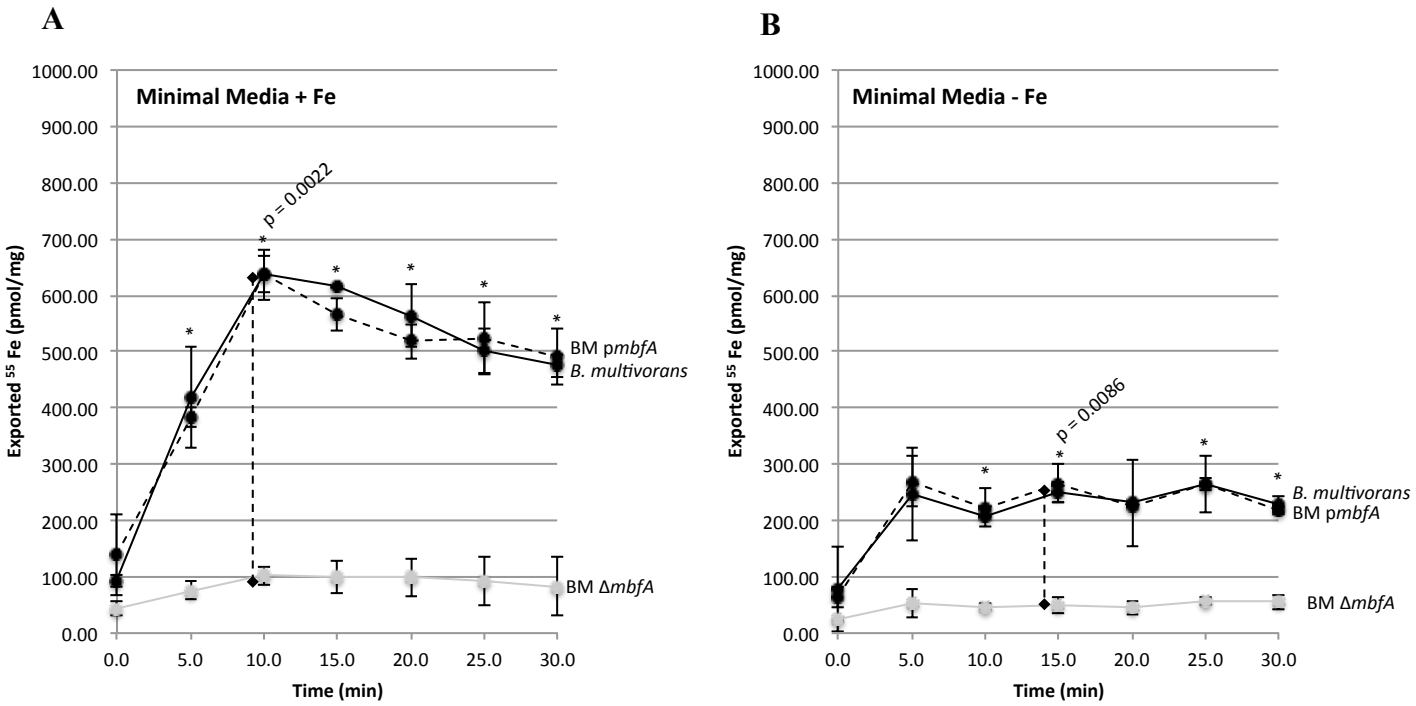

Figure 6.25: *Burkholderia multivorans* MbfA exports iron.

Measurement of ^{55}Fe export in *B. multivorans, B. multivorans* Δ*mbfA* (BM) and complemented *B. multivorans ΔmbfA* (BM p*mbfA*). The data presented represents the means and standard deviations obtained from three separate experiments. A: ^{55}Fe exported by *B. multivorans* compared to *B. multivorans* Δ*mbfA* (complemented and uncomplemented) under high iron conditions, statistically significant differences as determined by Students *t*-test ($p < 0.01$) at T = 10 min are indicated. B: ^{55}Fe exported as above but under minimal iron conditions, statistically significant differences as determined by Students *t*-test ($p < 0.01$) at T = 15 min are indicated.

In line with experimentation conducted for the pBAD*mbfA* and pBAD*At_VIT1* constructs transformed into *E. coli*, examination of the effect of hydrogen peroxide upon iron export rate was conducted with *B. multivorans* (Figure 6.26A). Addition of 100 μM H_2O_2 at T_0 resulted in a significant increase in ^{55}Fe export by 505 pmol mg^{-1} (55.7 %) at $T_{10,}$ compared to no hydrogen peroxide addition, whereas reduction of hydrogen peroxide concentrations though addition of 100 U catalase over the same time period decreased ^{55}Fe export by 294 pmol mg^{-1} (53.8 %).

To conduct an examination of iron export by *B. mulitvorans* MbfA under anaerobic conditions, modification to the propagation of the bacteria was made through addition of 20 mM sodium nitrate. *B. mulitvorans* is a facultatively anaerobic ß-proteobaceria

and requires addition of nitrate as a terminal electron acceptor to promote anaerobic growth. Anaerobic propagation prevented the export of ^{55}Fe, presumably through elimination of endogenous hydrogen peroxide production as a by-product of aerobic metabolism. Subsequent injection of 100 µM H_2O_2 at T_{15} resulted in the immediate export of ^{55}Fe at a comparable rate to that observed without H_2O_2 addition under aerobic culture (Figure 6.26B). These observations are consistent with those obtained from the *B. suis* 1330 MbfA expressed in *E. coli* and further demonstrate that iron export by MbfA is hydrogen peroxide dependent, for both the *B. suis* MbfA expressed in *E. coli* as well as MbfA of *B. multivorans*.

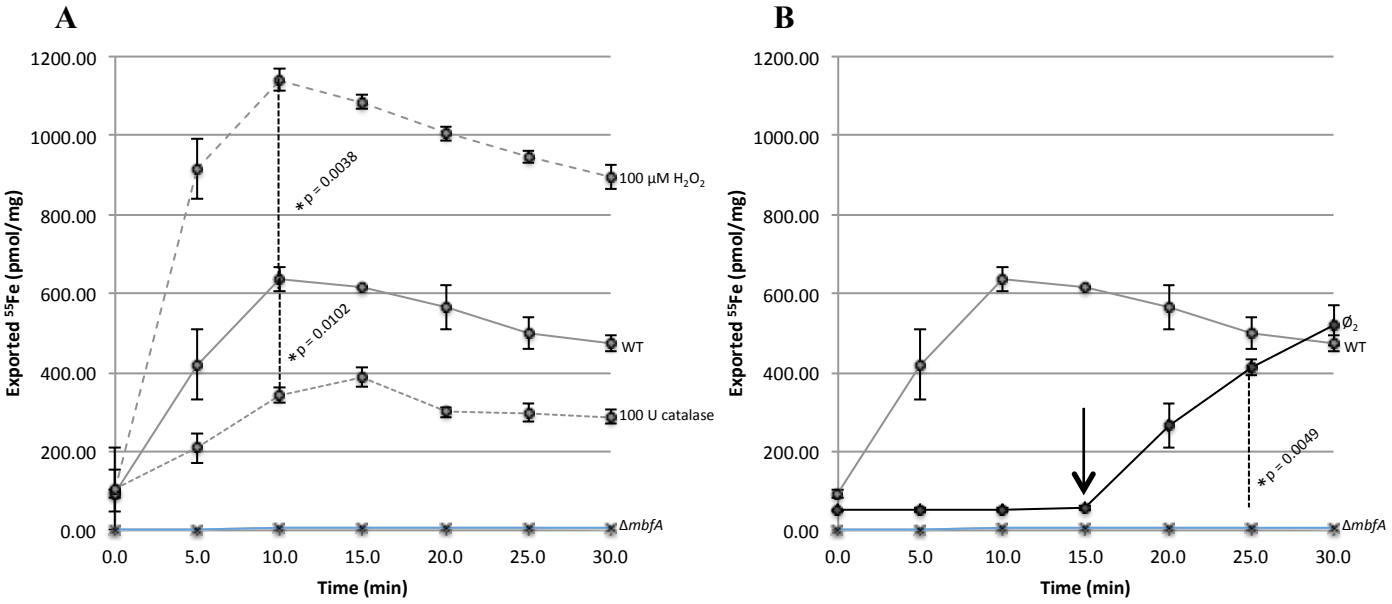

Figure 6.26: Hydrogen peroxide drives *Burkholderia multivorans* MbfA iron export.

Measurement of ^{55}Fe export from *B. multivorans* and *B. multivorans* Δ*mbfA*. The data presented represent the means and standard deviations obtained from three separate experiments. A: ^{55}Fe exported by *B. multivorans* in the presence of hydrogen peroxide and catalase, statistically significant differences as determined by Students *t*-test ($p < 0.01$) at T = 10 min are indicated. B: ^{55}Fe exported by *B. multivorans* under anaerobic conditions and with addition of 100 µM hydrogen peroxide at T = 15 min (arrow), statistically significant differences as determined by Students *t*-test ($p < 0.01$) at T = 25 min are indicated.

6.12: Export of iron potentiates disproportionation of hydrogen peroxide.

The ability MbfA, through the export of ferric iron, to elicit the disproportionation of H_2O_2 was assayed with Amplex Red (10-acetyl-3,7-dihydroxyphenoxazine) (ThermoFisher). A transformant *E. coli* MG1655 colony was inoculated into 5 ml LB (starting OD of 0.05), induced for 1 h once the OD reached 0.5 with 100 μM rhamnose, washed once with 10 ml cold WB then twice with TB and diluted to 1 OD ml^{-1}. For each measurement of H_2O_2 concentration, 100 μl of cells were added to 100 μl Amplex Red reagent and absorbance at 560 nm determined, then compared to a standard curve generated with known concentrations of H_2O_2. For each assay a measurement prior to addition (Pre) of 15 μM H_2O_2 (T_0) was made to ensure endogenous H_2O_2 concentrations were minimal, then every two minutes after H_2O_2 addition during the assay.

To ensure spontaneous disproportionation of hydrogen peroxide would not influence observed results, a control observation of 15 μM hydrogen peroxide in a 1 ml transport buffer solution (50 mM MES/TAPS pH 7.0) was conducted. The absorbance at 560 nm of Amplex Red remained stable over the 10 min assay period, enabling experimentation to progress without the need to consider spontaneous disproportionation. The addition of 1 OD *E. coli* LC106 to 15 μM H_2O_2 resulted in no significant reduction in H_2O_2 concentration (lack of catalase and alkyl hydroperoxidase, primary H_2O_2 scavengers in *E. coli* (Seaver and Imlay 2004)), whereas, addition of the parental wild type *E. coli* MG1655 resulted in rapid degradation of H_2O_2 (Figure 6.27A). Addition of *E. coli* LC106 pBAD*mbfA* to 15 μM H_2O_2 resulted in degradation of H_2O_2 at a constant rate until 4 min and there-after levels dropped slightly reaching a steady, low level. This rate of degradation was significantly greater than that of the vector control, but less effective than wild type *E. coli*. This demonstrates that MbfA is able to potentiate the disproportionation of H_2O_2, but the relative contributions afforded by Fenton reactions from exported iron and the erythrin domain peroxide reductase are unknown. To resolve this, 200 μM desferrioxamine were added to the assay, prior to addition to cells, allowing chelation of exported ferric iron, preventing disproportionation of H_2O_2 (Figure 6.28). In this way, the contribution of the peroxidase reaction at the erythrin domain could be quantified and subtracted from the total degradation, allowing determination of the contribution afforded by Fenton reactions (Figure 6.27B).

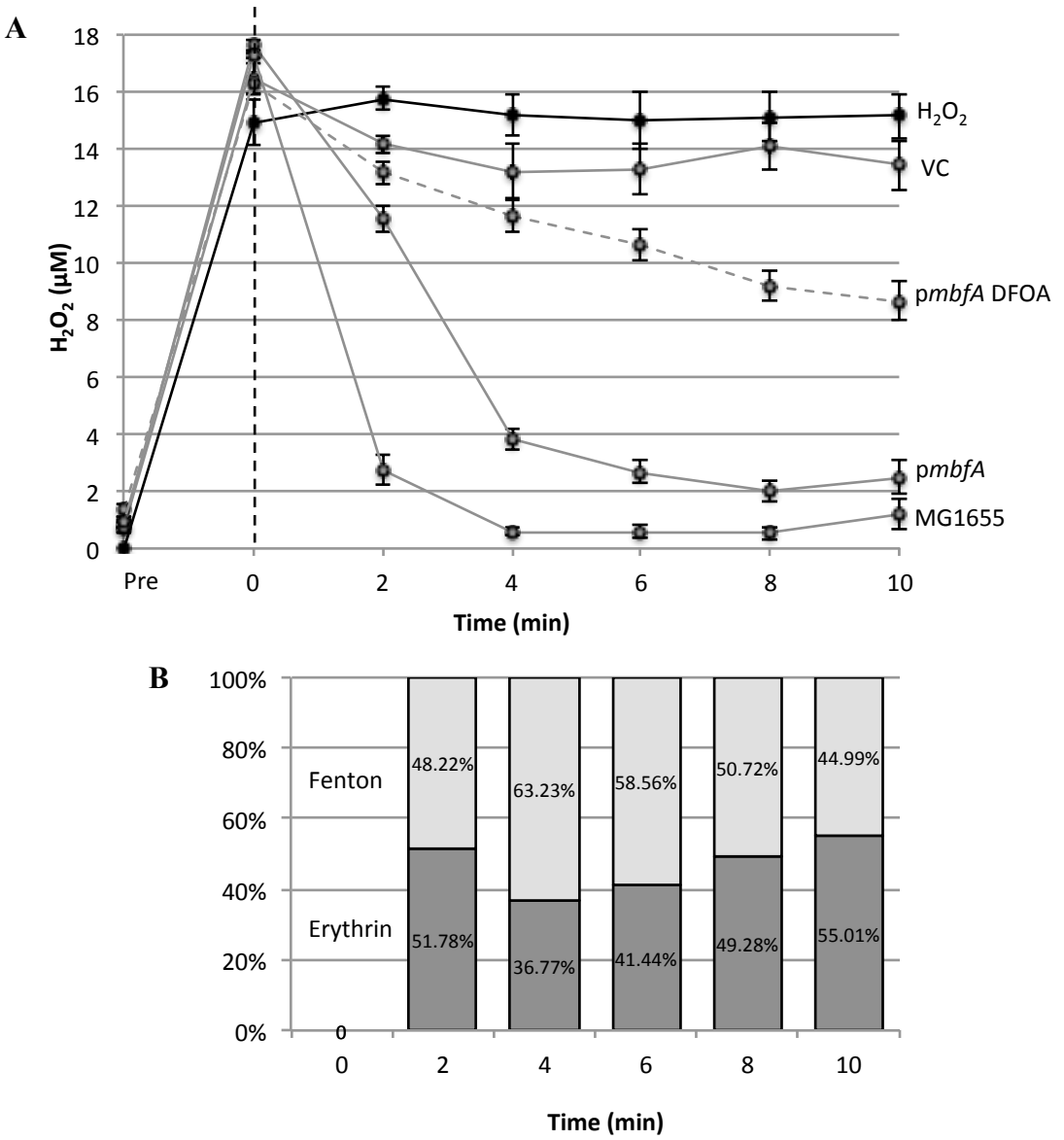

Figure 6.27: Disproportionation of hydrogen peroxide by MbfA.

A: Quantitation of the disproportionation of 15 μM H_2O_2 by *E. coli* LC106 transformed with pBADrham (vector control, VC) or pBAD*mbfA* with/without 200 μM desferrioxamine (DFOA) and *E. coli* MG1655. B: Relative H_2O_2 levels for VC minus those seen for p*mbfA*+DFOA, compared to levels for p*mbfA*+DFOA minus p*mbfA*-DFOA. This represents the relative loss of peroxide due to extracellular iron-induced Fenton chemistry and that driven by other MbfA mediated reactivity (i.e. peroxide reduction). Data shown are the means ± standard deviation of three independent experiments conducted in triplicate

Control reactions were conducted to demonstrate the effective protection of hydrogen peroxide disproportionation by ferrous and ferric iron when iron is chelated with the ferrous iron chelator 1,10–phenanthroline and the ferric iron chelator desferrioxamine (Figure 6.28).

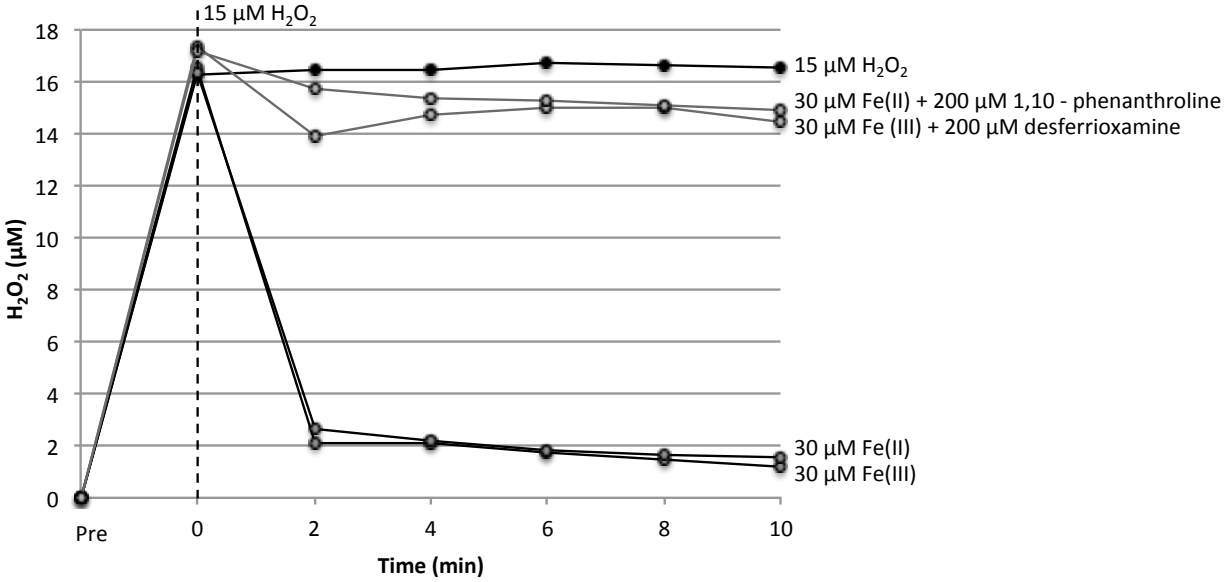

Figure 6.28: Disproportionation of hydrogen peroxide by iron is inhibited upon chelation.

Quantitation of the disproportionation of 15 µM H_2O_2 through exposure to 30 µM ferric and ferrous iron. Prevention of disproportionation through prior addition of 200 µM desferrioxamine or 1,10-phenanthroline, respectively. Data shown are the means of three independent experiments conducted in triplicate.

To determine if this novel mechanism for degradation of hydrogen peroxide could be physiologically relevant to *Brucella* spp. within the acidified BCV (pH 4.0 - 4.5 (Porte et al. 1999)), the assay was repeated at acidic pH. Adjustments in pH were made to TB. Results show no difference in hydrogen peroxide disproportionation under acidic conditions (Figure 6.29).

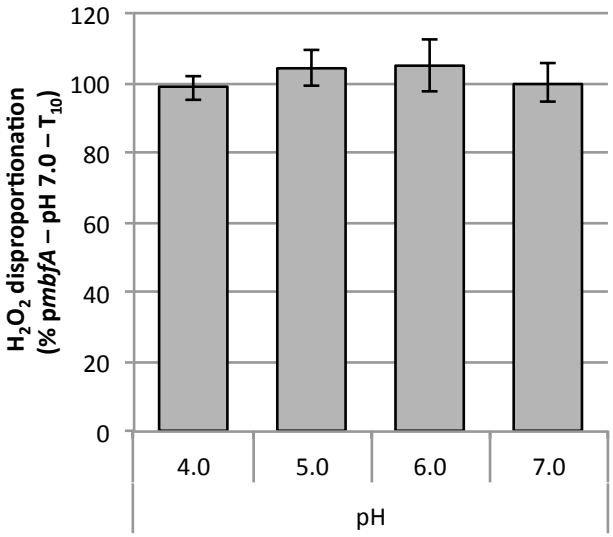

Figure 6.29: Effect of pH on disproportionation of hydrogen peroxide by MbfA. H_2O_2 disproportionation by *E. coli* LC106 p*mbfA* at pH 4.0, 5.0, 6.0 and 7.0. Data shown are the means ± standard deviation of three independent experiments conducted in triplicate.

6.13: MbfA protects from nitric oxide sensitisation to oxidative stress.

The phagolysosomal-like niche in which *Brucella* spp. are located during early stages of intracellular infection is characterised by the presence of both reactive oxygen and nitrogen species. Within the phagosome nitric oxide is generated from arginine and oxygen by inducible nitric oxide synthase (iNOS) (Fang 2004), nitric oxide (NO) is then able to react with superoxide (O_2^-) to generate toxic peroxynitrite ($ONOO^-$) (Radi et al. 1991). In addition to the generation of toxic byproducts, NO is also able to liberate stored iron from bacterioferritin (Le Brun et al. 1997). As well as inhibit catalase through the conversion of catalase compounds II and III to ferricatalase (Kim et al 2002); effectively stalling its catalytic activity, allowing lower concentrations of hydrogen peroxide to become toxic to the invading bacterium (Pacelli et al. 1995).

In addition, the physical properties of hydrogen peroxide, specifically its non-polar nature, allows it to freely diffuse across all biological membranes. It is important to note that not only can hydrogen peroxide diffuse into the invading organism, eliciting the redox stress required for bactericidal action, but also hydrogen peroxide will equally diffuse out of the phagolysosome. This results in hydrogen peroxide concentrations within the phagolysosome being low (4 - 30 μM) as it is impossible to concentrate it in any biological compartment. With this in mind, the requirement for nitric oxide, sensitizing invading bacteria to low concentrations of hydrogen peroxide becomes apparent. The synergism of NO and H_2O_2 mediated bacterial killing is highlighted by experimentation conducted by Ann Woodmansee; (Woodmansee and Imlay 2003). Nitric oxide was observed to accelerate the killing of *E. coli* through NO/H_2O_2 initiated Fenton reactions. However, it was of note that the killing of *E. coli* was protected by the addition of a cell permeable iron chelator.

Experimentation was conducted to examine the effect that NO has upon MbfA function and to determine whether MbfA is able to elicit a protective response to NO generated oxidative stress. Initially, the effect on cellular viability, measured by aerobic growth of a bacterial culture over 18 h, was determined with addition of up to 1 mM H_2O_2 or 50 μM NO (Figure 6.30). Nitric oxide was introduced into L broth as DEA NONOate (2-(N,N-diethylamino)-diazenolate-2-oxide). DEA NONOate is a nitric oxide donor, which is soluble in PBS and dissociates into a free amine and nitric oxide in a pH-dependent manner. At pH 7.4 and 37 °C, DEA NONOate has a half-life of 2 min and liberates 1.5 moles of NO per mole of parent compound. No deleterious effect was

observed upon the viability of *E. coli* MG1655 as optical densities were equivalent for cultures with no addition and with H_2O_2 or NO, at all concentrations, in the presence and absence of *mbfA*.

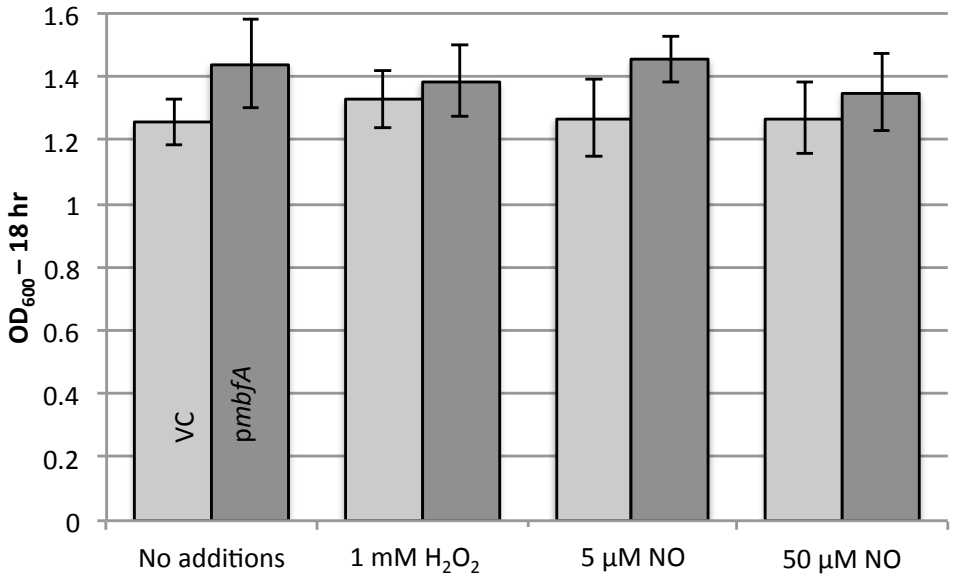

Figure 6.30: Growth of *E. coli* MG1655 with addition of H_2O_2 or NO.

Optical densities after 18 h aerobic growth of *E. coli* MG1655 pBAD*mbfA* or vector control (VC) in L broth with addition of 1 mM H_2O_2 or 5-50 µM NO. Data shown are the means ± standard deviation of three independent experiments conducted in triplicate. Rhamnose was present at 0.1 mM.

In contrast, when 5 μM NO was combined with 1 mM H_2O_2 this resulted in sensitivity of *E. coli* MG1655, but this effect was ameliorated with the expression of *mbfA* (Figure 6.31).

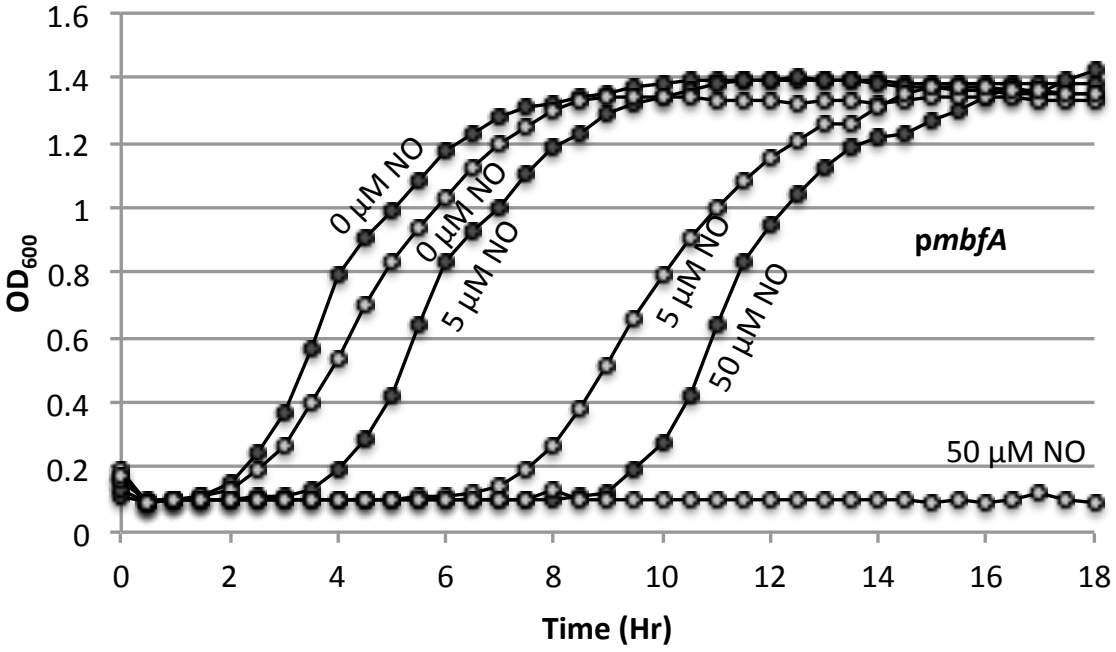

Figure 6.31: Growth of *E. coli* MG1655 with addition of H_2O_2 and NO in combination.

Growth of *E. coli* MG1655 pBAD*mbfA* (black circles) or vector control (VC, grey circles) in L broth with 1 mM H_2O_2 and 0, 5, or 50 μM NO. Data shown are the means of three independent experiments conducted in triplicate. Rhamnose was present at 0.1 mM.

Addition of 5 μM NO resulted in an increase in *E. coli* lag phase by ~6 h, compared to when no NO was added. When *E. coli* was transformed with pBAD*mbfA*, lag phase was reduced by ~3 h in the presence of 5 μM NO; this implies that expression of *mbfA* protects against the combined action NO and peroxide, and thus reduces losses in cellular viability. Similar, but more marked effects were observed with higher concentrations of NO. The synergistic effect of increased toxicity through combination of NO and H_2O_2 is most likely combated by MbfA mainly through the export of cellular iron which will degrade external H_2O_2. It is likely that the catalases and alkyl hydroperoxidases of wildtype *E. coli* fail to effectively combat peroxide stress when NO is present since NO would inhibit these haem-containing enzymes, as indicated above, whereas MbfA is haem-independent and so can be expected to be NO inert. Thus, MbfA is able to compensate for the inhibition of endogenous peroxidase and catalase activity by NO. Further, exported iron might also bind NO and thus limit its toxicity (Cooper 1999).

To further explore the combined impact of NO and H_2O_2, the effect of these two compounds on the *E. coli* catalase/alkyl-hydroperoxidase mutant (LC106) was examined (Figure 6.32A). NO caused a major increase in LC106 sensitivity to peroxide, which shows that the enhanced sensitivity of the wildtype to peroxide induced by NO is not simply a result of catalase/alkyl-hydroperoxide inhibition (in contrast to what was suggested above). In addition, MbfA was able to reverse this sensitivity. As suggested before, this is likely to be caused by MbfA increasing extracellular free iron concentration resulting in disproportionation of peroxide. However, NO may also act to enhance peroxide toxicity through binding to, and mobilization of, cellular iron (e.g. from Bfr) (Winstedt and von Wachenfeldt 2000) and/or through a range of direct NO toxicity activities within the cell (Beckman and Koppenol 1996). The potential action of NO in mobilization of cellular iron resulting in raised free cytosolic iron levels, is supported through the effect of NO on the streptonigrin (SNG) sensitivity of *E. coli* K-12 (MG1655) with and without MbfA. The results show that NO raises sensitivity to SNG for the vector control, but MbfA appears to reverse or even decrease sensitivity for the pBAD*mbfA* strain (Figure 6.32B). This is consistent with NO mobilization of iron which in turn enables its removal from the cell by MbfA; without MbfA this iron mobilisation would result in enhanced free-iron levels in the cytosol raising SNG toxicity, as observed.

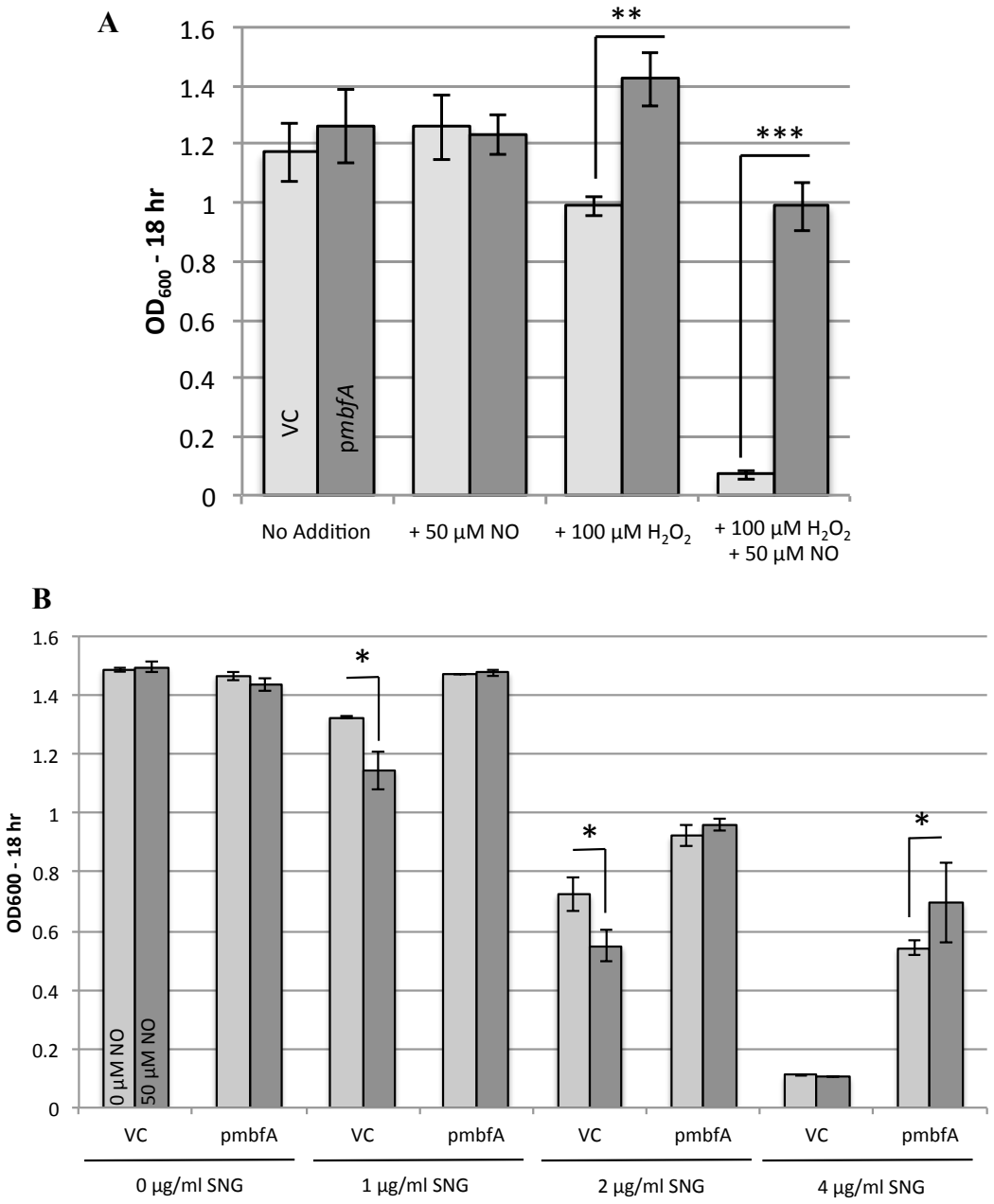

Figure 6.32: Protection of nitric oxide sensitisation to oxidative stress in *E. coli* by MbfA.

A: Optical density after 18 h aerobic growth of *E. coli* LC106 pBAD*mbfA* or vector control (VC) in LB with addition of 50 µM NO and/or 100 µM H_2O_2. B: Optical density after 18 h aerobic growth of *E. coli* MG1655 pBAD*mbfA* or vector control (VC) in LB with addition of 0 or 50 µM NO and streptonigrin (1-4 µg/ml). Data shown are the means ± standard deviation of three independent experiments conducted in triplicate and analysed using an unpaired, two tailed Student's *t*-test; * $P<0.05$, ** $P<0.01$ *** $P<0.001$. Rhamnose was present at 0.1 mM.

To determine whether the presence of NO has an impact on the rate of extracellular hydrogen peroxide disproportionation (as suggested above), H_2O_2 consumption by *E. coli* MG1655 and LC106 pBAD*mbfA* transformants was assessed with and without NO. The assay was conducted as described previously, however, 5 min before addition of hydrogen peroxide, DEA-NONOate was added to allow dissociation into NO.

Similar to previously observations, the *E. coli* LC106 vector control failed to degrade 15 µM H_2O_2; because of this, provision of 50 µM NO had no notable effect on H_2O_2 levels (Figure 6.33). Again, as before, *E. coli* LC106 (pBAD*mbfA*) showed rapid disproportionation of hydrogen peroxide, and addition of nitric oxide gave a slight increase in the initial (2 min) level of disproportion of hydrogen peroxide (Figure 6.33), although the difference was not significant. Thus, NO appears to have little impact on the extracellular degradation of hydrogen peroxide as mediated by MbfA. Thus, it can be assumed that MbfA is not inhibited by NO.

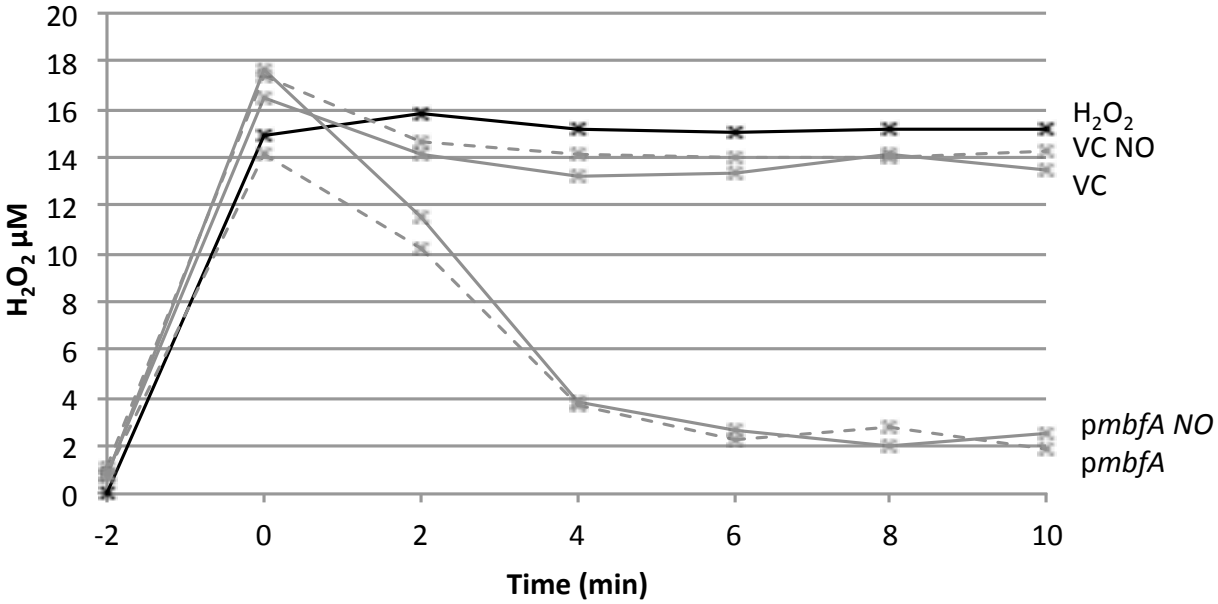

Figure 6.33: Effect of NO on disproportionation of hydrogen peroxide by MbfA in *E. coli* LC106.

Quantitation of the disproportionation of 15 µM H_2O_2 with Amplex Red. Samples were (as indicated): H_2O_2 only; *E. coli* LC106 vector control (VC) with 50 µM NO and H_2O_2 ; LC106 VC with H_2O_2 only; LC106 (pBAD*mbfA*) with 50 µM NO and H_2O_2; LC106 (pBAD*mbfA*) with H_2O_2 only. NO indicated by dashed lines. Data shown are the means of three independent experiments conducted in triplicate. Rhamnose was present at 0.1 mM.

In contrast, addition of nitric oxide to *E. coli* MG1655 resulted in a reduction in the rate of hydrogen peroxide disproportionation, although over a 10-min period total disproportionation was not dissimilar (Figure 6.34). In the absence of nitric oxide, *E. coli* MG1655 was able to disproportionate approximately 85-90% of total hydrogen peroxide within 2 min and 99% by 4 min. In comparison, for the vector control, nitric oxide addition led to decreased hydrogen peroxide disproportionation such that just 33 and 47% of total H_2O_2 was consumed at 2 and 4 min, respectively, which represents a greater than twofold decrease in consumption compared to the condition without NO (Figure 6.34).

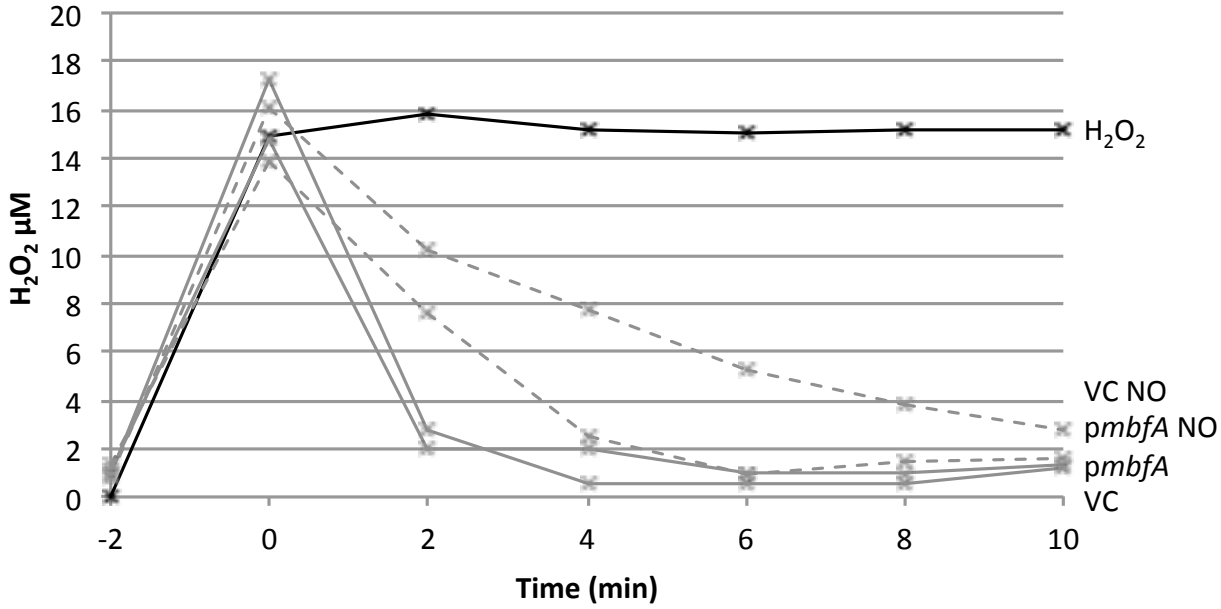

Figure 6.34: Effect of NO on disproportionation of hydrogen peroxide by MbfA in *E. coli* MG1655.

As above, except *E. coli* MG1655 was used in place of LC106.

For *E. coli* MG1655 with pBAD*mbfA*, the presence of NO again decreased the rate of hydrogen peroxide disproportionation but not to the same degree as seen for the vector control (Figures 6.34 and 6.35). Thus, expression of *mbfA* decreased hydrogen peroxide degradation, raising levels by ~threefold from by 7.8 to 2.6 µM at 4 min (compared to the VC). This suggests that, firstly, NO blocks the degradation of H_2O_2 by wildtype *E. coli* (presumably by inhibition of catalases and alkyl hyroperoxidases), and secondly, that MbfA is able to promote disproportionation of hydrogen peroxide in the presence of nitric oxide and thus compensate for catalase/alkyl hydroperoxidase inhibition by NO. Crucially, the data from Figure 6.33 show that MbfA is not negatively impacted

by NO (unlike catalases/alkylhyroperoxidases) which explains its ability to assist peroxide degradation in the wildtype when endogenous mechanisms are subject to NO inhibition. This 'resistance' of MbfA to NO could be important for survival of *Brucella* within the eBCV where combined exposure to NO and H_2O_2 is likely (Gross et al. 2004).

A comparison of the disproportionation of hydrogen peroxide after 4 min for *E. coli* MG1655 and LC106, +/-NO and +/-*mbfA* reveals that MbfA provides a significant increase in hydrogen peroxide degradation in all but one condition. No significant difference is observed for MbfA provision in *E. coli* MG1655 without NO addition (Figure 6.35).

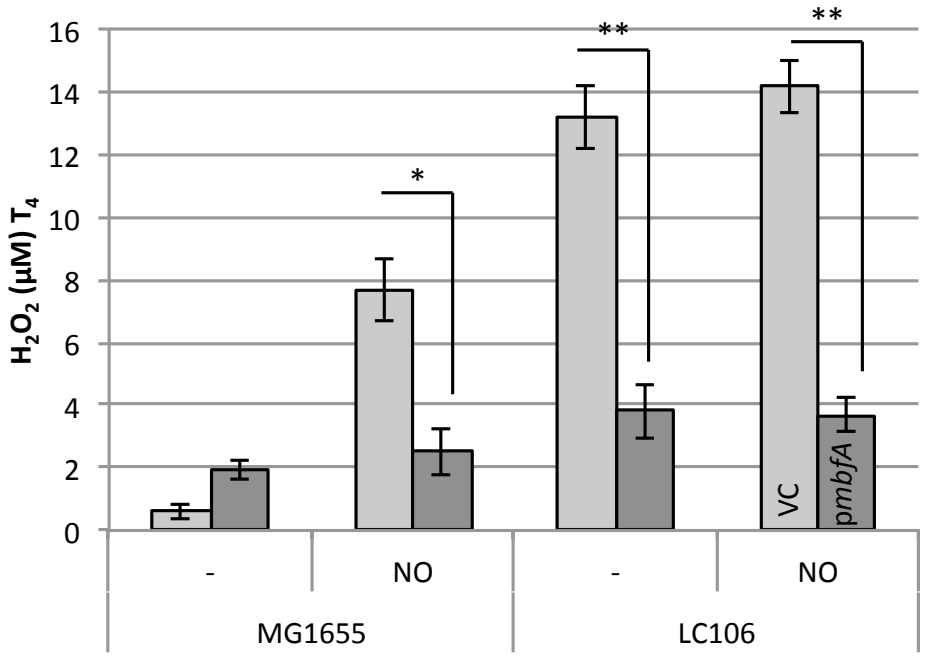

Figure 6.35: Comparison of effects of NO and endogenous catalases/peroxidase on hydrogen peroxide degradation by MbfA.

Data are derived from Figures 6.34-6.35 4 min. Data shown are the means ± standard deviation of three independent experiments conducted in triplicate and analysed using an unpaired, two tailed Student's *t*-test; * $P<0.05$, ** $P<0.01$ *** $P<0.001$

6.14: MbfA depletes the labile iron pool and iron stores.

To examine the effect of expression of *mbfA* on the intracellular concentration of iron within *E. coli*, measurement of total cellular iron was conducted using a ferrozine colorimetric assay. Strains were grown to mid-log phase before lysis by heating to 90 °C in the presence of an acidic ferrozine solution to allow determination of total iron content (Methods 2.5.2). Samples were standardized per mg of protein, as determined by Bradford assay (Methods 2.4.9).

Expression of *mbfA* in *E. coli* MG1655 resulted in significant reduction of total cellular iron at log phase (Figure 6.36) and this effect was reproduced in *E. coli* Δ*fur*, Δ*ryhB* and Δ*fur* Δ*ryhB* mutants. The expression of *mbfA* in *E. coli* MG1655 resulted in a reduction in total iron content by 5.3 μmoles/mg (23.5 %); larger decreases in total iron content were observed in *E. coli* Δ*fur*, Δ*ryhB* and Δ*fur* Δ*ryhB* strains: 8.1, 9.8 and 11.2 μmoles/mg (40.2, 46.8 and 53.8 %), respectively, compared to the wildtype. In the case of the *fur* mutant, the increased reduction in cellular iron levels mediated by MbfA could be related to the increased level of labile, free cytosolic iron caused by the deregulation of iron homeostasis (Nandal et al. 2010). For the *ryhB* mutant, an increase in Bfr levels is anticipated (Masse and Gottesman 2002) that might provide an increased source of intracellular iron for MbfA export (see below).

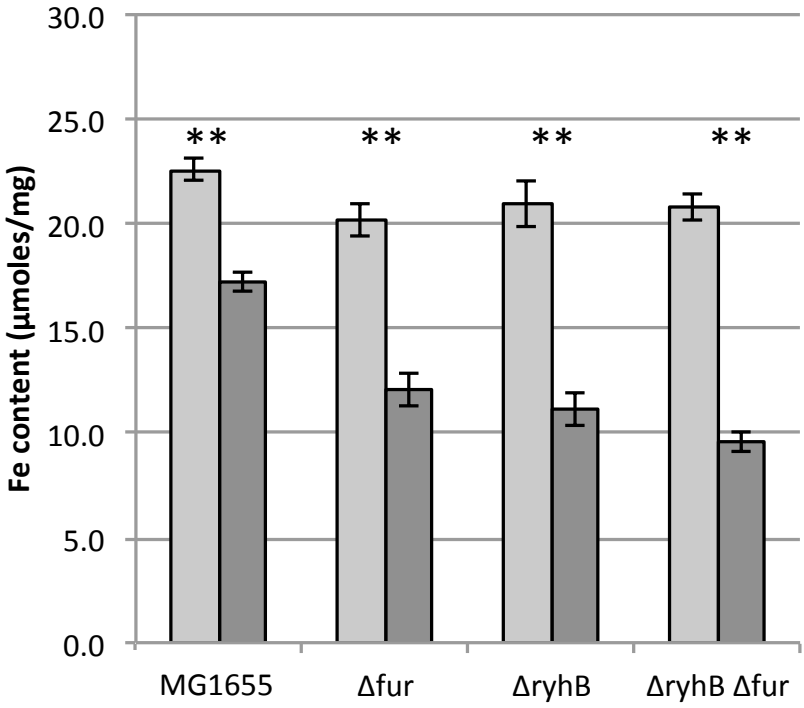

Figure 6.36: MbfA depletes cellular iron in *E. coli* with an increased effect seen for iron regulation mutants.

Total cellular iron was determined by colorimetric Ferrozine assay. Data shown are the means ± standard deviation of three independent experiments conducted in triplicate following growth to mid-log phase. Data was analysed using an unpaired, two tailed Student's *t*-test; * $P<0.05$, ** $P<0.01$ *** $P<0.001$. Rhamnose was present at 0.1 mM.

Deletion of *fur* results in de-regulation of iron uptake and storage; iron-uptake mechanism are constitutively expressed, whereas iron storage is repressed, as is incorporation of iron into proteins; these effects result in increased free intracellular iron concentrations compared to wild-type *E. coli*. This would make more free iron available for export which is reflected in the observed decreased iron content caused by expression of *mbfA* in the *fur* mutants with respect to levels observed for the wildtype. In contrast, deletion of *ryhB*, encoding a small 90-nucleotide non-coding RNA which acts to down-regulate iron-storage (bacterioferritin, Bfr) when iron is limited, results in constitutive expression of Bfr (Masse and Gottesman 2002). Provision of MbfA within the *ryhB* mutants, where this mutation is expected to result in less free iron due to excess Bfr iron storage capacity and raised expression of iron-protein genes, also resulted in reduction of total iron content in a similar fashion as seen for the *fur* mutants. This would be consistent with MbfA acting to drive the removal of iron from Bfr (note that FtnA is not RyhB controlled; (Nandal et al. 2010), suggesting that Bfr

might act as a source of intracellular iron for MbfA-mediated iron export; this possibility is further addressed below).

To further explore the hypothesis that MbfA not only depletes the labile iron pool but can also access cellular iron stores, examination of the total iron content of pBAD*mbfA* transformants of *E. coli ftnA, bfr, bfd* and *dps* mutants was conducted upon induction of *mbfA* expression (Figure 6.38). Examination of the total iron contents of *E. coli* Δ*ftnA,* Δ*dps* and Δ*ftnA* Δ*dps* mutants showed a significant reduction in total iron content with pBAD*mbfA* in all cases under inducing conditions. In contrast, deletion of *bfd* or *bfr*, or *bfr* and *bfd*, with or without *ftnA*, *dps*, and *dps* plus *ftnA*, gave no significant reduction in total iron content with pBAD*mbfA* (Figure 6.37). Thus, the MbfA-dependent reductions in total iron content were only seen when Bfr was present with Bfd. Deletion of the *bfr* gene or the adjacent 'bacterioferritin-associated ferredoxin' (Bfd) encoding gene (*bfd*) resulted in failure of MbfA to elicit a significant reduction in total iron content. This suggests that MbfA is able to deplete cellular iron stores in the form of Bfr (but not FtnA), presumably through an indirect mechanism, in a manner that depends also on Bfd. It is likely that iron removed from the cytoplasm by MbfA results in mobilization of iron from Bfr (as a homeostatic response to cytosolic free-iron depletion) which is then subject to MbfA-mediated export. It should be noted that Bfr is the sole recognized iron-storage protein within *Brucella* (Almiron and Ugalde 2010), so this mechanism would be expected to be applicable to most *Brucella* species. Also, *bfd* is induced by low iron (Fur dependent) and is considered to be involved in release of iron from Bfr through a reductive mechanism (Garg et al. 1996, Quail et al. 1996)

It is also possible that expression of *mbfA* prevents the accumulation of iron within Bfr (such that few iron stores are built up by Bfr) by reducing free intracellular iron availability, rather than by driving the removal of iron stores from Bfr. However, the higher iron content of the *bfd* mutant is not consistent with this theory although does match the hypothesis that MbfA is able to promote removal of iron from Bfr in a Bfd-dependent fashion. It is possible that both processes contribute to the role of Bfr in enabling an MbfA-dependent reduction in total-cellular iron.

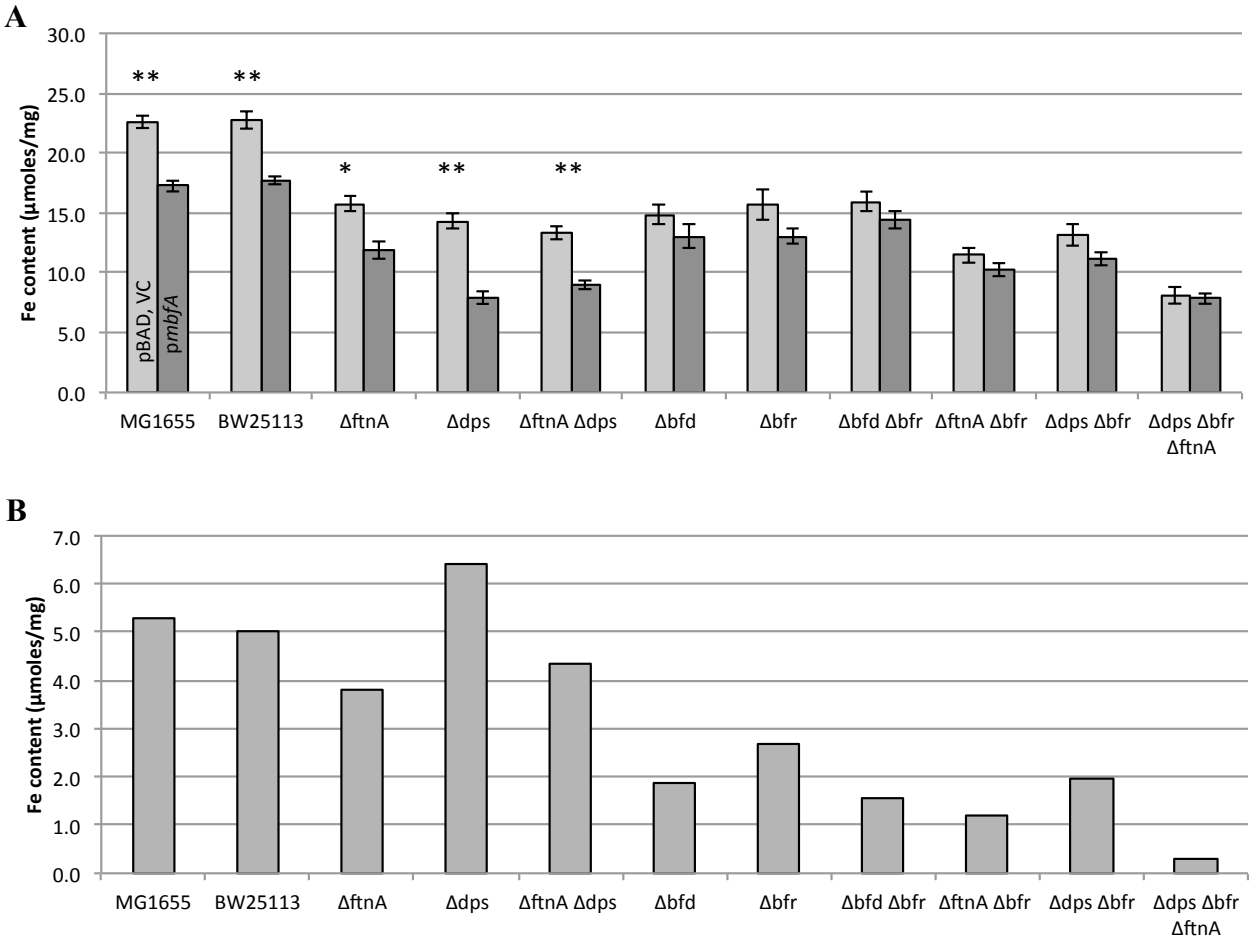

Figure 6.37: MbfA fails to significantly deplete cellular iron in *E. coli* Bfr and Bfd iron-storage defective strains.

A: Quantitation of total cellular iron in log phase by colorimetric Ferrozine assay. B: Difference in iron content with expression of MbfA (pBAD Fe/mg – pBAD*mbfA* Fe/mg) Data shown are the means ± standard deviation of three independent experiments conducted in triplicate and analysed using an unpaired, two tailed Student's *t*-test; * $P<0.05$, ** $P<0.01$ *** $P<0.001$. Rhamnose was present at 0.1 mM.

In addition to examination of the total iron status of *E. coli* strains, assessment of time dependent ferric-iron export was conducted to determine the concentrations of iron exported when *bfr* is either present or absent.

Iron export for *E. coli* MG1655 and *E. coli* Δ*dps* Δ*ftnA*, which both encode *bfr*, were compared to *E. coli* Δ*bfr* and Δ*bfr* Δ*dps* Δ*ftnA*, which both lack *bfr*, as well as a non-exporting control (*E. coli* MG1655 VC) (Figure 6.38, Table 6.1). Bfr^+ strains exported significantly more (~35 % at 16 min) iron over the time period assayed than Bfr^- *E. coli* strains, further supporting a role for Bfr in providing a source of iron available for export by MbfA. It is noteworthy that the absence of Bfr resulted in only an ~33% reduction in MbfA-dependent iron export, yet MbfA-dependent depletion of total cellular iron was decreased by 70%, from ~5 to 1.5 μmol/mg, through absence of Bfr (Figure 6.38). This discrepancy is likely to relate the longer time course for the experiments measuring cellular iron levels, where *mbfA* expression was induced throughout growth until the mid-log phase sampling point. The resulting cellular iron levels would reflect the combined action of iron uptake and MbfA-mediated release during the entire period of growth. In contrast, for the iron release experiments, assays were performed for just 32 min, one hour after *mbfA* induction, and are expected to represent the initial rates of iron export without influence of iron uptake.

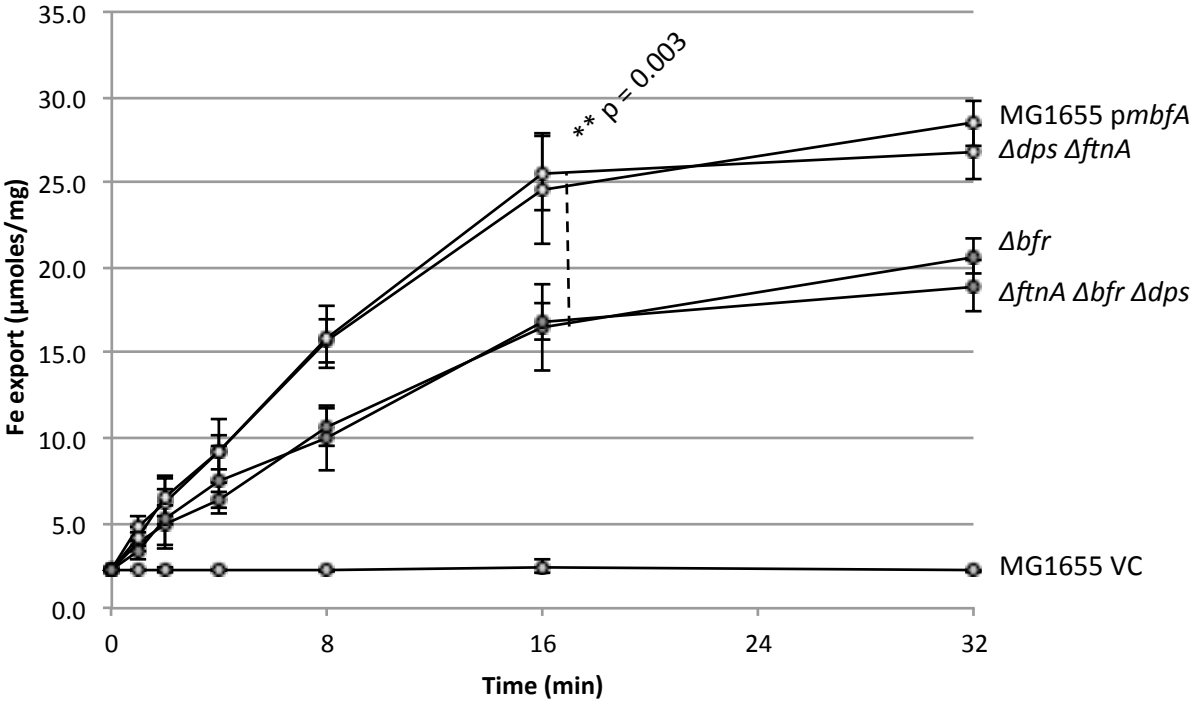

Figure 6.38: Time dependent export of cellular iron content by MbfA.

Export of iron as determined by ferrozine assay by *E. coli* MG1655 and mutant strains (Δ*bfr,* Δ*dps* Δ*ftnA* and Δ*ftnA* Δ*bfr* Δ*dps*) carrying pBAD*mbfA* compared to *E. coli* MG1655(pBADrham) vector control (VC) following growth to mid-log phase. Data shown are the means of three independent experiments conducted in triplicate and analysed using an unpaired, two tailed Student's *t*-test; * $P<0.05$, ** $P<0.01$ *** $P<0.001$. Rhamnose was present at 0.1 mM.

Table 6.1: Iron export rates

Strain (pBAD*mbfA*)	**Iron export rate (µmol/min/mg)**
MG1655	1.60
Δ*bfr*	1.54
Δ*dps* Δ*ftnA*	1.05
Δ*ftnA* Δ*bfr* Δ*dps*	1.03

Finally, the effect of various iron-metabolism defects on MbfA-induced resistance to 2 μg/ml streptonigrin resistance was tested to determine whether enhanced SNG toxicity resulting from increased cytosolic-free iron levels can be reversed by MbfA. As detailed previously, *E. coli* Δ*fur* has a high free iron content due to constitutive iron import and repressed iron storage, rendering this strain more sensitive to 2 μg/ml streptonigrin than the corresponding parental wild-type strain (Figure 6.39). Transformation of *E. coli* Δ*fur* with pBAD*mbfA* rescued the SNG-sensitive phenotype persumably through export of reactive iron resulting in lower cytosolic levels. Conversely, an *E. coli* mutant deficient (JC28) in all known high-affinity iron import systems was more resistant to 2 μg/ml strepotnigrin than the corresponding parental wild-type strain, such that the presence/absence of pBAD*mbfA* had no notable effect on growth.

Next, the effect of MbfA on the SNG-sensitivity of *E. coli* iron-storage mutants (Δ*dps* Δ*ftnA* Δ*bfr,* Δ*bfr* and Δ*dps* Δ*ftnA*) was tested. Strains lacking Bfr showed no significant increase in resistance to streptonigrin with expression of *mbfA*, but *E. coli* Δ*dps* Δ*ftnA* (*bfr* only) displayed a significant increase in resistance (Figure 6.40). This supports the hypothesis that Bfr stores iron that is readily available for release into the cytosol to provide free iron for metabolic purposes, thus raising susceptibility to killing by streptonigrin. The presence of Bfr in the wildtype did not result in MbfA-mediated enhancement of SNG-resistance, this effect was only seen in the *dps ftnA* mutant. The reason for this is unclear, but might be related to an increased SNG sensitivity resulting from Dps and FtnA absence.

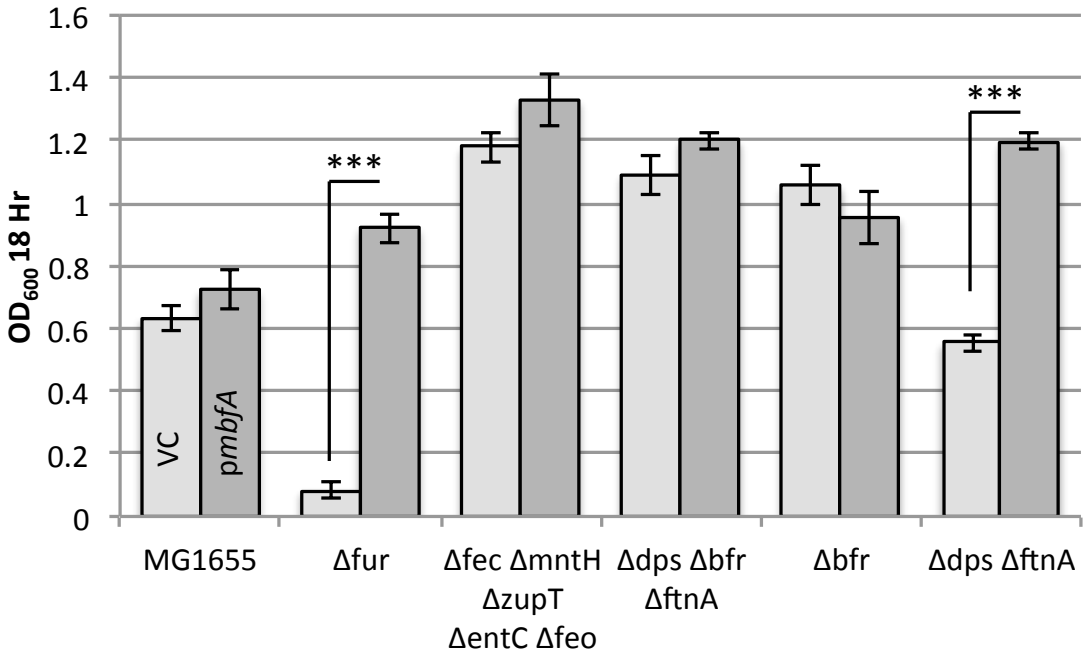

Figure 6.39: Effect of MbfA on resistance to streptonigrin dependent killing in *E. coli* iron-metabolism mutants.

Resistance of *E. coli* strains (as indicated, with pBADrham or pBAD*mbfA*) to 2 μg/ml streptonigrin. Data shown are the means ± standard deviation of three independent experiments conducted in triplicate and analysed using an unpaired, two tailed Student's *t*-test; * $P<0.05$, ** $P<0.01$ *** $P<0.001$.

6.15: Discussion:

The experiments described in this chapter focus upon the characterization of *Brucella suis* MbfA, but also examines the MbfA system in *Burkholderia multivorans* as well as VIT1 from *Arabidopsis thaliana*. The aim was to characterize the function of MbfA and how it might contribute to redox-stress resistance and virulence of *Brucella* spp..

Transformation of a plasmid expressing MbfA into an *E. coli* strain deficient in all high affinity iron uptake mechanisms (JC28) resulted in a reduction in growth in iron replete medium. Further MbfA-dependent growth reductions were observed when available iron was depleted through chelation. This phenotype provides evidence that expression of *mbfA* allows for export of cellular iron. Further to this, phenotypes were also observed which are consistent with iron export when MbfA was expressed in an *E. coli* peroxidase mutant (LC106). The transformed mutant and vector control were exposed to hydrogen peroxide, organic peroxide or redox mediators (methyl viologen) and differences in lag phase and final optical density were observed. In all cases, expression of *mbfA* resulted in an increase in cellular growth and decreased time to achieve log phase compared to the vector control. Although the erythrin domain of the MbfA protein is hypothesized to act as a peroxide reductase, the protection to the cell afforded by MbfA, in the presence of these redox active chemicals, cannot be directly attributed to this domain. It is possible that peroxides act as oxidants and are reduced at the erythrin domain, but also it is possible that exported iron is able to engage in Fenton reactions with these chemicals outside of the cell, affording cellular protection. It is of note that the activity seen *in vivo* for *mbfA* in *E. coli* indicates that low-level expression must result in good occupancy of the erythrin domain with a di-iron centre, thus, the high zinc content observed in the over-expressed domain results from its high abundance which appears to result in insufficient iron availability for di-iron site formation, enabling zinc occupation instead.

To aid in the resolution of how resistance to peroxides was achieved, the *VIT1* gene was cloned from *A. thaliana* into an inducible expression vector and transformed into *E. coli* LC106. VIT1 is known to act as an iron transport protein in *A. thaliana*, but has no erythrin domain therefore no peroxide reductase functionality. Expression of VIT1 in the presence of hydrogen peroxide in *E. coli* LC106 resulted in equivalent resistance to that achieved by MbfA, suggesting that resistance to peroxide induced stress may originate from reduction of the peroxides extracellularly through interactions with

exported iron. To add further to this observation, when the Vit1 domain of the MbfA protein was expressed in isolation, no resistance to peroxide was observed. This suggests that the erythrin domain is necessary to enable iron export by MbfA.

The predicted functionality of MbfA acting as an iron exporter was further supported by the results observed when *E. coli* wildtype and mutant strains were exposed to the iron dependent antibiotic streptonigrin. Exposure of *E. coli* strains to streptonigrin resulted in varying decreases in cellular growth, dependent upon the levels of free intracellular iron. The *E. coli fur* mutant (H1941) was more sensitive to streptonigrin than wildtype *E. coli* (MG1655), which in turn was more sensitive than the *E. coli* iron import mutant (JC28). In all cases, expression of MbfA, exporting intracellular iron, resulted in increases in resistance to streptonigrin. These results suggest that expression of *mbfA* drives export of cytosolic free iron which protects against the bactericidal action of streptonigrin through lowering concentrations of available iron able to interact with streptonigrin.

The development of a method for the quantitation of iron released from bacteria via resulted in the first direct quantitation of iron export by MbfA. Characterisation of the *Brucella suis* MbfA and *Arabidopsis thaliana* VIT1 were conducted in *E. coli* as a surrogate, whereas characterization of *Burkholderia multivornas* MbfA was conducted within the native host organism. Initial experiments provided reinforcement of previous observations that *mbfA* expression is controllable, on the $pBAD_{rham}$ plasmid, with addition of 0.1 mM rhamnose; observation of iron export was only observed with addition of inducer. To characterize the mechanism of iron export by MbfA, exported iron was monitored as increased and decreased (catalase addition) hydrogen peroxide concentrations were applied. Addition of hydrogen peroxide increase export rate, whereas, addition of catalase reduced export rate. Further to this, anaerobic propagation of *E. coli* MG1655, preventing *in vivo* hydrogen peroxide generation, resulted in complete cessation of iron export, which could be resumed immediately upon direct injection of de-gassed hydrogen peroxide.

To add further evidence for the requirement of both MbfA domains (erythrin and Vit1) to enable export of iron, quantitation of exported iron was determined when either domain was expressed in isolation. No iron export was observed in either case, however, expression of isolated domains *in trans* from two different plasmids in the

same cell resulted in a restoration of iron export, but at a fraction of that observed with native MbfA. Additionally, site-directed mutagenesis was used to selectively mutate four amino acids (D_{191}, M_{228}, E_{232} and Y_{268}), which present as potential iron coordinating ligands, to glycine. Mutagenesis allowed for the comparison of each MbfA variant's ability to export iron to the native MbfA. Mutation of M_{228}, E_{232} and Y_{268} resulted in no statistically significant differences in iron export to the un-edited MbfA, however mutation of D_{191} within TMH1 of the Vit1 domain resulted in significant reductions in export of iron. This observation was supported by a phenotypic observation in *E. coli* JC28 (iron uptake mutant). *E. coli* JC28 expressing pBAD*mbfA*D_{191} presented with significantly increased growth compared to the same strain expression pBAD*mbfA*. The increase in cellular growth can be attributed to a reduction in iron export with mutation of D_{191}.

The same series of hydrogen peroxide manipulation experiments was conducted with a comparison of wildtype *B. multivorans* to *B. multivorans* Δ*mbfA*, as well as with the VIT1 protein of *A. thaliana* expressed in *E. coli* MG1655. *B. multivorans* MbfA behaved in a very similar way to the MbfA from *B. suis* as iron was exported in a hydrogen peroxide dependent manner. However, advantages could be gained by observing MbfA within a native host, experimentation could be conducting regarding the expression of *mbfA* from its native promoter. The rate of iron export by *B. multivorans* MbfA was greatest when excess iron was supplied to the growth medium. In this way the *B. multivorans* cell is iron replete and suggests that *mbfA* is induced in response to high intracellular iron concentrations, allowing for the reduction in cellular iron content. Experimentation with *A. thaliana* VIT1 resulted in the observation that manipulation of hydrogen peroxide concentration did not influence the rate of iron export; leading to the determination that the VIT1 system exports iron in a hydrogen peroxide independent manner. This was to be expected due to the lack of an erythrin-like domain within the VIT1 protein. Experimentation with CCCP (proton ionophore) suggested that the VIT1 system, unlike MbfA, relies upon the proton motive force to enable iron translocation. Lastly, the dependence on hydrogen peroxide as an oxidant driving export influenced the redox state of the exported iron. H_2O_2 dependent systems lost an electron in the process of export and the exported iron was released to the medium as ferric iron, where as the H_2O_2 independent system maintained the ferrous iron oxidation state.

Final experimentation characterizing the function and mechanism of action of MbfA determined that the export of iron by MbfA results in numerous, beneficial effects. Export of iron from the cell results in the rapid disproportionation of external hydrogen peroxide though engagement of iron in Fenton reactions. This finding underpins the phenotypic observations that were conducted through the complementation of *E. coli* LC106 with MbfA and VIT1. Secondly, the export of cellular iron by MbfA protects the cell from nitric oxide sensitization to hydrogen peroxide (MbfA activity appears to be little affected by NO). Future work should be performed on the relative ability of the two separated domains (solo and *in trans*) to provide resistance to hydrogen peroxide in the presence and absence of nitric oxide. Lastly, the removal of iron from the cytoplasm by MbfA results in the mobilization of iron reserves from Bfr, which are in turn exported.

From the experiments described in this summary it was evident that the resistance to peroxide stress afforded to the cell through expression of *mbfA* is primarily conferred by export of iron from the cell which then engages in Fenton reactions that decompose peroxide externally in a fashion that is not harmful to the sensitive cellular machinery. To quantitate this, an assay was used to determine the effect of MbfA on the concentration external hydrogen peroxide over time. The *E. coli* strain lacking peroxidases (LC106) was unable to measurably degrade hydrogen peroxide over a 10 min period, but when complemented with MbfA, a rapid loss of hydrogen peroxide was observed. However, the issue was still apparent that the percentage contribution of peroxide degradation from the erythrin domain and Fenton reactions remained unresolved. To determine peroxide reduction at the erythrin domain in isolation, an extracellular iron chelator was added prior to the addition of hydrogen peroxide, this allowed the chelation of exported iron, preventing it from undertaking Fenton reactions. Hydrogen peroxide degradation under these conditions related to that solely occurring at the erythrin domain, which equated to ~20% of total hydrogen peroxide disproportionation. Therefore, as described in previous experiments, the majority of resistance to peroxides was achieved through the exported iron engaging in Fenton reactions outside of the cell.

With a detailed understanding gained of the mechanism that MbfA utilizes to export iron, experimentation was conducted to examine the role that nitric oxide plays within the phagosome of the macrophage. It was previously reported that NO and H_2O_2 act

synergistically in accelerating the killing of *E. coli* through a Fenton reaction mechanism (Woodmansee and Imlay 2003), and that this effect was reversed through the addition of a cell permeable iron chelator. This effect was examined with relation to *mbfA* expression. In isolation, addition of either 1 mM H_2O_2 or 50 μM NO gave no growth effect for *E. coli* MG1655, however when added together a synergistic killing effect was observed which was reduced with the expression of *mbfA*. The potential reasons for the increased sensitivity to hydrogen peroxide were postulated as being attributable to NO liberating stored iron from bacterioferritin and/or that NO binds the haem residues of catalase preventing detoxification of H_2O_2 (Hoshino et al. 1993, Brown 1995). In both cases, NO acts to sensitize the cell to hydrogen peroxide either by increasing available iron to engage in Fenton reactions within the cell, or by prevention of detoxification of H_2O_2.

To assess whether the presence of bacterioferritin (Bfr) and to a wider extent other iron storage proteins in *E. coli* (ferritin; FtnA and DNA-binding protein from starved cells; DPS) influenced the ability of MbfA to export iron from *E. coli*, quantitation of total iron content was performed for wildtype and mutant strains. Significant reductions in cellular iron content with expression of *mbfA* were only observed with deletion of *bfr* from the *E. coli* genome. In addition to this, the same *E. coli* iron storage mutants were assessed for their resistance to streptonigrin with *mbfA* expression. Deletion of all three iron storage mutants rendered *E. coli* more resistant to 2 μg/ml than wildtype *E. coli* with and without expression of *mbfA*. When Bfr was the sole iron storage protein in *E. coli*, sensitivity was comparable to that of wildtype *E. coli*, but MbfA expression resulted in significant protection. This suggests that Bfr acts as a reversible store of iron in *E. coli*.

The findings obtained suggest that MbfA acts as an NO-resistant, hydrogen peroxide dependent iron exporter. The biologically relevant consequences of exporting iron by *Brucella* are three-fold. First, MbfA specifically depletes intracellular ferrous iron concentrations, reducing the propensity for Fenton reactivity within the bacterial cytosol. Second, during export of ferric iron, the erythrin domain uses intracellular hydrogen peroxide as an oxidant, therefore further depleting the capacity for radical generation and ensuring that iron export only occurs when peroxides are present. Lastly, export of iron enables disproportionation of hydrogen peroxide outside of the bacterial cell, greatly limiting peroxide toxicity. This latter ability would be expected to

be particularly relevant in the macrophage where export of iron into the tight luminal space of the BCV should be highly effective in increasing iron concentration surrounding the *Brucella* in turn cell leading to efficient H_2O_2 decomposition. Thus, this relocalisation of H_2O_2-induced radical formation from the inside to the outside the bacterial cell provides a high degree of redox-stress resistance. Indeed, previous work has shown that high extracellular iron protects against peroxide, whereas high intracellular iron raises sensitivity (Cao et al. 2007, Nandal et al. 2010).

With respect to the use of hydrogen peroxide as a driving force for iron translocation in bacteria, this is not limited to the MbfA system. The *efeUOB* operon in *E. coli* O157:H7 and other bacteria encodes a high affinity ferrous iron transport system which is proposed to employ hydrogen peroxide as an oxidant facilitating iron translocation (Cao et al. 2007). This system and homologues thereof, are all thought to function to oxidise ferrous iron, located in the periplasm, to ferric iron at the periplasmically located EfeO protein, the electron generated during this oxidation step is transferred to the peroxide-reductase-like EfeB where it is used to reduce hydrogen peroxide. The ferric iron, bound to EfeO, is believed to pass its iron on to the ferric iron permease (EfeU), which then translocates the ferric iron into the cytosol. The substrates employed by EfeUOB are identical to those proposed for MbfA system, although the components involved in mediating the transport processes are quite distinct and the directionality of translocation is opposite. It both cases, hydrogen peroxide is used as an electron sink, to facilitate the oxidation and translocation of ferrous iron, whether this is for export or import is dependent upon the system.

From selected examples (Table 6.2) it is notable that organisms encoding EfeUOB-like iron importers do not encode MbfA-like iron export systems. The notion that both systems would be present in a single organism is counter intuitive as each employs peroxide to drive iron across the cytosolic membrane, but in reverse directions, and so their combined activities could result in a pointless futile cycle whereby peroxide promotes recycling of iron across the membrane. However, it is of interest that the *Brucella* spp. do encode a homologous, high affinity iron import system to EfeUOB, specified by the *ftrABCD* operon (Elhassanny et al. 2013). However, FtrABCD lacks any peroxide reductase component and is therefore unlikely to be peroxide dependent. This may, in part at least, explain the use of FtrABCD rather than EfeUOB in the *Brucellae*. Additionally, it is of note that when Vit-only versions of *mbfA* are observed

which lack an erythrin domain such as within *Neisseria flavescens*, the EfeUOB system is present.

Table 6.2: Gene identifiers of selected bacterial examples carrying either *mbfA* with *ftrABCD*, or *efeUOB* without *mbfA*.

MbfA Sub-family	Phyla	Organism	*mbfA* (AA Identity)	*ftrABCD* (AA Identity)	*efeUOB* (AA Identity)
Ib/c	α-proteobacteria	*Brucella suis*	BS1330_I1673 (100%)	BS1330_II0378 (100%)	N/A
	α-proteobacteria	*Bradyrhizobium japonicum*	BJS_07869 (58%)	N/A	N/A
	α-proteobacteria	*Agrobacterium tumefaciens*	ATCH_17048 (69%)	N/A	N/A
	β-proteobacteria	*Burkholderia multivorans*	BMULJ_05750 (16%)	BMULJ_02190 (66%)	N/A
	β-proteobacteria	*Paraburkholderia terrae*	WQE_38914 (17%)	WQE_37547 (71%)	N/A
	Actinobacteria	*Micrococcus luteus*	Mlut_04290 (15%)	N/A	N/A
	Bacteroidete	*Bacteroides fragilis*	BF9343_1281 (17%)	N/A	N/A
	Bacteroidete	*Fusobacterium ulcerans*	FUAG_02346 (21%)	N/A	N/A
IIp	β-proteobacteria	*Neisseria flavescens*	NEIFLAOT_00744 (10%)	N/A	NEIFLAOT_01857(50%)
	γ-proteobacteria	*Serratia marcescens*	SMDB11_1764 (8%)	N/A	SMDB11_RS10755 (74%)
	γ-proteobacteria	*Acinetobacter baumannii*	J504_1793 (7%)	N/A	A1S_1621 (26%)
	Actinobacteria	*Mycobacterium tuberculosis*	K875_03682 (10%)	N/A	K875_03222 (37%)
N/A	γ-proteobacteria	*Escherichia coli*	N/A	N/A	ECs1263 (100%)
	γ-proteobacteria	*Yersinia enterocolitica*	N/A	N/A	CH49_1371 (73%)

FtrABCD functions similarly to that of EfeUOB, in that ferrous iron is the transport substrate and is presumed to be oxidised during the uptake process. Also, like EfeUOB, FtrABCD carries a cupredoxin protein (FtrA) as well as an Ftr1-like ferric iron permease (FtrC) to import the ferric iron atom (Brickman and Armstrong 2012, Elhassanny et al. 2013). Differences arise in the way that the electron, generated from the ferrous iron oxidation, is dealt with. For FtrABCD, ferrous iron is believed to initially bind to the Cu-containing and periplasmic FtrB, where an electron is removed (possibly via FtrA) and then passed on to FtrD, a membrane-embedded polyferredoxin, where the electron is thought to be disposed of via unknown mechanism (Brickman and Armstrong 2012, Elhassanny et al. 2013). FtrABCD therefore, does not appear to rely upon the reduction of hydrogen peroxide and instead makes use of the polyferredoxin located within the inner membrane, as a sink for electrons. As indicated above, that hydrogen peroxide is not likely used as an oxidant for iron uptake in *Brucella* spp. is consistent with its use by MbfA for iron export instead (Figure 6.40).

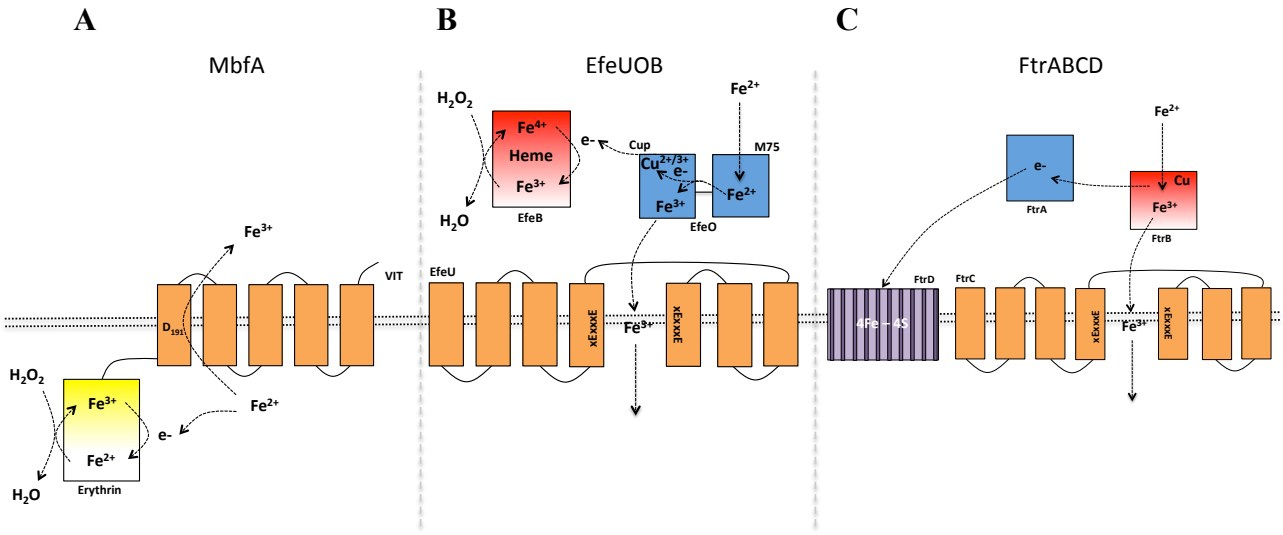

Figure 6.40: Schematic representation of the MbfA, EfeUOB and FtrABCD iron translocation mechanisms.

A: Intracellular ferrous iron is oxidised, the resulting released electron reduces the di-iron centre of the erythrin domain, allowing reduction of hydrogen peroxide. The resulting ferric iron atom is translocated to the periplasm. B: Extracellular ferrous iron is oxidised at the EfeO protein M75 domain, the electron passes to the EfeO cupredoxin domain (cup), and then on to the ferryl-haem group of EfeB, returning the haem group back to its resting state and enabling subsequent re-oxidation during reduction of hydrogen peroxide. The resulting ferric iron atom is translocated to the cytosol by EfeU. C: Extracellular ferrous iron is oxidised at the iron-binding site of the P19 protein

(FtrB), the released electron passed on to the periplasmic cupredoxin and is then shuttled to the iron-sulphur clusters of the membrane-bound polyferridoxin, FtrD, which may in turn feed the electron to the electron transport chain. The resulting ferric atom on FtrB is translocated to the cytosol via FtrC.

The above observation raises the hypothesis that bacterial spp. encoding MbfA-like iron export systems will encode FtrABCD-like rather than EfeUOB-like iron import systems, preventing opposing iron translocation process occurring upon exposure to H_2O_2. The converse should therefore be true, that bacterial spp. encoding EfeUOB-like iron import systems do not encode MbfA.

Chapter 7: Characterization of *mbfA* in *Brucella suis* 1330 and *Brucella melitensis* 16M

7.1: Rationale for the creation of *Brucella* spp. deletion mutants

To explore the role that MbfA plays with regards to intracellular survival and virulence in *Brucella* spp., the *mbfA* gene was deleted from the *Brucella suis* 1330 and *Brucella melitensis* 16M chromosomes by a targeted approach.

Given that *Brucella* spp. are hazard group three pathogens as defined by the Advisory Committee on Dangerous Pathogens (ACDP), as well as hazard group three Specified Animal Pathogen Order (SAPO) pathogens as defined by the Department for Environment, Food and Rural Affairs (DEFRA) and Overlap Select Agents as classified by the Center for Disease Control (CDC); all manipulations of *Brucella* spp. were conducted within the Defense Science and Technology Laboratory (DSTL) ACDP/ACGM containment level (CL) three laboratories.

To remove the target gene from the genomes of *Brucella suis* 1330 and *Brucella melitensis* 16M a non-polar unmarked gene excision approach was used in which the target gene was removed and an antibiotic resistance determinant (kanamycin) inserted in its place. This was achieved through the insertion of a suicide plasmid, via electroporation, into the *Brucella* spp. and recombination of that suicide plasmid with the *Brucella* genome via selective pressure applied by kanamycin. Integrants were cured through a second recombination event, selected for by resistance to sucrose, promoting the removal of the suicide plasmid backbone that encodes *sacB*. Upon the creation of *Brucella mbfA* mutants, a single clone was complemented with a replicating plasmid (limited to ten copies per cell in *Brucella* spp.) carrying the *mbfA* gene expressed from its native promoter.

To determine if *mbfA* aids in the intracellular survival and virulence of *Brucella* spp. the growth of wild-type and mutant derivative strains was assessed for their ability to grow under oxidative stress inducing conditions, as well as survival within cultured murine macrophages and *in vivo* within a mouse model.

7.2: Creation of *mbfA* deletion mutants in *Brucella suis* 1330 and *Brucella melitensis* 16M

Prior to the electroporation of plasmid DNA into *Brucella* suis 1330 and *Brucella melitensis* 16M it was ensured that stocks of the bacteria held at DSTL at -80C were viable and of smooth LPS phenotype. The virulence of the classical *Brucella* strains; *Brucella melitensis*, *Brucella abortus* and *Brucella suis* is associated with presence of the O-polysaccharide, with smooth LPS phenotypes generally being virulent and rough ones not. Smooth *Brucella* spp. colonies present as moist glistening circular convex colonies entire edges of 2-4 mm in diameter after growth for 2 days on TSA. However, spontaneous transition to the rough LPS phenotype is possible and is encouraged by the use of media with excessive moisture, unnecessary holding of cultures at room temperature and extended incubation periods. Rough cell phenotypes present with dry granular opaque and more brittle colonies that auto-agglutinate rapidly in broth culture, compared to smooth cultures which sediment slowly over time. A more comprehensive assessment of the smooth and rough phenotype on agar plates is achieved through flooding the plate with a 1:4 mixture of 10% crystal violet in ethanol and 1% ammonium oxalate in distilled water; smooth cells do not stain, whereas rough cells stain deep purple. Physical examination of *Brucella melitensis* after 3 days incubation at 37 °C on Brucella agar reveals small (approx. 1 mm diameter) moist circular colonies with entire edges. Additionally, *Brucella suis* colonies appear on average 3 mm in diameter with the same physical characteristics. This observation confirms the smooth LPS phenotype of these strains.

To prepare competent *Brucella* cells for receiving DNA by electroporation, one 10 µl loop of cells was scraped from a confluent TSA plate, which had been incubated at 37 °C for 3 days, and was re-suspended in 1 ml of room temperature H_2O. The cells were washed three times with 1 ml H_2O via centrifugation (3 min, 20 °C, 13,000 rpm), re-suspended in 200 µl of water before dividing into 50 µl aliquots. 5 µl of plasmid DNA was added to 50 µl of competent *Brucella* cells in a cooled 0.2 mm electroporation cuvette and electroportated (BioRad XCell electroporation system) at 400 Ω, 25 µF and 2.5 kV for 10 ms. Electroporated cells were allowed to recover in 1 ml SOC-B at 37 °C overnight before plating onto TSA with appropriate antibiotics and incubated at 37 °C for up to 5 days.

Prior to the construction of deletion mutants though the electroporation of the suicide plasmid construct into the *Brucella* species, the transformation efficiency of 1 µg of the replicating plasmid pBBR1-MCS4 (Amp^R) via the electroporation protocol described above into *Brucella melitensis* 16M and *Brucella suis* 1330 was determined. A transformation efficiency of $2.3x10^3$ cfu/µg was achieved with *B. melitensis* whilst an approximate one log higher transformational efficiency was achieved with *B. suis;* $1.4x10^4$ cfu/µg. This observation is consistent with the greater enumeration of *B. suis* bacteria present on Brucella agar plate cultures compared to *B. melitensis* after 3 days incubation at 37 °C.

Suicide and complementation plasmids (pEXΔ*mbfA*::Kn^R, pBBR4$mbfA_{melitensis}$, pBBR4$mbfA_{suis}$) were extracted from *E. coli* Top10 (Qiagen Plasmid Midi Prep) and concentration via ethanol precipitation to approx. 200 ng/µl DNA in H_2O and stored at -20 °C. Electroporation was repeated with pEXΔ*mbfA*::Kn^R and integrant *B. melitensis* and *B. suis* colonies were selected for through plating recovered cells on to TSA with 45 µg/ml kanamycin. Two presumptive *B. melitensis* integrants were recovered whilst *B. suis* yielded 25 colonies. The increased number of single homologous recombinations in *B. suis* was not unexpected due to the increased transformational efficiency.

To confirm the presence of a single homologous recombination of the suicide plasmid into the *Brucella melitensis* genome, colony PCR was conducted. To conduct this analysis the two kanamycin resistant *B. melitensis* colonies where taken into 100 µl of H_2O then heated and maintained at 96 °C for 10 minutes, ensuring complete loss of cellular viability. cPCR with primers specific to the kanamycin cassette (mbfAKn F/R) could then be undertaken at CL3 prior to the PCR samples being removed to a CL2 laboratory for agarose gel electrophoresis analysis (Figure 7.1) (Method 2.6.1). The presence of a 796 bp band indicates the single homologous recombination event within the integrant genome. *Brucella suis* colony boilates were unable to be created at the time of analysis, due to a Proof of Principle heat killing study on *B. suis* not having been undertaken – preventing the removal of all *B. suis* PCR materials from the CL3 laboratory.

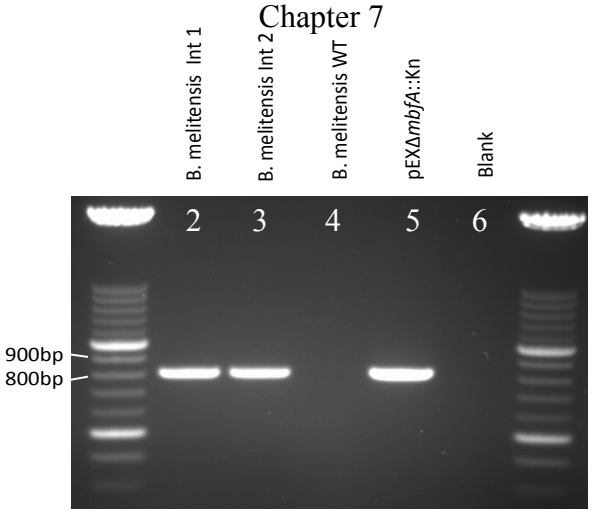

Figure 7.1: *Brucella melitensis* cPCR integrant confirmation

1% agarose gel electrophoretic analysis of cPCR of *B. melitensis* pEXΔ*mbfA*::Kn^R single homologous recombination integrants (primers specific to inserted kanamycin cassette). Tracks left to right: 1/7, molecular weight marker; 2, *B. melitensis* integrant 1 (796 bp); 3, *B. melitensis* integrant 2 (796 bp); 4, *B. melitensis* wild-type (negative control); 5, pEXΔ*mbfA*::Kn^R (positive control); 6, blank (PCR without DNA).

Both *B. melitensis* colonies and the positive control (pEX*mbfA*::kn plasmid) exhibited the expected 796 bp PCR band, whilst PCR from wild *type B. melitensis* did not exhibit any PCR product. This indicates that kanamycin resistant *B. melitensis* colonies result in 100% positive integrant selection. This can be taken as true for the *B. suis* colonies, which were unable to analyzed at the same time, that Kn^R colonies are integrants (later confirmed as integrants by PCR from extracted genomic DNA).

One *B. melitensis* and one *B. suis* integrant were inoculated into 1 ml of Brucella broth and incubated overnight at 37°C. The broth cultures were diluted ten-fold and 100 µl plated onto TSA with 10% sucrose and 45 µg/ml kanamycin and incubated at 37°C for 3 days to select for double homologous recombinants.

Eight single, isolated colonies, presumptive cured *B. melitensis* mutants, were selected for a second cPCR analysis with primers specific to the flanking region of DNA outside the 1kb flanking DNA used to allow for recombination (mbfA 1 kb F/R). A 154 bp larger PCR product was expected for *mbfA* mutants compared to the wild-type strains (Figure 7.2). The presence of a 3467 bp band rather than a 3313 bp indicates a double homologous recombination event.

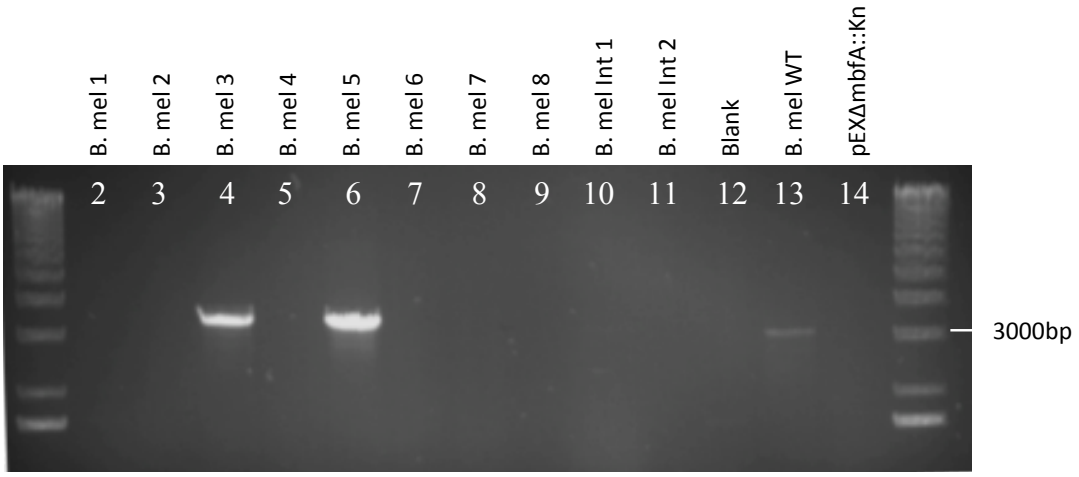

Figure 7.2: *Brucella melitensis* cPCR mutant confirmation

1% agarose gel electrophoretic analysis of cPCR of cured *Brucella melitensis* *mbfA*::Kn^R mutants with flanking primers. Tracks left to right: 1/15. molecular weight marker, 2-9. presumptive *B. melitensis mbfA* mutants (3467 bp), 10/11. *B. melitensis* integrants (negative control), 12. blank (PCR reaction without DNA), 13. *B. melitensis* wild-type (positive control – 3313 bp), 14. pEXΔ*mbfA*::Kn^R (negative control).

Two of the eight presumptive cured mutants presented with 3467 bp PCR products, suggesting a 25% success rate. With an *mbfA* mutant confirmed by cPCR in *B. melitensis*, genomic DNA preparations (Qiagen Gentra Puregene) were prepared from the eight presumptive cured mutants, one presumptive integrant and one wild-type *B. melitensis* and *B. suis* colonies. The DNA preparations were tested for sterility before removal to a CL2 laboratory via the inoculation of 10% of the DNA preparation in 10 fold excess Brucella broth and incubation for 7 days at 37 °C, followed by the incubation of 100 µl of broth on Brucella agar for a further 7 days at 37 °C. Plates presenting with no presumptive *Brucella* colonies were deemed sterile (Method 2.6.2).

The PCR reactions used to identify and confirm integrants and cured *Brucella melitensis* mutants were repeated for both *Brucella melitensis* and *Brucella suis* in a CL2 laboratory using the extracted genomic DNA (Figure 7.3A). To highlight the small increase in base pairs (154 bp), which determined the strain as a mutant rather than the wild type, the PCR products were analyzed after electrophoretic separation on an agarose gel directly adjacent to each other (Figure 7.3B). The presence of the 3467 bp band indicates a double homologous recombination event.

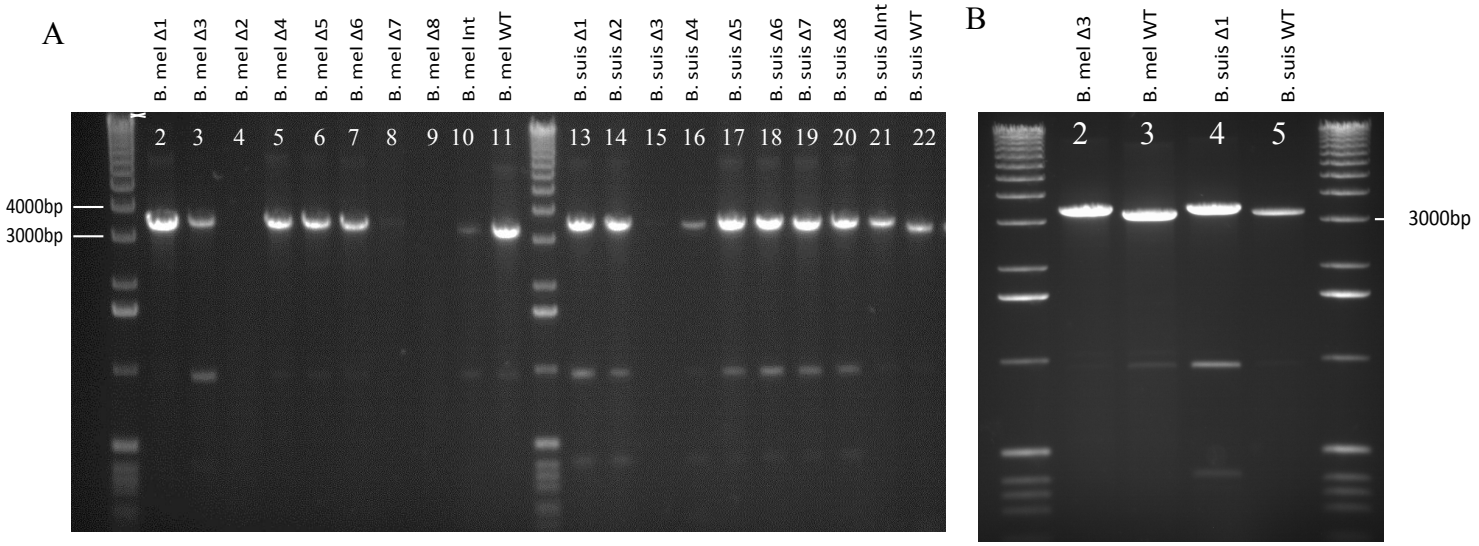

Figure 7.3: *B. melitensis* and *B. suis* genomic DNA PCR

A: 1% agarose gel electrophoretic analysis of PCR with gDNA of cured *B. melitensis* and *B. suis mbfA*::Kn^R mutants with flanking primers. Tracks left to right: 1/12. molecular weight marker, 2-9. presumptive *B. melitensis mbfA* mutants (3467 bp), 10. *B. melitensis* integrant (3467 bp), 11. *B. melitensis* wild-type (positive control – 3313 bp). 13-20. presumptive *B. suis mbfA* mutants (3467 bp), 21. *B. suis* integrant (3467 bp), 22. *B. suis* wild-type (positive control – 3313 bp). B: 1% agarose gel electrophoretic analysis of PCR with gDNA of *B. melitensis* Δ*mbfA*3, *B. suis* Δ*mbfA*1 and respective wild-type strains with flanking primers. Tracks left to right: 1/6. molecular weight marker, 2. *B. melitensis* Δ*mbfA*3 (3467 bp), 3. *B. melitensis* WT (3313 bp), 4. *B. suis* Δ*mbfA*3 (3467 bp), 5. *B. suis* WT (3313 bp).

Reproduction of the PCR reactions with *B. melitensis* genomic DNA resulted in five of the eight presumptive cured mutants presenting with 3467 bp (62.5 % successful cured mutants) compared to the two when analysed by cPCR. It is of note, that both cPCR positive cured integrants were both PCR positive when genomic DNA was analysed. Severn of the eight *B. suis* genomic extractions presented as PCR positive (87.5 %), with all PCR products separating to larger molecular weights than the respective wild-type control, indicating all isolates are mbfA deficient.

The genomic DNA from *B. melitensis* Δ*mbfA*3 and *B. suis* Δ*mbfA*1 was taken forward for a further confirmation of the mutant genotype by PCR using a combination of primers which would only yield a PCR product if a double recombination event had

taken place (mbfA F with mbfAkn R and mbfA R with mbfAKn F). The 5' flanking primer was paired with the 3' Kn^R primer for the left-hand reaction and the 3' flanking primer was paired with the 5' Kn^R primer for the right-hand reaction, allowing a comprehensive evaluation of the presence of the double recombination event and creation of the deletion mutant (Figure 7.4).

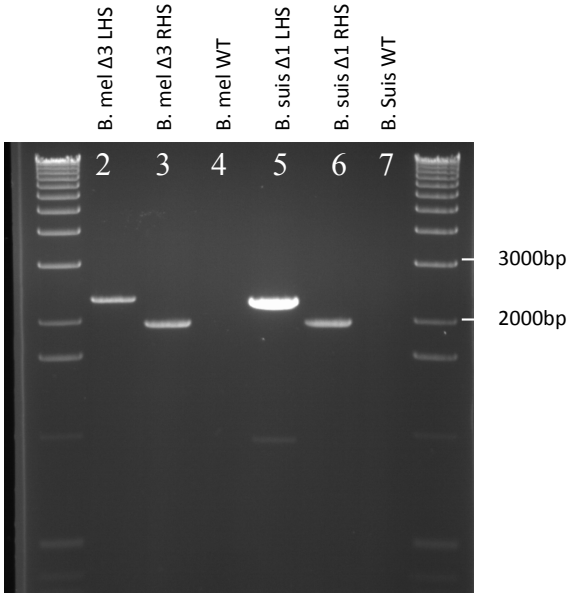

Figure 7.4: *B. melitensis* and *B. suis* mutant confirmation PCR

1% agarose gel electrophoretic analysis of PCR with gDNA of *B. melitensis* Δ*mbfA*3, *B. suis* Δ*mbfA*1 and respective wild-type strains with kanamycin and flanking primers. Tracks left to right: 1/8. molecular weight marker, 2. *B. melitensis* Δ*mbfA*3 LHS (2328 bp), 3. *B. melitensis* Δ*mbfA*3 RHS (2032 bp), 4. *B. melitensis* WT (negative control), 5. *B. suis* Δ*mbfA*1 LHS (2328 bp), 3. *B. suis* Δ*mbfA*1 RHS (2032bp), 4. *B. suis* WT (negative control).

The presence of 2328bp and 2032bp bands amplified from the mutant genome, and simultaneous absence from the wild-type genome indicate the removal of the target gene and replacement with the kanamycin cassette within the *mbfA* gene.

In addition to confirmation by PCR, the DNA sequence containing the mbfA deletion was sequenced. This would confirm that both, the *mbfA* gene had been removed and preplaced by the kanamycin cassette, as well as, ensuring that the *B. melitensis* wild-type strain encode the *mbfA* pseudogene through acquisition of the t55c SNP

The *mbfA* coding sequence and flanking regions of *B. melitensis* Δ*mbfA*3, *B. suis* Δ*mbfA*1 and their respective wild-type parental strains were amplified by PCR (mbfA 1 kb F/R) from the respective genomic DNA isolates. The amplified DNA was removed from residual oligonucleotides and free bases, and blunt end ligated into the pCR4-TOPO vector. The *Brucella* originating DNA was sequenced from the M13 forward and reverse sequencing primers (Figure 7.5).

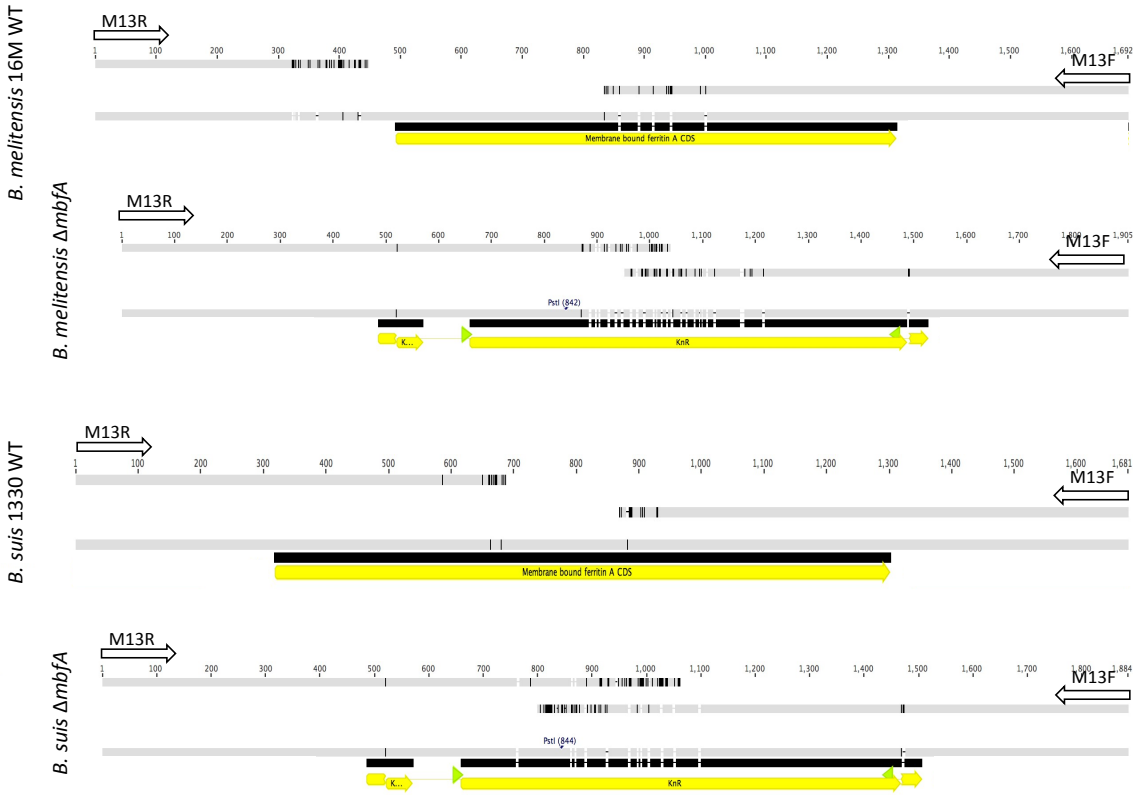

Figure 7.5: Sequence confirmation of *mbfA Brucella* mutants

Sanger sequencing reads of *B. melitensis* 16M WT, *B. melitensis* Δ*mbfA, B. suis* 1330 WT and *B. suis* Δ*mbfA* with M13 forward and reverse sequencing primers. Sequencing primers indicated with open arrows, *mbfA* and kanamycin genes indicated with yellow arrows.

The sequencing results confirmed that the mutant strains have deletions to the *mbfA* gene and replacement with the kanamycin gene and kanamycin promoter sequence. Additionally, confirmation of the t55c point mutation (glutamate to stop codon mutation) in the *mbfA* gene of *B. melitensis* 16M WT was observed, whilst this was absent in the *B. suis* strain, as expected.

Upon full confirmation of the deletion of the *mbfA* coding sequence from the genomes of *Brucella melitensis* 16M and *Brucella suis* 1330 complementation with pBBR4 series vectors was conducted.

Both *B. melitensis* and *B. suis* Δ*mbfA* strains were complemented with both the functional *B. suis mbfA*, or non-functional *B. melitensis mbfA* (pBBR$mbfA_{suis}$ and pBBR$mbfA_{melitensis}$) as well as empty vector control (pBBR4). Electroporations were conducted as described previously with selection of transformant strains conducted through plated onto Brucella agar (100 μg/ml ampicillin). Ampicillin resistant colonies were stored in glycerol stocks at -80 °C.

Table 7.1 lists the *Brucella* strains that have been created to characterize the function of *mbfA* in *Brucella suis* 1330 and *Brucella melitensis* 16M.

Table 7.1: Wild type and engineered *Brucella* spp. strains.

***Brucella* spp**	**Strain**	**Genotype**	**Antibiotic resistance**
B. melitensis	16M	WT	-
	Δ*mbfA*	Δ*mbfA*	Kn
	p$mbfA_{suis}$	Δ*mbfA* p$mbfA_{suis}$	Kn, Amp
	p$mbfA_{mel}$	Δ*mbfA* p$mbfA_{mel}$	Kn, Amp
B. suis	1330	WT	-
	Δ*mbfA*	Δ*mbfA*	Kn
	p$mbfA_{suis}$	Δ*mbfA* p$mbfA_{suis}$	Kn, Amp
	p$mbfA_{mel}$	Δ*mbfA* p$mbfA_{mel}$	Kn, Amp

7.3: Characterisation of *mbfA* deletion mutants of *Brucella suis* 1330 and *Brucella melitensis* 16M

To characterize the effect that the deletion of *mbfA* has upon the ability of *Brucella suis* 1330 and *Brucella melitensis* 16M to withstand loss of cellular viability through exposure to oxidative stress, three main experiments were proposed. First a growth curve monitoring the optical density over a 48 hour time period would be conducted in the presence of the two major factors contributing to oxidative stress experienced within the phagolysosome; hydrogen peroxide and ferrous iron (supplied as ferrous sulphate). Secondly, macrophage survival assays will be conducted and a comparison the number of intracellular bacteria determined during a time course experiment. Lastly, an *in vivo* study using a chronic infection mouse model will be conducted to identify if a significant difference is present between wild type and mutant *Brucella suis* strains. Individually and in combination these three assays will allow for a comprehensive review into the requirement of *mbfA* in *Brucella* spp. in terms of resistance to oxidative stress, intracellular survival and ability to maintain infection in a mammalian host, therefore determining if *mbfA* acts as a virulence factor in *Brucella* spp.

First an analysis of aerobic growth of *Brucella suis* 1330 and *Brucella melitensis* 16M wild type and *mbfA* mutants was monitored over a 48 hour time period at 37 °C 20 µl of 0.5 OD adjusted cells from an overnight *Brucella* culture was inoculated into 180 µl of Brucella broth with either hydrogen peroxide, ferrous sulphate or left with no addition as a control and optical densities at 620 nm were measured every 30 minutes for 48 hours with the Thermo Multiskan FC (Figure 7.6). Brucella broth (10.0 g/L pancreatic digest of casein, 10.0 g/L peptic digest of animal tissue, 2.0 g/L yeast extract, 5.0 g/L sodium chloride, 0.1 g/L sodium bisulphite, 1.0 g/L dextrose) was used as the base media in all experimentation; with supplementation of either with either 10 mM hydrogen peroxide or 5 mM ferrous iron made to examine resistance to oxidative stress.

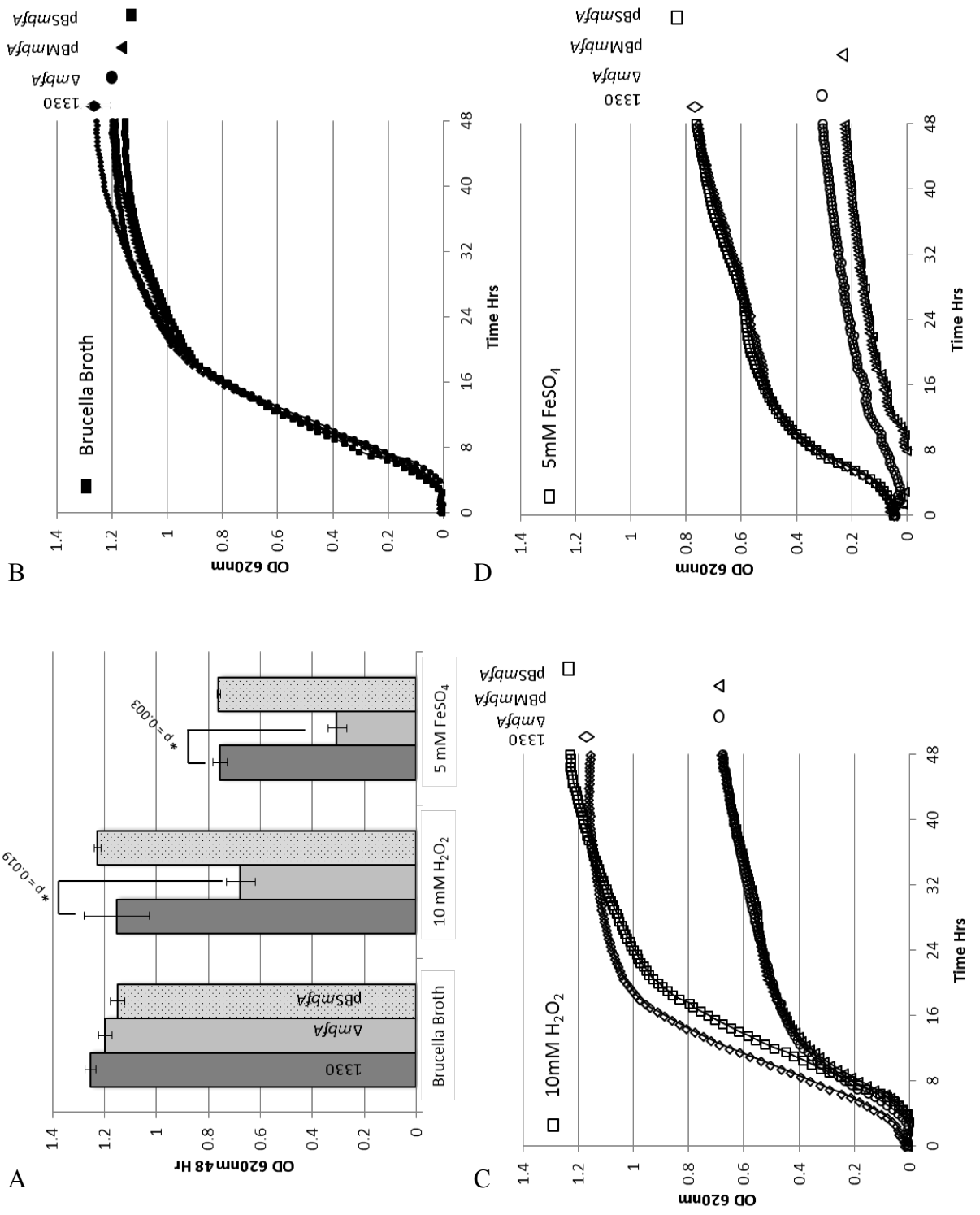

Figure 7.6. 48-hour growth curve of *B. suis* 1330, Δ*mbfA* and p*mbfA*.

All growth curves were conducted in 96 well plates in Brucella broth, supplementations are noted. A: Average optical density achieve for each strain after 48 hr growth. B: 48 hr growth curve. The data presented represents the means obtained from three separate experiments, the asterisk (*) denotes a statistically significant difference, between the data obtained for *B. suis* 1330 and *B. suis* Δ*mbfA* via a Students *T*-test ($P < 0.01$) at T = 48 h.

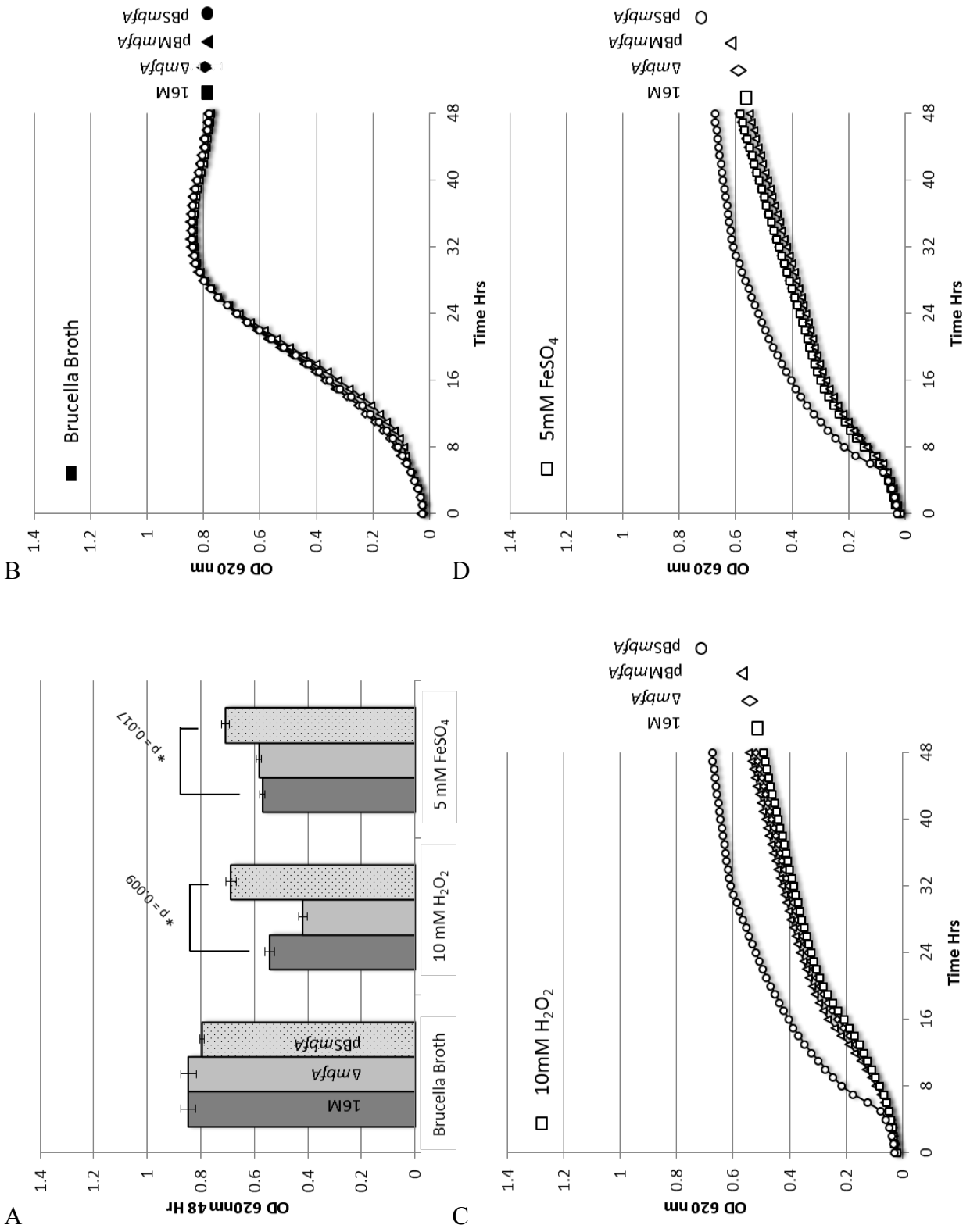

Figure 7.7. 48-hour growth curve of *B. melitensis* 16M, Δ*mbfA* and p*mbfA*.

As figure 7.6, *B. melitensis* in place of *B. suis*.

Aerobic growth over a 48 hour time course of *B. melitensis* in non-supplemented Brucella broth identifies growth to ½ maximal OD (0.42 OD units ~ 18 h) was achieved 5 h after that of *B. suis* (0.62 OD units ~ 13 h). As well as a reduced ½ maximal OD, a reduced optical density after 48 h (0.41 OD units) was visualized. This growth profile is consistent with the observation of smaller and less numerous *B. melitensis* colonies on Brucella agar compared to *B. suis*. Additionally, the less avid growth phenotype was apparent in both wild-type and Δ*mbfA B. melitensis* strains, suggesting that the reduction in *B. melitensis* growth is not *mbfA* dependent.

Supplementation of Brucella broth with 5 mM $FeSO_4$ resulted in a reduction in final optical density in all *Brucella* strains and derivatives. A greater reduction in optical density after 48 hr is observed in *B. suis* strains than *B. melitensis* (*B. suis* 1330 39.9% reduction; *B. melitensis* 16M 26.4% reduction) when comparing growth in supplemented and non-supplemented media. This suggests a greater resistance of *B. melitensis* 16M to iron associated oxidative stress than *B. suis* 1330. A hypothesis for greater redundancy in mechanisms relating to oxidative stress resistance is plausible although the mechanism for this resistance is unknown, and is not obvious upon examination of the *B. melitensis* genome.

B. suis Δ*mbfA* experienced greatest reduction in optical density – 0.452 OD units, compared to WT under the same iron supplemented condition, demonstrating an involvement of MbfA in protection against iron induced oxidative stress in *B. suis*. This effect was reversed with complementation of *mbfA* on a pBBR series vector. Deletion of *mbfA* in the cryptic *B. melitensis* 16M strain presented with no difference in optical density, but complementation with a functional copy of *B. suis mbfA* increased optical density by 0.124 OD units, suggesting that removal of *mbfA* via targeted mutation or through acquisition of SNP is detrimental to the protection against iron initiated oxidative stress in *B. melitensis*.

Supplementation of Brucella broth with 10 mM H_2O_2 resulted in similar observations to supplementation with ferrous iron; *B. suis* Δ*mbfA* experienced greatest reduction in optical density – 0.477 OD units and was complementable with p*mbfA*. *B. melitensis* 16M and Δ*mbfA* strains exhibit no significant difference in optical density, but complementation with a functional *mbfA* gene results in an increased resistance to H_2O_2 (0.268 OD unit increase).

Taken together these results suggest that *in vitro*, *mbfA* serves a role in protecting *Brucella* spp. from oxidative stress supplied via hydrogen peroxide and Fenton chemistry. As elucidated in previous chapters the mechanism for resisting oxidative stress by MbfA is likely due to the export of intracellular free iron, preventing the accumulation of hydroxyl radical damage generated as a byproduct of ferrous iron and hydrogen peroxide interactions. Exported iron will also function to engage in Fenton chemistry outside the cell preventing hydoxyl radical formation within the cell.

Given that *B. melitensis* strains are naturally cryptic for *mbfA,* suggestive of an evolutionary step away from its requirement in virulence, the results of this *in vitro* experimentation are unlikely representative of the interactions the *Brucella* spp. undertake *in vivo*. However, they do present evidence that MbfA provides measurable protective effects against iron and hydrogen peroxide initiated oxidative stress.

7.4: Immuno-detection of MbfA in *Brucella suis* 1330 and *Brucella melitensis* 16M

To further characterize the cryptic nature of the *B. melitensis mbfA* sequence and therefore lack of MbfA translation, Western blotting of whole cell extracts of *B. suis*, *B. melitensis* and derived mutants was conducted. Anti-rabbit, polyclonal antibodies were previously generated to the soluble N-terminal cytosolic erythrin domain of the MbfA protein, enabling probing for MbfA expression in *Brucella* strains.

To enable the collection of whole *Brucella* cells expressing *mbfA*, *B. suis*, *B. melitensis* and derived mutants were propagated in 5 ml Brucella broth over-night, before sub-culture into a further 5 ml Brucella broth supplemented with 10 mM hydrogen peroxide or 5mM ferrous sulphate. The cultures were incubated for 8 hr and 1 OD of cells pelleted by centrifugation at 13,000 rpm in a benchtop microfuge before re-suspension in 1 ml H_2O. The 1 ml suspensions were heat inactivated at 60 °C for 2 hrs, before the sterility of the suspension was assessed prior to removal to a CL2 laboratory (Method 2.6.2). The total protein content of the heat-killed cells was determined by a Bradford assay, using lysozyme to generate a standard curve. 10 µl of a 0.1 mg/ml normalized preparation was used to separate the isolated proteins by SDS-polyacrylamide gel electrophoresis and conduct a Western blot (Figure 7.8).

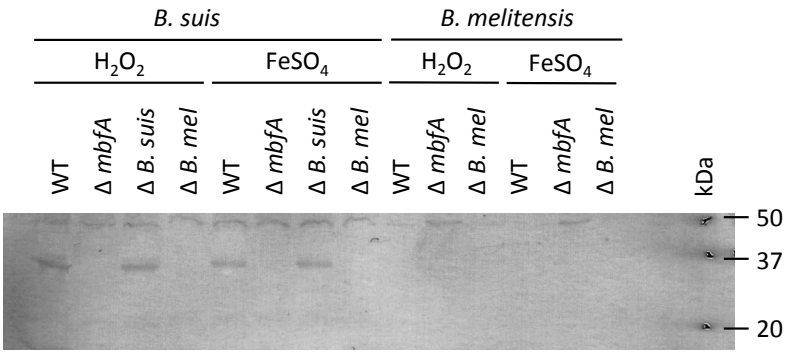

Figure 7.8: Western blot identification of MbfA

Immuno-detection of MbfA (anti-erythrin) from *B. suis* and *B. melitensis* whole cell extracts after 2 hour exposure to 10 mM H_2O_2 or 5 mM $FeSO_4$. MbfA: 36.4 kDa.

The Western blot highlights the absence of MbfA translation in response to hydrogen peroxide and ferrous iron in *B. melitensis* as well as engineered *B. suis mbfA* mutants, and *B. suis* mutant complemented with the *B. melitensis* pseudogene. MbfA is translated in the *B. suis* WT strain and when complemented with the *mbfA* sequence in a complementation plasmid.

7.5: Intracellular survival and replication of *B. suis* and *B. melitensis mbfA* mutants in J774.A1 murine macrophage

Building on the results observed *in vitro*, in which the presence of *mbfA* in *Brucella* spp. confers resistance to oxidative stress, the role that MbfA plays in regards to the intracellular survival of *Brucella* spp. will be elucidated through experimentation with J774.A1 murine macrophages. The relative survival of *B. suis* 1330, *B. melitensis* 16M and derivative Δ*mbfA* mutants will be compared to provide insight into MbfA function.

J774.A1 murine macrophages are an immortalized monocyte macrophage cell line isolated from the reticulum cell sarcoma of BALB/c mice. To enable maintenance and growth classical cell culture techniques are employed; J774.A1 macrophages were maintained in Dulbecco's modified Eagle's medium (DMEM) with 5% fetal bovine serum (FBS) and 2 mM L-glutamate and were incubated at 37 °C under a 5% CO_2 atmosphere. Upon 70-80% confluent growth in tissue culture flasks cells are split into fresh media to allow renewed propagation.

To conduct intracellular survival assays, $1x10^5$ J774.A1 macrophages were seeded per well in a 24 well plate in supplemented DMEM. After 24 hours growth at 37 °C and 5% CO_2, which provides sufficient time for attachment of macrophages to the 24-well plate and upon visualization of cellular monolayers, spent culture media was removed. Culture medium was replaced with 0.5 ml Leibovitz's L15 media containing approximately $1x10^7$ CFU/ml of the test organism, resulting in a multiplicity of infection (MOI) of 100:1. Leibovitz's L15 media was used in replacement of DMEM during intracellular survival assays conducted at CL3 due to the absence of an incubator supplying a 5% CO_2 atmosphere, through the requirement of containing CL3 pathogens in sealed containers during all manipulations outside the specified safety cabinet. Leibovitz's L15 media enables to buffering of pH to within required limits in the absence of CO_2. After 1.5 hours of infection, extracellular bacteria were killed by treatment with gentamicin (50 μg/ml) and maintained in Leibovitz's L-15 medium with gentamicin (2 μg/ml).

After removal of non-internalized *Brucella* via treatment with gentamycin, at pre-determined time points (0, 4, 24 and 48 hrs) macrophages were washed with PBS and lysed with 0.1% (vol:vol) triton X-100 in H_2O. To enumerate viable intracellular *Brucella* cells at each time point, macrophage cell lysates were serially diluted and

plated onto Brucella agar, then incubated for 3 days at 37 °C. CFU were counted and data was presented as CFU per well.

Prior to experimentation, preliminary studies were conducted to ensure 50 μg/ml gentamycin was bactericidal to all experimental *Brucella* strains. Gentamycin is an aminoglycoside, bactericidal antibiotic and functions through binding to the 30S subunit of the bacterial ribosome, interrupting bacterial protein synthesis. Studies have determined that the minimal bactericidal concentration (MBC), (the minimal concentration at which growth after 72 hours at 37 °C inhibited growth in broth and yielded no colonies for the corresponding agar subculture after 72 hours at 37 °C) of *Brucella melitensis*, and *Brucella suis* strains are between 4 and 32 μg/ml (Olsen and Carlson 2015). In line with this methodology, the effectiveness of the bactericidal action of 50 μg/ml gentamycin on *B. melitensis* and *B. suis* strains was examined. An overnight culture of *B. suis* and *B. melitensis* WT and Δ*mbfA* mutants was diluted to a standardized optical density of 0.5 OD units in Brucella broth. 100 μl of each *Brucella* culture was spread onto Brucella agar containing 50 μg/ml gentamicin; plates were incubated for 3 days at 37 °C then examined for colony forming units. In all cases, no *Brucella* colonies were observed. With confirmation of the bactericidal effect of gentamycin on *Brucella* survival, analysis of the intracellular survival of *B. suis* 1330, *B. melitensis* 16M and Δ*mbfA* mutants in J774.A1 murine macrophages was conducted (Figure 7.9).

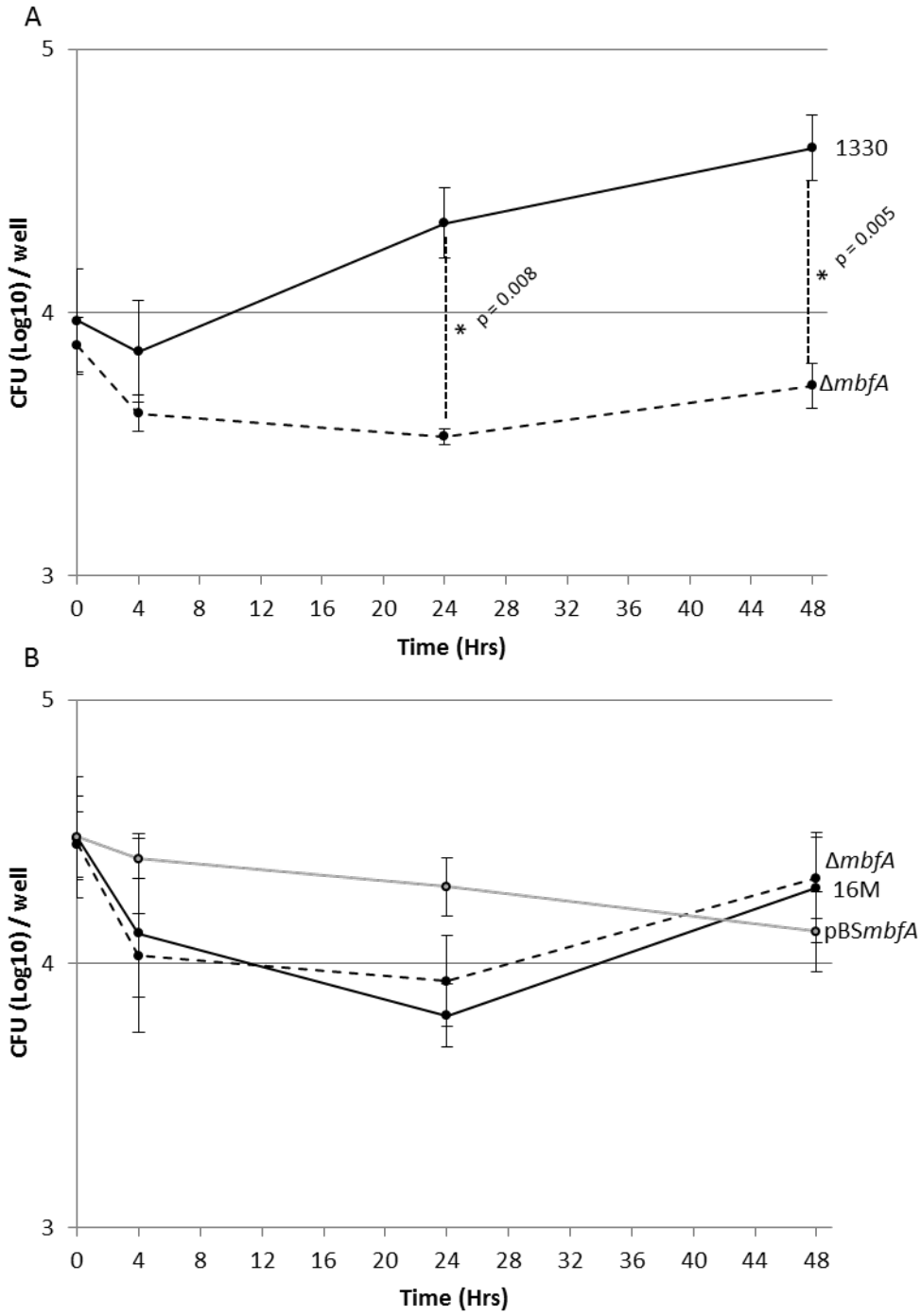

Figure 7.9: Intracellular survival and replication of *B. suis* 1330, *B. melitensis* 16M and derivative strains in J774.A1 murine macrophages.

1 x 10^5 J774.A1 macrophages were infected at an MOI of 100:1, at indicated times post-infection macrophages were lysed and the number of intracellular brucellae determined by serial dilution, plating and culture. (A) Survival and replication of *B. suis* 1330 and Δ*mbfA* and (B) *B. melitensis* 16M, Δ*mbfA* and p*mbfA*. The results are averages of n = 3 technical replicates and n = 3 biological replicates ± the standard deviation at each time point and analysed using an unpaired, two tailed Student's *t*-test.

Analysis of the intracellular survival profiles of *B. suis* and *B. melitensis* reveals that all strains exhibit an initial reduction in viable bacteria with in the first hours of macrophage infection. This is consistent with published literature; it is noted that up to 90% of ingested bacteria can be killed rapidly by the macrophage within the first 4 hours of infection (Celli et al. 2003), and represents the association with in the early Brucella containing vacuole (eBCV). In all wild type cases, after initial reductions in viable intracellular numbers, bacterial replication commences and increases in recoverable viable intracellular bacteria are observed.

B. suis 1330, *mbfA* expressing, is able to replicate at a greater rate and sooner during macrophage infection than the Δ*mbfA* mutant, which results in significantly less intracellular bacteria after 24 and 48 h. The deletion of *mbfA* from the *B. suis* 1330 genome results in an increased reduction (47%) of intracellular bacteria during residence within the eBCV (4-24 hours). This observation is consistent with MbfA providing protection against the respiratory burst generated by the macrophage during this period.

In comparison to *B. suis, B. melitensis* 16M, Δ*mbfA* or p*mbfA* strains all exhibit an increased number of bacteria entering macrophage at T_0 compared to *B. suis* strains; but present with differing percentage survival during the association within the eBCV depending upon *mbfA* genotype. *mbfA* defective strains experience an average 149% decrease in cellular viability after 4 h infection, whereas, *mbfA* expressing *B. melitensis* only suffers a 20% decrease in viable cell count over the same period, supporting the role of MbfA providing protection against oxidative stress.

It is of interest that *mbfA* expression during later macrophage infection is detrimental to *B. melitensis* viability. Post 24 h, *mbfA* defective *B. melitensis* strains begin replication but the *mbfA* expressing strain maintains a decreasing rate of reduction in cellular viability, this suggests that *mbfA* expression, although beneficial during early stage infection, is detrimental throughout the entire macrophage infection cycle. Removal of reactive free iron by MbfA protects against oxidative stress, but may disadvantage replication when environmental conditions are favourable. This suggests that *mbfA* in *Brucella melitensis* strains may act as an anti-virulence factor. The presence of MbfA, exporting iron during early stages of phogolysosomal localization is detrimental to the intracellular survival of *B. melitensis* at later time points. It is after 24 h that *B.*

melitensis is localized within the endoplasmic reticulum and when the requirement for iron to allow cellular replication is apparent. With the removal of iron by MbfA to counter oxidative stress, the propensity for replication is reduced.

A second interpretation of this data may suggest that the expression of *mbfA* in *Brucella melitensis* is completely advantageous. The assay conducted specifically identifies intracellular bacteria; the gentamycin in this assay specifically kills extracellular bacteria. We are therefore unable to enumerate bacteria that have completed their intracellular transition and have exited the macrophage as they will contact gentamycin. If *mbfA* is advantageous to *B. melitensis*, *mbfA* encoding strains may be able to transit through the macrophage quicker and exit the macrophage at a sooner time point. Under the conducted assay this would manifest as a reduction in intracellular bacteria, as is observed. Although this second conclusion can be drawn from the data, counter evidence exists which suggests that *mbfA* is not advantageous to *B. melitensis* strains.

Other lines of evidence counter the principle that *mbfA* is advantageous to *B. melitensis*. Firstly, from genetic analysis it is apparent that *B. melitensis* is currently in the process of genomic decay and *mbfA* is being lost from the genome as was detailed in the bioinformatics chapter. Clade I *B. melitensis* strains (including *B. melitensis Ether*) have acquired SNP's within the *mbfA* gene, two of which encode for stop codons and subsequently render the gene cryptic. If *mbfA* were advantageous to *B. melitensis* is it unlikely that a single point mutant resulting in a stop codons introduction would be maintained, let alone two.

Secondly, the results from these experiments are based upon the principle that the intracellular survival assay is based upon a model. To this fact, murine macrophages are being used as a representative model of human or in wider settings ruminant infections. The murine macrophage cell line J774.A1 possesses the $G_{169}D$ point mutation within the Slc11a1 (NRAMP1) gene rendering it non-functional, within humans and ruminants this mutation is not present and NRAMP is functional. Slc11a1 represents the major mechanism for host derived nutritional immunity directed towards the invading host. In the absence of Slc11a1 iron is not actively removed from the phagolysosome generating an altered environment as to that which is observed in humans and ruminants. Therefore results observed for the requirement of *mbfA* in intracellular survival of both *B. suis* and *B. melitensis* may not be a representative

model.

To address this concern, RAW264.7 murine macrophages, originally isolated from Slc11a1 non-functional BALB/c mice were obtained from Prof. Gunter Weiss (Medical University - Innsbruck) (Atkinson and Barton 1999) which have been transfected with the pHβA-1-neo plasmid containing either the full-length Slc11a1 cDNA (RAW-37) or an antisense-Slc11a1 construct (RAW-21).

The transfection of the functional Slc11a1 gene, with expression driving from the human β-actin promoter, will recreate conditions within the murine macrophage more representative of that observed in humans and ruminants. In the presence of Slc11a1/NRAMP1 – the requirement for MbfA to maintain cellular viability may be of greater requirement.

Laurence A. Guilloteau et al. (Guilloteau, Dornand et al. 2003) compared the intracellular survival of *Brucella melitensis* H38S (smooth virulent strain) within the RAW264.7 transfectant cell lines R21 (*Nramp1* deficient) and R37 (*Nramp1* expressing) provided by C. H. Barton. Their examinations revealed that there was no difference in the replication rates of *B. melitensis* H38S in the RAW264 transfectants, leading them to conclude that "In contrast to infections with *Salmonella, Leishmania,* and *Mycobacterium,* the expression of the *Nramp1* gene appears to be of limited importance for the natural resistance of mice to *Brucella*." Their work further noted that it was only during initial stages (first week) of *B. melitensis* H38S infection of a NRAMP1 resistant mouse that spleen and liver counts were increased compared to a NRAMP1 sensitive mouse. By the second week of infection, no differences were observable in bacteria isolated from spleens or livers.

Although this study determined that NRAMP1 was of little importance to the resistance of *B. melitensis* infection in mice, the importance of NRAMP1 in influencing the intracellular survival of *mbfA* encoding *Brucella* spp. (*B. suis* or *B. abortus*) has not been examined. To address this, intracellular survival assays with the RAW264.7 transfectant cell lines R21 and R37 were conducted with *B. suis* 1330 and *B. suis* Δ*mbfA*.

7.6: Intracellular survival and replication of *B. suis* and *B. melitensis* in RAW264.7 NRAMP1 transfectant murine macrophage

RAW264.7 -R21 and -R37 macrophage cell lines were generously supplied by Prof. G. Weiss, whilst anti-NRAMP1 antibodies were supplied by Dr. H. Barton. Prior to conducting macrophage survival assays with *Brucella*, the NRAMP1 status of the transfectant cell lines was determined via Western blotting. The anti-NRAMP1 antibodies supplied were generated to amino acids 1-54 of the murine NRAMP1 (Slc11a1) protein sequence, and were routinely used at a dilution of 1:1000 (Atkinson and Barton 1999). $1x10^6$ macrophage cells were collected from RAW264.7 R21 and R37 cell lines, as well as from the J774.A1 macrophage cell line used previously. Whole cell lysates were prepared for each cell line through passage of the cell solution in SDS-PAGE buffer through a syringe (advise was given not to boil samples before analysis as NRAMP1 would aggregate and not separate during electrophoresis), before separation by SDS-PAGE and immuno-blotting (Figure 7.10). It is of note that NRAMP1 is glycosylated, and hence results in a non-distinct band upon immuno-detection.

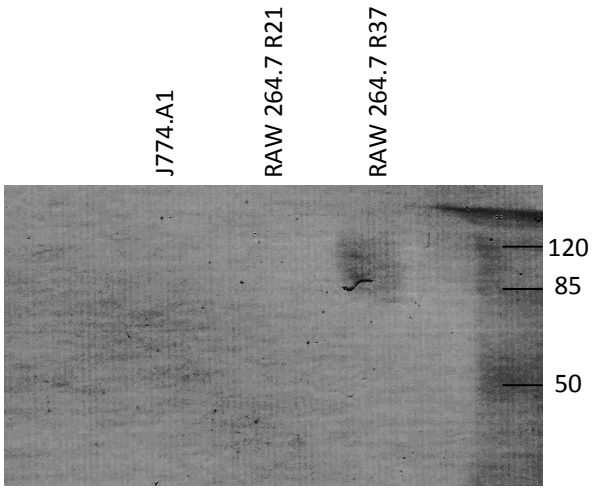

Figure 7.10: Western blot identification of NRAMP1

Immuno-detection of NRAMP1 from J774.A1, RAW264.7-R21 and RAW264.7-R37 macrophages. NRAMP1: 90-100 kDa.

An approx. 100 kDa product, consistent with the presence of NRAMP1 was only observed from RAW264.7-R37 macrophage. This confirms the genotype of both J774.A1 and RAW264.7-R21 as NRAMP1 deficient, whilst RAW264.7-R37 as NRAMP1 expressing.

Macrophage survival assays conducted with transfectant RAW264.7 murine macrophages where conducted in the same way as was described for J774.A1 macrophages assays, with one exception; geneticin G418 was included at a concentration of 0.5 mg/ml within DMEM during propagation of macrophages to provide selective pressure to ensure the maintenance of the pHβA-1-neo harboring the antisense- or sense-Slc11a1 cDNA.

Analysis of the intracellular survival of *B. suis* 1330, Δ*mbfA* and p*mbfA*, as well as *B. melitensis* 16M and p*mbfA* were compared in RAW264.7 R21 and R37 macrophages simultaneously (Figure 7.11).

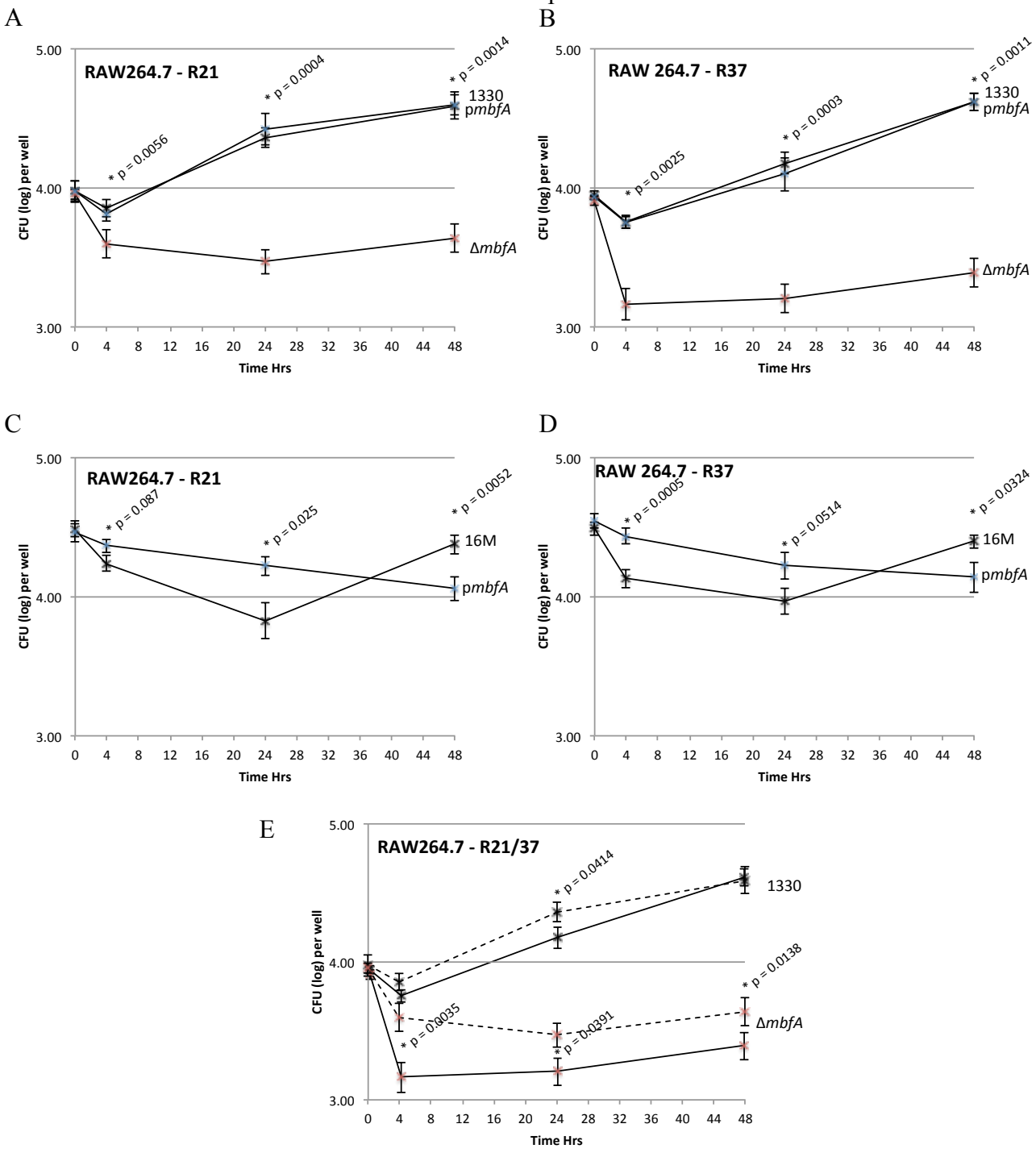

Figure 7.11: Intracellular survival and replication of *B. suis* 1330, *B. melitensis* 16M and derivative strains in RAW264.7 R21 and R37 macrophages.

1 x 10^5 RAW264.7 R21 and R37 macrophages were infected at an MOI of 100:1, at indicated times post-infection macrophages were lysed and the number of intracellular brucellae determined by serial dilution, plating and culture. (A) Survival and replication of *B. suis* 1330 Δ*mbfA* and p*mbfA* in R21 macrophage, (B) *B. suis* 1330 Δ*mbfA* and p*mbfA* in R37 macrophage, (C) *B. melitensis* 16M and p*mbfA* in R21 macrophage and (D) *B. melitensis* 16M and p*mbfA* in R37 macrophage, (E) *B. suis* 1330 and Δ*mbfA* in R21 and R37 macrophages. The results are averages of n = 3 technical replicates and n

= 3 biological replicates ± the standard deviation at each time point and analysed using an unpaired, two tailed Student's *t*-test.

The replication profiles of all *B. suis*, *B. melitensis* and derived *mbfA* mutant and complemented strains examined in RAW264.7-R21 macrophages were directly comparable to those observed in J774.A1 macrophages. This is expected, as both cell lines are *Nramp1* deficient – this observation acted as a control as it ensured that the results observed in RAW264.7-R37 macrophages was comparable with previous intracellular survival observations. In contrast, the intracellular survival of *B. suis,* derived *mbfA* mutant and complemented mutant strains, when examined in RAW264.7-R37 macrophages (*Nramp1* encoding) were significantly hampered compared to that of *Nramp1* deficient macrophages.

Comparing the number of viable *B. suis* cells, from all strains, that entered R21 and R37 macrophages (survival at T_0) revealed no significant difference in *Brucella* infectivity. At T_0, R21 macrophages presented with 9.3 x 10^3 bacterial cells/well compared to 8.5 x 10^3 cells/well with in R37 macrophage, a difference of 8.8%. This demonstrates that *Nramp1* genotype does not alter *Brucella* entry into macrophage and all strains present with the same infectivity.

The presence of NRAMP1, within the phagolysosome, decreases *B. suis* intracellular survival in all wild-type and derived strains compared to when NRAMP1 is absent, during early phases of macrophage infection (T_4 and T_{24}). Significantly, the largest reduction in viable intracellular cells resulted when *mbfA* is absent from *B. suis* (Figure 7.11 E).

A reduction of 16.8 % in viable *B. suis* 1330 cells ($p = 0.0241$) is observed when comparing R21 to R37 macrophages after 4 hours; this increases to a 33.9 % reduction ($p = 0.0642$) after 24 hours. No significant difference is observed after 48 hours, as numbers of viable *B. suis* differ only by 6.67 %. This is suggestive that the presence of NRAMP1 is detrimental to the survival of *Brucella* cells during transit of the bacterium from the phagolysosomal-associated eBCV to the ER-associated rBCV, as is observed through decreases in viable *Brucella* between 4 and 24 hours, time points when *Brucella* are known to be associated with this cellular compartment. It is of note that wild-type and complemented *B. suis mbfA* mutant present equivalent intracellular

survival from four hours after engulfment, 6.7 x 10^3 and 5.6 x 10^3 respectively (16.8 % difference) to 48 hours after engulfment, 3.9 x 10^4 and 4.2 x 10^4 respectively (6.7 % difference). This displays effective expression of *mbfA in trans* from the pBBR-4 plasmid, functionally complementing the deletion of *mbfA* in the constructed *mbfA* mutant.

When *mbfA* is removed from the *B. suis* genome, much larger decreases in viable cell counts are observed when comparing R21 to R37 macrophages throughout the assay, from T_4 to T_{48}. After 4 hours a 63.7 % reduction ($p = 0.0004$) in *B. suis* Δ*mbfA* viable cells is observed when comparing counts from R21 to R37, this decreases to a 46.3 % reduction by 24 hours ($p = 0.0294$) and 43.8 % by 48 hours post infection ($p = 0.0378$). Taken together these viable cell counts display a significant reduction in *B. suis* intracellular survival when located in the phagolysosome with *Nramp1* expression in the absence of *mbfA*. This bactericidal effect is mediated by NRAMP1; exporting iron from the phagolysosome promotes conditions where hydrogen peroxide is able to accumulate to a concentration where sufficient quantities can ingress into the *Brucella* cell. The subsequent creation of free radicals leads to cellular damage and loss of cellular viability, this effect is exasperated by the deletion of *mbfA* from *B. suis* as NRAMP1-dependent export of iron progresses without competition from the export of iron by MbfA. .This therefore, provides evidence for the hypothesis that MbfA functions to aid *B. suis* viability within the phagolysosome though export of iron and acts as a virulence factor for *B. suis*.

This observation is not repeated in *B. melitensis* however. As with *B. suis*, there is no significant difference with the number of *B. melitensis* able to enter macrophages. But as with observations made with J774.A1 macrophage, more *B. melitensis* bacteria were able to enter RAW264.7 cells than *B. suis* strains, at an average of half a log increase. In contrast to *B. suis*, the presence of NRAMP1 within RAW264.7 macrophages was not detrimental to the intracellular survival of *B. melitensis* 16M (smallest p value over four time points comparing R21 to R37 *B. melitensis* 16M viable cells = 0.451). This observation is in agreement with those collected by Guilloteau et al. (Guilloteau et al. 2003) who determined that "there was no difference between *in vitro* replication rates of *B. melitensis* H38S in *Nramp1* RAW264 transfectant macrophages". The authors conclude that the *Nramp1* gene of little importance for the natural resistance of mice to *Brucella melitensis,* this is in contrast infections with *Salmonella, Leishmania,* and

Mycobacterium where the presence of *Nramp1* is detrimental to intracellular survival.

The complementation of *B. melitensis* 16M with *B. suis mbfA* (pBBR*mbfA*) yielded significant increases in the survival of intracellular bacteria at T_4 and T_{24} in both R21 and R37 macrophages when compared to wild-type *B. melitensis* (naturally cryptic *mbfA*). No differences were present when comparing across macrophage strains, suggesting that MbfA provides a growth advantage during early macrophage infection which is not NRAMP1 dependent.

7.7: Role of *mbfA* during *B. suis* infection of mouse

To determine if the reduced intracellular survival of *B. suis* Δ*mbfA* within cultured murine macrophages results in a reduction in virulence, an *in vivo* study was conducted. The mouse model is widely used to assess the virulence of *Brucella* spp. and derived mutants, and was employed in this instance. The colonization of the spleen, liver and blood was compared within mice infected with either *B. suis* 1330 or *B. suis* Δ*mbfA* over an 8 week period.

Experimental infection in the murine model with *Brucella* spp. results in a chronic infection that can routinely be maintained for up to 12 weeks (Nymo et al. 2016) but can persist for up to 6 months (Enright et al. 1990). In general, *Brucella* infection can occur via the digestive or inhalation routes, and upon crossing the respective mucosal barrier the organisms are able to reach regional lymph nodes. Bacterial replication occurs within macrophages and a bacteremic phase of infection must follow to allow colonization of the spleen and liver, establishing a systemic and persistent infection. Experimental infection of mice occurs mostly through three routes: intraperitoneal, digestive and nasal (aerosol), with the intraperitoneal (IP) route being the most frequently used in published literature. The IP route of infection establishes a persistent infection with rapid systemic distribution and high bacterial loads in the liver and spleen (Grillo et al. 2012), this method of bacterial delivery was used in this study.

The replication profile of a *Brucella* infection in the mouse model can be divided into four separate and distinct phases (Grillo et al. 2012). First, the onset of the infection is marked by colonisation of the animal in the first 48 h post infection. Secondly, an acute phase of infection presents, extending from approximately the third day post infection to the time point at which colony forming units (CFU) reach a maximum, generally between 2 and 3 weeks. Next, a chronic infection phase, which correlates to a plateau in CFU that can last up to 8 weeks. Finally, a chronic-declining phase, which as previously stated may last up to 6 months post infection; during this period a slow elimination of the bacteria occurs.

To evaluate the role that MbfA plays in resistance to bacterial killing during macrophage engulfment, a comparison between organ colonisation profiles of forty 6 to 8 week old female BALB/c mice was conducted. BALB/c mice were obtained from Charles River Laboratories UK, and all work was conducted according to the Animal (Scientific Procedures) Act 1986.

Mice which had undertaken a 5 day acclimatisation period were challenge by the IP route with 5 x 10^4 cells of the wild type or mutant *Brucella suis* strains. Five mice per group were culled at 1, 2, 4 and 8 weeks post infection. To prepare the inoculum of *B. suis* strains for challenging the BALB/c mice via the IP route, both wild type and mutant strains were grown on Brucella agar for 2 days at 37 °C. Trial inoculums were prepared to determine a relationship between the optical density of suspended cells against CFU/ml (Figure 7.12). It was determined that *Brucella* cells harvested into PBS and adjusted to a standardized optical density of 0.005 would correspond to a challenge dose of approx. 5 x 10^4. Enumeration of the final challenge dose revealed that 7.0 x 10^5 CFU/ml were present for *B. suis* 1330, and 7.9 x 10^5 CFU/ml for *B. suis* Δ*mbfA*. Optimum challenge dose was 5 x 10^5 CFU/ml (5 x 10^4 CFU/0.1 ml).

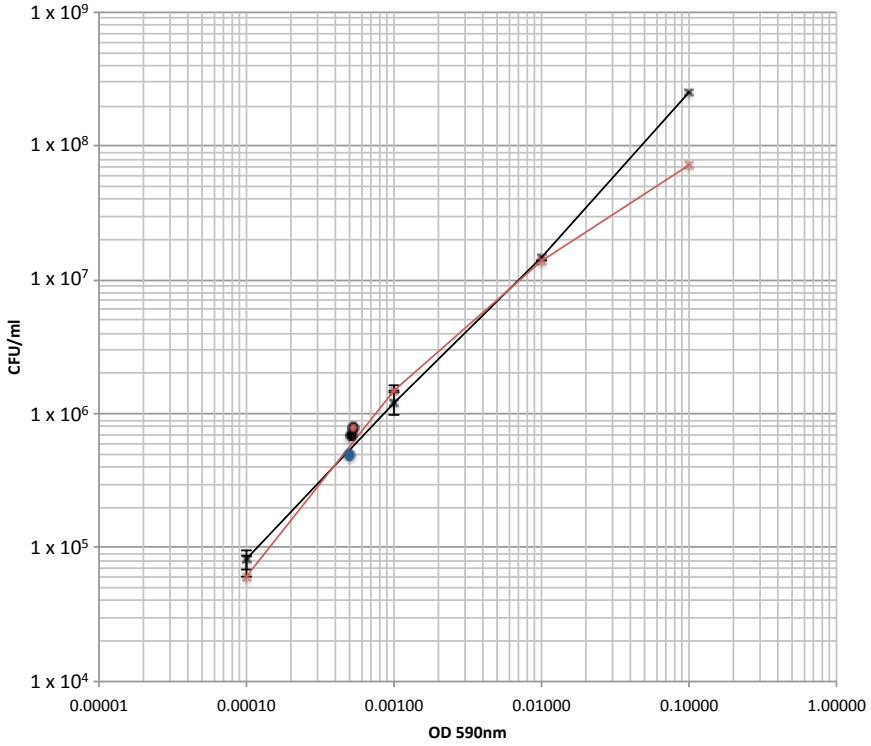

Figure 7.12: Standardisation of colony-forming unit numbers to optical density.
Enumeration of CFU from decreasing optical densities of *B. suis* 1330 (black) and *B. suis* Δ*mbfA* (red) cultures. Black dot, *B. suis* 1330 (black line) challenge dose; red dot, *B. suis* Δ*mbfA* (red line) challenge dose**;** blue dot, target challenge dose.

Following inoculation, five mice per experimental group were culled at 1, 2, 4 and 8 weeks post-infection. Each mouse was terminally anaesthetised by inhalation of halothane prior to collection of blood via cardiac puncture followed by culling by cervical dislocation, a schedule 1 method. Subsequently, post-mortems were conducted to allow for the collection of the spleen and liver. Each organ was weighed then homogenized in PBS with 0.1% Triton X-100, serially diluted and plated to enumerate viable *Brucella* at each time point.

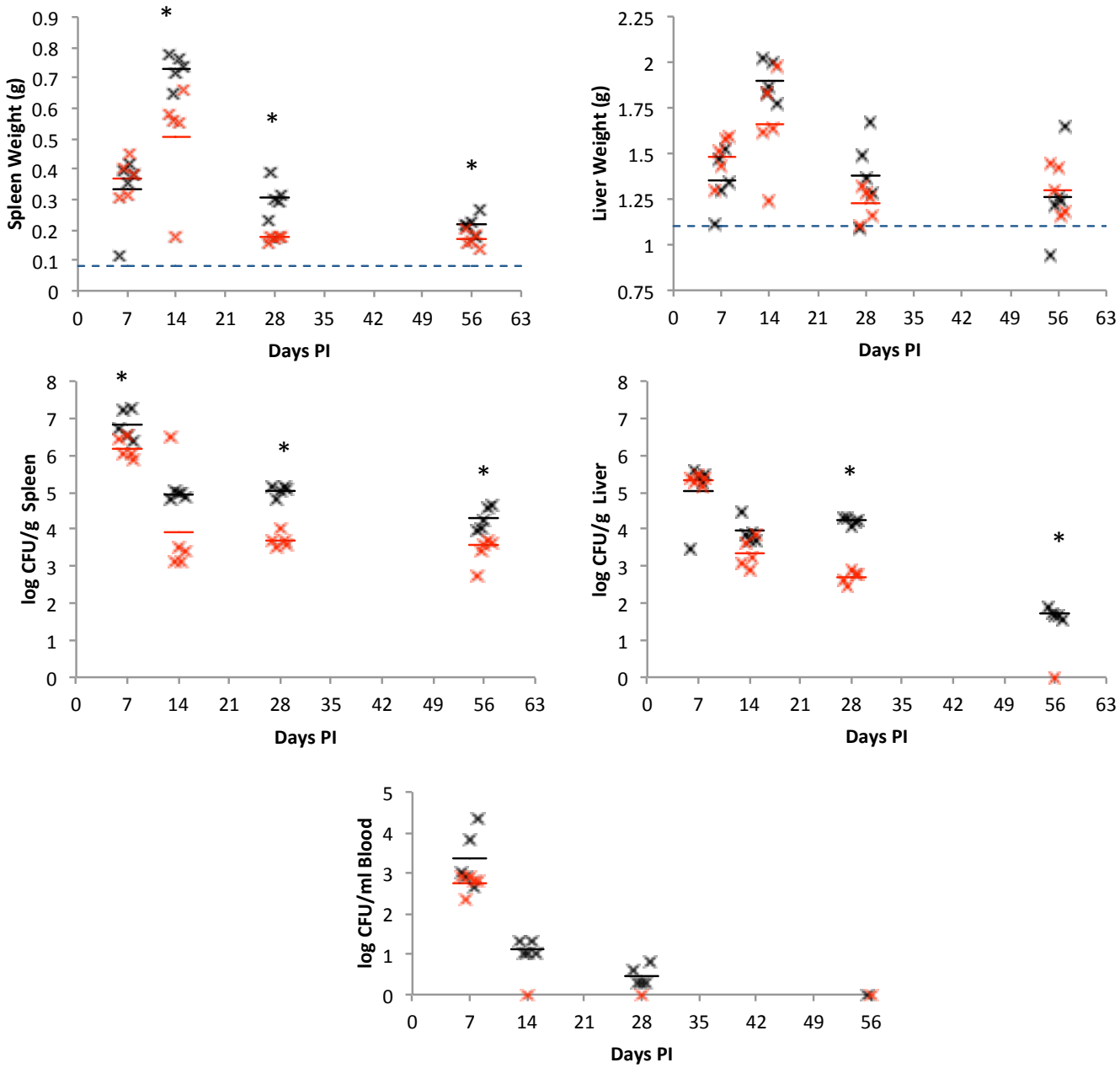

Figure 7.13: Spleen, liver and blood bacterial counts and organ weights.

Log bacterial counts per organ per gram for *B. suis* 1330 (black) and *B. suis* Δ*mbfA* (red) in spleens, livers and blood of BALB/c mice after intraperitoneal (IP) inoculation of $5x10^4$ colony forming units (CFU) of bacteria, along with organ weights for corresponding samples. The asterisk (*) denotes a statistically significant difference as determined by a Student's *t*-test ($P < 0.01$). Dotted horizontal line indicates 'normal' weights for uninfected controls, and horizontal bars indicate average (mean) values.

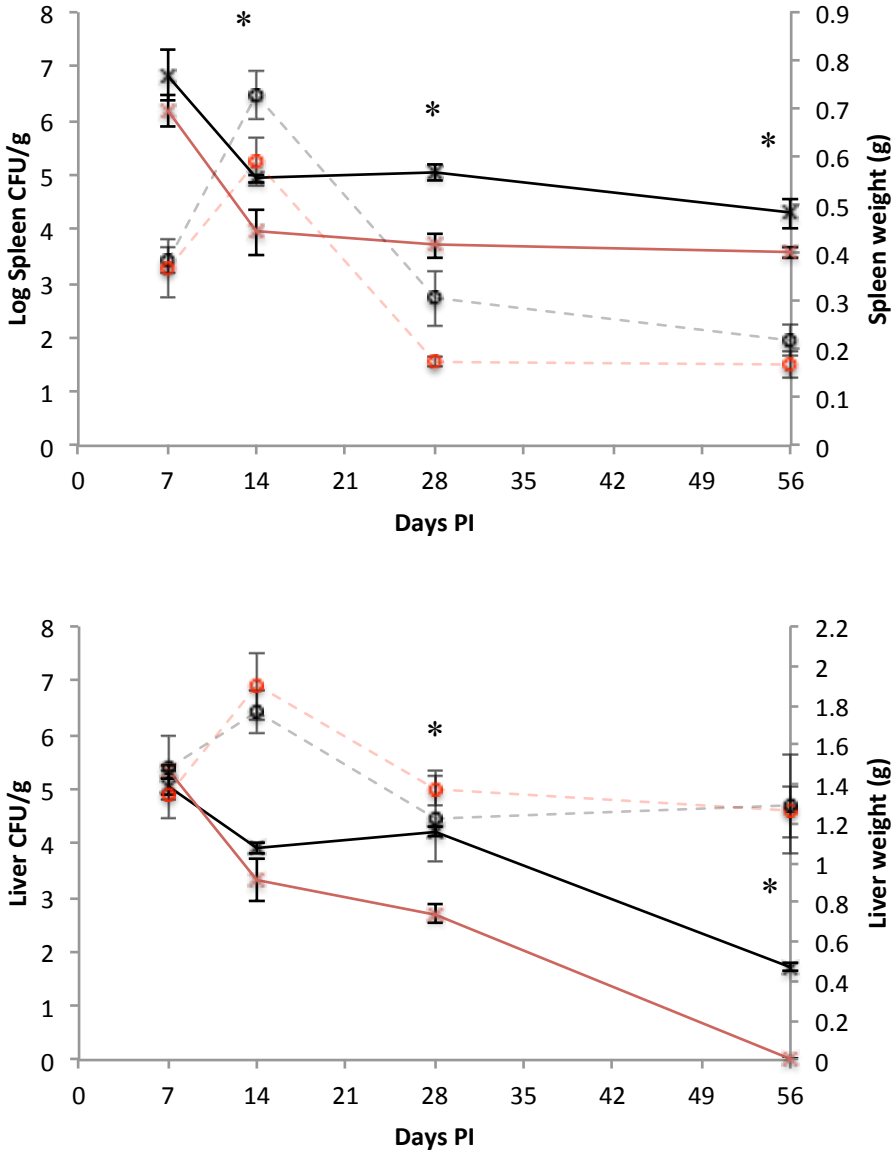

Figure 7.14: Comparison of bacterial counts and organ weights for spleen and liver.

Data are derived from the figure above. Average organ weights (broken lines) and average log bacterial counts (solid lines) for *B. suis* 1330 (black) and *B. suis* Δ*mbfA* (red) in spleens and livers of BALB/c mice. Results are expressed as means ± one standard deviation. The asterisk (*) denotes a statistically significant difference as determined by a Students *T*-test ($P < 0.01$) for average log bacterial counts.

The number of Δ*mbfA* bacteria recovered from the spleen, liver and blood were consistently significantly less than the numbers obtained for the wild-type strain from 14 days post-infection onwards. This therefore suggests that *mbfA* is required for virulence of *B. suis* in the murine model. It should be noted that the reduced *B. suis* Δ*mbfA* survival after 14 weeks compared to the wild-type was achieved despite a slightly higher inoculum used for Δ*mbfA* (11.4% higher CFU count) than that for WT.

Supplementary to this primary observation, the organ weight data gathered reveals a peak in both liver and spleen weights at 14 days post infection, with a 9.1 times increase in mean spleen weight for *B. suis* 1330 and 7.4 times increase for *B. suis* Δ*mbfA* compared to the average, uninfected spleen weight (0.08 g). Similar observations were made for the liver, an increase in weight of 1.73 times was observed with infection with *B. suis* 1330 and 1.60 times increase for *B. suis* Δ*mbfA* compared to the average, uninfected liver weight (1.1 g). The inflammation of the liver was accompanied by a pale colouration, compared to normal healthy tissue. It should be noted that there is a greater likelihood of variation between liver weights due to difficulties in isolating the entire organ during post-mortem. The multi-lobed nature of the liver renders it difficult to ensure that all lobes are excised, generating the possibility that the whole liver will not have been removed. Despite this technical limitation, the standard error between samples was not excessively high.

Over the first two weeks post-infection, the *B. suis* Δ*mbfA* strain gave a lower number of recoverable cells from the spleen, with respect to those recovered for the wild-type strain (*B. suis* Δ*mbfA* 2.495 log reduction with respect to the inoculum; *B. suis* 1330 1.688 log reduction). Over the 4 and 8 weeks post infection period, the numbers of recoverable viable cells from the spleen remained relatively constant for both strains, although reductions in CFU's were still seen in the liver, with the *B. suis* Δ*mbfA* strain again displaying a greater reduction which culminated in clearance of this strain from the liver by 8 weeks post infection, whereas the wildtype remained present at 1.9×10^2 cells/g. The infection pattern seen in the spleen resembles that previously reported with an initial 'acute phase' giving a peak recovery (seen at 7 days here), followed by a chronic phase with a CFU plateau that lasts ~10 weeks. A final 'chronic decline phase' can last more than 36 weeks and so would not be observed in the data provided here which does not extend beyond 8 weeks (High et al. 2007).

Previous reports have shown that the spleen and liver are the most infected organs in mice following challenge with virulent smooth *Brucella* species (Grillo et al. 2012), with one-two logs lower CFU/g in the liver than the spleen (Cheers and Cone 1974), as seen above. The infection level is reported to be consistently higher in the spleen and infection is usually cleared from the liver after 3-4 weeks (Pardon and Marly 1976), although here the wildtype remained associated with the liver even at 8 weeks. It is thought that the spleen protects the liver from major infection since the level of liver infection is greatly increased when the spleen is removed (Braude and Spink 1951).

In addition to the examination of CFU's within murine organs, recordings were made of individual mouse weights (g) on each day post-infection (weekdays only) as well as one day prior to infection (Figure 7.15).

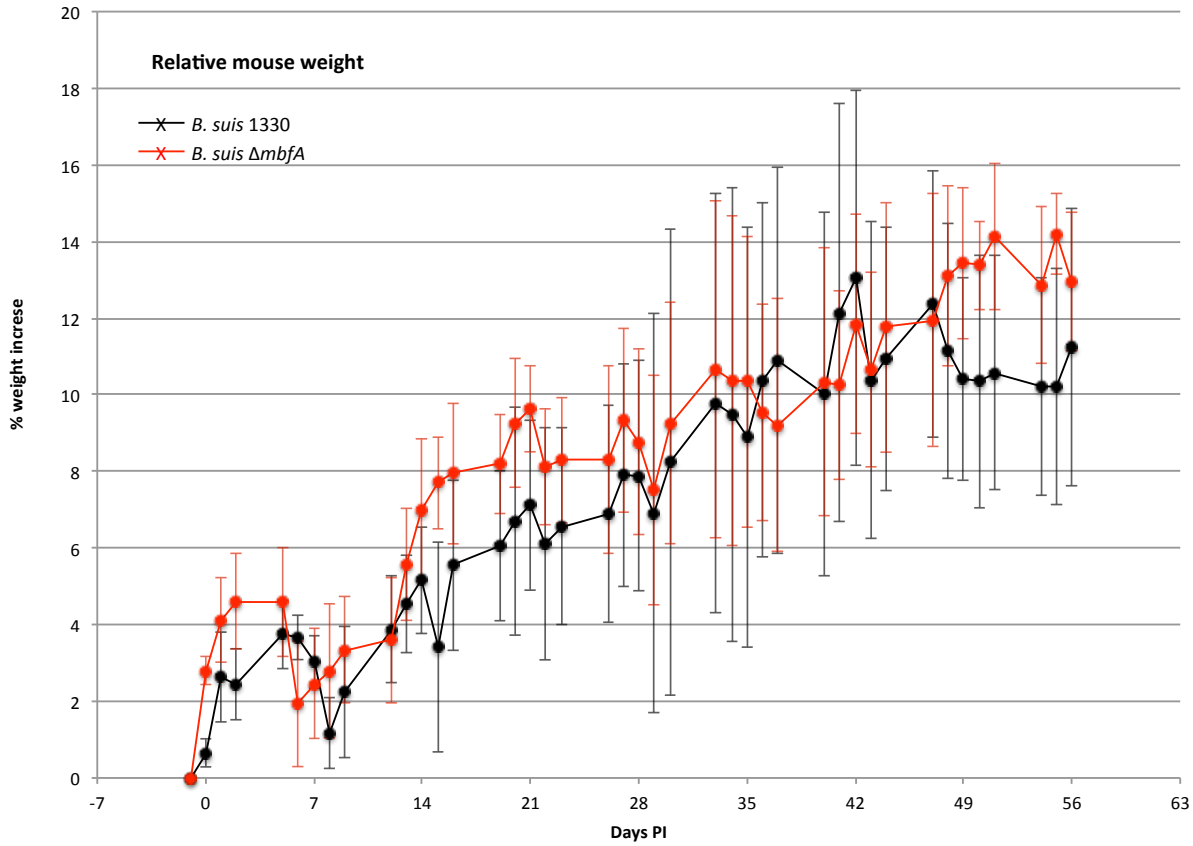

Figure 7.15: Average change in mouse weight following infection with wildtype and MbfA-deficient *B. suis.*

Average increase in whole animal weight of *B. suis* 1330 and *B. suis* Δ*mbfA* infected BALB/c mice (n = 40) over the 8 week post infection period. Five mice from each group were culled at day 7, 14, 28 and 56. Results are expressed as means ± one standard deviation.

The average animal weight increase for *B. suis* 1330 and *B. suis* Δ*mbfA* infected BALB/c mice was not significantly different, despite the significantly decreased recovery of *B. suis* Δ*mbfA* from infected mice. This result represents the chronic and non-lethal model that the mouse represents in terms of Brucellosis disease. Infection with wild type, virulent *B. suis* did not cause weight loss or significant decreasing in weight increase over time. The average absolute weight of mice infected with *B. suis* 1330 one day prior to infection was 19.57 g whilst mice infected with *B. suis* Δ*mbfA* was 19.70 g, with the average weight after 8 weeks post infection being 21.84 g for *B.*

suis 1330 and 22.64 g for *B. suis* Δ*mbfA* (Figure 7.16).

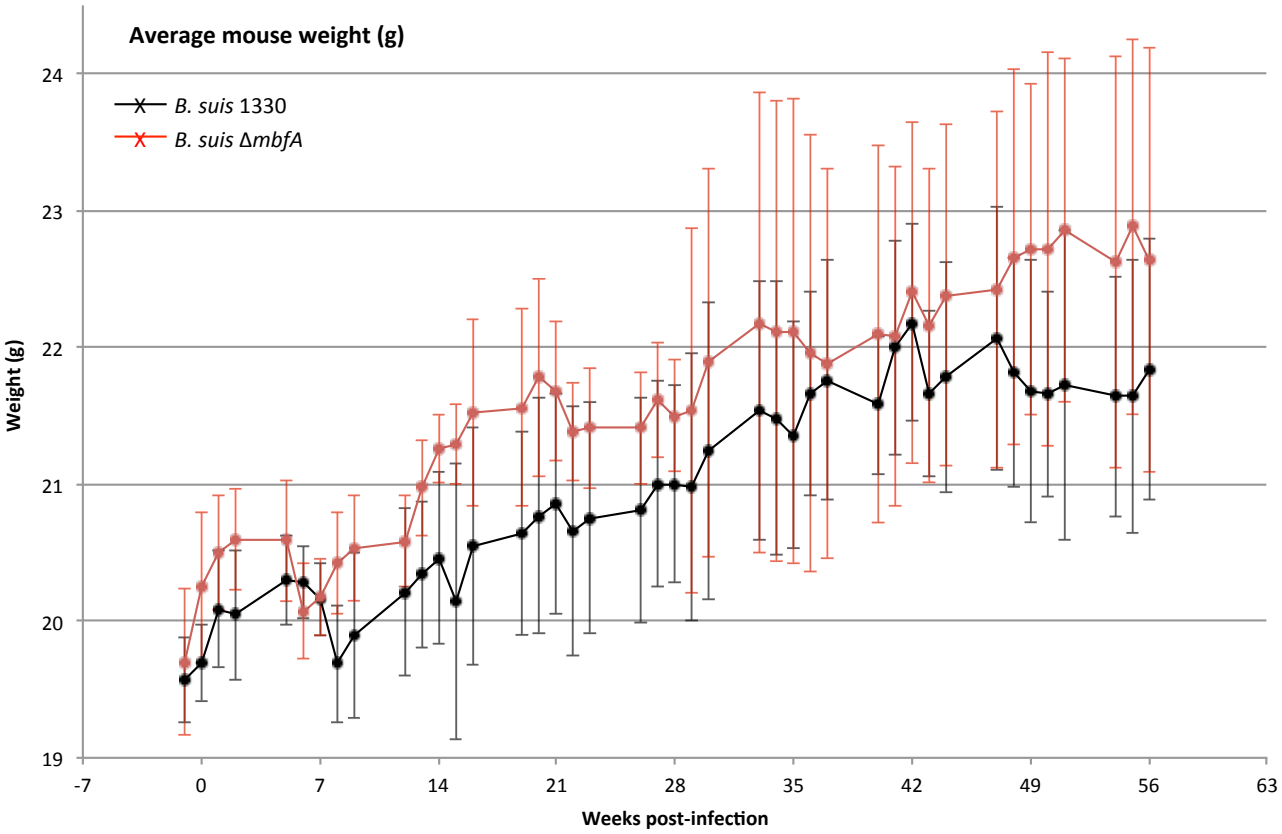

Figure 7.16: Average absolute mouse weight following infection with wildtype and MbfA-deficient *B. suis*.

Average increase in absolute whole animal weight of *B. suis* 1330 and *B. suis* Δ*mbfA* infected BALB/c mice (n = 40) over the 8 week post infection period. Five mice from each group were culled at day 7, 14, 28 and 56. Results are expressed as means ± one standard deviation.

Absolute average animal weights reflect those of changes in animals weights, with a steady increase over the 8-week infection period. However, it is of note that on average, *B. suis* Δ*mbfA* infected mice was consistently heavier than *B. suis* 1330 infected mice. This observation indicates that, despite randomisation of mice receiving inocula, heavier mice were inoculated with *B. suis* Δ*mbfA*, rather than any effect of the *mbfA* mutation on body weight.

Supplementary to the recording of whole animal weights, the animal's general condition was examined for indications of distress and clinical signs indicative of disease. A score was assigned to each animal each day post-infection; if observations indicated that the animal was succumbing to the infection, actions could then be taken to cull the

animal at a humane end-point. During this study, 16 animals displayed minor clinical signs (visible starring around the neck) for a maximum of 1 day only during the entire course of the infection. These minor symptoms further support the chronic and non-lethal infection that Brucellosis presents in the murine model.

Taken together, the data collected from whole animal weights, clinical signs, organ weights and CFU's per organ, support the hypothesis that *mbfA* is required for optimal virulence of *B. suis* in the murine model.

7.8: Discussion

In summary, experiments reported in this chapter included the creation of *B. suis* 1330 and *B. melitensis* 16M *mbfA* deletion mutants, *in vitro* growth assays, macrophage survival assays and *in vivo* virulence assays. Together these experiments have provided evidence that *mbfA* is required for efficient intracellular survival of *B. suis* 1330 in macrophages and for full virulence of this organism in mice.

The creation of *B. suis* 1330 and *B. melitensis* 16M *mbfA* deletion mutants was achieved via the delivery of a suicide plasmid harboring an in frame deletion of the *mbfA* gene, substituted with a kanamycin resistance cassette. Targeted PCR and Sanger sequencing techniques were then used to confirm the genotypes of the deletion mutants. Upon confirmation of the *B. suis* 1330 and *B. melitensis* 16M Δ*mbfA* strains, *in vitro* characterisation of the resistance to hydrogen peroxide and ferrous sulphate was conducted through comparison of growth curves. The deletion of *mbfA* from the *B. suis* genome resulted in significant reduction in culture optical density upon exposure to H_2O_2 or $FeSO_4$ when compared to the wildtype strain or a complemented mutant strain. In contrast, deletion of *mbfA* from the *B. melitensis* genome did not result in any attenuation in growth compared to the wildtype strain highlighting the cryptic nature of *mbfA* in *B. melitensis* strains. Complementation of either wildtype *B. melitensis* (cryptic *mbfA*) or the engineered mutant (Δ*mbfA*) with the functional *mbfA* from *B. suis* resulted in significantly increased resistance to both to H_2O_2 and $FeSO_4$. It was observed that *B. melitensis* strains are slower growing in broth culture, but are more resistant to ferrous iron related oxidative stress than *mbfA*-encoding *B. suis*. To support these observations, immuno-detection of MbfA was conducted; MbfA was detected with exposure to H_2O_2 or $FeSO_4$ in strains with functional MbfA, but was absent when H_2O_2 or $FeSO_4$ was removed or when *mbfA* was deleted or cryptic.

To determine if *mbfA* contributed to the intracellular survival within macrophages of *Brucella* spp., enumerations of viable *Brucella* cells over 48 h were made in J774.A1 (NRAMP1$^-$) as well as RAW 264.7 (NRAMP1$^{+/-}$) murine macrophages. In summary, deletion of *mbfA* from *B. suis* resulted in significant attenuation of intracellular survival in NRAMP1$^-$ macrophages (J774.A1/RAW 264.7 - R21). Despite the natural lack of *mbfA* expression in *B. melitensis* intracellular growth was observed but was increased when a functional copy of *mbfA* was supplied. When enumerations of viable cells were

conducted from NRAMP1$^+$ macrophage (RAW 264.7 - R37), a greater attenuation in intracellular growth was observed with the deletion of *mbfA* in *B. suis* compared to NRAMP1$^-$ macrophages. This experiment demonstrated that the deletion of *mbfA* from *B. suis* results in an attenuation of survival and replication within macrophages. The observation that *B. suis* Δ*mbfA* yields significantly fewer CFU at 24 and 48 h post-infection in both NRAMP1$^{+/-}$ macrophages (with significantly fewer in NRAMP1$^+$ macrophages) suggests that MbfA protects *B. suis* 1330 from succumbing to the oxidative stress encountered within the eBCV. Interestingly, the presence of NRAMP1 is more detrimental to cellular survival in an *mbfA* mutant than when NRAMP1 is absent. This is consistent with the suggestion that NRAMP1 and MbfA have antagonistic roles in moving iron out of, and into, the lumen of the eBCV. This finding suggests that nutritional immunity plays a large role in *Brucella* survival within the phagosome than previously suggested: in the absence of NRAMP1, H_2O_2-quenching iron is not exported from the phagosome lumen and can therefore disproportionate hydrogen peroxide, rendering the phagosome less bactericidal. An *mbfA* mutant strain is therefore able to replicate to higher numbers in NRAMP1$^-$ than in an NRAMP1-expressing macrophages since luminal iron levels are higher which in part compensates for lack of MbfA activity. The ability of MbfA to lower H_2O_2 exposure within the eBCV of macrophage by countering the action of NRAMP1, correlates with the reduced virulence observed for *B. suis* Δ*mbfA* in the murine model. Experimental infection of BALB/c mice with *B. suis* Δ*mbfA* resulted in a significant reduction of viable bacteria isolated from spleen, liver and blood over time in comparison to wildtype *B. suis*. Notably *mbfA* deficient *B. suis* were eliminated from the blood by day 14 post infection compared to day 56 for wildtype *B. suis*, in addition to a reduced splenic colonization throughout the infection period. This highlights the reduced ability *mbfA* deficient *B. suis* has in surviving intracellularly within splenic macrophages, resulting in fewer extracellular *Brucella* entering the blood.

The murine infection model for Brucellosis research represents a good model of infection compared to that seen in the natural host (pig/goat/cow). However, there are differences between experimental infection of mice and disease observed in animal hosts and humans, the most notable being that *Brucella* are not significantly shed during infection of mice – reducing horizontal transmission (Grillo et al. 2012).

Consideration of the temporal and spatial recruitment of host proteins to the BCV during *Brucella* intracellular life identifies rationales for the requirement of MbfA. After phagocytosis of *Brucella* by the macrophage, *Brucella* shapes the BCV from a phagosomal-like vesicle into an autophagosome/ER-like vesicle where replication ultimately takes place. The BCV interacts with the early endosome characterised by the presence of early endosomal markers (Pizarro-Cerda et al. 1998) late endosome (Starr et al. 2008) and ER, whilst preventing lysosome fusion (Pizarro-Cerda et al. 1998).

During initial stages of BCV transit, internalised *Brucella* experience the respiratory burst generated by NADPH phagocyte oxidase (PhoX) as well as exposure to NO generated by inducible nitric oxide synthase (iNOS) which produce an antimicrobial activity (Jiang et al. 1993) (Figure 7.17). Evidence that *Brucella* experience the respiratory burst was determined by treating macrophages with methylene blue (enhances respiratory burst activity). Treated cells experienced increased intracellular killing but was reversible through the addition of catalase or superoxide dismutase (Jiang et al. 1993). Many intracellular bacteria experience early exposure (minutes to hours post infection) to the respiratory burst and NO. In experimental *Salmonella* infections, the respiratory burst and NO radical production contribute significantly to the anti-*Salmonella* activity of the macrophage (Mastroeni et al. 2000, Vazquez-Torres et al. 2000), whilst early recruitment of iNOS is also observed in macrophages infected with *Mycobacterium* spp. (Miller et al. 2004). But, NADPH oxidase-dependent killing of *Salmonella* was limited to the initial phase of infection, whereas RNS, generated by iNOS, exhibited an extended role in limiting residual bacterial replication through a sustained bacteriostatic effect (Vazquez-Torres et al. 2000). The co-localisation of NADPH oxidase and iNOS in the early phagosome (eBCV) enables interaction between ROS and RNS which play a synergistic role in bacterial killing as NO can potentiate H_2O_2 killing of bacteria (Pacelli et al. 1995). It is of notable interest that *Burkholderia cenocepacia,* which do not encode *mbfA*, may combat this synergistic effect by delaying the association of NADPH oxidase by approx. 6 h within the *B. cenocepacia* containing vacuole (BcCV) (Keith et al. 2009).

The NRAMP1 protein is expressed in the membranes of late endosomes of macrophages (Blackwell et al. 2000, Forbes and Gros 2001) (Figure 7.17) and is thought to function by removing iron into the cytoplasm, conferring resistance to intracellular pathogens including *Salmonella typhimurium* in mice (Fritsche et al. 2012)

by reducing available iron for growth. *Nramp1* expression was first associated with decreased phagosomal iron content by Gomes and Appelberg; 1998 who determined that this activity influenced the growth of *Mycobacterium avium* within the macrophage through starvation of the pathogen of iron (Gomes and Appelberg 1998), additionally *Nramp1* expression resulted in decreased cellular iron loads (Atkinson and Barton 1998). Since *Brucella* does not replicate in the eBCV, any lack of iron imposed by NRAMP1 is unlikely to exert any starvation effect, instead the removal of iron is presumed to favour the preservation of H_2O_2.

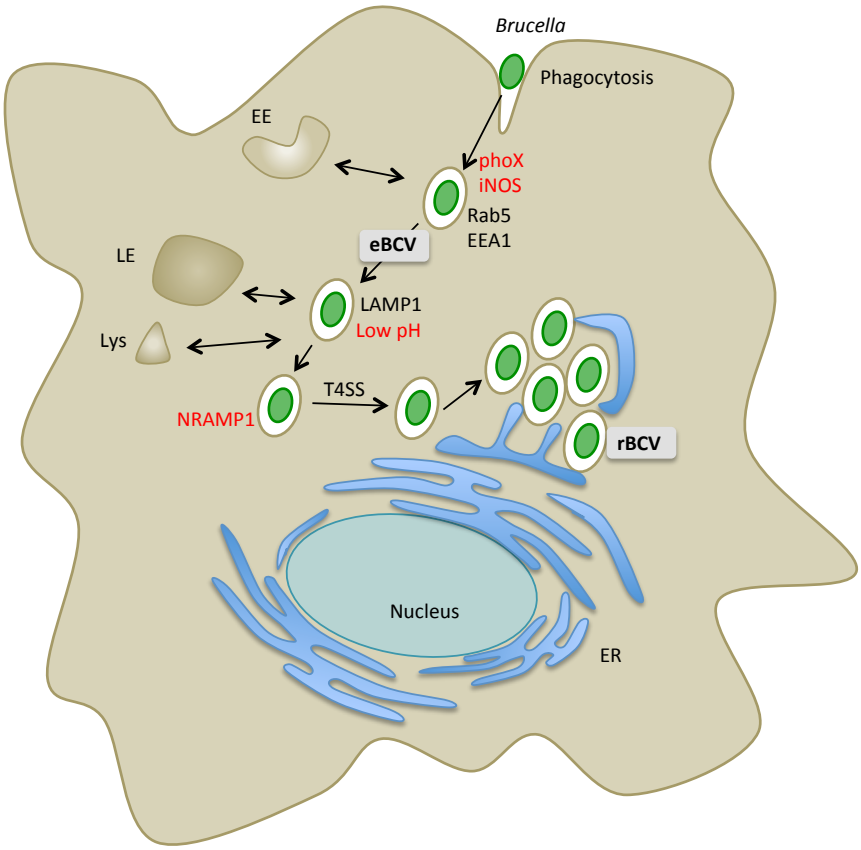

Figure 7.17: Schematic representation of *Brucella* intracellular trafficking in mammalian cells

Brucella spp. reside within a vacuole termed the *Brucella* containing vacuole (BCV) which traffics along the endocytic pathway interacting with early endosome (EE), late endosomes (LE) and lysosomes (Lys). Interaction with the lysosome provides cues for induction of the VirB T4SS, from which VirB type IV effector proteins redirect the BCV to fuse with the endoplasmic reticulum (ER) creating the rBCV.

The distinct separation of the recruitment of NADPH oxidase and iNOS before NRAMP1 to the BCV may play an important role in the survival of *Brucella*. MbfA exporting iron in response to Irr-sensed redox stress, as generated by NADPH oxidase, allows degradation of peroxide in the BCV lumen, thus enhancing catalase mediated disproportionation of H_2O_2 in the *Brucella* cytoplasm, which in the presence of iNOS-generated NO may be inhibited. As the BCV matures and NRAMP1 is recruited, MbfA-dependent iron release will reduce peroxide levels and raise luminal iron levels such that the withdrawal of iron by NRAMP1 would be less effective in preserving peroxide. Additionally, iron released by MbfA into the lumen of the BCV could be later reabsorbed by *Brucella* through induction of FtrABCD, once in the rBCV, when peroxide levels are diminished, enabling growth to progress.

Despite a proposed rationale for the requirement of MbfA in *Brucella* spp. it is clear that *B. melitensis* strains are *mbfA* deficient, but remain virulent. One explanation for the maintenance of virulence of *B. melitensis* strains is that they transit to the ER faster than other *Brucella* spp.. Experimental infection of JEG-3 trophoblasts with *B. abortus* and *B. suis* showed residence within single membrane, acidic, LAMP1 inclusions 24 h post infection, whilst *B. melitensis* was located within BCVs positive for calnexin (ER marker) (Salcedo et al. 2013). These observations suggest that *B. melitensis* may be able to move through the phagosomal pathway at an accelerated rate compared to other *Brucella* spp. reaching the replicative niche within the ER sooner. In addition, *B. abortus* replication rate was slower than that of *B. melitensis* – suggesting that the ER-derived BCVs are a more suited niche for *Brucella* intracellular replication (Salcedo et al. 2013). These observations are supported by the experiments displayed in Figure 7.9, where *B. melitensis* 16M was observed to be more infectious in J774.A1 macrophages where the bacteria replicated to higher numbers within macrophage than their *B. suis* 1330 and *B. suis* Δ*mbfA* counterparts.

The lack of *mbfA* expression in *B. melitensis* as well as the accelerated transit to the ER-associated replicative niche compared to *B. abortus* and *B. suis* points towards a different strategy for redox stress avoidance in *B. melitensis*. A quicker transit through the eBCV stages within the macrophage allows for a reduced exposure to NADPH oxidase, iNOS and NRAMP1, preventing loss of cellular viability. Additionally, the maintenance of cellular iron (lack of export of MbfA) prevents the requirement of iron

acquisition before cellular proliferation enabling faster initiation of replication. The loss of *mbfA* does not present a burden to *B. melitensis* strains, which is the most infectious of the *Brucella* species, possibly because this species possesses other mechanisms for countering the redox-stress imposed by macrophages.

Examination of literature detailing the characterization of redox stress relief and iron uptake mechanisms allows additional context to be given to role that MbfA plays within *Brucella* and the BCV. *Brucella* spp. encode a single periplasmic catalase, a homolog of the *katE* gene of *E. coli* (haem catalase) (Sha et al. 1994), which is dispensable. Although the catalase protects against hydrogen peroxide supplied *in vitro*, a *B. melitensis* deletion mutant retains full virulence in the natural host (Gee et al. 2004). As NO is expected to inhibit haem catalases during *Brucella* localization in the BCV, rendering it non-functional, deleting the gene may have no impact on virulence. However, *in vitro* experiments, conducted in the absence of NO, show that catalase functions as expected. In addition, the examination of a *katE* and *ahpC* double mutant in *B. abortus* (Steele et al. 2010) suggests that *B. abortus* can degrade hydrogen peroxide without the expression of the major respiratory antioxidants, catalase and alkyl hydroperoxidase. This therefore suggests that additional enzymes are present within *Brucella* spp. that are able to degrade hydrogen peroxide, thus providing speculative evidence for MbfA activity.

In addition to catalase, *Brucella* spp. express two superoxide dismutase, a cytoplasmic Mn-SOD (*sodA*) (Sriranganathan et al. 1991) as well as, a periplasmic Cu-Zn SOD (*sodC*) (Stabel et al. 1994). Both SodA and SodC were identified independently as being required for intracellular survival of *B. abortus* during early stages of infection in macrophages (Gee et al. 2005) (Martin et al. 2012), but in isolation were not required for full virulence *in vivo* (Latimer et al. 1992, Tatum et al. 1992). This suggests that redundancy between the two SODs is experienced, masking the effect of a single deletion *in vivo*, but also that SOD is required primarily during the early stages of BCV inhabitation due to the temporal recruitment of NADPH oxidase to the BCV; once within the rBCV exposure to redox stress is limited.

Chapter 8: Discussion

8.1: Summary of experimental observations

In summary, the experimental findings of this thesis detail the role that a novel iron transport system, MbfA, plays in *Brucella* pathogenicity and intracellular survival.

Bioinformatical analysis of the *mbfA* sequence from *Brucella suis* 1330 identified that the protein was organized into an N-terminal erythrin domain and a C-terminal, membrane embedded (vacuolar iron transporter) Vit1 domain. Examination of additional bacteria phyla for examples of MbfA-like sequences revealed that four distinct variants of the MbfA protein were encoded by both prokarya and eukarya, and that the five transmembrane helix organization of the VIT domain was extensively conserved. A closer examination of the *mbfA* sequence from *Brucella* spp. identified that *B. melitensis* strains had acquired one or, in some cases, two SNPs, introducing stop codons to the sequence rendering *mbfA* in these strains cryptic. Analysis of the upstream region of DNA from the *mbfA* start codon showed high sequence similarity to the iron control element (ICE) box, allowing predictions to conditions in which *mbfA* is expressed in *Brucella*.

The first experimental steps taken were to clone the *mbfA* gene from *B. melitensis* 16M into a high copy number plasmid for further manipulations. Due to the presence of interfering SNPs in the *B. melitensis mbfA* sequence, site directed mutagenesis (SDM) was used to revert the mutations regenerating the *mbfA* sequence found in *B. suis*. The *B. suis* variant of the *mbfA* gene was cloned into controllable expression vectors (rhamnose, arabinose and IPTG) to enable the observation of phenotypes in *E. coli* strains. Additionally, suicide and complementation vectors were generated to enable the deletion of *mbfA* from the *B. suis* and *B. melitensis* genomes by replacement with a kanamycin cassette. The soluble erythrin domain was cloned into a T7 RNA polymerase promoter containing plasmid to enable the overexpression and subsequent extraction of recombinant protein.

Creation of the pET plasmid harboring the erythrin domain from *mbfA* enabled the generation of sufficient quantities of recombinant erythrin protein to facilitate its purification by chromatographic methods. The incorporation of a C-terminal His-tag enabled initial purification of erythrin by nickel affinity chromatography, which was

followed by anion exchange chromatography to yield high concentrations and homogeneity of erythrin. The purified homogenous erythrin protein allowed further experiment, including: the generation of polyclonal antibodies in rabbits, facilitating the immune-detection of MbfA in *E. coli* and *Brucella*. Also, the formation of apo-erythrin (metal free) through the chelation of bound metals, which were subsequently removed by dialysis, enabling the recreation of a di-iron form of erythrin through the titration of ferrous iron. The di-iron centre of the erythrin was first characterized by ICP-OES and ESI-MS spectroscopy techniques, which confirmed the association of two iron atoms per protein monomer. This in turn allowed the examination of the reduction (sodium dithionite) and oxidation (hydrogen peroxide) of the di-iron centre spectroscopically at 360-480 nm. Thermal shift assays indicated that, in addition to iron, zinc, manganese and cadmium were also able to bind the di-iron binding site. This knowledge facilitated directed attempts to generate protein crystals; crystallization trials were conducted on iron, manganese and zinc centred erythrin.

The first experimentation conducted with *B. suis mbfA* was with the controllable expression vector $pBAD_{rham}$ transformed in *E. coli*. Phenotypes were observed, consistent with the export of iron through the expression of *mbfA,* in an *E. coli* strain deficient in all iron acquisition mechanisms (*E. coli* JC28), an *E. coli fur* mutant (*E. coli* H1941) and an *E. coli* catalase/alkyl hydroperoxidase mutant (*E. coli* LC106). This supported the notion that MbfA affords *Brucella* spp. increased intracellular survival capacity through exporting iron to counter redox stress. To determine whether *mbfA* expression influenced the intracellular iron content of the *E. coli* strains, resistance to streptonigrin was used as a probe. Streptonigrin is an iron dependent antibiotic, thus, increased resistance to streptonigrin upon *mbfA* expression would represent a removal of reactive intracellular iron. In all examined *E. coli* strains, expression of *mbfA* increased resistance to streptonigrin highlighting the proposed function of MbfA.

To quantitatively measure the efflux of iron by MbfA, a protocol was developed to utilize the sensitivity of detection of the radioisotope ^{55}Fe by liquid scintillation counting. The presence of ^{55}Fe in cellular supernatants collected after expression of *mbfA* from wildtype *E. coli* represented effluxed intracellular iron by MbfA. The rate of iron efflux of iron was observed to be biochemically controlled by the presence of hydrogen peroxide. During aerobic respiration H_2O_2 is generated which then facilitates iron export by MbfA, however, when additional H_2O_2 was introduced the iron export

rate increased, conversely, when an additional catalase was added, consuming H_2O_2, the rate of iron export reduced. This was further demonstrated by culturing *E. coli* anaerobically, which prevented the generation of hydrogen peroxide thus eliminating iron export. This series of experiments highlighted the combined roles that the erythrin and Vit1 domains play in MbfA, facilitating iron export. Results suggest that an electron from intracellular ferrous iron is likely removed to facilitate the reduction of hydrogen peroxide at the di-iron centre of the erythrin domain; the oxidized iron atom is then translocated across the membrane. In the absence of hydrogen peroxide, the electron flow from the iron waiting to be exported is interrupted and export is prevented. This biochemical control ensures that the scares iron resources of the cell are maintained in the absence of redox stress and that export is only initiated when damaging H_2O_2 is present.

To investigate this system in more detail, the erythrin and Vit1 domains of MbfA were separated from one another and expressed in isolation. No iron export was observed in either case, supporting the evidence acquired previously that both domains are required for iron transport. Despite this, the vacuolar iron transport system (VIT1) of *A. thaliana* and *P. falciparum* are reported, as well as hypothetically, type II *mbfA* like proteins, to facilitate iron transport whilst lacking an erythrin domain. To examine the mechanism of iron transport by VIT1, *A. thaliana VIT1* was codon optimized and cloned into an inducible vector, enabling expression in *E. coli,* and thus quantitation of ^{55}Fe export. No biochemical control of VIT1 was observed as iron was exported constitutively during all manipulations of hydrogen peroxide concentrations. The proton motive force was found to facilitate the translocation of iron by this system as titration of the protonophore CCCP greatly reduced iron export, whilst little impacting MbfA activity. Colorimetric quantification with the ferrous iron specific chelator ferrozine enabled determination of the redox state of the exported iron; ferric iron was exported by MbfA but ferrous iron by VIT1, reflecting the involvement of an oxidation step in export of iron by the MbfA system.

From initial phenotypic examinations of *mbfA* expression it was observed that MbfA was able to protect against hydrogen peroxide induced redox stress. A colourmetric Amplex Red hydrogen peroxide assay was used to monitor the rapid disproportionation of H_2O_2 by wildtype *E. coli* and lack of such activity in a catalase/alkyl hydroperoxidase deficient strain (*E. coli* LC106). This formed the experimental basis to

examine the ability of MbfA to facilitate H_2O_2 degradation. Expression of *mbfA* in *E. coli* LC106 resulted in H_2O_2 degradation, but the relative contributions afforded by reduction at the erythrin domain and the degradation of extracellular peroxide by exported iron were unknown. To resolve this, the extracellular ferric iron chelator desferrioxamine was added to quench extracellular iron allowing quantitation of hydrogen peroxide reduction at the erythrin domain to be calculated; up to 80% of hydrogen peroxide disproportionation was facilitated by exported iron Fenton reactions.

With a detailed understanding gained of the mechanism that MbfA utilizes to export iron and afford resistance to hydrogen peroxide, the role that nitric oxide plays within the phagosome of the macrophage in inhibiting bacterial catalase/hydroperoxidase was investigated. In isolation, addition of either H_2O_2 or NO presented with no growth reduction for *E. coli* MG1655, however when added together a synergistic killing effect was observed possibly through the inhibition of catalase/hydroperoxidase; this effect was markedly reduced with the expression of MbfA. This observation demonstrates a mechanism for intracellular survival within the phagosome as NO inhibition of catalase can be circumvented by expression of *mbfA*, reducing hydrogen peroxide that would otherwise accumulate and cause cellular damage.

Although export of iron by MbfA is unique in terms of mechanism and biochemical control, it is of acknowledgement that recent work conducted with the Gram-positive bacteria *Bacillus subtilis* and *Listeria monocytogenes* has identified an ATPase system specific for export of iron (Guan et al. 2015 and Pi et al. 2016). The *B. subtilis* PfeT protein functions as a ferrous iron efflux pump that protects the cell against iron toxicity as measured by resistance to the iron dependent antibiotic, streptonigrin. This evidence was supported by the examination of an engineered *pfeT* deletion mutant, which accumulated elevated levels of intracellular iron as determined by ICP-OES (Guan et al. 2015). Similarly, the *L. monocytogenes* FrvA protein was shown *in vitro* to function as a divalent cation specific ATPase that was induced with exposure to ferrous iron and that complementation of the *B. subtilis pfeT* deletion strain (Guan et al. 2015) with *frvA* increased resistance to iron (Pi et al. 2016).

The first experimentation directly upon *Brucella* was to generate *mbfA* deletion mutants within *B. suis* 1330 and *B. melitensis* 16M; this was conducted by a targeted approach removing the *mbfA* gene and replacing it with a kanamycin resistance cassette. The resistance of wildtype and *mbfA* deficient *Brucella* spp. to ferrous sulphate and hydrogen peroxide was assessed through examination of growth curves and this revealed that *B. suis* Δ*mbfA* is more susceptible to redox mediated killing than wildtype. However, Δ*mbfA B. melitensis* grew equivalently to the wildtype due to the naturally cryptic *mbfA* encoded by this strain. Complementation of *B. melitensis* with a functional copy of *mbfA* from *B. suis* increased resistance to redox stress suggesting that the loss of MbfA function in *B. melitensis* is deleterious under the conditions employed. Next, the intracellular survival of the *Brucella* stains was examined within NRAMP1$^-$ (J774.A1/RAW264-R21) and NRAMP1$^+$ (RAW264-R37) murine macrophages. Deletion of *mbfA* from *B. suis* resulted in significant attenuation of intracellular survival in all examined macrophages, but greatest attenuation was observed for the deletion of *mbfA* in *B. suis* in NRAMP1$^+$ macrophages. In support of this, experimental infection of BALB/c mice with *B. suis* Δ*mbfA* resulted in a significant reduction of viable bacteria isolated from spleen, liver and blood over time in comparison to wildtype *B. suis*.

8.2: MbfA promotes *Brucella* intracellular survival and is required for virulence

Many bacterial species, including *Brucella*, have an absolute requirement for iron; its acquisition during host colonization is paramount in enabling virulence and propagation. *Brucella* spp. are able to acquire iron from multiple sources, including: ferric iron – acquisition mediated by the siderophores 2,3-dihydroxybenzoic acid (DHBA) and Brucebactin, as well as ferric chelates; ferrous iron - acquisition via the high affinity FtrABCD system; and haem, via BhuATUV. *In vivo* studies have elucidated that the high-affinity ferrous iron and haem transport systems which are fully expressed during stationary phase during location in the rBCV are absolutely required for virulence during chronic infection; deletion of *ftrA* (periplasmic ferrous iron binding protein) or *bhuA* (OM haem transporter) in *Brucella abortus* result in attenuation in macrophage and mouse models (Paulley et al. 2007, Elhassanny et al. 2013). However, ferric iron acquisition systems are dispensable as siderophore-iron import systems are not required for replication in macrophages or for chronic infection of BALB/c mice (Bellaire et al. 1999), as was demonstrated with an *entC* (isochorismate synthase – 2,3-DHBA synthesis) mutant. This lack of requirement for ferric-iron import can be attributed to the niche that *Brucella* species occupy within the host; the reduced nature of the intracellular environment and the low pH of the BCV (Gonzalez Carrero et al. 2002) would be expected to favour the ferrous iron oxidation state over the ferric state, rendering ferric uptakes systems redundant.

Iron homeostasis is regulated by the iron response regulator (Irr) in Rhizobiales of the alpha-proteobacteria including *Brucella* spp.; Irr promotes the transcription of iron-uptake genes in response to low iron concentrations, and represses their expression in response to high intracellular iron and oxidative stress (Yang et al. 2006). During iron replete conditions, expression of iron storage (*bfr*) and export (*mbfA*) genes is stimulated to maintain iron concentrations within tight parameters (Jaggavarapu and O'Brian 2014). The ability for *Brucella* spp. to not only store iron, but also to export excess free intracellular iron, represents a novel mechanism for maintaining iron homeostasis and combating redox stress. The export of iron by MbfA allows rapid counteraction of oxidative stress imparted though the processes such as the respiratory burst of the macrophage, thus promoting survival. This mechanism enables utilisation of intracellular iron to directly combat the toxicity exerted by H_2O_2 in the external environment, increasing likelihood of survival under redox-stress conditions.

The results described in this thesis have enabled a new hypothesis for the function of MbfA in *Brucella* spp. to be established. MbfA acts to export intracellular iron from the *Brucella* cell in a hydrogen peroxide dependent manner. The MbfA-mediated export of iron is controlled both genetically and biochemically. The genetic control is through the de-repression of *mbfA* expression by Irr, which is degraded when cellular iron concentrations are high or upon exposure to hydrogen peroxide (Yang et al. 2006); the biochemical control is achieved as iron export is driven by hydrogen peroxide reduction at the erythrin domain (Chapter 6.7). These two levels of control would be expected to allow *Brucella* to exert great control over the rate at which iron, an essential micronutrient, is released from the cell.

Iron export by MbfA involves oxidation of intracellular ferrous iron to the ferric form; this redox reaction is believed to involve the release of an electron from Fe^{2+} (during export to the periplasm) which is then used for the reduction of hydrogen peroxide to water. This mechanism would be expected to lower the concentration of both total intracellular iron and free cytosolic iron, which has the propensity to initiate Fenton chemistry generating damaging radicals, when hydrogen peroxide is present. MbfA's action of exporting iron further aids redox-stress resistance during the intracellular survival of *B. suis* in macrophages through several additional means. Exporting iron into the eBCV lumen acts as a direct counter to the function of NRAMP1. NRAMP1 removes divalent metal cations from the phagosomal lumen; the reason for this activity is reported to be to generate conditions of nutritional immunity, restricting invading bacteria of essential nutrients. However, as suggested here, the removal of redox active metals would also enhance the preservation of hydrogen peroxide within the luminal space. Generation of hydrogen peroxide in the phagosome (and related intracellular bodies such as the eBCV) is one of the primary mechanisms of attack against the invading bacterium. As hydrogen peroxide is non-polar it diffuses across all biological membranes, therefore its synthesis cannot lead to high concentrations inside cells which are found at 2-50 μM in phagosomes (Slauch 2011), a concentration which is below that required for bactericidal action (*E. coli* 15 mM) (Pericone et al. 2000). Such sub-lethal concentrations are maximized through the release of nitric oxide, which acts as a potentiator of redox stress through two means: firstly, it stalls haem catalases/peroxidases, preventing the degradation of hydrogen peroxide; secondly, it reacts with hydrogen peroxide to create toxic peroxynitrite. The removal of iron by MbfA can be considered to counter both of these macrophage mechanisms. Iron

removed from *Brucella* would limit free-radical generation by hydrogen peroxide in proximity to sensitive cellular components (e.g. DNA), it would also re-populate the phagosomal (or eBCV) luminal space with iron, driving disproportionation of hydrogen peroxide (Chapter 6.12). In summary, the H_2O_2-driven export of iron into the phagosomal/eBCV lumen by MbfA would be expected to directly counter the respiratory burst activities of the macrophage by:

- Reducing intracellular H_2O_2,
- Lowering intracellular iron levels,
- Counteracting the action of NRAMP1 by raising extracellular iron levels,
- Promoting the disproportionation of hydrogen peroxide outside of the cell, preventing ingress into the cell, and
- Compensating for the inhibition of catalases/peroxidase by NO.

The above mechanism represents a novel approach for thwarting the innate-immune system by a pathogen. It is paramount to the successfulness of *Brucella* spp. pathogenesis that cellular viability is maintained as it transits through its intracellular niches in the host macrophage (phagolysosome to ER). It is evident from *in vitro* and *in vivo* experimentation that the presence of *mbfA* in *Brucella suis* 1330 confers significant protection to macrophage-associated killing and survival in the host, allowing greater numbers of bacteria to disseminate and maintain infection.

8.3: MbfA contribution to *Brucella* spp. pathogenesis.

The primary requisite of a bacterial organism is to propagate. Although *Brucella* is able to survive and replicate within macrophages, to maximize this propagation, infection of the greatest numbers of hosts is desirable, therefore an ability to disseminate to new hosts is required. In the case of *Brucella* infection, despite significant symptoms, pathogenesis of Man is limited and appears to be a "dead-end" in terms of bacterial transmission and dissemination. This is primarily due to the lack of infectivity of trophoblasts of the placenta in pregnant individuals and hence ineffective mechanisms of transmission from host to host (the major mechanism of spread in animals is by contact with infected birthing fluids and tissues).

Brucella utilizes MbfA to survive the 'nutritional immunity' and redox stress that are imparted as a consequence of inhabiting the phagolysosome (eBCV) of a macrophage. Since *Brucella* does not replicate in the eBCV, any lack of iron imposed by NRAMP1 is

unlikely to exert any starvation effect. The type-4 secretion system (T4SS), a major virulence factor of *Brucella*, allows release of *Brucella* from the endosomal niche and establishment of an ER niche (the rBCV). During infection of human or non-pregnant ruminants, *Brucella* persists within macrophages of the spleen and represents a chronic infectious state (Hanot Mambre et al. 2015). It is only when a ruminant host becomes pregnant that *Brucella* is able to infect the trophoblasts of the placenta. The same mechanisms of intracellular survival as used in the macrophage are required to transit *Brucella* to the ER of the trophoblast (Salcedo et al. 2013). However, within the ER of trophoblasts (the rBCV), T4SS-induced ER stress causes release of the pathogen, which are able to grow to concentrations approaching 10^{11}/g extracellularly, causing acute inflammation, resulting in abortion of the foetus. As a result, dissemination of the bacterium is promoted and transmission through the herd is most likely achieved through licking of the foetus by other animals (Byndloss and Tsolis 2016).

With this assessment of the pathogenesis of *Brucella*, the role that MbfA plays in the survival of the bacteria during early stages of infection is highlighted. Encountering oxidative stress upon engulfment by professional macrophages during host infection represents a preliminary barrier to *Brucella* establishing a replicative niche in the phagosome leading to a chronic infection; the results presented herein show that MbfA plays a role in limiting such oxidative stress and promoting the chronic infectious state.

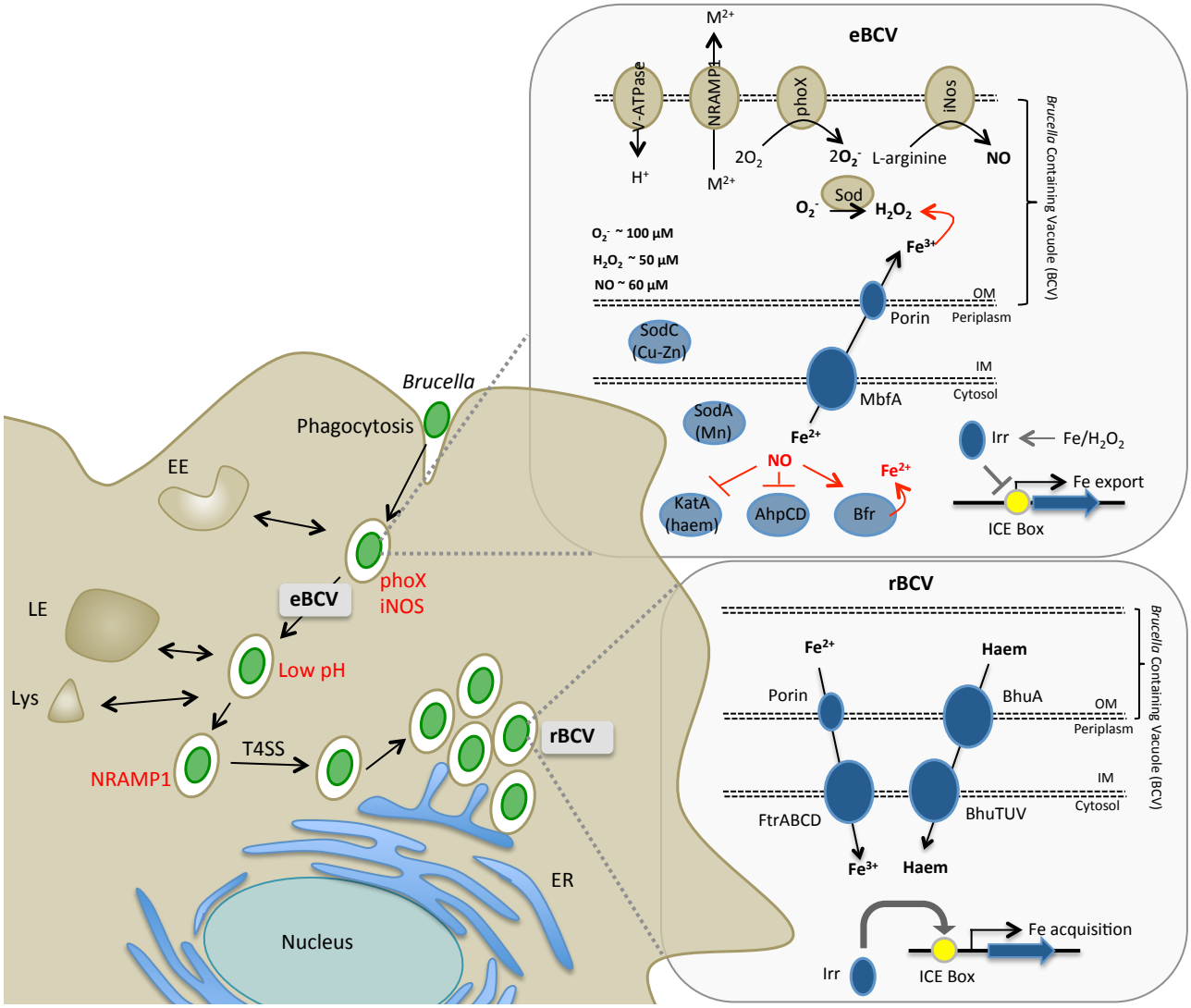

Figure 8.1: Schematic representation of *Brucella* survival in eBCV and rBCV

Brucella spp. reside within a vacuole termed the *Brucella* containing vacuole (BCV) which traffics along the endocytic pathway interacting with early endosome (EE), late endosomes (LE) and lysosomes (Lys) characterizing the eBCV, before T4SS effector proteins facilitate fusing with the endoplasmic reticulum (ER) generating the rBCV. Top insert depicts interactions between *Brucella* and the macrophage within the eBCV, which is dominated by redox stress imposed by the respiratory burst of the macrophage. MbfA acts to compensate for NO-inhibited catalase/alkylhydroperoxidase by exporting iron to catalyse peroxide disproportionation in the eBCV lumen. Bottom insert depicts switch of iron metabolism from export to import via FtrABCD and BhuATUV, upon relief of redox stress within the rBCV. Note the role of Irr in reciprocal regulation of both MbfA and FtrABCD expression in response to iron and peroxide levels.

8.4: Inclusion of MbfA in future vaccine development

There are currently several licensed live attenuated *Brucella* vaccines that are available for use in livestock. S19 and RB51 for *Brucella abortus*, Rev 1 for *Brucella melitensis* and S2 for *Brucella suis*. The effectiveness of these vaccines is dependent upon the host species and all are virulent in humans. These limitations present the requirement for the development of a vaccine that meets all ideal vaccine characteristics. The ideal *Brucella* vaccine would:

- be live and induce a strong type 1 helper immune response, would not induce antibodies, that interfere with current serological tests, and
- would be attenuated sufficiently so as not cause disease to animals or humans (Ko and Splitter 2003).

The current *B. abortus* vaccine strain, S19, is a live attenuated strain, but maintains a smooth LPS phenotype which induces antibodies that interfere with serological examinations of *Brucella* herd prevalence. Attenuation is primarily achieved through a 702 bp deletion located within the erythritol metabolism locus. Failure of *Brucella* to metabolise erythritol (an energy source found mainly within the placenta of livestock), prevents replication of *Brucella* to extremely high concentrations and thus avoids abortion of the foetus. Despite this, immunisation of pregnant cattle by the subcutaneous route can result in up to a 3.2% abortion rate (Beckett and MacDiarmid 1985) and 100% when immunised intravenously (Taylor and MacDiarmid 1949). To avoid complications with serological tests the RB51 vaccine was developed and replaced the S19 vaccination in the USA in 1996. RB51 was developed through passage of *B. abortus* 2308 on sub-inhibitory concentrations of rifampicin and selection of rough colony phenotypes. RB51 was found to be safer to administer to pregnant cows intravenously, with a 25% abortion rate, but does not protect cattle against *B. suis* infection (Olsen and Hennager 2010), and is still infectious to humans (Ashford et al. 2004).

Vaccination against *B. melitensis* is conducted with the *B. melitensis* Rev 1 vaccine, a live attenuated vaccine created through passage on streptomycin medium until resistant clones developed (Elberg and Faunce 1957). Unlike the RB51 vaccine, Rev 1 maintains the smooth LPS phenotype and hence interferes with serological diagnosis. However, the Rev 1 vaccine is effective in preventing *Brucella* infection in goats and sheep, but this strain is still virulent to humans (Blasco and Diaz 1993). In addition, the

B. suis S2 vaccine, like the Rev 1 vaccine, was developed through serial passage and retains the smooth LPS phenotype, yet it remains effective at vaccinating sheep, goats, sows and cows against *B. suis* infection.

Recent vaccine development has focused upon introducing targeted deletions to characterised virulence factors followed by testing for loss of virulence in mice. Efforts in *B. abortus* have focused on mutation of purine biosynthesis genes (*purL purD* and *purE*) (Alcantara et al. 2004), however these deletions did not sufficiently attenuate *B. abortus*. In contrast, mutation of the lipid A fatty acid transporter (*bacA*) (Ferguson et al. 2004), ferrochelatase (*hemH*) (Almiron et al. 2001) and type 4 secretion system (*virB*) (den Hartigh et al. 2004) resulted in high attenuation in mice, but efficacy in cattle is yet to be assessed. Similarly, in *B. suis*, deletion of the aromatic amino acid biosynthesis gene (*aroC*) (Foulongne et al. 2001) results in loss of virulence in mice, but efficacy is yet to be determined. In contrast, deletion of the erythritol metabolism gene *eryC* in *B. suis* (Burkhardt et al. 2005) did not reduce virulence, therefore this mutant is not sufficiently attenuated for investigation in pigs. Lastly, the development of rough *B. melitensis* mutants through the deletion of core and O-polysaccaride synthesis genes (*wbkF*, *per* and *waa*) was less effective than Rev1 in sheep.

These efforts summarise the difficulty in establishing a safe and effective vaccination against Brucellosis, and highlights the requirement for the identification of addition virulence factors which can be targeted during vaccine development. It appears that, in isolation, the deletion of a single virulence factor does not yield vaccine efficacy that is equivalent or greater than that achieved by a vaccine generated 50 years ago. It is therefore likely that a combination of targeted deletions would be required to increase the efficiency of any newly developed vaccine. With this in mind, the reduced virulence that is exhibited through infection of mice with *B. suis* Δ*mbfA* could be combined with additional mutants such as erythritol metabolism to generate a sufficiently attenuated live *Brucella* vaccine. Clearly, such a strategy would not be applicable to *B. melitensis*.

8.5: *mbfA* phylogeny - rationale for the cryptic nature of *mbfA* in *Brucella melitensis* strains

The presence of *mbfA* is not restricted to *Brucella* spp., MbfA is widely conserved across the alpha-proteobacteria, in particularly the *Rhizobiales* order. The function that MbfA plays within these bacterial species is likely to bear relationship to that indicated by this study in *Brucella* spp.. Many bacteria of the *Rhizobiales* order play an important role in the development of the root nodule of leguminous plants; a symbiotic relationship is established between the plant root and the bacteria, in which the bacterial enzyme nitrogenase fixes atmospheric nitrogen generating ammonium, which is consumed, by the plant.

During development of the plant root nodule before development of the mature root bacteroid, the bacterial species activates the plant immune system, triggering release of redox active chemicals. The expression of *mbfA* under these environmental conditions is therefore likely to aid in survival of bacteria in the mature root bacteroid through the same iron export mechanism as described for *Brucella*. Not only do many alpha-proteobacteria encounter conditions of oxidative stress (although many bacteria encounter oxidative stress but do not encode *mbfA*), the intracellular niches that these bacteria inhabit are characterised by very small luminal spaces. This spatial restriction allows for maximum benefit of redox detoxification by export of iron, as exported iron is not diluted throughout a large luminal space.

A search of MbfA-like amino acid sequences across both the Prokarya and Eukarya identified four distinct variants of MbfA-like sequences, denoted Ia, Ib, Ic and II (Chapter 3.2). Variant Ib denotes the abundant MbfA variant present in the alpha-proteobacteria consisting of an N-terminal erythrin domain, characterised by the presence of four iron-binding motifs (2 x ExxH and 2 x E-6-Y), and a C- terminal, five transmembrane helix bearing, vacuolar iron transporter domain. Ia MbfA variants exhibit a C-terminal VIT domain but no N-terminal erythrin domain; these variants were only observed in *Bartonella* spp.. MbfA of *B. quintana* and *B. bacilliformis* both have N-terminal domains but these domains do not resemble erythrin, nor are they similar to other *Bartonella* MbfA N-terminal domains. *Bartonella* represent an interesting bacterial genus, they are opportunistic pathogens that reside primarily within erythrocytes and are transmitted via fleas, ticks and mosquitoes. The residence within erythrocytes is reflected in the iron uptake capabilities of these pathogens, many iron

transport systems present in closely related *Brucella* spp. have been lost in the *Bartonella* genome through the process of genome reduction. Examination of the *B. quintana* genome reveals that a haem uptake system (*hutABC*) and a ferrous iron uptake system (*sitABCD*) remain the only mechanisms for iron assimilation. In addition to minimal iron uptake machinery, they lack the traditional iron-storage proteins FtnA, Dps and Bfr and no not encode catalase (Nijssen et al. 2009, Liu and Biville 2013). Taken together, these genetic traits suggest that *mbfA* may play a significant role in both iron homeostasis and oxidative stress resistance in *Bartonella* spp.. Thus, the Ia *mbfA* variants are most likely fulfilling a function to mitigate redox stress through the alteration of iron homeostasis via iron export.

In addition to Ia *mbfA* variants, Ic variants encode an N-terminal erythrin domain; in addition to this they have an approximate 85 amino acid insertion between transmembrane helix 2 and 3, which translates to a large cytoplasmic loop in the VIT domain. This cytoplasmic loop is also present in type II MbfA variants but it differs from that of type Ic variants due to the complete absence of an N-terminal erythrin domain. In this way, type II MbfA variants are directly comparable to the CCC1 system described in *S. cerevisiae* and VIT1 in *A. thaliana*. Examples of type Ic variants are present in both Gram-negative (beta-Proteobacteria) and Gram-positive bacteria (Actinobacteria). The additional cytoplasmic loop within these variants is well conserved but its purpose is unknown.

In contrast, the type II MbfA variants (CCC1/VIT1-like proteins) are conserved across not only Gram-negative (beta/gamma/delta-Proteobacteria) and Gram-positive bacteria (Actinobacteria/Firmicutes) but also eukaryotic domains including: alveotata/euglenoza (*Plasmodium falciparum/Toxoplasma gondii*), fungi (*S. cerevisiae/A. niger*), plantae (*A. thaliana*) and amoebozoa.

Although prokaryotes and eukaryotes encode a well-conserved type II MbfA (CCC1/VIT1), which in strict terms is a VIT1 protein, the mechanism in which the transport of iron is utilised the role of these proteins in oxidative stress and regulation of iron homeostasis would be expected to differ from that of classical bacterial MbfAs. It is assumed that MbfA will be located in the inner membrane of all bacteria and would function to export iron out of the cell, however, in eukaryotes, evidence is present to suggest that VIT1 is utilised to transport iron into a storage vacuole. Such a mechanism

cannot be deployed by prokaryotes since they lack internal, membrane-bound organelles, although the use of iron-storage proteins provides a similar capacity. The reason for the use of iron-storing vacuoles in yeast, plants and protozoa in place of ferritin molecules is unclear, although yeast lacks ferritins so has not alternative option. Experimentation on VIT1 systems has focus primarily on the CCC1 iron transport system in *S. cerevisiae* and VIT1 system in *A. thaliana*, but more recently, experimentation has characterised the function of the VIT1 system in *P. falciparum* where a role in regulating iron homeostasis in response to oxidative stress was described (Slavic and Krishna 2016). Iron was determined to be transported into a cytoplasmic vacuole, as is also seen in *S. cerevisiae* and *A. thaliana* (Li et al. 2001, Kim et al. 2006). *P. falciparum*, like *Brucella*, is an intracellular parasite. However, the iron exporting processes mediated by VIT1 and MbfA, respectively, are quite distinct in that in one case the iron is sequestered and the other the iron is externalised. Additionally, the niche that each intracellular parasite resides differs, *Plasmodium* within erythrocytes whilst *Brucella* within macrophage. This suggests quite different purposes for these proteins in assisting the virulence within their respective hosts. The work reported herein provides added detail to such studies at it confirms the iron export capacity of VIT1, shows that the exported iron is in the form of ferrous iron, and indicates that the process is driven by the PMF (Chapter 6.9).

As outlined above, the expression of *mbfA* appears to present as a beneficial mechanism for bacterial survival through efficient regulation of iron homeostasis to prevent excess damaging oxidative stress. However, examination of the *B. melitensis mbfA* sequence and subsequent *in vitro* experimentation reveals that all *B. melitensis* strains have acquired at least one (and in some cases two) SNP's rendering *mbfA* cryptic. This observation is puzzling as *B. melitensis* strains are very pathogenic to humans and induce abortions in a wide range of animal hosts, yet lack MbfA which is shown in this thesis to be a *B. suis* as a virulence factor. Further, provision of function MbfA to *B. melitensis* provides little advantage during redox stress and may even be detrimental in the macrophage (Chapter 7.5), acting as an anti-virulence factor which might favour selection against its expression through the acquisition of point mutations. This poses the question, why isn't MbfA beneficial to virulence in *B. melitensis*?

MbfA in *B. melitensis* may be acting in several ways; one possibility is that it promotes the initial survival of *B. melitensis*, as is observed, but this increased virulence is

detrimental to the "stealthy" nature of *Brucella* pathogenesis. Perhaps MbfA makes *B. melitensis* too successful resulting in a greater immune response to infection – providing a less favourable niche for colonisation. Another possibility is that removal of iron during the eBCV stage resulting in detoxification of peroxide in the eBCV could be detrimental to the survival of *B. melitensis* due to the loss of bacterial iron stores that might reduce subsequent replication in the rBCV phase. In either case, *B. melitensis* remains an effective pathogen in the absence of *mbfA*, and a precise reason for the loss of the gene is unclear.

In summary, the work reported in this thesis shows that MbfA provides a new mechanism by which iron homeostasis can be adjusted to combat oxidative stress. In addition, the results provided here represent the first characterisation of a dedicated prokaryotic iron export system with a clear physiological purpose. Further, this work contributes towards current knowledge on eukaryotic intracellular iron trafficking.

Chapter 9: Appendix

9.1: DNA and Protein molecular markers

A

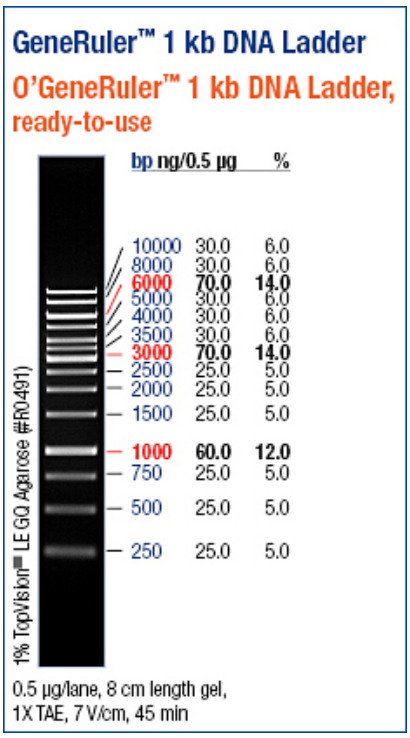

B

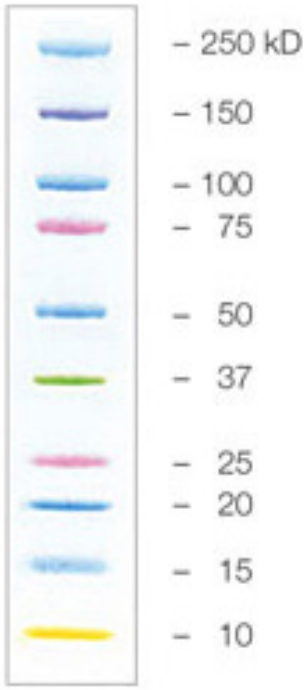

Figure 9.1: DNA (A) and Protein (B) molecular markers

9.2: Brucella suis 1330 nucleotide and amino acid sequences

Table 9.1: *mbfA* nucleotide sequence

Brucella suis 1330 chromosome I - 1622586-1621603 complement (984 bp)**.** Locus tag: BS1330_I1673

Position	Sequence
1	ATGTTCAGCC GATTCTTCCG TAATGACCGA CGCTCTTTCG ATTCGCTTTC TGAACAGGAA
61	ATTCTGGCGC TTGCCATATC CTCCGAGGAG GATGATGCCC GCATCTATCT GGCTTATGCC
121	GATGGCCTGC GCGACGAGTT TCCGCAATCG GCGAAGATTT ACGAGCAGAT GGCCGCAGAG
181	GAACACGACC ACCGCGCAGC ACTGATTGAG CGGCATAAGG CCCGCTTTGG CGACCGGATT
241	CCGCTGATCC GCCGCGAGCA TGTCAGTGGC TATTATGATC GCAAGCCGGA CTGGCTGGTG
301	CGTCCGCTCG GCATCGACAA GGTGCGTGAG GCCGCCTCCG AGATGGAGGA ACAGGCTTAT
361	CGTTTCTATG TCGAGGCGGC CAAGCGCGTC AGCGATGCAG ACACGCGCAA ACTGCTGGGT
421	GACCTTGCCC AGCAGGAAAA ACAGCACGAA GCCAAGGCTG AATCGCTGGA ACACACGCTG
481	ACACCGGATA ATGTGCAGGA TGAGGAACGC GCCGCCGAGC GCAAGCAATT CATCCTCACC
541	TATATCCAGC CTGGCCTTGC GGGCCTGATG GACGGCTCCG TCTCGACACT CGCACCGATC
601	TTTGCCGCCG CCTTTGCCAC GCAGGATACA TGGCAGACCT TTCTGGTTGG CCTTTCCGCC
661	TCGGTCGGCG CCGGTATTTC GATGGGCTTT ACAGAAGCCG TGCATGACGA CGGCAAGCTG
721	TCGGGACGCG GCTCGCCGAT CAAGCGCGGC ATTTCATGCG GCGTCATGAC GACGCTGGGC
781	GGGCTTGGTC ACAGCCTGCC CTATCTGATC AAGGATTTCT GGACTGCGAC AAGCATCGCC
841	GTGATCCTTG TCTTCTTCGA GCTCTGGGCC ATTGCCTTCA TTCAGAACCG CTATATGGAA
901	ACGCCCTTCT TCCGCGCCGC ACTCCAGGTC GTTTTTGGCG GTGCGCTCGT CCTGGCGGCG
961	GGCATATTGA TCGGCAGCGC CTGA

Table 9.2: MbfA amino acid sequence

Hypothetical membrane protein (327 AA); Locus tag: WP_004690452

Position	Sequence
1	MFSRFFRNDR RSFDSLSEQE ILALAISSEE DDARIYLAYA DGLRDEFPQS AKIYEQMAAE
61	EHDHRAALIE RHKARFGDRI PLIRREHVSG YYDRKPDWLV RPLGIDKVRE AASEMEEQAY
121	RFYVEAAKRV SDADTRKLLG DLAQQEKQHE AKAESLEHTL TPDNVQDEER AAERKQFILT
181	YIQPGLAGLM DGSVSTLAPI FAAAFATQDT WQTFLVGLSA SVGAGISMGF TEAVHDDGKL
241	SGRGSPIKRG ISCGVMTTLG GLGHSLPYLI KDFWTATSIA VILVFFELWA IAFIQNRYME
301	TPFFRAALQV VFGGALVLAA GILIGSA

Table 9.3: MbfA amino acid frequency

Molecular weight: 36.433 kDa

Isoelectric point: 5.27

Amino Acid	Frequency	Percentage (%)
A	41	12.5
C	1	0.3
D	21	6.4
E	25	7.6
F	19	5.8
G	24	7.3
H	8	2.4
I	21	6.4
K	12	3.7
L	31	9.5
M	7	2.1
N	3	0.9
P	10	3.1
Q	14	4.3
R	24	7.3
S	22	6.7
T	14	4.3
V	16	4.9
W	4	1.2
Y	10	3.1

9.3: MbfA multiple sequence alignments

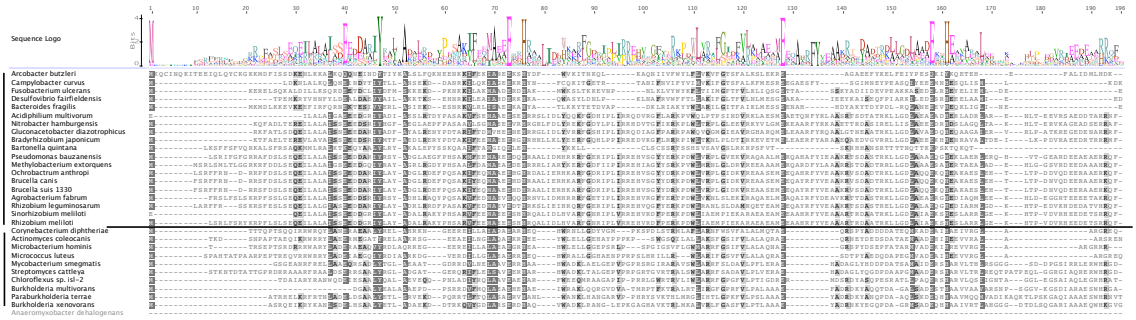

Figure 9.2: Alignment of prokaryotic and eukaryotic MbfA erythrin domain

Multiple sequence alignment of prokaryotic and eukaryotic MbfA erythrin domains.

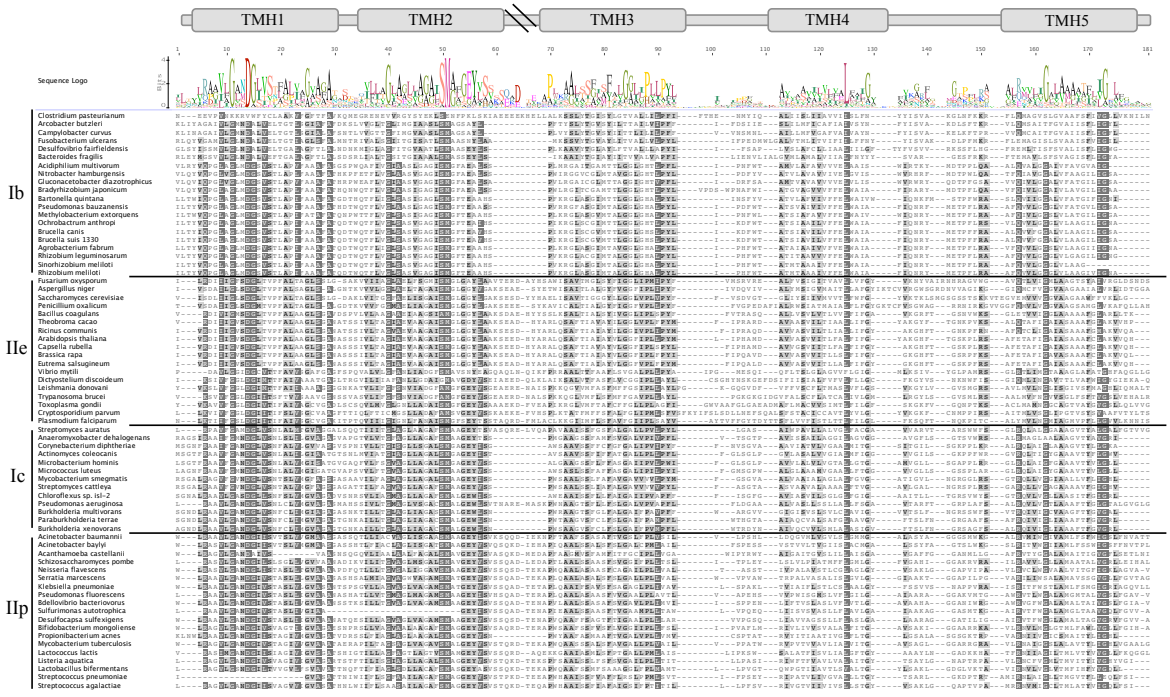

Figure 9.3: Alignment of prokaryotic and eukaryotic MbfA transmembrane helices

Multiple sequence alignment of prokaryotic and eukaryotic MbfA transmembrane helices

Figure 9.4: Alignment of prokaryotic and eukaryotic MbfA cytoplasmic loop

Multiple sequence alignment of prokaryotic and eukaryotic MbfA cytoplasmic loop.

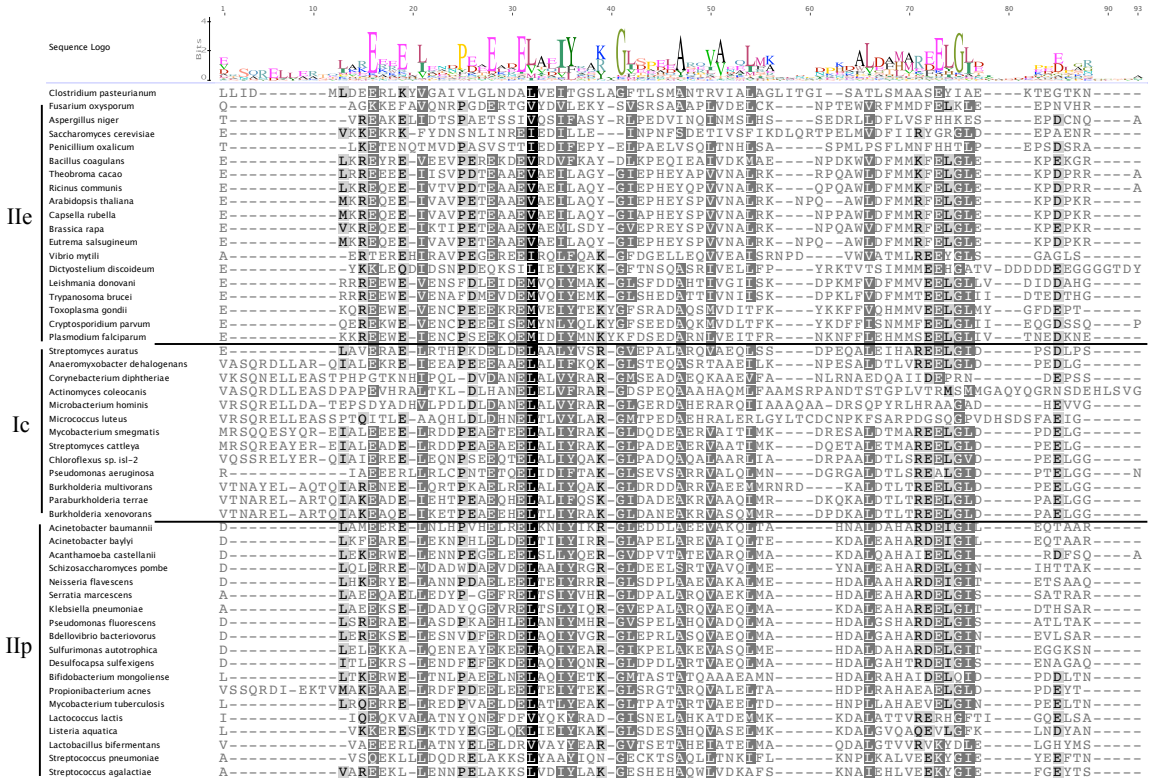

9.4: *B. suis* 1330 iron metabolism and redox stress genes

Table 9.4: *B. suis* 1330 iron metabolism and redox stress genes

Product	Gene Symbol	Start	End	Base Pairs	AA
Catalase	katA	336392	337915	1524	507
Ferric iron ABC transporter, permease protein	sfuC1	676714	678432	1719	572
Ferric iron ABC transporter, iron-binding protein	sfuA1	678504	679520	1017	338
Ferric iron ABC transporter, ATP-binding protein	sfuB1	679646	680680	1035	344
Ferric iron ABC transporter, ATP-binding protein	sfuC2	698847	699908	1062	353
Ferric iron ABC transporter, permease protein	sfuA2	699905	702130	2226	741
Ferric iron ABC transporter, iron-binding protein	sfuB2	702265	703290	1026	341
Periplasmic protein p19	ftrA	362050	362598	549	182
putative exported protein	ftrB	362626	363000	375	124
High-affinity iron permease	ftrC	363007	363843	837	278
Polyferredoxin	ftrD	363804	365237	1434	477
Heme-degrading monooxygenase	bhuQ	541582	541896	315	104
ATP-binding component	bhuV	735357	736154	798	265
Permease component	bhuU	736151	737149	999	332
Periplasmic substrate-binding component	bhuT	737191	738225	1035	344
TonB-dependent siderophore receptor	bhuA	1192352	1194337	1986	661
Hypothetical transmembrane iron-regulated protein	mbfA	1621603	1622586	984	327
Bacterioferritin	bfr	542630	543115	486	161
Non-specific DNA-binding protein Dps	dps	2071065	2071547	483	160
Manganese transport protein	mntH	1399842	1401131	1290	429
alkyl hydroperoxide reductase D	ahpD	687040	687567	528	175
Alkyl hydroperoxide reductase protein C	ahpC	687647	688201	555	184
Manganese uptake regulation protein	mur	1603397	1603867	471	156
Iron-responsive regulator	irr	2097917	2098321	405	134
Iron-responsive repressor	rirA	541004	541465	462	153
Zinc uptake regulation protein	zur	1116283	1116720	438	145
Enterobactin synthetase	entD	9684	10316	633	210
2,3-dihydroxybenzoate-2,3-dehydrogenase	entA	10399	11175	777	258
Isochorismatase [brucebactin]	entB	11175	12047	873	290
2,3-dihydroxybenzoate-AMP ligase [brucebactin]	entE	12099	13718	1620	539
Isochorismate synthase [brucebactin]	entC	13825	15000	1176	391
Siderophore biosynthesis non-ribosomal peptide synthetase modules	entF	15141	16481	1341	446
Iron compound ABC transporter, periplasmic iron compound-binding protein	fatB	653662	654591	930	309
Iron compound ABC transporter, permease protein	fatD	654648	655610	963	320
Iron compound ABC transporter, permease protein	fatC	655603	656556	954	317
Iron compound ABC transporter, ATP-binding protein	fatE	656553	657311	759	252
TonB-dependent receptor	fiu	986784	988814	2031	676

Vitamin B12 ABC transporter, ATPase component	fepD	1304414	1305190	777	258
Vitamin B12 ABC transporter, permease component	fepC	1305187	1306188	1002	333
Vitamin B12 ABC transporter, B12-binding component	fepB	1306181	1307020	840	279
Outer membrane vitamin B12 receptor	cir	1307034	1309019	1986	661
Superoxide dismutase [Fe]	sodA	561022	561621	600	199
Superoxide dismutase [Cu-Zn]	sodC	682572	683093	522	173
Biopolymer transport protein	exbB	1611752	1612630	879	292
Biopolymer transport protein	exbD	1612636	1613130	495	164
TonB-dependent receptor	tonB	1613127	1614053	927	308
Periplasmic zinc-binding protein	znuA	1113345	1114349	1005	334
Zinc ABC transporter, ATP-binding protein	znuC	1114576	1115472	897	298
Zinc ABC transporter, permease protein	znuB	1115426	1116286	861	286

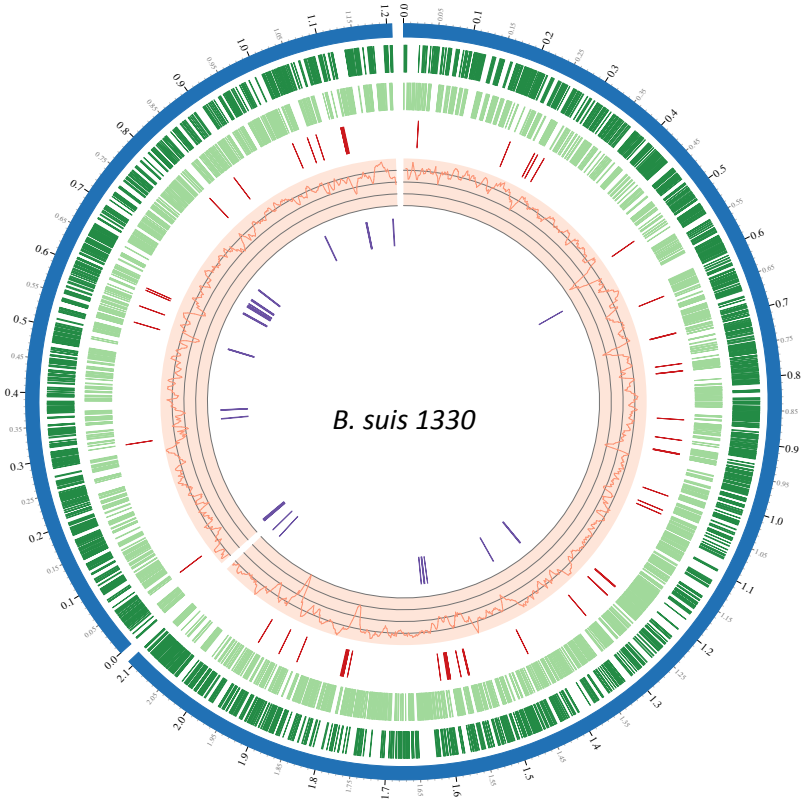

Figure 9.5: *B. suis* 1330 genome map

Genome map of *B. suis* 1330. Chromosome I: 2.11 Mp Chromosome II: 1.21 Mp. Annotations from outside to inside: coding sequences - sense strand, (dark green), coding sequences - antisense strand (light green), tRNA's (red), GC% plot (orange), iron and redox stress related genes (purple).

9.5: Thermal shift assay screen matrix

Actual screen stocks contain concentrations twice that of which is displayed. The concentration is halved by the addition of the protein and the SYPRO orange probe.

Table 9.5: pH screen

	1	2	3	4	5	6	7	8	9	10	11	12
A	Water	Water	4 M urea	100 mM citric acid pH 4.1	100 mM citric acid pH 4.6	100 mM citric acid pH 5.1	100 mM acetic acid pH 4.2	100 mM acetic acid pH 4.7	100 mM acetic acid pH 5.2	100 mM succinic acid pH 4.4	100 mM succinic acid pH 4.9	100 mM succinic acid pH 5.4
B	100 mM malic acid pH 4.3	100 mM malic acid pH 4.8	100 mM malic acid pH 5.3	100 mM tartaric acid pH 4.3	100 mM tartaric acid pH 4.8	100 mM tartaric acid pH 5.3	100 mM propionic acid pH 4.3	100 mM propionic acid pH 4.8	100 mM propionic acid pH 5.3	100 mM malonic acid pH 5.2	100 mM malonic acid pH 5.7	100 mM malonic acid pH 6.2
C	100 mM citric acid pH 5.5	100 mM citric acid pH 6.0	100 mM citric acid pH 6.5	100 mM succinic acid pH 5.6	100 mM succinic acid pH 6.1	100 mM succinic acid pH 6.6	100 mM MES pH 5.6	100 mM MES pH 6.1	100 mM MES pH 6.6	100 mM maleic acid pH 5.7	100 mM maleic acid pH 6.2	100 mM maleic acid pH 6.7
D	100 mM sodium cacodylate pH 5.7	100 mM sodium cacodylate pH 6.2	100 mM sodium cacodylate pH 6.7	100 mM ADA pH 6.1	100 mM ADA pH 6.6	100 mM ADA pH 7.1	100 mM bisTRIS pH 6.1	100 mM bisTRIS pH 6.6	100 mM bisTRIS pH 7.1	100 mM ACES pH 6.3	100 mM ACES pH 6.8	100 mM ACES pH 7.3
E	100 mM phosphate pH 6.3	100 mM phosphate pH 6.8	100 mM phosphate pH 7.3	100 mM PIPES pH 6.3	100 mM PIPES pH 6.8	100 mM PIPES pH 7.3	100 mM imidazole pH 6.6	100 mM imidazole pH 7.1	100 mM imidazole pH 7.6	100 mM MOPS pH 6.6	100 mM MOPS pH 7.1	100 mM MOPS pH 7.6
F	100 mM bisTRIS propane pH 6.6	100 mM bisTRIS propane pH 7.1	100 mM bisTRIS propane pH 7.6	100 mM HEPES pH 7.0	100 mM HEPES pH 7.5	100 mM HEPES pH 8.0	100 mM tricine pH 7.5	100 mM tricine pH 8.0	100 mM tricine pH 8.5	100 mM EPPS pH 7.5	100 mM EPPS pH 8.0	100 mM EPPS pH 8.5
G	100 mM TRIS pH 7.7	100 mM TRIS pH 8.2	100 mM TRIS pH 8.7	100 mM bicine pH 7.7	100 mM bicine pH 8.2	100 mM bicine pH 8.7	100 mM TAPS pH 7.9	100 mM TAPS pH 8.4	100 mM TAPS pH 8.9	100 mM bisTRIS propane pH 8.5	100 mM bisTRIS propane pH 9.0	100 mM bisTRIS propane pH 9.5
H	100 mM boric acid pH 8.6	100 mM boric acid pH 9.1	100 mM boric acid pH 9.6	100 mM CHES pH 8.8	100 mM CHES pH 9.3	100 mM CHES pH 9.8	100 mM glycine pH 9.2	100 mM glycine pH 9.7	100 mM glycine pH 10.2	100 mM CAPS pH 9.9	100 mM CAPS pH 10.4	100 mM CAPS pH 10.9

Table 9.6: Salt screen

	1	2	3	4	5	6	7	8	9	10	11	12
A	Water	Water	4 M urea	3.0 M Gu-HCl	1.0 M Gu-HCl	0.8 M Gu-HCl	0.6 M Gu-HCl	0.4 M Gu-HCl	0.2 M Gu-HCl	5 mM Gu-HCl	0.5 M Na_3 citrate	0.2 M Na_3 citrate
B	1.5 M Na_2 malonate	1.0 M Na_2 malonate	0.8 M Na_2 malonate	0.6 M Na_2 malonate	0.4 M Na_2 malonate	0.2 M Na_2 malonate	1.5 M $(NH_4)_2SO_4$	1.0 M $(NH_4)_2SO_4$	0.8 M $(NH_4)_2SO_4$	0.6 M $(NH_4)_2SO_4$	0.4 M $(NH_4)_2SO_4$	0.2 M $(NH_4)_2SO_4$
C	1.5 M NaCl	1.0 M NaCl	0.8 M NaCl	0.6 M NaCl	0.4 M NaCl	0.2 M NaCl	1.5 M NH_4Cl	1.0 M NH_4Cl	0.8 M NH_4Cl	0.6 M NH_4Cl	0.4 M NH_4Cl	0.2 M Na2 NH_4Cl
D	1.0 M $MgSO_4$	0.8 M $MgSO_4$	0.6 M $MgSO_4$	0.4 M $MgSO_4$	0.2 M $MgSO_4$	1.0 M Na_2SO_4	0.8 M Na_2SO_4	0.6 M Na_2SO_4	0.4 M Na_2SO_4	0.2 M Na_2SO_4	0.5 M KCl	0.2 M KCl
E	0.5 M LiCl	0.2 M LiCl	0.5 M RbCl	0.2 M RbCl	0.5 M CsCl	0.2 M CsCl	0.4 M NaF	0.1 M NaF	1.5 M NaBr	0.4 M NaBr	0.1 M NaBr	0.4 M NaI
F	0.1 M NaI	0.4 M $MgCl_2$	5 mM $MgCl_2$	5 mM $CaCl_2$	5 mM $SrCl_2$	1 mM $ZnCl_2$	0.1 mM $ZnCl_2$	1 mM $NiCl_2$	0.1 mM $NiCl_2$	5 mM $MnCl_2$	0.5 mM $MnCl_2$	1 mM $CoCl_2$
G	0.1 mM $CoCl_2$	1 mM $CuSO_4$	0.1 mM $CuSO_4$	1 mM $CdSO_4$	5 mM EDTA pH 7.5	5 mM EGTA pH 7.5	magic triangle	2 mM $La(NO_3)_3$	2 mM $PrCl_3$	2 mM $NdCl_3$	2 mM $SmCl_3$	2 mM $EuCl_3$
H	2 mM $GdCl_3$	2 mM $DyCl_3$	2 mM $HoCl_3$	2 mM $YbCl_3$	2 mM $LuCl_3$	5 mM Na_2HPO_4	5 mM Na_3VO_4	5 mM Na_2WO_4	5 mM Na_2MoO_4	5 mM DTT	5 mM TCEP	5 mM β-mercapto ethanol

Table 9.7: Metal screen

	1	2	3	4	5	6	7	8	9	10	11	12
A	H_2O	1 µM $MnCl_2$	1 µM $FeCl_3$	1 µM $Fe(NH_4)_2(SO_4)_2$	1 µM $CoCl_2$	1 µM $NiSO_4$	1 µM $CuCl_2$	1 µM $ZnSO_4$	1 µM MoO_3	1 µM $CdCl_2$	1 µM $Pb(NO_3)_2$	1 µM $VOSO_4$
B	H_2O	5 µM $MnCl_2$	5 µM $FeCl_3$	5 µM $Fe(NH_4)_2(SO_4)_2$	5 µM $CoCl_2$	5 µM $NiSO_4$	5 µM $CuCl_2$	5 µM $ZnSO_4$	5 µM MoO_3	5 µM $CdCl_2$	5 µM $Pb(NO_3)_2$	5 µM $VOSO_4$
C	4M Urea	10 µM $MnCl_2$	10 µM $FeCl_3$	10 µM $Fe(NH_4)_2(SO_4)_2$	10 µM $CoCl_2$	10 µM $NiSO_4$	10 µM $CuCl_2$	10 µM $ZnSO_4$	10 µM MoO_3	10 µM $CdCl_2$	10 µM $Pb(NO_3)_2$	10 µM $VOSO_4$
D	4M Urea	50 µM $MnCl_2$	50 µM $FeCl_3$	50 µM $Fe(NH_4)_2(SO_4)_2$	50 µM $CoCl_2$	50 µM $NiSO_4$	50 µM $CuCl_2$	50 µM $ZnSO_4$	50 µM MoO_3	50 µM $CdCl_2$	50 µM $Pb(NO_3)_2$	50 µM $VOSO_4$
E	20 mM MES	100 µM $MnCl_2$	100 µM $FeCl_3$	100 µM $Fe(NH_4)_2(SO_4)_2$	100 µM $CoCl_2$	100 µM $NiSO_4$	100 µM $CuCl_2$	100 µM $ZnSO_4$	100 µM MoO_3	100 µM $CdCl_2$	100 µM $Pb(NO_3)_2$	100 µM $VOSO_4$
F	20 mM MES	500 µM $MnCl_2$	500 µM $FeCl_3$	500 µM $Fe(NH_4)_2(SO_4)_2$	500 µM $CoCl_2$	500 µM $NiSO_4$	500 µM $CuCl_2$	500 µM $ZnSO_4$	500 µM MoO_3	500 µM $CdCl_2$	500 µM $Pb(NO_3)_2$	500 µM $VOSO_4$
G	Dithionite	1mM $MnCl_2$	1 mM $FeCl_3$	1 mM $Fe(NH_4)_2(SO_4)_2$	1 mM $CoCl_2$	1 mM $NiSO_4$	1 mM $CuCl_2$	1 mM $ZnSO_4$	1 mM MoO_3	1 mM $CdCl_2$	1 mM $Pb(NO_3)_2$	1mM $VOSO_4$
H	Dithionite	2 mM $MnCl_2$	2 mM $FeCl_3$	2 mM $Fe(NH_4)_2(SO_4)_2$	2 mM $CoCl_2$	2 mM $NiSO_4$	2 mM $CuCl_2$	2 mM $ZnSO_4$	2 mM MoO_3	2 mM $CdCl_2$	2 mM $Pb(NO_3)_2$	2mM $VOSO_4$

9.6: Crystallisation screening conditions

Table 9.8: PACT premier HT-96 – Conditions A1-D12

PACT *premier*™ HT-96 / FX-96 Conditions A1-D12 MD1-36 / MD1-36-FX

Well #	Conc.	Salt	Conc.	Buffer	pH	Conc.	Precipitant
A1			0.1 M	SPG	4.0	25 % w/v	PEG 1500
A2			0.1 M	SPG	5.0	25 % w/v	PEG 1500
A3			0.1 M	SPG	6.0	25 % w/v	PEG 1500
A4			0.1 M	SPG	7.0	25 % w/v	PEG 1500
A5			0.1 M	SPG	8.0	25 % w/v	PEG 1500
A6			0.1 M	SPG	9.0	25 % w/v	PEG 1500
A7	0.2 M	Sodium chloride	0.1 M	Sodium acetate	5.0	20 % w/v	PEG 6000
A8	0.2 M	Ammonium chloride	0.1 M	Sodium acetate	5.0	20 % w/v	PEG 6000
A9	0.2 M	Lithium chloride	0.1 M	Sodium acetate	5.0	20 % w/v	PEG 6000
A10	0.2 M	Magnesium chloride hexahydrate	0.1 M	Sodium acetate	5.0	20 % w/v	PEG 6000
A11	0.2 M	Calcium chloride dihydrate	0.1 M	Sodium acetate	5.0	20 % w/v	PEG 6000
A12	0.01 M	Zinc chloride	0.1 M	Sodium acetate	5.0	20 % w/v	PEG 6000
B1			0.1 M	MIB	4.0	25 % w/v	PEG 1500
B2			0.1 M	MIB	5.0	25 % w/v	PEG 1500
B3			0.1 M	MIB	6.0	25 % w/v	PEG 1500
B4			0.1 M	MIB	7.0	25 % w/v	PEG 1500
B5			0.1 M	MIB	8.0	25 % w/v	PEG 1500
B6			0.1 M	MIB	9.0	25 % w/v	PEG 1500
B7	0.2 M	Sodium chloride	0.1 M	MES	6.0	20 % w/v	PEG 6000
B8	0.2 M	Ammonium chloride	0.1 M	MES	6.0	20 % w/v	PEG 6000
B9	0.2 M	Lithium chloride	0.1 M	MES	6.0	20 % w/v	PEG 6000
B10	0.2 M	Magnesium chloride hexahydrate	0.1 M	MES	6.0	20 % w/v	PEG 6000
B11	0.2 M	Calcium chloride dihydrate	0.1 M	MES	6.0	20 % w/v	PEG 6000
B12	0.01 M	Zinc chloride	0.1 M	MES	6.0	20 % w/v	PEG 6000
C1			0.1 M	PCTP	4.0	25 % w/v	PEG 1500
C2			0.1 M	PCTP	5.0	25 % w/v	PEG 1500
C3			0.1 M	PCTP	6.0	25 % w/v	PEG 1500
C4			0.1 M	PCTP	7.0	25 % w/v	PEG 1500
C5			0.1 M	PCTP	8.0	25 % w/v	PEG 1500
C6			0.1 M	PCTP	9.0	25 % w/v	PEG 1500
C7	0.2 M	Sodium chloride	0.1 M	HEPES	7.0	20 % w/v	PEG 6000
C8	0.2 M	Ammonium chloride	0.1 M	HEPES	7.0	20 % w/v	PEG 6000
C9	0.2 M	Lithium chloride	0.1 M	HEPES	7.0	20 % w/v	PEG 6000
C10	0.2 M	Magnesium chloride hexahydrate	0.1 M	HEPES	7.0	20 % w/v	PEG 6000
C11	0.2 M	Calcium chloride dihydrate	0.1 M	HEPES	7.0	20 % w/v	PEG 6000
C12	0.01 M	Zinc chloride	0.1 M	HEPES	7.0	20 % w/v	PEG 6000
D1			0.1 M	MMT	4.0	25 % w/v	PEG 1500
D2			0.1 M	MMT	5.0	25 % w/v	PEG 1500
D3			0.1 M	MMT	6.0	25 % w/v	PEG 1500
D4			0.1 M	MMT	7.0	25 % w/v	PEG 1500
D5			0.1 M	MMT	8.0	25 % w/v	PEG 1500
D6			0.1 M	MMT	9.0	25 % w/v	PEG 1500
D7	0.2 M	Sodium chloride	0.1 M	Tris	8.0	20 % w/v	PEG 6000
D8	0.2 M	Ammonium chloride	0.1 M	Tris	8.0	20 % w/v	PEG 6000
D9	0.2 M	Lithium chloride	0.1 M	Tris	8.0	20 % w/v	PEG 6000
D10	0.2 M	Magnesium chloride hexahydrate	0.1 M	Tris	8.0	20 % w/v	PEG 6000
D11	0.2 M	Calcium chloride dihydrate	0.1 M	Tris	8.0	20 % w/v	PEG 6000
D12	0.002 M	Zinc chloride	0.1 M	Tris	8.0	20 % w/v	PEG 6000

Table 9.9: PACT premier HT-96 – Conditions E1-H12

PACT *premier*™ HT-96 / FX-96 Conditions E1-H12 MD1-36 / MD1-36-FX

Well #	Conc.	Salt	Conc.	Buffer	pH	Conc.	Precipitant
E1	0.2 M	Sodium fluoride				20 % w/v	PEG 3350
E2	0.2 M	Sodium bromide				20 % w/v	PEG 3350
E3	0.2 M	Sodium iodide				20 % w/v	PEG 3350
E4	0.2 M	Potassium thiocyanate				20 % w/v	PEG 3350
E5	0.2 M	Sodium nitrate				20 % w/v	PEG 3350
E6	0.2 M	Sodium formate				20 % w/v	PEG 3350
E7	0.2 M	Sodium acetate trihydrate				20 % w/v	PEG 3350
E8	0.2 M	Sodium sulfate				20 % w/v	PEG 3350
E9	0.2 M	Potassium sodium tartrate tetrahydrate				20 % w/v	PEG 3350
E10	0.02 M	Sodium/potassium phosphate				20 % w/v	PEG 3350
E11	0.2 M	Sodium citrate tribasic dihydrate				20 % w/v	PEG 3350
E12	0.2 M	Sodium malonate dibasic monohydrate				20 % w/v	PEG 3350
F1	0.2 M	Sodium fluoride	0.1 M	Bis-Tris propane	6.5	20 % w/v	PEG 3350
F2	0.2 M	Sodium bromide	0.1 M	Bis-Tris propane	6.5	20 % w/v	PEG 3350
F3	0.2 M	Sodium iodide	0.1 M	Bis-Tris propane	6.5	20 % w/v	PEG 3350
F4	0.2 M	Potassium thiocyanate	0.1 M	Bis-Tris propane	6.5	20 % w/v	PEG 3350
F5	0.2 M	Sodium nitrate	0.1 M	Bis-Tris propane	6.5	20 % w/v	PEG 3350
F6	0.2 M	Sodium formate	0.1 M	Bis-Tris propane	6.5	20 % w/v	PEG 3350
F7	0.2 M	Sodium acetate trihydrate	0.1 M	Bis-Tris propane	6.5	20 % w/v	PEG 3350
F8	0.2 M	Sodium sulfate	0.1 M	Bis-Tris propane	6.5	20 % w/v	PEG 3350
F9	0.2 M	Potassium sodium tartrate tetrahydrate	0.1 M	Bis-Tris propane	6.5	20 % w/v	PEG 3350
F10	0.02 M	Sodium/potassium phosphate	0.1 M	Bis-Tris propane	6.5	20 % w/v	PEG 3350
F11	0.2 M	Sodium citrate tribasic dihydrate	0.1 M	Bis-Tris propane	6.5	20 % w/v	PEG 3350
F12	0.2 M	Sodium malonate dibasic monohydrate	0.1 M	Bis-Tris propane	6.5	20 % w/v	PEG 3350
G1	0.2 M	Sodium fluoride	0.1 M	Bis-Tris propane	7.5	20 % w/v	PEG 3350
G2	0.2 M	Sodium bromide	0.1 M	Bis-Tris propane	7.5	20 % w/v	PEG 3350
G3	0.2 M	Sodium iodide	0.1 M	Bis-Tris propane	7.5	20 % w/v	PEG 3350
G4	0.2 M	Potassium thiocyanate	0.1 M	Bis-Tris propane	7.5	20 % w/v	PEG 3350
G5	0.2 M	Sodium nitrate	0.1 M	Bis-Tris propane	7.5	20 % w/v	PEG 3350
G6	0.2 M	Sodium formate	0.1 M	Bis-Tris propane	7.5	20 % w/v	PEG 3350
G7	0.2 M	Sodium acetate trihydrate	0.1 M	Bis-Tris propane	7.5	20 % w/v	PEG 3350
G8	0.2 M	Sodium sulfate	0.1 M	Bis-Tris propane	7.5	20 % w/v	PEG 3350
G9	0.2 M	Potassium sodium tartrate tetrahydrate	0.1 M	Bis-Tris propane	7.5	20 % w/v	PEG 3350
G10	0.02 M	Sodium/potassium phosphate	0.1 M	Bis-Tris propane	7.5	20 % w/v	PEG 3350
G11	0.2 M	Sodium citrate tribasic dihydrate	0.1 M	Bis-Tris propane	7.5	20 % w/v	PEG 3350
G12	0.2 M	Sodium malonate dibasic monohydrate	0.1 M	Bis-Tris propane	7.5	20 % w/v	PEG 3350
H1	0.2 M	Sodium fluoride	0.1 M	Bis-Tris propane	8.5	20 % w/v	PEG 3350
H2	0.2 M	Sodium bromide	0.1 M	Bis-Tris propane	8.5	20 % w/v	PEG 3350
H3	0.2 M	Sodium iodide	0.1 M	Bis-Tris propane	8.5	20 % w/v	PEG 3350
H4	0.2 M	Potassium thiocyanate	0.1 M	Bis-Tris propane	8.5	20 % w/v	PEG 3350
H5	0.2 M	Sodium nitrate	0.1 M	Bis-Tris propane	8.5	20 % w/v	PEG 3350
H6	0.2 M	Sodium formate	0.1 M	Bis-Tris propane	8.5	20 % w/v	PEG 3350
H7	0.2 M	Sodium acetate trihydrate	0.1 M	Bis-Tris propane	8.5	20 % w/v	PEG 3350
H8	0.2 M	Sodium sulfate	0.1 M	Bis-Tris propane	8.5	20 % w/v	PEG 3350
H9	0.2 M	Potassium sodium tartrate tetrahydrate	0.1 M	Bis-Tris propane	8.5	20 % w/v	PEG 3350
H10	0.02 M	Sodium/potassium phosphate	0.1 M	Bis-Tris propane	8.5	20 % w/v	PEG 3350
H11	0.2 M	Sodium citrate tribasic dihydrate	0.1 M	Bis-Tris propane	8.5	20 % w/v	PEG 3350
H12	0.2 M	Sodium malonate dibasic monohydrate	0.1 M	Bis-Tris propane	8.5	20 % w/v	PEG 3350

Table 9.10: JCSG-plus HT-96 – Conditions A1-D12

JCSG-*plus* HT-96 Wells A1- D12 MD1–40

Well #	Conc.	Salt	Conc.	Buffer	pH	Conc.	Precipitant
A1	0.2 M	Lithium sulfate	0.1 M	Sodium acetate	4.5	50 % w/v	PEG 400
A2		None	0.1 M	Sodium citrate	5.5	20 % w/v	PEG 3000
A3	0.2 M	Ammonium citrate dibasic		None		20 % w/v	PEG 3350
A4	0.02 M	Calcium chloride dihydrate	0.1 M	Sodium acetate	4.6	30 % v/v	MPD
A5	0.2 M	Magnesium formate dihydrate		None		20 % w/v	PEG 3350
A6	0.2 M	Lithium sulfate	0.1 M	Phosphate/citrate	4.2	20 % w/v	PEG 1000
A7		None	0.1 M	CHES	9.5	20 % w/v	PEG 8000
A8	0.2 M	Ammonium formate		None		20 % w/v	PEG 3350
A9	0.2 M	Ammonium chloride		None		20 % w/v	PEG 3350
A10	0.2 M	Potassium formate		None		20 % w/v	PEG 3350
A11	0.2 M	Ammonium phosphate monobasic	0.1 M	Tris	8.5	50 % v/v	MPD
A12	0.2 M	Potassium nitrate		None		20 % w/v	PEG 3350
B1	0.8 M	Ammonium sulfate	0.1 M	Citrate	4.0		None
B2	0.2 M	Sodium thiocyanate		None		20 % w/v	PEG 3350
B3		None	0.1 M	BICINE	9.0	20 % w/v	PEG 6000
B4		None	0.1 M	HEPES	7.5	10 % w/v	PEG 8000
						8 % v/v	Ethylene glycol
B5		None	0.1 M	Sodium cacodylate	6.5	40 % v/v	MPD
						5 % w/v	PEG 8000
B6		None	0.1 M	Phosphate/citrate	4.2	40 % v/v	Ethanol
						5 % w/v	PEG 1000
B7		None	0.1 M	Sodium acetate	4.6	8 % w/v	PEG 4000
B8	0.2 M	Magnesium chloride hexahydrate	0.1 M	Tris	7.0	10 % w/v	PEG 8000
B9		None	0.1 M	Citrate	5.0	20 % w/v	PEG 6000
B10	0.2 M	Magnesium chloride hexahydrate	0.1 M	Sodium cacodylate	6.5	50 % v/v	PEG 200
B11	1.6 M	Sodium citrate tribasic dihydrate pH 6.5		None			None
B12	0.2 M	Potassium citrate tribasic monohydrate		None		20 % w/v	PEG 3350
C1	0.2 M	Sodium chloride	0.1 M	Phosphate/citrate	4.2	20 % w/v	PEG 8000
C2	1.0 M	Lithium chloride	0.1 M	Citrate	4.0	20 % w/v	PEG 6000
C3	0.2 M	Ammonium nitrate		None		20 % w/v	PEG 3350
C4		None	0.1 M	HEPES	7.0	10 % w/v	PEG 6000
C5	0.8 M	Sodium phosphate monobasic monohydrate	0.1 M	Sodium HEPES	7.5		None
	0.8 M	Potassium phosphate monobasic		None			
C6		None	0.1 M	Phosphate/citrate	4.2	40 % v/v	PEG 300
C7	0.2 M	Zinc acetate dihydrate	0.1 M	Sodium acetate	4.5	10 % w/v	PEG 3000
C8		None	0.1 M	Tris	8.5	20 % v/v	Ethanol
C9		None	0.1 M	Sodium/potassium phosphate	6.2	25 % v/v	1,2-Propandiol
						10 %v/v	Glycerol
C10		None	0.1 M	BICINE	9.0	10 % w/v	PEG 20,000
						2 % v/v	1,4-Dioxane
C11	2.0 M	Ammonium sulfate	0.1 M	Sodium acetate	4.6		None
C12		None		None		10 % w/v	PEG 1000
						10 % w/v	PEG 8000
D1		None		None		24 % w/v	PEG 1500
						20 % v/v	Glycerol
D2	0.2 M	Magnesium chloride hexahydrate	0.1 M	Sodium HEPES	7.5	30 % v/v	PEG 400
D3	0.2 M	Sodium chloride	0.1 M	Sodium/potassium phosphate	6.2	50 % v/v	PEG 200
D4	0.2 M	Lithium sulfate	0.1 M	Sodium acetate	4.5	30 % w/v	PEG 8000
D5		None	0.1 M	HEPES	7.5	70 % v/v	MPD
D6	0.2 M	Magnesium chloride hexahydrate	0.1 M	Tris	8.5	20 % w/v	PEG 8000
D7	0.2 M	Lithium sulfate	0.1 M	Tris	8.5	40 % v/v	PEG 400
D8		None	0.1 M	Tris	8.0	40 % v/v	MPD
D9	0.17 M	Ammonium sulfate		None		25.5 % w/v	PEG 4000
						15 % v/v	Glycerol
D10	0.2 M	Calcium acetate hydrate	0.1 M	Sodium cacodylate	6.5	40 % v/v	PEG 300
D11	0.14 M	Calcium chloride dihydrate	0.07 M	Sodium acetate	4.6	14 % v/v	2-Propanol
						30 % v/v	Glycerol
D12	0.04 M	Potassium phosphate monobasic		None		16 % w/v	PEG 8000
						20 % v/v	Glycerol

Table 9.11: JCSG-plus HT-96 – Conditions E1-H12

JCSG-*plus* HT-96 Wells E1 – H12 MD1–40

Well #	Conc.	Salt	Conc.	Buffer	pH	Conc.	Precipitant
E1	1.0 M	Sodium citrate tribasic dihydrate	0.1 M	Sodium cacodylate	6.5		None
E2	2.0 M	Ammonium sulfate	0.1 M	Sodium cacodylate	6.5		None
	0.2 M	Sodium chloride					
E3	0.2 M	Sodium chloride	0.1 M	HEPES	7.5	10 % v/v	2-Propanol
E4	1.26 M	Ammonium sulfate	0.1 M	Tris	8.5		None
	0.2 M	Lithium sulfate					
E5		None	0.1 M	CAPS	10.5	40 % v/v	MPD
E6	0.2 M	Zinc acetate dihydrate	0.1 M	Imidazole	8.0	20 % w/v	PEG 3000
E7	0.2 M	Zinc acetate dihydrate	0.1 M	Sodium cacodylate	6.5	10 % v/v	2-Propanol
E8	1.0 M	Ammonium phosphate dibasic	0.1 M	Sodium acetate	4.5		None
E9	1.6 M	Magneisum sulfate heptahydrate	0.1 M	MES	6.5		None
E10		None	0.1 M	BICINE	9.0	10 % w/v	PEG 6000
E11	0.16 M	Calcium acetate hydrate	0.08 M	Sodium cacodylate	6.5	14.4 % w/v	PEG 8000
						20 % v/v	Glycerol
E12		None	0.1 M	Imidazole	8.0	10 % w/v	PEG 8000
F1	0.05 M	Cesium chloride	0.1 M	MES	6.5	30 % v/v	Jeffamine® M-600
F2	3.2 M	Ammonium sulfate	0.1 M	Citrate	5.0		None
F3		None	0.1 M	Tris	8.0	20 % v/v	MPD
F4		None	0.1 M	HEPES	7.5	20 % v/v	Jeffamine® M-600
F5	0.2 M	Magnesium chloride hexahydrate	0.1 M	Tris	8.5	50 % v/v	Ethylene glycol
F6		None	0.1 M	BICINE	9.0	10 % v/v	MPD
F7	0.8 M	Succinic acid pH 7.0		None			None
F8	2.1 M	DL-Malic acid pH 7.0		None			None
F9	2.4 M	Sodium malonate dibasic monohydrate pH 7.0		None			None
F10	1.1 M	Sodium malonate dibasic monohydrate	0.1 M	HEPES	7.0	0.5 % v/v	Jeffamine® ED-2003
F11	1.0 M	Succinic acid	0.1 M	HEPES	7.0	1 % w/v	PEG 2000 MME
F12		None	0.1 M	HEPES	7.0	30 % v/v	Jeffamine® M-600
G1		None	0.1 M	HEPES	7.0	30 % v/v	Jeffamine® ED-2003
G2	0.02 M	Magnesium chloride hexahydrate	0.1 M	HEPES	7.5	22 % w/v	Poly(acrylic acid sodium salt) 5100
G3	0.01 M	Cobalt(II) chloride hexahydrate	0.1 M	Tris	8.5	20 % w/v	Polyvinylpyrrolidone
G4	0.2 M	TMAO	0.1 M	Tris	8.5	20 % w/v	PEG 2000 MME
G5	0.005 M	Cobalt(II) chloride hexahydrate	0.1 M	HEPES	7.5	12 % w/v	PEG 3350
	0.005 M	Cadmium chloride hemi(pentahydrate)					
	0.005 M	Magnesium chloride hexahydrate					
	0.005 M	Nickel(II) chloride hexahydrate					
G6	0.2 M	Sodium malonate dibasic monohydrate		None		20 % w/v	PEG 3350
G7	0.1 M	Succinic acid		None		15 % w/v	PEG 3350
G8	0.15 M	DL-Malic acid		None		20 % w/v	PEG 3350
G9	0.1 M	Potassium thiocyanate		None		30 % w/v	PEG 2000 MME
G10	0.15 M	Potassium bromide		None		30 % w/v	PEG 2000 MME
G11	2.0 M	Ammonium sulfate	0.1 M	BIS-Tris	5.5		None
G12	3.0 M	Sodium chloride	0.1 M	BIS-Tris	5.5		None
H1	0.3 M	Magnesium formate dihydrate	0.1 M	BIS-Tris	5.5		None
H2	1.0 M	Ammonium sulfate	0.1 M	BIS-Tris	5.5	1 % w/v	PEG 3350
H3		None	0.1 M	BIS-Tris	5.5	25 % w/v	PEG 3350
H4	0.2 M	Calcium chloride dihydrate	0.1 M	BIS-Tris	5.5	45 % v/v	MPD
H5	0.2 M	Ammonium acetate	0.1 M	BIS-Tris	5.5	45 % v/v	MPD
H6	0.1 M	Ammonium acetate	0.1 M	BIS-Tris	5.5	17 % w/v	PEG 10,000
H7	0.2 M	Ammonium sulfate	0.1 M	BIS-Tris	5.5	25 % w/v	PEG 3350
H8	0.2 M	Sodium chloride	0.1 M	BIS-Tris	5.5	25 % w/v	PEG 3350
H9	0.2 M	Lithium sulfate	0.1 M	BIS-Tris	5.5	25 % w/v	PEG 3350
H10	0.2 M	Ammonium acetate	0.1 M	BIS-Tris	5.5	25 % w/v	PEG 3350
H11	0.2 M	Magnesium chloride hexahydrate	0.1 M	BIS-Tris	5.5	25 % w/v	PEG 3350
H12	0.2 M	Ammonium acetate	0.1 M	HEPES	7.5	45 % v/v	MPD

Abbreviations: Bis Tris; Bis-(2-hydroxyethyl)imino-tris(hydroxymethyl)methane, **CAPS**; N-Cyclohexyl-3-aminopropanesulfonic acid, **CHES**; 2-(N-Cyclohexylamino)ethane Sulfonic Acid, **HEPES;** 2-(4-(2-Hydroxyethyl)-1-piperazinyl)ethanesulfonic Acid, **Na HEPES**; 2-(4-(2-Hydroxyethyl)-1-piperazinyl)ethanesulfonic Acid Sodium Salt, **MES**; 2-(N-morpholino)ethanesulfonic acid, **MPD;** 2,4-methyl pentanediol, **PEG**; Polyethylene glycol (2K, 6K , 8K and 10K correspond to the molecular weight, in thousands of Daltons, of PEG), **TMAO:** Trimethylamine N-oxide, **Tris**; 2-Amino-2-(hydroxymethyl)propane-1,3-diol.

References

Abdul-Tehrani, H., A. J. Hudson, Y. S. Chang, A. R. Timms, C. Hawkins, J. M. Williams, P. M. Harrison, J. R. Guest and S. C. Andrews (1999). "Ferritin mutants of *Escherichia coli* are iron deficient and growth impaired, and *fur* mutants are iron deficient." J Bacteriol **181**(5): 1415-1428.

Agnoli, K., S. Schwager, S. Uehlinger, A. Vergunst, D. F. Viteri, D. T. Nguyen, P. A. Sokol, A. Carlier and L. Eberl (2012). "Exposing the third chromosome of *Burkholderia cepacia* complex strains as a virulence plasmid." Mol Microbiol **83**(2): 362-378.

Alcantara, R. B., R. D. Read, M. W. Valderas, T. D. Brown and R. M. Roop, 2nd (2004). "Intact purine biosynthesis pathways are required for wild-type virulence of *Brucella abortus* 2308 in the BALB/c mouse model." Infect Immun **72**(8): 4911-4917.

Alexander, B., P. R. Schnurrenberger and R. R. Brown (1981). "Numbers of *Brucella abortus* in the placenta, umbilicus and fetal fluid of two naturally infected cows." Vet Rec **108**(23): 500.

Almiron, M., M. Martinez, N. Sanjuan and R. A. Ugalde (2001). "Ferrochelatase is present in *Brucella abortus* and is critical for its intracellular survival and virulence." Infect Immun **69**(10): 6225-6230.

Almiron, M. A. and R. A. Ugalde (2010). "Iron homeostasis in *Brucella* abortus: the role of bacterioferritin." J Microbiol **48**(5): 668-673.

Anderson, E. S., J. T. Paulley, D. A. Martinson, J. M. Gaines, K. H. Steele and R. M. Roop, 2nd (2011). "The iron-responsive regulator irr is required for wild-type expression of the gene encoding the heme transporter BhuA in *Brucella abortus* 2308." J Bacteriol **193**(19): 5359-5364.

Anderson, T. D., N. F. Cheville and V. P. Meador (1986). "Pathogenesis of placentitis in the goat inoculated with *Brucella abortus*. II. Ultrastructural studies." Vet Pathol **23**(3): 227-239.

Andrews, S. C. (2010). "The Ferritin-like superfamily: Evolution of the biological iron storeman from a rubrerythrin-like ancestor." Biochim Biophys Acta **1800**(8): 691-705.

Angerer, A., B. Klupp and V. Braun (1992). "Iron transport systems of *Serratia marcescens.*" J Bacteriol **174**(4): 1378-1387.

Ashford, D. A., J. di Pietra, J. Lingappa, C. Woods, H. Noll, B. Neville, R. Weyant, S. L. Bragg, R. A. Spiegel, J. Tappero and B. A. Perkins (2004). "Adverse events in humans associated with accidental exposure to the livestock brucellosis vaccine RB51." Vaccine

22(25-26): 3435-3439.

Atkinson, P. G. and C. H. Barton (1998). "Ectopic expression of Nramp1 in COS-1 cells modulates iron accumulation." FEBS Lett **425**(2): 239-242.

Atkinson, P. G. and C. H. Barton (1999). "High level expression of Nramp1G169 in RAW264.7 cell transfectants: analysis of intracellular iron transport." Immunology **96**(4): 656-662.

Baldwin, C. L., X. Jiang and D. M. Fernandes (1993). "Macrophage control of *Brucella abortus*: influence of cytokines and iron." Trends Microbiol **1**(3): 99-104.

Beckett, F. W. and S. C. MacDiarmid (1985). "The effect of reduced-dose *Brucella abortus* strain 19 vaccination in accredited dairy herds." Br Vet J **141**(5): 507-514.

Beckman, J. S. and W. H. Koppenol (1996). "Nitric oxide, superoxide, and peroxynitrite: the good, the bad, and ugly." Am J Physiol **271**(5 Pt 1): C1424-1437.

Bellaire, B. H., P. H. Elzer, C. L. Baldwin and R. M. Roop, 2nd (1999). "The siderophore 2,3-dihydroxybenzoic acid is not required for virulence of *Brucella abortus* in BALB/c mice." Infect Immun **67**(5): 2615-2618.

Bellaire, B. H., R. M. Roop, 2nd and J. A. Cardelli (2005). "Opsonized virulent *Brucella abortus* replicates within nonacidic, endoplasmic reticulum-negative, LAMP-1-positive phagosomes in human monocytes." Infect Immun **73**(6): 3702-3713.

Bhubhanil, S., J. Chamsing, P. Sittipo, P. Chaoprasid, R. Sukchawalit and S. Mongkolsuk (2014). "Roles of *Agrobacterium tumefaciens* membrane-bound ferritin (MbfA) in iron transport and resistance to iron under acidic conditions." Microbiology **160**: 863-871.

Blackwell, J. M. (2001). "Genetics and genomics in infectious disease susceptibility." Trends Mol Med **7**(11): 521-526.

Blackwell, J. M., S. Searle, T. Goswami and E. N. Miller (2000). "Understanding the multiple functions of Nramp1." Microbes Infect **2**(3): 317-321.

Blasco, J. M. and R. Diaz (1993). "*Brucella melitensis* Rev-1 vaccine as a cause of human brucellosis." Lancet **342**(8874): 805.

Boschiroli, M. L., S. Ouahrani-Bettache, V. Foulongne, S. Michaux-Charachon, G. Bourg, A. Allardet-Servent, C. Cazevieille, J. P. Liautard, M. Ramuz and D. O'Callaghan (2002). "The *Brucella suis virB* operon is induced intracellularly in macrophages." Proc Natl Acad Sci U S A **99**(3): 1544-1549.

Braude, A. I. and W. W. Spink (1951). "Studies in the pathology and pathogenesis of experimental brucellosis. III. Investigations pertaining to the function of the spleen." J Infect Dis **89**(3): 272-276.

Brickman, T. J. and S. K. Armstrong (2012). "Iron and pH-responsive FtrABCD ferrous iron

utilization system of *Bordetella* species." Mol Microbiol **86**(3): 580-593.

Brown, G. C. (1995). "Reversible binding and inhibition of catalase by nitric oxide." Eur J Biochem **232**(1): 188-191.

Burkhardt, S., M. P. Jimenez de Bagues, J. P. Liautard and S. Kohler (2005). "Analysis of the behavior of *eryC* mutants of *Brucella suis* attenuated in macrophages." Infect Immun **73**(10): 6782-6790.

Byndloss, M. X. and R. M. Tsolis (2016). "*Brucella* spp. Virulence Factors and Immunity." Annu Rev Anim Biosci **4**: 111-127.

Byrd, T. F. and M. A. Horwitz (1989). "Interferon gamma-activated human monocytes downregulate transferrin receptors and inhibit the intracellular multiplication of *Legionella pneumophila* by limiting the availability of iron." J Clin Invest **83**(5): 1457-1465.

Cao, J., M. R. Woodhall, J. Alvarez, M. L. Cartron and S. C. Andrews (2007). "EfeUOB (YcdNOB) is a tripartite, acid-induced and CpxAR-regulated, low-pH Fe^{2+} transporter that is cryptic in *Escherichia coli* K-12 but functional in *E. coli* O157:H7." Mol Microbiol **65**(4): 857-875.

Carrica Mdel, C., I. Fernandez, R. Sieira, G. Paris and F. A. Goldbaum (2013). "The two-component systems PrrBA and NtrYX co-ordinately regulate the adaptation of *Brucella abortus* to an oxygen-limited environment." Mol Microbiol **88**(2): 222-233.

Celli, J., C. de Chastellier, D. M. Franchini, J. Pizarro-Cerda, E. Moreno and J. P. Gorvel (2003). "*Brucella* evades macrophage killing via VirB-dependent sustained interactions with the endoplasmic reticulum." J Exp Med **198**(4): 545-556.

Cheers, C. and R. E. Cone (1974). "Effect of polyadenine: polyuridine on brucellosis in conventional and congenitally athymic mice." J Immunol **112**(4): 1535-1539.

Cockrell, A., S. P. McCormick, M. J. Moore, M. Chakrabarti and P. A. Lindahl (2014). "Mossbauer, EPR, and modeling study of iron trafficking and regulation in Delta *ccc1* and CCC1-up *Saccharomyces cerevisiae*." Biochemistry **53**(18): 2926-2940.

Cooper, C. E. (1999). "Nitric oxide and iron proteins." Biochim Biophys Acta **1411**(2-3): 290-309.

Delrue, R. M., M. Martinez-Lorenzo, P. Lestrate, I. Danese, V. Bielarz, P. Mertens, X. De Bolle, A. Tibor, J. P. Gorvel and J. J. Letesson (2001). "Identification of *Brucella* spp. genes involved in intracellular trafficking." Cell Microbiol **3**(7): 487-497.

DelVecchio, V. G., V. Kapatral, R. J. Redkar, G. Patra, C. Mujer, T. Los, N. Ivanova, I. Anderson, A. Bhattacharyya, A. Lykidis, G. Reznik, L. Jablonski, N. Larsen, M. D'Souza, A. Bernal, M. Mazur, E. Goltsman, E. Selkov, P. H. Elzer, S. Hagius, D.

O'Callaghan, J. J. Letesson, R. Haselkorn, N. Kyrpides and R. Overbeek (2002). "The genome sequence of the facultative intracellular pathogen *Brucella melitensis*." Proc Natl Acad Sci U S A **99**(1): 443-448.

den Hartigh, A. B., Y. H. Sun, D. Sondervan, N. Heuvelmans, M. O. Reinders, T. A. Ficht and R. M. Tsolis (2004). "Differential requirements for VirB1 and VirB2 during *Brucella abortus* infection." Infect Immun **72**(9): 5143-5149.

Elberg, S. S. and K. Faunce, Jr. (1957). "Immunization against *Brucella* infection. VI. Immunity conferred on goats by a nondependent mutant from a streptomycin-dependent mutant strain of *Brucella melitensis*." J Bacteriol **73**(2): 211-217.

Elhassanny, A. E., E. S. Anderson, E. A. Menscher and R. M. Roop, 2nd (2013). "The ferrous iron transporter FtrABCD is required for the virulence of *Brucella abortus* 2308 in mice." Mol Microbiol **88**(6): 1070-1082.

Elzer, P. H., M. E. Kovach, R. W. Phillips, G. T. Robertson, K. M. Peterson and R. M. Roop, 2nd (1995). "*In vivo* and *in vitro* stability of the broad-host-range cloning vector pBBR1MCS in six *Brucella* species." Plasmid **33**(1): 51-57.

Enright, F. M., L. N. Araya, P. H. Elzer, G. E. Rowe and A. J. Winter (1990). "Comparative histopathology in BALB/c mice infected with virulent and attenuated strains of *Brucella abortus*." Vet Immunol Immunopathol **26**(2): 171-182.

Fang, F. C. (2004). "Antimicrobial reactive oxygen and nitrogen species: concepts and controversies." Nat Rev Microbiol **2**(10): 820-832.

Fellay, R., J. Frey and H. Krisch (1987). "Interposon mutagenesis of soil and water bacteria: a family of DNA fragments designed for *in vitro* insertional mutagenesis of gram-negative bacteria." Gene **52**(2-3): 147-154.

Ferguson, G. P., A. Datta, J. Baumgartner, R. M. Roop, 2nd, R. W. Carlson and G. C. Walker (2004). "Similarity to peroxisomal-membrane protein family reveals that *Sinorhizobium* and *Brucella* BacA affect lipid-A fatty acids." Proc Natl Acad Sci U S A **101**(14): 5012-5017.

Forbes, J. R. and P. Gros (2001). "Divalent-metal transport by NRAMP proteins at the interface of host-pathogen interactions." Trends Microbiol **9**(8): 397-403.

Foulongne, V., K. Walravens, G. Bourg, M. L. Boschiroli, J. Godfroid, M. Ramuz and D. O'Callaghan (2001). "Aromatic compound-dependent *Brucella suis* is attenuated in both cultured cells and mouse models." Infect Immun **69**(1): 547-550.

Franz, D. R., C. D. Parrott, and E. T. Takafuji (1997). "The US biological warfare and biological defense programs." Medical aspects of chemical and biological warfare 426.

Frawley, E. R., M. L. Crouch, L. K. Bingham-Ramos, H. F. Robbins, W. Wang, G. D. Wright

and F. C. Fang (2013). "Iron and citrate export by a major facilitator superfamily pump regulates metabolism and stress resistance in *Salmonella* Typhimurium." Proc Natl Acad Sci U S A **110**(29): 12054-12059.

Fritsche, G., M. Nairz, S. J. Libby, F. C. Fang and G. Weiss (2012). "Slc11a1 (Nramp1) impairs growth of *Salmonella enterica* serovar typhimurium in macrophages via stimulation of lipocalin-2 expression." J Leukoc Biol **92**(2): 353-359.

Garcia-del Portillo, F., J. W. Foster, M. E. Maguire and B. B. Finlay (1992). "Characterization of the micro-environment of *Salmonella* typhimurium-containing vacuoles within MDCK epithelial cells." Mol Microbiol **6**(22): 3289-3297.

Garg, R. P., C. J. Vargo, X. Cui and D. M. Kurtz, Jr. (1996). "A [2Fe-2S] protein encoded by an open reading frame upstream of the *Escherichia coli* bacterioferritin gene." Biochemistry **35**(20): 6297-6301.

Gee, J. M., M. E. Kovach, V. K. Grippe, S. Hagius, J. V. Walker, P. H. Elzer and R. M. Roop, 2nd (2004). "Role of catalase in the virulence of *Brucella melitensis* in pregnant goats." Vet Microbiol **102**(1-2): 111-115.

Gee, J. M., M. W. Valderas, M. E. Kovach, V. K. Grippe, G. T. Robertson, W. L. Ng, J. M. Richardson, M. E. Winkler and R. M. Roop, 2nd (2005). "The *Brucella abortus* Cu,Zn superoxide dismutase is required for optimal resistance to oxidative killing by murine macrophages and wild-type virulence in experimentally infected mice." Infect Immun **73**(5): 2873-2880.

Gibson, D. G., L. Young, R. Y. Chuang, J. C. Venter, C. A. Hutchison, 3rd and H. O. Smith (2009). "Enzymatic assembly of DNA molecules up to several hundred kilobases." Nat Methods **6**(5): 343-345.

Gomes, M. S. and R. Appelberg (1998). "Evidence for a link between iron metabolism and Nramp1 gene function in innate resistance against *Mycobacterium avium*." Immunology **95**(2): 165-168.

Gonzalez Carrero, M. I., F. J. Sangari, J. Aguero and J. M. Garcia Lobo (2002). "*Brucella abortus* strain 2308 produces brucebactin, a highly efficient catecholic siderophore." Microbiology **148**(Pt 2): 353-360.

Grass, G., M. Otto, B. Fricke, C. J. Haney, C. Rensing, D. H. Nies and D. Munkelt (2005). "FieF (YiiP) from *Escherichia coli* mediates decreased cellular accumulation of iron and relieves iron stress." Arch Microbiol **183**(1): 9-18.

Griggs, D. W., B. B. Tharp and J. Konisky (1987). "Cloning and promoter identification of the iron-regulated cir gene of *Escherichia coli*." J Bacteriol **169**(12): 5343-5352.

Grillo, M. J., J. M. Blasco, J. P. Gorvel, I. Moriyon and E. Moreno (2012). "What have we

learned from brucellosis in the mouse model?" Vet Res **43**: 29.

Groftehauge, M. K., N. R. Hajizadeh, M. J. Swann and E. Pohl (2015). "Protein-ligand interactions investigated by thermal shift assays (TSA) and dual polarization interferometry (DPI)." Acta Crystallogr D Biol Crystallogr **71**(Pt 1): 36-44.

Gross, A., S. Bertholet, J. Mauel and J. Dornand (2004). "Impairment of *Brucella* growth in human macrophagic cells that produce nitric oxide." Microb Pathog **36**(2): 75-82.

Guan, G., A. Pinochet-Barros, A. Gaballa, S. J. Patel, J. M. Arguello and J. D. Helmann (2015). "PfeT, a P1B4 -type ATPase, effluxes ferrous iron and protects *Bacillus subtilis* against iron intoxication." Mol Microbiol **98**(4): 787-803.

Guilloteau, L. A., J. Dornand, A. Gross, M. Olivier, F. Cortade, Y. L. Vern and D. Kerboeuf (2003). "Nramp1 is not a major determinant in the control of *Brucella melitensis* infection in mice." Infect Immun **71**(2): 621-628.

Gupta, N., F. Bonomi, D. M. Kurtz, Jr., N. Ravi, D. L. Wang and B. H. Huynh (1995). "Recombinant *Desulfovibrio vulgaris* rubrerythrin. Isolation and characterization of the diiron domain." Biochemistry **34**(10): 3310-3318.

Halling, S. M., B. D. Peterson-Burch, B. J. Bricker, R. L. Zuerner, Z. Qing, L. L. Li, V. Kapur, D. P. Alt and S. C. Olsen (2005). "Completion of the genome sequence of *Brucella abortus* and comparison to the highly similar genomes of *Brucella melitensis* and *Brucella suis*." J Bacteriol **187**(8): 2715-2726.

Hamza, I., S. Chauhan, R. Hassett and M. R. O'Brian (1998). "The bacterial irr protein is required for coordination of heme biosynthesis with iron availability." J Biol Chem **273**(34): 21669-21674.

Hanot Mambres, D., A. Machelart, J. M. Vanderwinden, C. De Trez, B. Ryffel, J. J. Letesson and E. Muraille (2015). "In Situ Characterization of Splenic *Brucella melitensis* Reservoir Cells during the Chronic Phase of Infection in Susceptible Mice." PLoS One **10**(9): e0137835.

Hantke, K. (1990). "Dihydroxybenzoylserine--a siderophore for *E. coli*." FEMS Microbiol Lett **55**(1-2): 5-8.

High, K. P., R. Prasad, C. R. Marion, G. G. Schurig, S. M. Boyle and N. Sriranganathan (2007). "Outcome and immune responses after *Brucella abortus* infection in young adult and aged mice." Biogerontology **8**(5): 583-593.

Hoshino, M., K. Ozawa, H. Seki and P. C. Ford (1993). "Photochemistry of nitric oxide adducts of water-soluble iron(III) porphyrin and ferrihemoproteins studied by nanosecond laser photolysis." Journal of the American Chemical Society **115**(21): 9568-9575.

Irving, H. and R. J. P. Williams (1953). "637. The stability of transition-metal complexes." Journal of the Chemical Society (Resumed)(0): 3192-3210.

Jaggavarapu, S. and M. R. O'Brian (2014). "Differential control of *Bradyrhizobium japonicum* iron stimulon genes through variable affinity of the iron response regulator (Irr) for target gene promoters and selective loss of activator function." Mol Microbiol **92**(3): 609-624.

Jiang, X., B. Leonard, R. Benson and C. L. Baldwin (1993). "Macrophage control of *Brucella abortus*: role of reactive oxygen intermediates and nitric oxide." Cell Immunol **151**(2): 309-319.

Kall, L., A. Krogh and E. L. Sonnhammer (2004). "A combined transmembrane topology and signal peptide prediction method." J Mol Biol **338**(5): 1027-1036.

Kaufmann, A. F., M. I. Meltzer and G. P. Schmid (1997). "The economic impact of a bioterrorist attack: are prevention and postattack intervention programs justifiable?" Emerg Infect Dis **3**(2): 83-94.

Ke, Y., X. Yuan, Y. Wang, Y. Bai, J. Xu, H. Song, L. Huang and Z. Chen (2012). "Genome sequences of *Brucella melitensis* 16M and its two derivatives 16M1w and 16M13w, which evolved in vivo." J Bacteriol **194**(19): 5489.

Ke, Y., X. Yuan, Q. Zhen, Y. Wang, T. Li, Y. Sun, H. Song, L. Huang, D. Wang, B. Cui, K. Mao and Z. Chen (2012). "Genome sequence of *Brucella melitensis* S66, an isolate of sequence type 8, prevalent in China." J Bacteriol **194**(19): 5451.

Keith, K. E., D. W. Hynes, J. E. Sholdice and M. A. Valvano (2009). "Delayed association of the NADPH oxidase complex with macrophage vacuoles containing the opportunistic pathogen *Burkholderia cenocepacia*." Microbiology **155**(Pt 4): 1004-1015.

Kelley, L. A. and M. J. Sternberg (2009). "Protein structure prediction on the Web: a case study using the Phyre server." Nat Protoc **4**(3): 363-371.

Kim, S. A., T. Punshon, A. Lanzirotti, L. Li, J. M. Alonso, J. R. Ecker, J. Kaplan and M. L. Guerinot (2006). "Localization of iron in *Arabidopsis* seed requires the vacuolar membrane transporter VIT1." Science **314**(5803): 1295-1298.

Ko, J. and G. A. Splitter (2003). "Molecular host-pathogen interaction in brucellosis: current understanding and future approaches to vaccine development for mice and humans." Clin Microbiol Rev **16**(1): 65-78.

Koppenol, W. H. (2001). "The Haber-Weiss cycle--70 years later." Redox Rep **6**(4): 229-234.

Koster, W. L., L. A. Actis, L. S. Waldbeser, M. E. Tolmasky and J. H. Crosa (1991). "Molecular characterization of the iron transport system mediated by the pJM1 plasmid in *Vibrio anguillarum* 775." J Biol Chem **266**(35): 23829-23833.

Latimer, E., J. Simmers, N. Sriranganathan, R. M. Roop, 2nd, G. G. Schurig and S. M. Boyle (1992). "*Brucella abortus* deficient in copper/zinc superoxide dismutase is virulent in BALB/c mice." Microb Pathog **12**(2): 105-113.

Le Brun, N. E., S. C. Andrews, G. R. Moore and A. J. Thomson (1997). "Interaction of nitric oxide with non-haem iron sites of *Escherichia coli* bacterioferritin: reduction of nitric oxide to nitrous oxide and oxidation of iron(II) to iron(III)." Biochemical Journal **326**(Pt 1): 173-179.

Lestrate, P., R. M. Delrue, I. Danese, C. Didembourg, B. Taminiau, P. Mertens, X. De Bolle, A. Tibor, C. M. Tang and J. J. Letesson (2000). "Identification and characterization of *in vivo* attenuated mutants of *Brucella melitensis*." Mol Microbiol **38**(3): 543-551.

Li, L., O. S. Chen, D. McVey Ward and J. Kaplan (2001). "CCC1 is a transporter that mediates vacuolar iron storage in yeast." J Biol Chem **276**(31): 29515-29519.

Liu, M. and F. Biville (2013). "Managing iron supply during the infection cycle of a flea borne pathogen, *Bartonella henselae*." Front Cell Infect Microbiol **3**: 60.

Lopez-Goni, I., I. Moriyon and J. B. Neilands (1992). "Identification of 2,3-dihydroxybenzoic acid as a *Brucella abortus* siderophore." Infect Immun **60**(11): 4496-4503.

Lown, J. W. (1983). "The mechanism of action of quinone antibiotics." Mol Cell Biochem **55**(1): 17-40.

Lumppio, H. L., N. V. Shenvi, A. O. Summers, G. Voordouw and D. M. Kurtz, Jr. (2001). "Rubrerythrin and rubredoxin oxidoreductase in *Desulfovibrio vulgaris*: a novel oxidative stress protection system." J Bacteriol **183**(1): 101-108.

Martin, D. W., J. E. Baumgartner, J. M. Gee, E. S. Anderson and R. M. Roop, 2nd (2012). "SodA is a major metabolic antioxidant in *Brucella abortus* 2308 that plays a significant, but limited, role in the virulence of this strain in the mouse model." Microbiology **158**(Pt 7): 1767-1774.

Martinez, M., R. A. Ugalde and M. Almiron (2005). "Dimeric *Brucella* abortus Irr protein controls its own expression and binds haem." Microbiology **151**(Pt 10): 3427-3433.

Martinez, M., R. A. Ugalde and M. Almiron (2006). "Irr regulates brucebactin and 2,3-dihydroxybenzoic acid biosynthesis, and is implicated in the oxidative stress resistance and intracellular survival of *Brucella abortus*." Microbiology **152**(Pt 9): 2591-2598.

Martinez-Guerrero, C. E., R. Ciria, C. Abreu-Goodger, G. Moreno-Hagelsieb and E. Merino (2008). "GeConT 2: gene context analysis for orthologous proteins, conserved domains and metabolic pathways." Nucleic Acids Res **36**(Web Server issue): W176-180.

Masse, E. and S. Gottesman (2002). "A small RNA regulates the expression of genes involved in iron metabolism in *Escherichia coli*." Proc Natl Acad Sci U S A **99**(7): 4620-4625.

Mastroeni, P., A. Vazquez-Torres, F. C. Fang, Y. Xu, S. Khan, C. E. Hormaeche and G. Dougan (2000). "Antimicrobial actions of the NADPH phagocyte oxidase and inducible nitric oxide synthase in experimental salmonellosis. II. Effects on microbial proliferation and host survival in vivo." J Exp Med **192**(2): 237-248.

McHugh, J. P., F. Rodriguez-Quinones, H. Abdul-Tehrani, D. A. Svistunenko, R. K. Poole, C. E. Cooper and S. C. Andrews (2003). "Global iron-dependent gene regulation in *Escherichia coli*. A new mechanism for iron homeostasis." J Biol Chem **278**(32): 29478-29486.

Miller, B. H., R. A. Fratti, J. F. Poschet, G. S. Timmins, S. S. Master, M. Burgos, M. A. Marletta and V. Deretic (2004). "*Mycobacteria* inhibit nitric oxide synthase recruitment to phagosomes during macrophage infection." Infect Immun **72**(5): 2872-2878.

Mills, M. and S. M. Payne (1997). "Identification of *shuA*, the gene encoding the heme receptor of *Shigella dysenteriae*, and analysis of invasion and intracellular multiplication of a *shuA* mutant." Infect Immun **65**(12): 5358-5363.

Nairz, M., G. Fritsche, P. Brunner, H. Talasz, K. Hantke and G. Weiss (2008). "Interferon-gamma limits the availability of iron for intramacrophage *Salmonella* typhimurium." Eur J Immunol **38**(7): 1923-1936.

Nandal, A., C. C. Huggins, M. R. Woodhall, J. McHugh, F. Rodriguez-Quinones, M. A. Quail, J. R. Guest and S. C. Andrews (2010). "Induction of the ferritin gene (*ftnA*) of *Escherichia coli* by $Fe^{(2+)}$-Fur is mediated by reversal of H-NS silencing and is RyhB independent." Mol Microbiol **75**(3): 637-657.

Nijssen, E., S. Cescau, M. Vayssier-Taussat, J. Wang and F. Biville (2009). "Identification of mechanisms involved in iron and haem uptake in *Bartonella birtlesii*: *in silico* and *in vivo* approaches." Clin Microbiol Infect **15 Suppl 2**: 118-119.

Nordlund, P. and H. Eklund (1995). "Di-iron-carboxylate proteins." Curr Opin Struct Biol **5**(6): 758-766.

Nymo, I. H., M. A. Arias, J. Pardo, M. P. Alvarez, A. Alcaraz, J. Godfroid and M. P. Jimenez de Bagues (2016). "Marine Mammal *Brucella* Reference Strains Are Attenuated in a BALB/c Mouse Model." PLoS One **11**(3): e0150432.

O'Callaghan, D., C. Cazevieille, A. Allardet-Servent, M. L. Boschiroli, G. Bourg, V. Foulongne, P. Frutos, Y. Kulakov and M. Ramuz (1999). "A homologue of the *Agrobacterium tumefaciens* VirB and *Bordetella pertussis* Ptl type IV secretion systems is essential for intracellular survival of *Brucella suis*." Mol Microbiol **33**(6): 1210-1220.

O'Donnell, S. M. and G. R. Janssen (2001). "The initiation codon affects ribosome binding and translational efficiency in *Escherichia coli* of cI mRNA with or without the 5'

untranslated leader." J Bacteriol **183**(4): 1277-1283.

Ojeda, J. F., D. A. Martinson, E. A. Menscher and R. M. Roop, 2nd (2012). "The *bhuQ* gene encodes a heme oxygenase that contributes to the ability of *Brucella abortus* 2308 to use heme as an iron source and is regulated by Irr." J Bacteriol **194**(15): 4052-4058.

Olsen, S. C. and S. A. Carlson (2015). "*In vitro* bactericidal activity of aminoglycosides, including the next-generation drug plazomicin, against *Brucella* spp." Int J Antimicrob Agents **45**(1): 76-78.

Olsen, S. C. and S. G. Hennager (2010). "Immune responses and protection against experimental *Brucella suis* biovar 1 challenge in nonvaccinated or *B. abortus* strain RB51-vaccinated cattle." Clin Vaccine Immunol **17**(12): 1891-1895.

Pacelli, R., D. A. Wink, J. A. Cook, M. C. Krishna, W. DeGraff, N. Friedman, M. Tsokos, A. Samuni and J. B. Mitchell (1995). "Nitric oxide potentiates hydrogen peroxide-induced killing of *Escherichia col*i." J Exp Med **182**(5): 1469-1479.

Pardon, P. and J. Marly (1976). "Resistance of *Brucella abortus* infected mice to intravenous or intraperitoneal *Brucella* reinfection." Ann Immunol (Paris) **127**(1): 57-70.

Paulley, J. T., E. S. Anderson and R. M. Roop, 2nd (2007). "*Brucella abortus* requires the heme transporter BhuA for maintenance of chronic infection in BALB/c mice." Infect Immun **75**(11): 5248-5254.

Paulsen, I. T., R. Seshadri, K. E. Nelson, J. A. Eisen, J. F. Heidelberg, T. D. Read, R. J. Dodson, L. Umayam, L. M. Brinkac, M. J. Beanan, S. C. Daugherty, R. T. Deboy, A. S. Durkin, J. F. Kolonay, R. Madupu, W. C. Nelson, B. Ayodeji, M. Kraul, J. Shetty, J. Malek, S. E. Van Aken, S. Riedmuller, H. Tettelin, S. R. Gill, O. White, S. L. Salzberg, D. L. Hoover, L. E. Lindler, S. M. Halling, S. M. Boyle and C. M. Fraser (2002). "The *Brucella suis* genome reveals fundamental similarities between animal and plant pathogens and symbionts." Proc Natl Acad Sci U S A **99**(20): 13148-13153.

Pericone, C. D., K. Overweg, P. W. Hermans and J. N. Weiser (2000). "Inhibitory and bactericidal effects of hydrogen peroxide production by *Streptococcus pneumoniae* on other inhabitants of the upper respiratory tract." Infect Immun **68**(7): 3990-3997.

Pi, H., S. J. Patel, J. M. Arguello and J. D. Helmann (2016). "The *Listeria monocytogenes* Fur-regulated virulence protein FrvA is an Fe(II) efflux P1B4 -type ATPase." Mol Microbiol **100**(6): 1066-1079.

Pizarro-Cerda, J., S. Meresse, R. G. Parton, G. van der Goot, A. Sola-Landa, I. Lopez-Goni, E. Moreno and J. P. Gorvel (1998). "*Brucella abortus* transits through the autophagic pathway and replicates in the endoplasmic reticulum of nonprofessional phagocytes." Infect Immun **66**(12): 5711-5724.

Pizarro-Cerda, J., E. Moreno, V. Sanguedolce, J. L. Mege and J. P. Gorvel (1998). "Virulent *Brucella abortus* prevents lysosome fusion and is distributed within autophagosome-like compartments." Infect Immun **66**(5): 2387-2392.

Pope, C. D., W. O'Connell and N. P. Cianciotto (1996). "*Legionella pneumophila* mutants that are defective for iron acquisition and assimilation and intracellular infection." Infect Immun **64**(2): 629-636.

Porte, F., J. P. Liautard and S. Kohler (1999). "Early acidification of phagosomes containing *Brucella suis* is essential for intracellular survival in murine macrophages." Infect Immun **67**(8): 4041-4047.

Qi, Z. and M. R. O'Brian (2002). "Interaction between the bacterial iron response regulator and ferrochelatase mediates genetic control of heme biosynthesis." Mol Cell **9**(1): 155-162.

Quail, M. A., P. Jordan, J. M. Grogan, J. N. Butt, M. Lutz, A. J. Thomson, S. C. Andrews and J. R. Guest (1996). "Spectroscopic and voltammetric characterisation of the bacterioferritin-associated ferredoxin of *Escherichia coli.*" Biochem Biophys Res Commun **229**(2): 635-642.

Radi, R., J. S. Beckman, K. M. Bush and B. A. Freeman (1991). "Peroxynitrite-induced membrane lipid peroxidation: the cytotoxic potential of superoxide and nitric oxide." Arch Biochem Biophys **288**(2): 481-487.

Ratledge, C. and L. G. Dover (2000). "Iron metabolism in pathogenic bacteria." Annu Rev Microbiol **54**: 881-941.

Ravi, N., B. C. Prickril, D. M. Kurtz, Jr. and B. H. Huynh (1993). "Spectroscopic characterization of ^{57}Fe-reconstituted rubrerythrin, a non-heme iron protein with structural analogies to ribonucleotide reductase." Biochemistry **32**(33): 8487-8491.

Rodionov, D. A., M. S. Gelfand, J. D. Todd, A. R. Curson and A. W. Johnston (2006). "Computational reconstruction of iron- and manganese-responsive transcriptional networks in alpha-proteobacteria." PLoS Comput Biol **2**(12): e163.

Roop, R. M., 2nd, J. M. Gaines, E. S. Anderson, C. C. Caswell and D. W. Martin (2009). "Survival of the fittest: how *Brucella* strains adapt to their intracellular niche in the host." Med Microbiol Immunol **198**(4): 221-238.

Ruangkiattikul, N., S. Bhubhanil, J. Chamsing, P. Niamyim, R. Sukchawalit and S. Mongkolsuk (2012). "*Agrobacterium tumefaciens* membrane-bound ferritin plays a role in protection against hydrogen peroxide toxicity and is negatively regulated by the iron response regulator." FEMS Microbiol Lett **329**(1): 87-92.

Rudolph, G., H. Hennecke and H. M. Fischer (2006). "Beyond the Fur paradigm: iron-controlled gene expression in rhizobia." FEMS Microbiol Rev **30**(4): 631-648.

Rudolph, G., G. Semini, F. Hauser, A. Lindemann, M. Friberg, H. Hennecke and H. M. Fischer (2006). "The Iron control element, acting in positive and negative control of iron-regulated *Bradyrhizobium japonicum* genes, is a target for the Irr protein." J Bacteriol **188**(2): 733-744.

Salcedo, S. P., N. Chevrier, T. L. Lacerda, A. Ben Amara, S. Gerart, V. A. Gorvel, C. de Chastellier, J. M. Blasco, J. L. Mege and J. P. Gorvel (2013). "Pathogenic brucellae replicate in human trophoblasts." J Infect Dis **207**(7): 1075-1083.

Sankari, S. and M. R. O'Brian (2014). "A bacterial iron exporter for maintenance of iron homeostasis." J Biol Chem **289**(23): 16498-16507.

Seaver, L. C. and J. A. Imlay (2004). "Are respiratory enzymes the primary sources of intracellular hydrogen peroxide?" J Biol Chem **279**(47): 48742-48750.

Sha, Z., T. J. Stabel and J. E. Mayfield (1994). "*Brucella abortus* catalase is a periplasmic protein lacking a standard signal sequence." J Bacteriol **176**(23): 7375-7377.

Shea, C. M. and M. A. McIntosh (1991). "Nucleotide sequence and genetic organization of the ferric enterobactin transport system: homology to other periplasmic binding protein-dependent systems in *Escherichia coli*." Mol Microbiol **5**(6): 1415-1428.

Sieira, R., D. J. Comerci, L. I. Pietrasanta and R. A. Ugalde (2004). "Integration host factor is involved in transcriptional regulation of the *Brucella abortus virB* operon." Mol Microbiol **54**(3): 808-822.

Slauch, J. M. (2011). "How does the oxidative burst of macrophages kill bacteria? Still an open question." Mol Microbiol **80**(3): 580-583.

Slavic, K. and S. Krishna (2016). "A vacuolar iron-transporter homologue acts as a detoxifier in *Plasmodium*." Nature Comm. **7**: 10403.

Smith, H., A. E. Williams, J. H. Pearce, J. Keppie, P. W. Harris-Smith, R. B. Fitz-George and K. Witt (1962). "Foetal erythritol: a cause of the localization of *Brucella abortus* in bovine contagious abortion." Nature **193**: 47-49.

Smith, L. D. and T. A. Ficht (1990). "Pathogenesis of *Brucella*." Crit Rev Microbiol **17**(3): 209-230.

Sperry, J. F. and D. C. Robertson (1975). "Erythritol catabolism by *Brucella abortus*." J Bacteriol **121**(2): 619-630.

Sriranganathan, N., S. M. Boyle, G. Schurig and H. Misra (1991). "Superoxide dismutases of virulent and avirulent strains of *Brucella abortus*." Vet Microbiol **26**(4): 359-366.

Stabel, T. J., Z. Sha and J. E. Mayfield (1994). "Periplasmic location of *Brucella abortus* Cu/Zn superoxide dismutase." Vet Microbiol **38**(4): 307-314.

Starr, T., T. W. Ng, T. D. Wehrly, L. A. Knodler and J. Celli (2008). "*Brucella* intracellular

replication requires trafficking through the late endosomal/lysosomal compartment." Traffic **9**(5): 678-694.

Steele, K. H., J. E. Baumgartner, M. W. Valderas and R. M. Roop, 2nd (2010). "Comparative study of the roles of AhpC and KatE as respiratory antioxidants in *Brucella abortus* 2308." J Bacteriol **192**(19): 4912-4922.

Stephens, D. L., M. D. Choe and C. F. Earhart (1995). "*Escherichia coli* periplasmic protein FepB binds ferrienterobactin." Microbiology **141 (Pt 7)**: 1647-1654.

Tan, K. K., Y. C. Tan, L. Y. Chang, K. W. Lee, S. S. Nore, W. Y. Yee, M. N. Mat Isa, F. L. Jafar, C. C. Hoh and S. AbuBakar (2015). "Full genome SNP-based phylogenetic analysis reveals the origin and global spread of *Brucella melitensis*." BMC Genomics **16**: 93.

Tatum, F. M., P. G. Detilleux, J. M. Sacks and S. M. Halling (1992). "Construction of Cu-Zn superoxide dismutase deletion mutants of *Brucella abortus*: analysis of survival *in vitro* in epithelial and phagocytic cells and *in vivo* in mice." Infect Immun **60**(7): 2863-2869.

Thompson, J. M., H. A. Jones and R. D. Perry (1999). "Molecular characterization of the hemin uptake locus (*hmu*) from *Yersinia pestis* and analysis of hmu mutants for hemin and hemoprotein utilization." Infect Immun **67**(8): 3879-3892.

Vazquez-Torres, A., J. Jones-Carson, P. Mastroeni, H. Ischiropoulos and F. C. Fang (2000). "Antimicrobial actions of the NADPH phagocyte oxidase and inducible nitric oxide synthase in experimental salmonellosis. I. Effects on microbial killing by activated peritoneal macrophages *in vitro*." J Exp Med **192**(2): 227-236.

Winstedt, L. and C. von Wachenfeldt (2000). "Terminal oxidases of *Bacillus subtilis* strain 168: one quinol oxidase, cytochrome aa(3) or cytochrome bd, is required for aerobic growth." J Bacteriol **182**(23): 6557-6564.

Winterbourn, C. C., M. B. Hampton, J. H. Livesey and A. J. Kettle (2006). "Modeling the Reactions of Superoxide and Myeloperoxidase in the Neutrophil Phagosome: Implications for microbial killing." Journal of Biological Chemistry **281**(52): 39860-39869.

Woodmansee, A. N. and J. A. Imlay (2003). "A mechanism by which nitric oxide accelerates the rate of oxidative DNA damage in *Escherichia coli*." Mol Microbiol **49**(1): 11-22.

Wyckoff, E. E., D. Duncan, A. G. Torres, M. Mills, K. Maase and S. M. Payne (1998). "Structure of the *Shigella dysenteriae* haem transport locus and its phylogenetic distribution in enteric bacteria." Mol Microbiol **28**(6): 1139-1152.

Yang, J., H. R. Panek and M. R. O'Brian (2006). "Oxidative stress promotes degradation of the Irr protein to regulate haem biosynthesis in B*radyrhizobium japonicum*." Mol Microbiol

60(1): 209-218.